



STUDIECENTRUM VOOR KERNENERGIE
CENTRE D'ÉTUDE DE L'ÉNERGIE NUCLÉAIRE

00/C070033/JDB/BNe/P-2

CORA PROJECT TRUCK-II [FAS 63561]

WINDOCUMENT

J.D. Barnichon and B. Neerdael
(SCK•CEN)
J. Grupa (NRG)
A. Vervoort (KULeuven)

Waste & Disposal Department
SCK•CEN, Mol, Belgium

R-3409

January 2000

DISTRIBUTION LIST

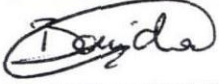
CORA Commission (12)
NRG, Mr. J. Grupa (1)
KULeuven, Prof. A. Vervoort (1)
ESV Praclay (2)

SCK•CEN central documentation/library (2)
Documentation Waste and Disposal Program (5)

SCK•CEN :

Mr. P. Govaerts (1)
General Manager
Mr. L. Veuchelen (1)
Contract Manager
Mr. G. Collard (1)
Head Research Unit Waste and Dismantling
Mr. B. Neerdael (1)
Department Head Waste and Disposal
Mr. M. Buyens (1)
Project Leader Exploitation URF
Mr. J. Marivoet (1)
Project Leader Performances
Mr. M. Put (1)
Project Leader R&D Disposal
Mr. P. Van Iseghem (6)
Project Leader Waste Characterization and Compatibility
Mr. J. Verstricht (1)
Project Leader PRACLAY
Mr. J.D. Barnichon

This document has been written and approved by:

		Date	Approval
Author:	Jean-Dominique Barnichon	25/01/00	
Verified by:	Geert Volckaert	25/01/00	
Approved by:	Bernard Neerdael	00/01/26	

RESTRICTED

All property right and copyright are reserved. Any communication or reproduction of this document, and any communication or use of its content without explicit authorization is prohibited. Any infringement to this rule is illegal and entitles to claim damages from the infringer, without prejudice to any other right in case of granting a patent of registration in the field or intellectual property. SCK•CEN, Boeretang 200, B-2400 Mol.

CORA PROJECT TRUCK-II
[FAS 63561]

J.D. Barnichon and B. Neerdael (SCK•CEN)
J. Grupa (NRG)
A. Vervoort (KULeuven)

R-3409

Contractnr: FAS 63561

Waste & Disposal Department
SCK•CEN, Mol, Belgium

January 2000

Foreword

The TRUCK-II project has been carried out with SCK•CEN as co-ordinator (Waste and Disposal Department), and with NRG and KULeuven ('Mining unit' of the Civil Engineering Department) under the CORA reference FAS 63561 and during the period 01/08/1998 - 10/07/1999.

The activities of the consortium have been distributed as follows:

- KULeuven, as author of the TRUCK-I project, brings the necessary information on the basic mine design and evaluates with the other partners the possible alternatives and their consequences in terms of repository area and planning (section 3.3);
- NRG is in charge of providing a procedure for retrievability in clay according to the concept(s) selected (chapter 4), in agreement and with the support of the partners as well as the evaluation of costs based on its previous experience for similar exercise in salt (chapter 5), and also some background information in the disposal concept (section 3.5);
- SCK•CEN is, beside the co-ordination, in charge of the estimation of the mechanical parameters for the Boom clay at 500 m depth (chapter 2), the optimisation of the mining concept from the thermal point of view (section 3.2), and the optimisation from the hydro-mechanical point of view (section 3.4), together with some background information on backfilling and sealing (section 3.5).

A large input to this project is the experimental programme related to the mechanical parameters determined on Boom Clay core samples taken at different depths in both Belgium and the Netherlands. This laboratory test campaign was decided in the course of the project, taking the opportunity of available core samples recently taken in the framework of the ONDRAF/NIRAS programme and in accordance with the wishes of the representative of the TRAKTOR programme to get a set of basic mechanical parameters required to launch this programme. The experimental programme had not only to be added within the planning of the TRUCK-II project, which of course led to a delay of several months, it also brought a huge increase of activities in follow-up and interpretation, taking into account sometime^s rather specific results and associated uncertainties in the further development of the project.

As it can be expected from such rather limited study tackling new large research issues and launching a new experimental programme, a number of questions arising during the study still needs to be

solved now. The conclusions that can be drawn from this work require more developments and confirmation before they can be put into practice. Based on these considerations, possible themes for further research were identified and discussed between the partners.

In order to ensure the necessary exchange of information and discussion with the partners, about 8 bilateral or trilateral meetings have been organised, partly in connection with the POC meetings organised at the NITG office. The main results of the project were presented of the CORA Commission held on the 24th June 1999.

To clarify the context of this TRUCK-II report, two main interfaces within the CORA program are worth to be mentioned:

- *the interface METRO – TRUCK-II*

The METRO (Modellen voor veiligheid en Economische aspecten van Terughaalbare opberging van hoog-Radioactief afval in de diepe Ondergrond) project refers to costs and performance of reference concepts as well for salt as for clay host rocks and requires therefore the needed information on mining aspects and associated models.

The interface was easily provided as the representative of NRG within the TRUCK-II project was previously involved in the METRO project;

- *the interface TRAKTOR – TRUCK-II*

The TRAKTOR (Transport van RADionucliden opgeslagen in Klei van Tertiaire ORigine) project started in the course of the TRUCK-II project so that the interface was automatically provided. The TRAKTOR project needed to get a basic set of geomechanical parameter values which could be determined using core samples from the same origin and test results performed in the same laboratory (UCL-Louvain-La-Neuve, B).

SCK•CEN could also take advantage in its evaluation of mechanical parameters of the information previously gathered in the CAR projects performed by NITG.

Executive summary

The TRUCK-II project investigates the retrievable disposal, at a depth of 500 m in the Boom Clay formation, of the radioactive waste generated by the Dutch nuclear programme.

It originated from the TRUCK-I project that focused on the study of the repository layout based mainly on mining considerations, on the host rock properties known at a depth of 225 m (Mol site), and on conservative thermal load conditions. This first study needed to be refined, taking advantage of the experience gained in Belgium at SCK•CEN for more than two decades with the same generic host rock, and of newly available data.

More realistic mechanical parameters for the Boom clay at a depth relevant for the Dutch concept, (500 m) are obtained from literature and from cores taken at five different depths and locations.

In addition, a more realistic thermal load is considered, taking into account both the time decay of the heat produced by the Cogema canisters and the effect of the cooling period before disposal. Good agreement is observed between the semi-analytical and numerical approach used.

From these more realistic mechanical parameters and thermal load conditions, the repository is optimised in terms of layout (distances between the different access and disposal galleries), timing and costs. Timing and financial aspects are studied for the whole repository, i.e. for high level heat-generating waste, medium level waste and low level waste. However, construction aspects (mechanical parameters, feasibility, excavated and disturbed zone) and conceptual aspects (dimensions, lining, overpack, backfill, temperature, cooling time, retrievability) are studied only for the part of the repository that relates to the high level heat-generating waste.

Results from the literature study suggest that, at greater depths, the rock properties become more beneficial for mining. However, this idea is not supported by the experimental results carried out here: the obtained friction angle at 500 m depth is about 9°, whereas the reference value known at Mol (225 m) reads 18°. This unexpected trend, which is unfavourable for mining, is not fully understood and would deserve additional work.

As a result from the thermal study, the following minimum repository area per Cogema canister that complies with the thermal disturbance criterion ($\Delta T \leq 4^\circ\text{C}$ at a boundary, 50 m above the repository) is obtained: 271, 179 and 141 m²/canister respectively for 50, 75 and 100 years cooling time.

Construction and timing aspects lead to the selection of two alternative configurations in addition to the one proposed in TRUCK-I: a network of 30 m × 30 m or 30 m × 18 m instead of the reference network of 50 m × 50 m. These alternative configurations can only be used if the diameter of the disposal cells is also reduced. Such a layout modification results in a decrease in length of the primary and secondary galleries by 40 to 60 %, and in a decrease in the corresponding repository area by 65 to 80 %. However, this depends essentially on the number of machines working at the same time.

The retrievability of the high level heat-generating waste is complicated due to the high radiation fields surrounding this waste. Therefore, a disposal cell (canister, buffer and backfill materials) has been designed that allows safe emplacement and retrieval of a waste canister, based on present-day technology.

A preliminary cost estimation indicates that the cost may range between Mfl 1500 and Mfl 2700. These are undiscounted costs in Dutch guilders, price value 1994. The dominant cost component is the cost of the underground construction: the tunnels' cost represents between 48 % to 60 % of the total cost, and the shafts cost between 14 % to 37 % of the total cost. Optimisation of the section for non-heat generating wastes is possible. Assuming that about 70% less tunnel length is sufficient to dispose the same amount of canisters, the estimated costs could decrease to Mfl 900 or Mfl 1900 for an optimised design.

Should further studies be considered, they should include new hydro-mechanical laboratory tests to confirm or deny the obtained unexpected trends, and an optimisation of the repository layout and cost (especially the lining cost) for all types of waste.

Samenvatting

Het TRUCK-II project onderzoekt de terughaalbare opslag van radioactief afval, dat voortkomt uit het Nederlands nucleair programma, op een diepte van 500 m in de Boomse kleilaag.

Het TRUCK-II project spruit voort uit het TRUCK-I project dat geconcentreerd was op de studie van een ondergronds opslag ontwerp dat hoofdzakelijk gebaseerd was op mijnbouw beschouwingen, op de eigenschappen van het gastgesteente op een diepte van 225 m (site te Mol) en op conservatieve thermische belastingcondities. Deze voorafgaandelijke studie diende verfijnd, voordeel halend uit de ervaring die verkregen werd in België door het SCK•CEN gedurende meer dan twee decennia van onderzoek in hetzelfde oorspronkelijk gastgesteente, en met de recentelijk beschikbare gegevens.

Meer realistische mechanische parameters voor de Boomse Klei op een diepte die relevant is voor het Nederlandse concept (500 m), werden bekomen uit een literatuurstudie en op stalen van de Boomse Klei die genomen werden op vijf verschillende dieptes en locaties.

Bovendien werd een meer realistische thermische belasting beschouwd, rekening houdend met het tijdsverval van de warmteafgifte voortgebracht door een Cogema vat en met het effect van de koelperiode voorafgaand aan de berging. Een goede overeenkomst tussen de semi-analytische en de numerische benadering werd vastgesteld.

Gebaseerd op deze meer realistische mechanische parameters en thermische belasting wordt de ondergrondse berging geoptimaliseerd op het vlak van de lay-out (afstanden tussen de verschillende toegangs- and bergingsgalerijen); de timing en de kosten. De timing en de financiële aspecten worden bestudeerd voor de ganse ondergrondse berging, d.w.z. voor hoog radioactief warmte-afgevend afval, middelactief afval en laag actief afval. De constructie aspecten (mechanische parameters, haalbaarheid, uitgegraven en verstoorde zone) en de conceptuele aspecten (afmetingen, bekleding, extra verpakking, opvulmateriaal, temperatuur, koeltijd, terughaalbaarheid) worden enkel bestudeerd voor het deel van de ondergrondse berging dat betrekking heeft op het hoog radioactief warmte-afgevend afval.

De resultaten van de literatuurstudie suggereren dat, op grotere dieptes, de kleieigenschappen gunstiger worden voor mijnbouw. Niettemin wordt dit idee niet ondersteund door de experimentele resultaten die hier werden bekomen: de vastgestelde wrijvingshoek op 500 m diepte bedraagt 9°, terwijl de referentiewaarde die hier in Mol gekend is (225 m) 18° bedraagt. Deze onverwachte trend, die ongunstig is voor mijnbouw, wordt niet ten volle begrepen en zou bijkomend werk waard zijn.

Als een resultaat van de thermische studie wordt de volgende minimale bergingsoppervlakte per Cogema vat die in overeenstemming met het thermische verstoringskriterium ($\Delta T \leq 4$ °C aan de grenslaag, 50 m boven de bergingsplaats), verkregen: 271, 179 en 141 m²/vat respectievelijk voor 50, 75 en 100 jaar koeltijd.

Constructie en tijdsverdelingsaspecten leiden tot de keuze van twee alternatieve concepten aanvullend op diegene die voorgesteld werden in TRUCK-I: een netwerk van 30 m × 30 m of 30 m × 18 m in plaats van het referentie netwerk van 50 m × 50 m. Deze alternatieve ontwerpen kunnen enkel

gebruikt worden indien de diameter van de bergingscellen ook verminderd wordt. Zulke ontwerpaanpassing resulteert in een vermindering van de lengte van primaire en secundaire galerijen met 40 tot 60 % en in een vermindering van de overeenkomstige bergingsoppervlakte van 65 tot 80 %. Niettemin hangt dit essentieel af van het aantal machines die tegelijkertijd werken.

De terughaalbaarheid van het hoog radioactief warmte-afgevend afval is ingewikkeld omwille van de hoge stralingsvelden die dit afval omgeven. Daarom wordt een bergingscel (canister, buffer en opvulmateriaal) ontworpen die een veilige plaatsing en terugname van een afvalvat toelaat, gebaseerd op de huidige technologie.

Een voorafgaandelijke kosten schatting geeft aan dat de kost kan variëren tussen 1500 Mfl en 2700 Mfl. Dit zijn bruto kosten in Nederlandse guldens, gebaseerd op de waarde in 1994. De belangrijkste kost is de kost van de ondergrondse constructie: de kosten van de tunnels vertegenwoordigen 48% tot 60 % van de totale kosten terwijl de kosten voor de schachten liggen tussen 14% en 37% van de totale kosten. Optimalisatie van de sectie voor de berging van niet-warmte-afgevend afval is mogelijk. Indien men aanneemt dat ongeveer 70% minder tunnellenge voldoende is voor de berging van dezelfde hoeveelheid canisters, kan de geschatte kost verminderen tot 900 Mfl of 1900 Mfl voor een geoptimaliseerd ontwerp.

Indien verdere studies zouden ondernomen worden, dan zouden die nieuwe hydro-mechanische labotesten moeten omvatten om de bekomen onverwachte trends te bevestigen of te ontkennen, alsook een optimalisatie van de uitvoering van de berging en de kosten (vooral de kosten van de bekleding) voor alle afval types.

Abbreviations

CSL : Critical State Line
HLW : High Level radioactive Waste
HM : HydroMechanical
ILW : Intermediate Level radioactive Waste
LLW : Low Level radioactive Waste
MCC : Modified Cam Clay
NCL : Normal Consolidation Line
SWL : SWelling Line

Latin letters

C : intersection of the failure with the q axis
 C_{ijkl}^* : effective elastic constitutive matrix
 C_p : specific heat [$\text{J}\cdot\text{kg}^{-1}\cdot\text{K}^{-1}$]
 C_u : undrained shear strength
 c' : effective cohesion
 E : Young's modulus
 E_{th}, E_1, E_2, E_c : heat energy [J]
 e : void ratio
 f : yield function
 g : flow potential
 G : elastic shear modulus
 h : repository (half)thickness
 h : height of the HM model
 I_p : plasticity index
 K : elastic bulk modulus (undrained)
 K' : elastic effective bulk modulus
 k_T : thermal diffusivity
 M : slope of the CSL in the p' - q plane
 m : mass of a canister
 n : porosity
 P : thermal power [W]
 P_0 : thermal power generated by one canister at reactor unloading [W]
 p' : effective pressure
 p_c : preconsolidation pressure
 p_0 : half preconsolidation pressure
 p_1 : reference pressure
 q : stress deviator
 \mathbf{q} : heat flux [$\text{W}\cdot\text{m}^{-2}$]
 q_v : volume heat flux [$\text{W}\cdot\text{m}^{-3}$]
 q_{v0} : initial volume heat flux [$\text{W}\cdot\text{m}^{-3}$]
 r_1 : radius of secondary galleries

r_2 : radius of disposal cells
 s_2 : spacing between secondary galleries in a horizontal plane
 s_3 : spacing between tertiary galleries (or disposal cells) in a horizontal plane
 T : temperature
 t : time [s]
 t_C : cooling time since reactor unloading
 t_{GD} : time since disposal in repository
 V : specific volume
 V_λ : specific volume on the NCL at p_1
 V_κ : specific volume on the SWL at p_1
 v : total volume
 v_s : solid volume
 w : water content
 z : depth

Greek letters

$\Delta()$: increment
 δ_{ij} : Kronecker delta
 ϵ_{ij} : strain tensor
 ϵ_v^p : volumic plastic strain
 ϕ : effective friction angle
 γ_d : dry weight
 γ_s : specific weight
 γ_{sat} : saturated weight
 κ : SWL slope
 λ : NCL slope
 λ_T : thermal conductivity
 ν : Poisson's ratio
 ρ_s : specific density
 ρ_{sat} : saturated density
 ρ_w : water density
 $\sigma_{ij}, \sigma'_{ij}$: total and effective stress tensor
 ω : decay parameter

Symbols

$(\cdot), \frac{d(\cdot)}{dt}$: time derivative

Table of contents

1. Framework and scope	1
1.1. Introduction	1
1.2. Background information from the TRUCK-I project	2
1.2.1. General	2
1.2.2. Layout	3
1.2.3. Planning and time schedule	4
1.3. Scope of the TRUCK-II project	5
1.4. References	6
2. Estimation of realistic values for mechanical properties of Boom Clay at 500 m depth	11
2.1. Introduction	11
2.2. Time-independent mechanical behaviour of Boom clay	11
2.2.1. Mohr-Coulomb elastoplastic model	11
2.2.2. Modified Cam-clay elastoplastic model	12
2.3. Literature study on the evolution of Boom clay geomechanical parameters with depth 14	
2.3.1. Information available on the Boom clay	14
2.3.2. Information obtained on other clay formations	18
2.3.3. Representativeness of the available evolution laws for the Boom clay and consequences for the TRUCK-II project	19
2.4. Laboratory testing programme on Boom clay cores	20
2.4.1. Available core-drilled boreholes	20
2.4.2. Available Boom clay cores and selection of samples	21
2.4.3. Description of the testing programme	25
2.4.4. Consolidated Triaxial Undrained tests (CTU)	26
2.4.5. Isotropic Consolidation tests (IC)	27
2.5. Summary of the results	27
2.6. Discussion about the experimental results	29
2.7. Conclusions and implications for the TRUCK-II project	33
2.8. References	33
3. Optimisation of the design of the disposal facility	35
3.1. Introduction	35
3.2. Optimisation of a repository design from a thermal point of view	36
3.2.1. Starting assumptions	36
3.2.2. Thermal power generated per canister	36
3.2.3. Initial thermal field and canister temperatures	38
3.2.4. Basic configuration	38
3.2.5. Boundary conditions, properties and loading	39
3.2.6. Resolution methods	42
3.2.6.1. Analytical solution	42
3.2.6.2. Finite difference solution	43
3.2.7. Results	43
3.2.7.1. 1-D analytical results	43
3.2.7.2. 3-D finite difference results	47
3.2.8. Proposal of a repository configuration acceptable from a thermal point of view	54
3.3. Selection of alternatives based on configuration and timing of disposal	54
3.3.1. Comparison of 6 configurations	56
3.3.2. Time planning	58
3.3.3. Conclusions	60

3.4.	Optimisation of a repository design from a hydromechanical point of view	61
3.4.1.	Influence of the mechanical parameters obtained from the testing programme	61
3.4.2.	Details about the three-dimensional models considered	64
3.4.3.	Excavation of the secondary gallery	67
3.4.4.	Excavation of the disposal cell	67
3.4.5.	Conclusions	68
3.5.	Support and backfill of the galleries and disposal cells	69
3.5.1.	Initial Design of the Disposal Cell for HLW-canisters	69
3.5.2.	Backfill	71
3.6.	References	73
4.	Procedure for retrieval of a HLW canister	75
4.1.	Disposal and retrieval of a HLW-canister without overpack	75
4.2.	Disposal and retrieval of a HLW-canister with overpack	79
4.3.	Further considerations	83
4.3.1.	Radiation protection	83
4.3.2.	Generic designs	84
4.3.3.	Damage to the overpack or to the lining of the disposal cell	84
4.3.4.	Monitoring	84
5.	Cost estimate of a disposal facility in clay	85
5.1.	Introduction	85
5.2.	Cost estimates per phase in the disposal process	86
5.2.1.	Costs of research and development	86
5.2.2.	Costs of site screening and evaluation	86
5.2.3.	Costs of construction of the facility	86
5.2.3.1.	Surface constructions	86
5.2.3.2.	Shafts	87
5.2.3.3.	Underground infrastructure; tunnelling	88
5.2.3.4.	Personnel costs during operation and construction	91
5.2.4.	Costs of operation of the facility	91
5.2.4.1.	Cost of a watertight lining of a disposal cell	91
5.2.4.2.	Packaging and disposal of the waste	92
5.2.4.3.	Personnel costs during disposal operation	92
5.2.4.4.	Prolonged operation without disposal	92
5.2.5.	Costs of decommissioning and closure	93
5.3.	Results	93
5.4.	Comparison with the cost estimate provided by Belgium (SCK•CEN and ONDRAF)	94
5.5.	Conclusions	95
5.6.	References	96
6.	Conclusions and recommendations	97
	Appendix A - Dose rate calculations	A-3
	Appendix B - Mechanical analysis	A-7
	Appendix C - Hydromechanical modelling	A-9
	Appendix D - Analytical solution for the function f_{ω}	A-43
	Appendix E - Report on the geomechanical tests performed at UCL-LGC	A-45

1. Framework and scope

1.1. Introduction

The vitrified High Level radioactive Waste (HLW) from the Dutch nuclear power plants will probably be stored in a surface facility for 50 to 100 years, followed by a period of 50 to 300 years of retrievable storage. However, the waste must be isolated from the environment for a much longer period - at least several hundred thousand years. Research is therefore carried out to find long lasting solutions. Since other countries with nuclear power plants are faced with the same problem, a lot of the research is often performed in international co-operation. This is also the case for this project, where together with NRG two Belgian partners are involved: SCK·CEN and KU Leuven.

At SCK·CEN the possibility of disposing the radioactive waste in a deep underground clay formation has been studied for about 20 years. The clay layer under investigation, the Boom clay, has a number of properties that are favourable for a disposal facility:

- the clay layer is geologically stable. This means that we expect that this layer will be unchanged for millions of years to come;
- the Boom clay has a number of chemical/physical properties favourable to isolate the waste from aquifers in the geosphere;
- this clay is generally classified as a 'plastic' clay, in the sense that the elastic domain is quite limited and that irreversible phenomena appear rapidly under loading. Possible cracks in the clay layer during construction and operation phases or as a result of seismic events will close with time by creeping of the clay.

The results obtained to date from the research performed by SCK·CEN confirm that the clay layer is a suitable host rock for a disposal facility.

The Boom clay formation is also present under the Netherlands. Until recently however, research in the Netherlands focused on disposal in salt formations. In 1996, the scientific commission appointed by the Ministry of Economic Affairs that is managing the research on radioactive waste disposal (CORA) decided to start research into the possibility of disposing waste in clay formations.

The results of the Belgian research do not apply right away to the situation in The Netherlands. Two important differences are:

- The Dutch government has stated that all waste should be disposed of in such a way that it will be retrievable for a lengthy period of time.
- CORA is of the opinion that the waste should be disposed of at a larger depth than that currently being considered in Belgium (500 m instead of 225 m). This is because future glaciations may result in disturbances at larger depths in the Netherlands than in Belgium.

Further, some assumptions, taken from the Belgian programme, need confirmation in a further stage of the research. In particular, the reference thermal criteria used in section 3.2.1 (4°K at the top of the clay layer) would need to be refined but might even not be applicable in the Dutch context.

The TRUCK-II project should contribute to answer the following two questions:

- What are the (rock mechanical/mining engineering) properties of the Boom clay layer at a depth of 500 m?
- In what way can the high level radioactive waste be disposed of in this clay layer, such that the option to retrieve it in a relative simple way is left open?
- What are the costs of such a disposal facility?

Other issues, such as the isolation performance of the facility, are studied in the METRO-project.

1.2. Background information from the TRUCK-I project

1.2.1. General

Within the TRUCK-I project, a global mine design was made for the disposal of the different types of waste generated in the Netherlands: high-level heat generating waste, long-lived waste (not generating heat) and middle/low level radioactive waste (M/LLW). The same quantities were used as for the A strategy in the OPLA study (Grupa, 1998).

The host material is a clay formation with a minimum thickness of about 100 m. The design took the retrievability requirement into account, by imposing the constraint that each canister of high level waste has to be individually retrievable for at least a period of 50 to 300 years (TU Delft, 1993).

An additional factor having a direct impact on the mine design was that in the Netherlands a minimum depth of 500 m is imposed for the storage of radioactive waste. This minimum cover is related to the observed depth of glacial erosion channels.

The following principles were further applied to the mine design:

- i) The three types of waste are stored in three separated zones (see Figure 1.1a). It allows to take different actions for each waste type (e.g. sealing off, keeping open or retrieving waste).
- ii) Each zone is surrounded by a barrier of clay with a width of minimum 50 m. The barriers do not only allow to delineate clearly the different parts of the mine, but they also allow to isolate the highly radioactive parts from the rest of the repository. The number of tunnels intersecting these barriers is as much as possible limited (only two intersections per zone). It results in the additional advantage that sealing off an entire zone can be done relatively quickly and easily.
- iii) Within each zone, a regular mesh of tunnels is excavated, resulting in square or rectangular blocks of clay between the tunnels. In one direction access tunnels are excavated whereas the storage/disposal are built in the orthogonal direction. The blocks of clay left in situ between galleries are required for stability reasons (see further).

The main factors influencing the mine design were the stability of the individual tunnels and of the mine as a whole, and the problem induced by the temperature rise as a consequence of the storage of the heat generating high-level radioactive waste.

The most important question to be answered by the TRUCK-I project was whether the construction of a mine would be feasible taking the above mentioned constraints into consideration. An evaluation of the total length of shafts and tunnels was carried out, as well as the total volume of excavated and filling material, the total surface area required and the time required to excavate the shafts and the tunnels, to store the canisters and to fill the access tunnels. The calculations indicated that the construction of a mine under the modelled constraints is feasible indeed.

When TRUCK-I was carried out, no information was available on the mechanical and thermal characteristics of clay at a depth of 500 m. The available values for a depth of about 200 m were used in the calculations and it was assumed that these values were a conservative approach for clay at a depth of 500 m. In other words it was assumed that the clay would be at least as strong at a depth of 500 m, as it is at a depth of 200 m and that the heat conductivity would be the same or larger. The laboratory experiments carried out within the TRUCK-II project showed that these assumptions were well conservative (see chapter 2).

1.2.2. Layout

The Belgian reference concept for underground disposal was used for designing the mine layout. The mine consists of one level only, in the middle part of a thick clay layer. Apart from two vertical shafts, only circular horizontal tunnels are excavated. The three types of waste are stored in three different zones of the disposal facility (see Figure 1.1a), separated by a barrier of at least 50 m wide:

- High level heat generating waste: area of 400 m x 1000 m
- High level non heat generating waste: area of 1350 m x 1000 m
- Middle and low level waste: area of 800 m x 1000 m.

The area covered by the entire mine is about 4 km².

The proposed final layout, illustrated in Figure 1.1b, allows to excavate a new zone next to the existing ones at any time with a limited additional investment in the main infrastructure.

The following different types of tunnels can be distinguished:

- Primary galleries: these are the main drifts of the mine and the galleries connecting them. These primary galleries, as main transport roads enabling access to the various parts of the mine, have to remain open, at least as long as a particular part of the mine has to remain accessible.
- Secondary galleries: they are parallel to the shaft-shaft connection. They give access to the waste storage galleries and can remain open after storage of the waste to allow easy access for retrieval purposes. If desired, they can at a later stage be totally sealed off.
- Tertiary or storage galleries are smaller diameter galleries (inside diameter of 2.2 m), perpendicular to the secondary galleries. These storage galleries are sealed off as soon as the waste (canisters, drums or containers) has been brought in place.

For both types of high level waste, only one container is placed in each tertiary heading. In Figure 1.2, the transition secondary-tertiary gallery and the position of the high level waste canister are shown. The tertiary galleries are dead-ended and have a length of 15 m from the centre of the secondary galleries, as shown in Figure 1.3. The distance between the secondary galleries is in the three zones equal to 50 m. The distance between the tertiary galleries is 40 m for the zones in which no heat is generated and has been increased to 50 m for the heat generating zone, resulting in a square pattern for the latter. According to this layout, 304 storage points (16x19) are available for the storage of the 300 high level heat generating waste canisters.

In Table 1.1, the total length of all excavations (including shafts and all types of tunnels) and their volume have been compiled. In total, more than 1.4 million m³ of ground has to be excavated. Nearly 500 thousand m³ filling material is required to fill up all the voids and galleries.

Table 1.1. Total excavation length and total volume excavated (from Van de Steen and Vervoort, 1998).

Phase	Activity	Internal diameter (m)	External diameter (m)	Length (m)	Volume (1000 m ³)
1a	Shafts	5.0	6.2	1040	31.4
1b	Shaft area	4.3	5.4	388	8.9
2a	Connecting gallery	3.5	4.6	1095	18.2
2b	Basic primary layout	3.5	4.6	5086	84.5
3	Primary galleries	3.5	4.6	8086	134.4
4	Secondary galleries	3.5	4.6	47779	794.0
5a	Tertiary galleries MLW	2.2	3.2	17434	140.2
5b	Tertiary galleries HLW	2.2	3.2	20320	163.4
	Total	-	-	101227	1375.1

1.2.3. Planning and time schedule

In total, eight different phases were considered. The first five covered the excavation period. The sixth is the real storage of the waste and the backfilling of the voids surrounding the canisters. The filling of the primary and secondary tunnels is considered in the last two phases. In Table 1.2, an overview is given of all phases. It was assumed that the next phase would only start if the previous phase is completely finished. Hence, the entire mine could be excavated, a long time before the start of the underground storage of the canisters. Similarly, the filling of the primary and secondary galleries has not to follow immediately after the storage. The various assumptions on excavation rate, time to position machines, number of machines, storage rate, filling rate are given in (Van de Steen and Vervoort, 1998).

The total time required to excavate the entire mine complex is estimated to be 2950 working days. This would correspond to about 13 years (46 workings weeks of 5 days considered in one year). If one would be able to increase the speed of excavating by 50 % (from 10 to 15 m/day), but keeping the

same time for e.g. repositioning, the total time period is only reduced by about 600 working days. Under these conditions the mine could be finished in about 10 years.

If the three types of waste were stored in successive phases, it would require 2060 working days or about 9 years. To store the middle and low level radioactive waste requires 1126 working days or just below 5 years. The storage time for the two types of high level radioactive waste is less: 302 working days for the heat generating waste and 632 working days for the non heat generating waste.

The final filling of the secondary and primary galleries would require maximum 815 working days or 3.5 years. This could be reduced if one works at the same time in the various zones.

In conclusion, a minimum period of about 20 years should be provided for, between starting the shaft excavation and sealing off the repository, in case no major delays are experienced between the consecutive phases.

Table 1.2. Overview of time schedule for the excavation of the mine, the storage of the waste and possible successive closure (from Van de Steen and Vervoort, 1998).

Phase	Activity	Time required (# working days)	Total time period since start
Excavation			
1a	Shaft	380	
1b	Shaft area	85	465
2	Basic primary layout	320	785
3	Primary galleries	290	1075
4	Secondary galleries	1000	2075
5	Tertiary galleries	875	2950
Storage			
6a	HLW (Warm)	302	-
6b	HLW (Cold)	632	-
6c	MLW	1126	-
Filling			
7	Secondary galleries		
7a	HLW (Warm)	172	-
7b	HLW (Cold)	537	-
8	Primary galleries		
8a	HLW (Warm)	50	-
8b	HLW (Cold)	56	-

1.3. Scope of the TRUCK-II project

The project TRUCK-II is mainly aimed at applying the experience gained within the HADES project at SCK•CEN to the retrievable concept developed for the high level and long lived waste in the Netherlands, based on previous studies for salt formations (NRG) and on a preliminary design of the 'mine' performed by K.U.Leuven in the frame of the TRUCK-I project, summarised in the previous section. According to this objective, we will refer further in this document to the concept of High-Level heat emitting Waste (abbreviated in this report as HLW).

Within the numerous aspects which are relevant for such a storage/disposal system, we are focussing to constructional (mechanical parameters, feasibility, excavated disturbed zone) and conceptual (dimensions, lining, overpack, backfill, temperature, cooling time) aspects.

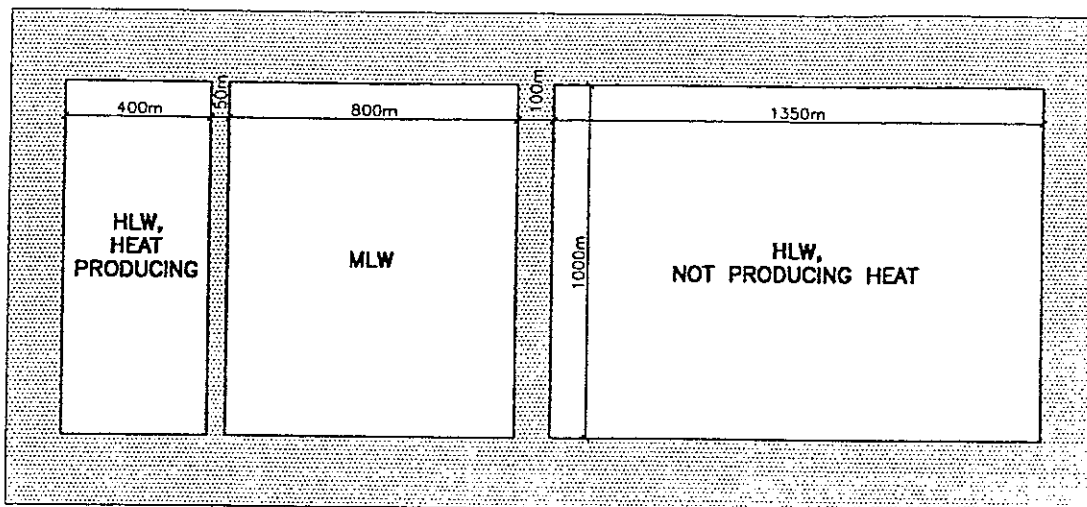
In Figure 1.4, a scheme is presented of the set-up of the TRUCK-II project. The new input or assumptions that are different in TRUCK-II in comparison with TRUCK-I are the more realistic thermal computations, the alternatives for the dimensions of the tertiary galleries (smaller diameter and shorter holes), and the better knowledge of the mechanical properties of Boom clay at 500 m depth. For the latter, a large part of this project has therefore been devoted to the determination of reliable data by carrying out (under the umbrella of the TRAKTOR programme) a rather extended experimental programme on undisturbed Boom Clay core samples from different locations and depths.

Essentially based on thermal calculations, different diameters and lengths of secondary and tertiary galleries are taken into account and further evaluated in terms of optimal configuration and planning. The corresponding alternatives are confirmed after being submitted to more detailed hydro-mechanical calculations based on convenient codes and realistic parameter values.

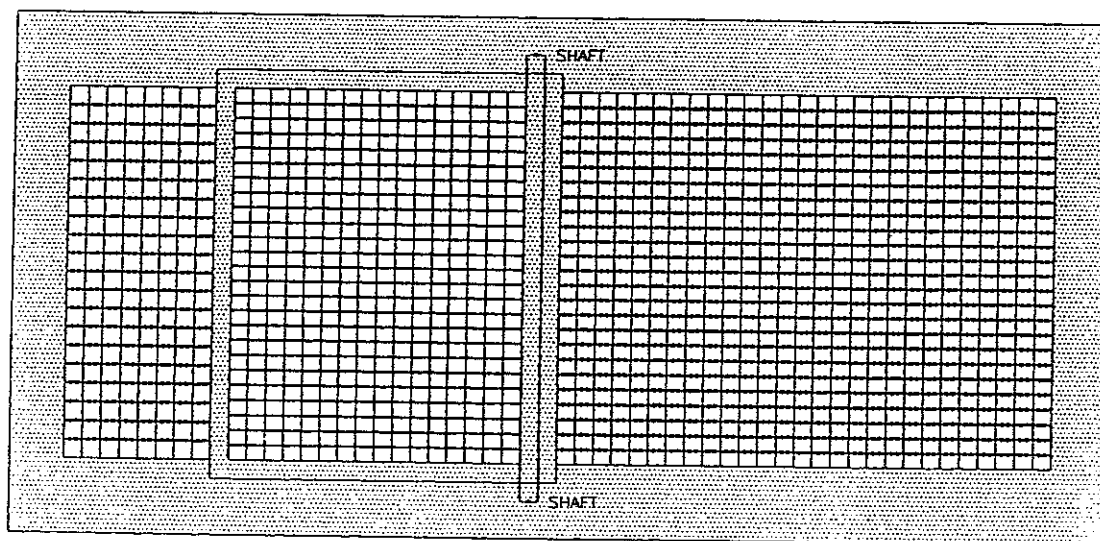
After a cost evaluation of a disposal facility for radioactive waste in a deep underground clay layer based on the available information, the document presents recommendations for further research.

1.4. References

- Grupa J. 1998. Overzichtslijst OPLA strategie A, Personal communication.
- Technische Universiteit Delft. 1993. OPLA Iia: Terughaalbaarheid van radioactief afval. In: *Bijlage, Eindrapport aanvullend onderzoek van fase I: samenvatting van de deelstudies*.
- Van de Steen B. and Vervoort A. 1998. *Mine design in clay*. CORA-project TRUCK-I, K.U.Leuven.



a: View of three separated zones (horizontal plane)



b: Tertiary or waste storage galleries (horizontal plane)

Figure 1.1. TRUCK-I mine layout of waste disposal (from Van de Steen and Vervoort, 1998).

1. Framework and scope

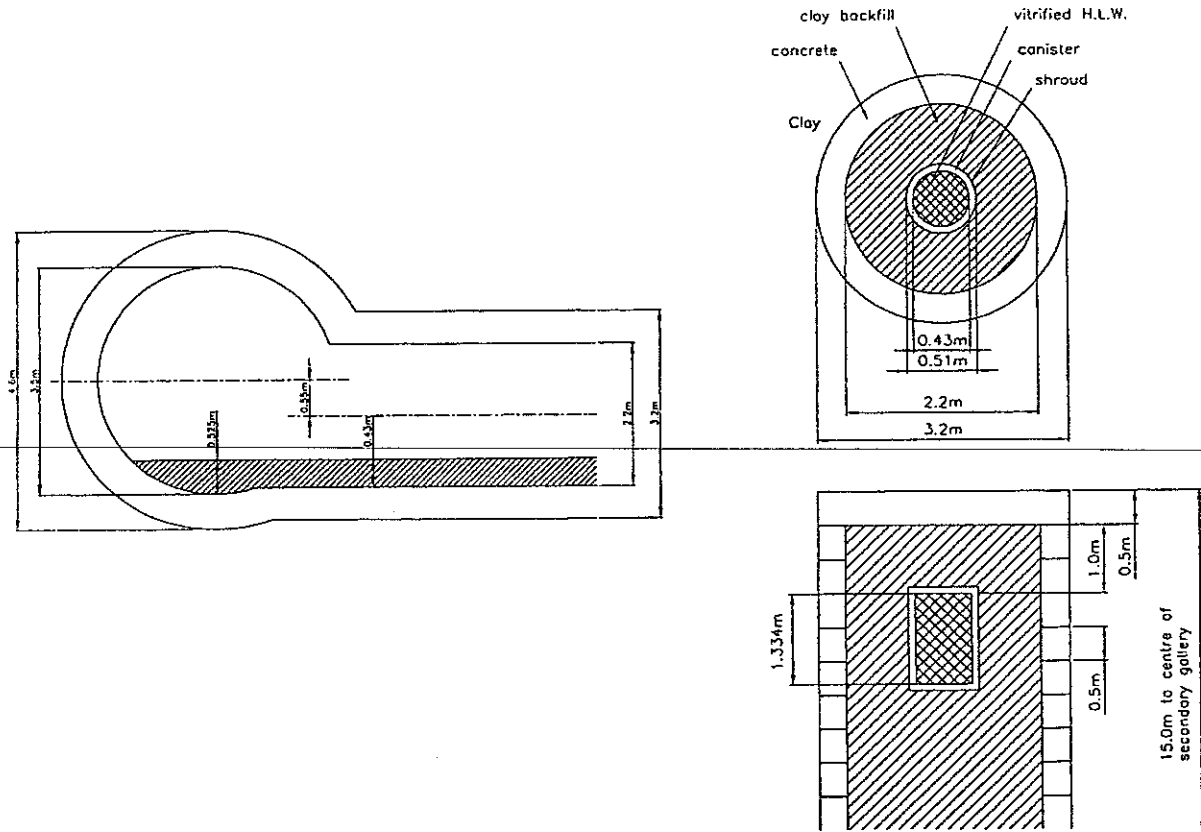


Figure 1.2. Transition secondary gallery-tertiary gallery and position of the high level waste canister in the tertiary gallery (from Van de Steen and Vervoort, 1998).

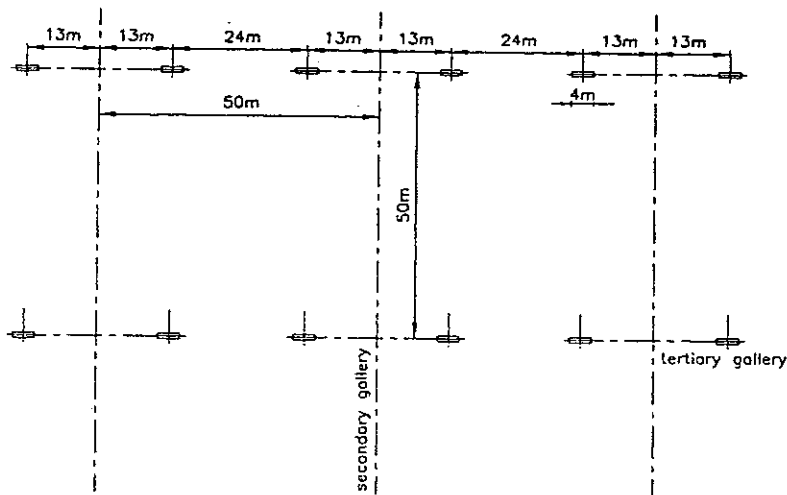


Figure 1.3. Basic grid pattern of 50 m x 50 m for the heat generating high level waste (from Van de Steen and Vervoort, 1998).

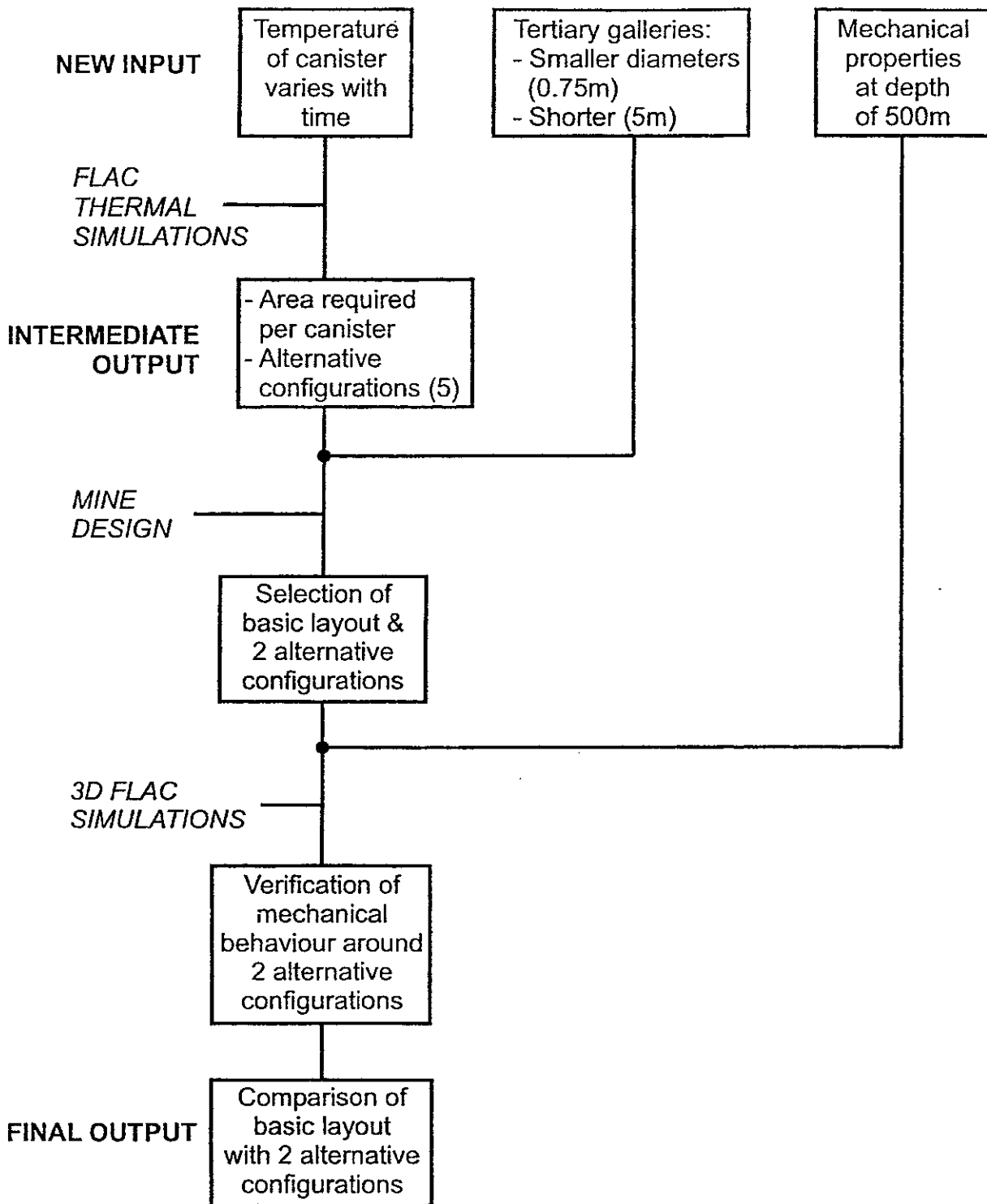


Figure 1.4. Overview of the TRUCK-II approach.

2. Estimation of realistic values for mechanical properties of Boom Clay at 500 m depth

2.1. Introduction

It is of prime importance to evaluate or determine what are the mechanical characteristics of the Boom clay formation at a depth of about 500 metres. Only time-independent mechanical characteristics are considered here (elastic and plastic properties). Assuming the clay behaviour is isotropic, the elastic coefficients then resume to the bulk K and the shear G modulus (or alternatively the Young modulus E and the Poisson ratio ν). Depending of the plasticity model that is considered to best approximate the Boom clay behaviour, the following plastic parameters are also required:

- the effective cohesion c' and the effective friction angle ϕ' if the Mohr-Coulomb yield criterion is considered,
- the preconsolidation pressure p_c , the slopes λ and κ of the normal consolidation line and swelling line, and the specific volume V (or the porosity n) if the Cam-clay criterion is considered.

2.2. Time-independent mechanical behaviour of Boom clay

In this study, yielding of soils/rocks is considered to result either from a purely frictional behaviour (Mohr-Coulomb) or from a combination of frictional and volumetric behaviour (Modified Cam-clay). The resulting basic formulation for these two models is described below, considering the drained behaviour.

2.2.1. Mohr-Coulomb elastoplastic model

This model is based on linear elasticity (Hooke's law),

$$\dot{\sigma}'_{ij} = C^e_{ijkl} \dot{\epsilon}_{kl} \quad (2.1)$$

where the drained elastic tensor C^e_{ijkl} is defined by

$$C^e_{ijkl} = 2G \delta_{ik} \delta_{jl} + \left(K' - \frac{2}{3}G \right) \delta_{ij} \delta_{kl} \quad (2.2)$$

and where K' and G represent respectively the drained bulk modulus and the shear elastic modulus.

In this model, yielding (i.e. the transition from elasticity to plasticity) results mainly from the *deviatoric* part of the loading, or more rigorously from the ratio between the stress deviator and the effective mean stress, which must remain below a given level. The Mohr-Coulomb criterion is defined by the function f

$$f \equiv c' + \sigma'_n \tan \phi' - \tau = 0 \quad (2.3)$$

and is represented in the σ'_n - τ effective stress space by a straight line (see Figure 2.1), with c' the drained cohesion and ϕ' the drained friction angle.

Additionally, the dilation angle ψ is required to define the direction of plastic strain increments, and more particularly the volumetric plastic strain. Usually, this criterion represents fairly well the behaviour of 'compact' rocks such as limestone, granite. However, it must be pointed out that, when

dealing with porous rocks such as chalks and clays or sand-like soils, the Mohr-Coulomb criterion becomes less appropriate as it is unable to reproduce the volumetric yielding observed for such materials.

To summarise, in addition to the classical drained elastic parameters K' and G (or E' and ν'), the Mohr Coulomb criterion requires the definition of the following three parameters: the drained cohesion c' , the drained friction angle ϕ' and the dilation angle ψ .

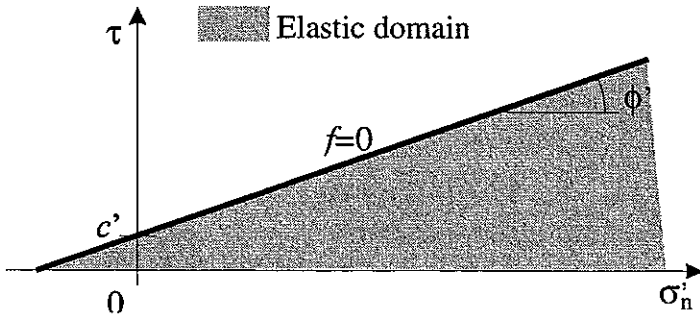


Figure 2.1. The Mohr-Coulomb yield criterion.

2.2.2. Modified Cam-clay elastoplastic model

Consider now materials for which yielding is a combination of both frictional and volumetric yielding, which agrees with experimental results obtained from soils and clays (Britto & Gunn, 1987). A classical representation of such behaviour has been proposed through the critical state family of constitutive laws, of which the Modified Cam-Clay (MCC) model is the most famous. The MCC model is based on non-linear elasticity, with a plastic formulation incorporating the critical state concept.

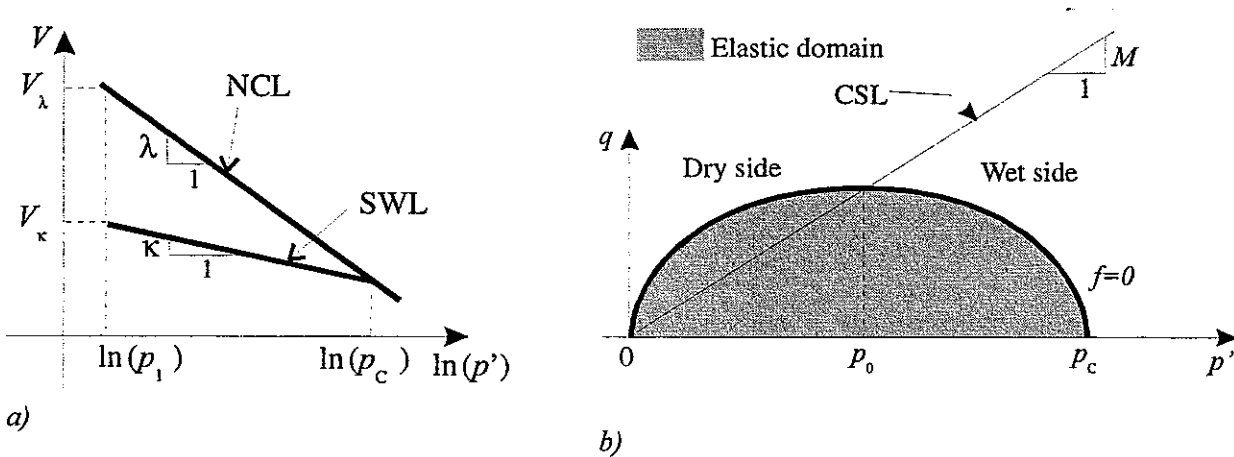


Figure 2.2. Modified Cam-clay model: a) representation of the NCL and SWL in the $\ln(p')$ - V space, b) yield surface in the p' - q space.

Let us recall the definition of specific volume V (v is the total volume, v_s the solid volume)

$$V = \frac{v}{v_s} = 1 + e = \frac{1}{1-n} \quad (2.4)$$

From isotropic consolidation tests, the Normal Consolidation Line (NCL) is defined by

$$V = V_\lambda - \lambda \ln \frac{p'}{p_1} \quad (2.5)$$

and the isotropic elastic SWelling Line (SWL) by

$$V = V_\kappa - \kappa \ln \frac{p'}{p_1} \quad (2.6)$$

where λ and κ are the slope of the NCL and SWL in the V - $\ln(p)$ space. V_λ represents the specific volume on the NCL at a reference pressure p_1 and V_κ is the specific volume at the same reference pressure for a given preconsolidation pressure p_c (see Figure 2.2a). Non-linear elasticity is considered, in which the evolution of the drained elastic bulk modulus K' with p' is obtained from (2.6) and gives

$$K' = \frac{V p'}{\kappa} \quad (2.7)$$

Given a constant drained Poisson ratio ν' , the drained elastic shear modulus G' is then evaluated from

$$G' = \frac{3K'(1-2\nu')}{2(1+2\nu')} \quad (2.8)$$

though such assumption is not strictly valid from thermodynamics. The plastic part of the Modified Cam-Clay (MCC) model is based on an elliptical yield function f defined in the $(p'-q)$ stress space by

$$f \equiv (p' - p_0)^2 + \frac{q^2}{M^2} - p_0^2 = 0 \quad (2.9)$$

where p' represents the effective pressure

$$p' = -\frac{\sigma'_{kk}}{3} = -\frac{I_\sigma}{3} \quad (2.10)$$

q the second invariant of the stress deviator $\hat{\sigma}_{ij}$

$$q = \sqrt{\frac{3}{2} \hat{\sigma}_{ij} \hat{\sigma}_{ij}} = \sqrt{3} II_{\hat{\sigma}} \quad \text{with} \quad \hat{\sigma}_{ij} = \sigma_{ij} + p \delta_{ij} \quad (2.11)$$

M the slope of the Critical State Line (CSL) which is related to the drained friction angle ϕ' through

$$M = \frac{6 \sin \phi'}{3 + \sin \phi'} \quad (2.12)$$

and p_0 represents half of the preconsolidation pressure p_c (see Figure 2.2b)

$$p_0 = \frac{1}{2} p_c \quad (2.13)$$

The other main features of this model lie in the definition of a hardening rule describing the evolution of p_0 as a function of volumetric plastic strains $\dot{\epsilon}_v^p$ by

$$\dot{p}_0 = \frac{p_0}{\lambda - \kappa} \dot{\epsilon}_v^p \quad (2.14)$$

and in the associated plasticity (i.e. the flow potential g corresponds to the yield surface f). It results that this model predicts a different plastic volumetric behaviour depending on the overconsolidation ratio (wet and dry side, see Figure 2.2b). For further details about its formulation, refer e.g. to Gens and Potts (1988).

To summarise, in addition to the drained friction angle ϕ' , the Modified Cam-clay criterion requires the definition of the following three parameters: the slope λ of the NCL and the slope κ of the SWL in the $\ln(p')$ - V space, and the preconsolidation pressure p_c .

2.3. Literature study on the evolution of Boom clay geomechanical parameters with depth

Within the framework of the TRUCK-II project, representative geomechanical parameters for the Boom clay are required at the depth of approximately 500 m as it is the target depth for the Dutch HLW disposal in the Rupelian clays. As a first step, the variation of the geomechanical parameters as a function of depth is studied (interval 100 m – 500 m).

Depending on the considered constitutive model, the evolution of several parameters is required. For the Mohr-Coulomb model, the variation of the elastic parameters E' and ν' (or G and K') and of the plastic parameters c' and ϕ' is required. For the modified Cam-clay model, the evolution of parameters λ , κ and p_c is required.

Firstly, information available on the Boom clay is presented. Then, comparison with some other clay formations is given in section 2.3.2. Eventually, the reliability of the proposed relationships for the Boom clay is discussed.

2.3.1. Information available on the Boom clay

Obviously, all the publications directly linked with the Boom clay formation at the Mol site at the depth of -223 m were previously known at SCK•CEN out of the framework of the TRUCK-II project (see for instance Bonne et al., 1985; Horseman et al., 1987; Mair et al., 1992; Neerdael et al., 1992; Bernier and Neerdael, 1996; Horseman and McEwen, 1996; Knowles et al., 1996). As all these references relate to studies for the Belgian HLW repository concept, they all consider the Boom clay at the depth of about -225 m (which is the depth corresponding to the Mol underground laboratory). Some work has been carried out in the past to study the evolution of Boom clay geomechanical characteristics with depth, which results are presented hereafter, together with an up-dating of these studies.

- From borehole measurements, the evolution of the Boom clay dynamic Young modulus with depth is limited (Rijkers, 1998).
- Referring to Antwerp samples of Boom clay ranging from 0 to 50 m depth, De Beer (1977) proposed the following linear evolution of the undrained shear strength C_u as a function of depth z

$$C_u = 0.75 + 0.035 \cdot z \quad (2.15)$$

where C_u is given in bars and z in m.

- Using later measurements of Boom clay samples at the Mol site, ranging from 180 to 250 m depth, and reporting them on the same plot (see Figure 2.3), we propose the following adjusted linear regression

$$C_u = 1.002 + 0.02488 \cdot z \quad (2.16)$$

However, the variation of C_u with depth is likely to be non-linear as shown on Figure 2.3. Thus, we also propose the following power relation as a better approximation for C_u than the relation (2.16)

$$C_u = 0.3272 \cdot z^{0.5464} \quad (2.17)$$

In any case, there is a large uncertainty on the extrapolation of C_u at 500 m depth due to a large scattering of data obtained from the Mol site.

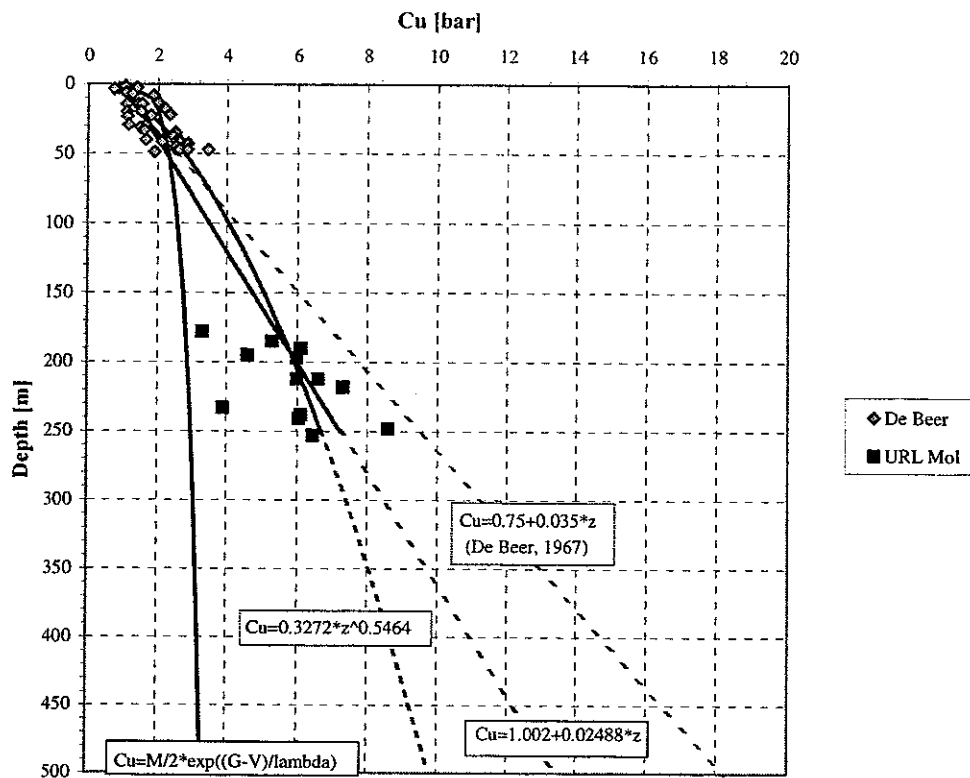


Figure 2.3. Undrained shear strength obtained from unconsolidated undrained triaxial tests on Antwerp and Mol Boom clay samples (diamond-shaped and square points) with some proposed regressions functions.

- Under normally consolidated condition (n.c.), Horseman et al. (1987) proposed for the Boom clay a relation between the undrained shear strength C_u and the consolidation pressure $p_{c(n.c.)}$

$$C_u = p_{c(n.c.)} \cdot 0.269 \quad (2.18)$$

and also showed that the Boom clay verifies fairly well the general relation proposed by Skempton (1957) for normally consolidated clays

$$\frac{C_u}{p_{c(n.c.)}} = 0.11 + 0.0037 \cdot I_p \quad (2.19)$$

where I_p is the plasticity index. Based on the MCC model, they also gives the relation

$$\frac{C_u}{p_{c(n.c.)}} = 0.5 \cdot M \left(2^{-\Lambda_0} \right) \quad (2.20)$$

where Λ_0 is the critical state pore pressure parameter defined by

$$\Lambda_0 = 1 - \frac{\kappa}{\lambda} \quad (2.21)$$

Using this relation, the value $\Lambda_0 = 0.85$ is obtained, which then leads to $M = 0.96$ from (2.20). Using equation (2.20) and $\Lambda_0 = 0.58$ (Horseman et al., 1987) for the Boom clay at Mol site, the value of $M = 0.80$ is obtained, which is also very close to the direct value obtained from triaxial experiments ($M = 0.81$).

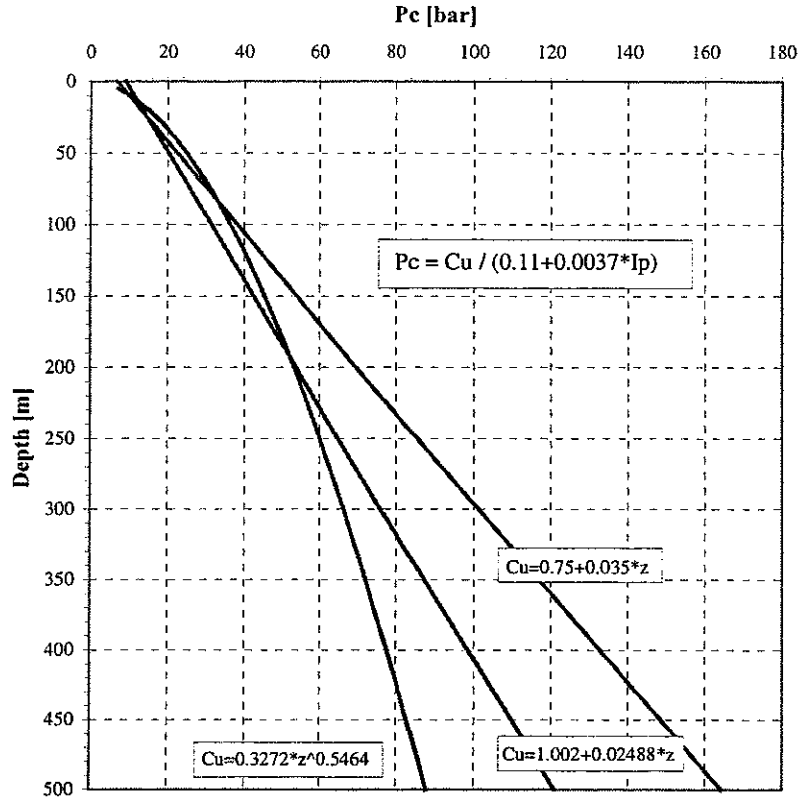


Figure 2.4. Preconsolidation pressure obtained from Skempton relation using different C_u estimations.

- Wood (1990, page 259) proposed a relation based on the MCC model

$$C_u = \frac{M}{2} \exp\left(\frac{\Gamma - V}{\lambda}\right), \text{ with } \Gamma = N - (\lambda - \kappa) \ln 2 \quad (2.22)$$

Using Boom clay parameters from Mol site, and computing the evolution of specific volume as a function of depth from the SWL and NCL, this relation is plotted in Figure 2.3. It seems to underestimate C_u for large depth values.

- Using the C_u values given by relations (2.15), (2.16) and (2.17), the profiles of preconsolidation pressure p_c obtained from (2.19) (with a constant value $I_p = 0.32$) are presented on Figure 2.4.
- The critical state framework includes an evolution law for the elastic bulk modulus K and for the porosity n as a function of the mean pressure p . With these relations and using parameters that are known at the Mol site (depth of 225 m), K and n can be extrapolated at the depth of 500 m. Some assumptions are required to obtain the values of p , especially on the K_0 value and on the rock density value. Here, an isotropic stress state is assumed (i.e. $K_0 = 1$), resulting in a pressure p equal to the column weight

$$p = \rho_{\text{sat}} \cdot g \cdot z \quad (2.23)$$

with $\rho_{\text{sat}} = (1 - n) \cdot \rho_s + n \cdot \rho_w$

where ρ_{sat} is the density (assumed to be constant) of the saturated porous medium (bulk density), ρ_s and ρ_w the specific and water density. Here the value $\rho_{\text{sat}} = 2000 \text{ kg}\cdot\text{m}^{-3}$ is adopted, which corresponds to the value at Mol site ($\rho_s \approx 2700 \text{ kg}\cdot\text{m}^{-3}$, $\rho_w = 1000 \text{ kg}\cdot\text{m}^{-3}$, $n \approx 0.4$).

Firstly, the specific volume V depends on the pressure p through equations (2.5) and (2.6). As an example, its evolution has been computed here for depths ranging between 225 to 1000 m, and

using Mol parameters at 225 m: $\lambda = 0.13$, $\kappa = 0.02$, $p_0 = 22.5$ bars. With an initial porosity $n_0 = 0.45$, the corresponding porosity profile is presented on Figure 2.5a together with two points obtained from Rijkers (1998). Note the change of slopes at 600 m depth, which corresponds to the transition from elasticity to plasticity (equal to p_c under isotropic loading). Note also that such porosity changes result in density changes, which have been neglected here. The value $\kappa = 0.08$ gives a second porosity profile (see Figure 2.5a) which match^o very closely the two points obtained from Rijkers (1998).

Secondly, the elastic bulk modulus K depends on p and V through equation (2.7), which then results in a non-linear dependence on p (see Figure 2.5b).

These results represent the theoretical evolution of n and K for Mol samples which would have been loaded down to 500 m depth under a drained stress path (i.e. at a very low rate).

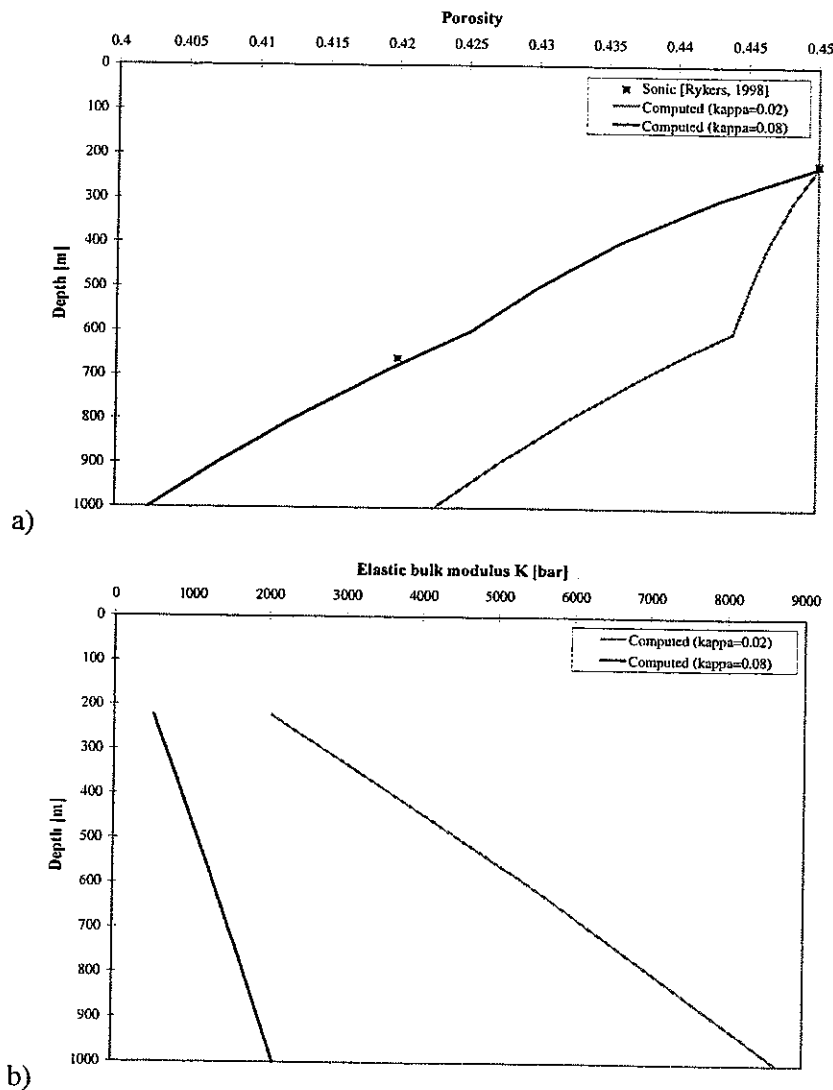


Figure 2.5. a) evolution of porosity with depth: theoretically computed from critical state model (solid lines) for two κ values and obtained from sonic measurements (points); b) theoretical evolution of bulk modulus with depth for two κ values.

However, it is uncertain whether or not these results are representative of the in-situ Boom clay at 500 m because they are based on evolution laws derived from laboratory experiments in which

some factors of the consolidation process are not considered (e.g. thermal and chemical effects). Therefore, the evolution laws (2.5), (2.6) and (2.7) may lead to geomechanical parameters which can differ significantly from their real values at 500 m depth.

2.3.2. Information obtained on other clay formations

When looking at some other geological clay formations, very little work has been published on the depth evolution of geomechanical parameters of clays from 0 to about 500 m depth. The most probable reason for that comes from the difficulty to obtain samples of the same clay at different depths, and especially at several hundred meters which is not a common depth for most civil engineering investigations. For instance, Cripps and Taylor (1986) summarised the geomechanical properties of the main British Tertiary clay deposits for relatively shallow depth (ranging between 0 to 40 m).

Several authors have proposed evolution laws (either linear or non-linear) of some parameters with depth (i.e. with mean stress) for given rock types:

- based on a large number of in-situ seismic cone tests, Shibuya and Tanaka (1996) proposed an evolution law of the Holocene clay elastic shear modulus G_f with the vertical stress

$$G_f = A (e_0)^{-\beta} (\sigma'_v)^n \quad (2.24)$$

where σ'_v is given in kPa and e_0 is the in-situ void ratio, and where

$$A = 5, \quad \beta = 1.5, \quad n = 0 \quad (2.25)$$

- Wroth and Wood (1978) proposed a relation between C_u and the liquidity index,
- Rubey and Hubbert (1959), see e.g. Magara (1980), proposed a law to describe the variation of porosity n with depth (i.e. the compaction)

$$n = n_0 \exp^{-cz} \quad (2.26)$$

where n_0 is the porosity at $z = 0$ and c is a constant.

- Changes in porosity induce non-linear variations in permeability k , which can be represented by the Kozeny-Carman law

$$k = cste \cdot \frac{n^s}{(1-n)^r} \quad (2.27)$$

where s and r are exponents, or more recently by Lamoureux-Var (1997)

$$k = A \cdot e^r \quad (2.28)$$

where e is the void ratio and r an exponent.

In the framework of radioactive waste disposals, several host rock formations have been studied throughout Europe, and their main geomechanical properties are summarised in Table 2.1.

Table 2.1. Properties of several potential host rocks for different disposal concepts throughout Europe (adapted from NEA, 1995).

	clay mineral (% wt)	Burial depth (m)	Bulk density	w (% dry wt)	n (%)	Rc (MPa)	E (MPa)	ν	ϕ (°)	C (Mpa)	λ	κ	ϕ' (°)	p_c (MPa)	ν'
Boom Clay (B)	60	200	1.9-2.1	19-24	36-40	2.0-2.2	200-400	0.4-0.45	4	1	0.11-0.16	0.02-0.05	18-22	5-6	0.125-0.2
Opalinus Clay (CH)	40-80	500-1000	2.5-2.6	4-12	3-12	4-8	2000-3000	0.35	20-30	2-3					
Tourmemire argillite (F)	25-50	200-250	2.3-2.6	1-4	7-14	32-37	9700-15300	0.16-0.28	19-35	1-1.8					
Gard silt (F)	30-40	300-1500	2.2-2.6	<10	10-15	10-100	4000-25000	0.3							
Est argillite (F)	40-45	350-550	2.2-2.3	4-8	10-15	18-30	3000-10000	0.3							
Blue clay (I)	35-89	0-1000	1.4-2.2	20-30	20	0.5-3.5			21-21	0.1					
San Pedro clay (S)	52-96	100-500	2.5-2.8	6-30		6.5-11.5	100-1300		19-52	0.07-0.08					
Oxford clay (UK)	40-58	265	2.0-2.4	9-20	20-36	1-4	100-300								

with w : water content; n: porosity; Rc: uniaxial strength.

2.3.3. Representativeness of the available evolution laws for the Boom clay and consequences for the TRUCK-II project

In the previous section, some relations have been proposed to describe the evolution with depth (ranging between 0 to 500 m) of some parameters: undrained shear strength C_u , preconsolidation pressure p_c , porosity n , bulk modulus K , shear modulus G . These relations are based either on the critical state framework (for n and K) or on large number of tests performed at different depths (for C_u , p_c and G), which results in two main difficulties for determining them.

The first important difficulty comes from the wide origin of the used data, which leads to variations of the following factors:

- the size of the samples in case of laboratory experiments,
- the method that is used for sampling (extraction/coring method, conservation method),
- the human error (preparation of the samples, interpretation of the results),
- the method that is used for measuring the parameters (although different types of in-situ measurements and laboratory experiments may be used to estimate a given parameter, they generally do not give the same results).

As the final results depend upon all these factors, it is therefore very difficult/uncertain to build accurate evolution laws (as a function of depth) from such heterogeneous data sets.

The second important difficulty comes from the wide depth range which should be investigated: it is very unlikely to have data all over the depth range [0;225] m as most of the Boom clay samples come either from depths of 0 to 40 m (common civil engineering works) or from 225 m (Mol site).

Therefore, the relations proposed in the previous section for the evolution of C_u , p_c and G are likely to be unreliable in the depth range 0-225 m due to the wide origin of data they are built from, and their extrapolation to depth of 500 m would be very inaccurate.

As a consequence for the TRUCK-II project, the use of such unrepresentative evolution laws would lead to doubtful results, e.g. in term of plastic zone extent and support pressure.

A much better approach to build this evolution law for Boom clay would be to measure, using the same experimental method (ideally the same laboratory team), the same parameters for Boom clay samples coming from different depths, provided such samples are available.

2.4. Laboratory testing programme on Boom clay cores

Following the conclusions of the previous section, it was decided to check whether recent Boom clay cores at different depths were available.

Fortunately, four boreholes have been drilled recently by ONDRAF/NIRAS between October 1996-April 1998 in the framework of the performance assessment of the Belgian concept for geological disposal of HLW. These boreholes have several interesting aspects with respect to the TRUCK-II project. Firstly, all the four boreholes have been drilled recently so the cores were still in a 'fresh' state (they also have been conditioned similarly). Secondly, the same coring method has been used to extract the cores. Thirdly, due to the regional geology, the depth of the Boom clay is different for each of the four boreholes.

It provided us with the opportunity to build a programme of laboratory tests in order to measure geomechanical parameters for Boom clay coming from four different depths but from the same horizon (Putte member), and under the same experimental conditions. Due to the limited number of cores that were available and to the limited budget allocated to these tests, the core quality was investigated by X-ray computerized tomography scanning, which allowed to extract as homogeneous as possible samples from the cores. This programme has been defined in agreement between SCK•CEN and the Civil Engineering Department of the Louvain-La-Neuve University (UCL-LGC), within the framework of the TRAKTOR project.

Later in this project, some cores were made available from the Blija borehole in the Netherlands. Although there may not be an exact correlation between the Belgian and the Dutch Rupelian clay series (particularly about the location of the Putte member), and although the coring method was not the same as for the Belgian cores, they have been added to the project due to the large depth they are coming from (between 455 m and 478 m).

2.4.1. Available core-drilled boreholes

After discussion with NIRAS/ONDRAF, we selected four boreholes that have been drilled recently in Belgium (Doel 2b, Zoersel, Mol 1 and Weelde 1, see Figure 2.6 for location). Although the whole Boom clay section has been cored for each borehole (see Table 2.2), all the cores were not available as a part of them is used for other purposes (permeability measurements, migration experiments...). Lately, the Boom clay has also partially been cored at the Blija borehole (northern Netherlands) at depth ranging between 455 m and 478 m.

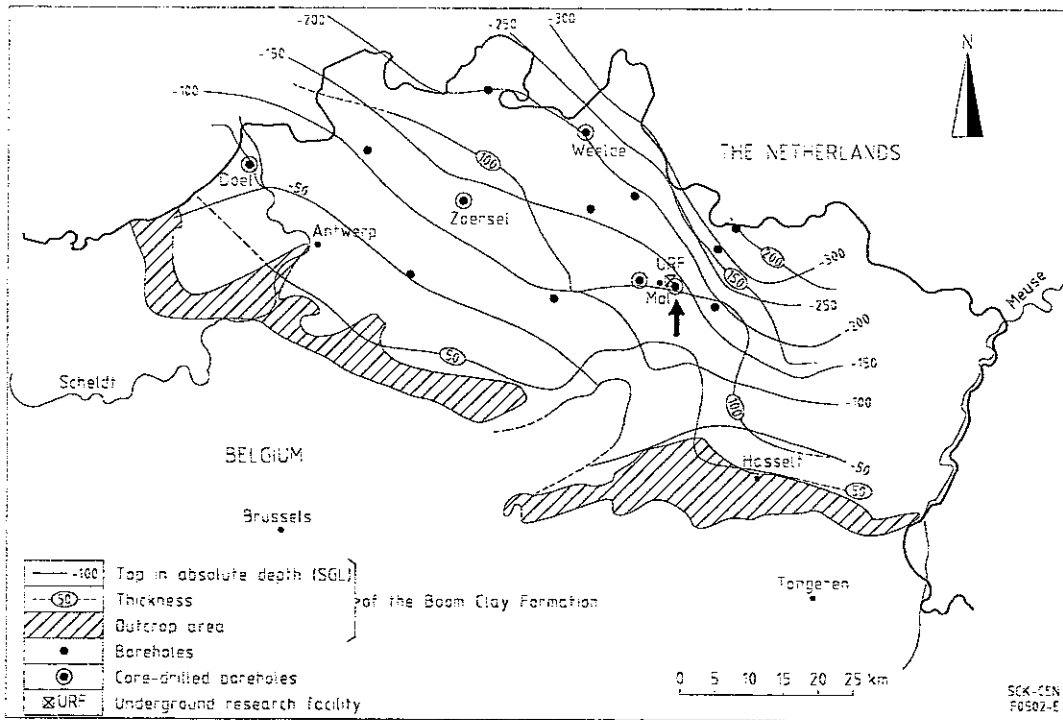


Figure 2.6. Location of the Doel, Zoersel, Mol and Weelde boreholes in Belgium.

Table 2.2. Characteristics of the Doel, Zoersel, Mol and Weelde and Blija boreholes

Borehole	Drilling date	cored range [m]
Doel 2B (B)	Apr 1998	53-114
Zoersel (B)	Oct 1996	90-188
Mol 1 (B)	May 1997	191-294
Weelde 1 (B)	May 1997	244-385
Blija (NL)	Oct 1998	454.5-455; 478-478.5

→ (20 km NMO van Leenwarden)

In order to derive representative evolution laws of geomechanical parameters as a function of depth for the Boom clay, the tests must ideally be performed on samples of different depths, but which all correspond to the same lithological unit.

2.4.2. Available Boom clay cores and selection of samples

Here, we decided to follow as closely as possible the level of the Boom clay which corresponds to the depth of -225 m at the Mol URF, and which belongs to the Putte member. Based on borehole logs, the correlation between the four selected boreholes and the cores availability led to the selection of five cores, which characteristics are reported in Table 2.3.

The available cores (provided by NIRAS/ONDRAF) have all been sampled using the same coring technique (patent of SMET Boring N.V.), with an original diameter of 10 cm, and disposed in a PVC tubing. Later, the geological description of the cored section required to truncate a two cm thick slice along the cores, which afterwards have been vacuum-sealed. Although the resulting core section is no longer circular (see Figure 2.7), there is still enough material to extract two samples for geomechanical tests (diameter = 38 mm, length = 76 mm).

Table 2.3. Characteristics of the Doel, Zoersel, Mol, Weelde and Blija cores studied.

Sample	Core number	CT Scan name	Depth [m]
Doel 2B	63c	AV Doel	69.5
Zoersel	38c	AV Zoer	121.0
Mol 1	76c	AV Mol 1c	225.0
Mol 1	80c	AV Mol 1	229.0
Weelde 1	87c	Weelde 87	313.1
Weelde 2	86c	Weelde 86	313.5
Blija			455
Blija			478

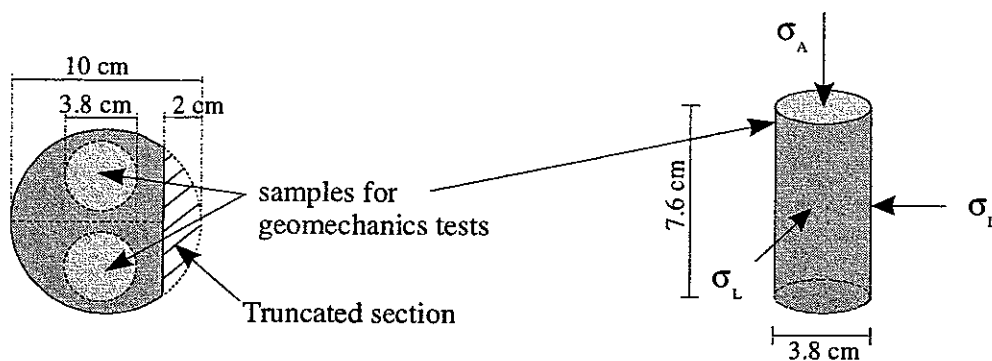


Figure 2.7. Location of geomechanical samples in the cores, and geometry.

The quality of each core reported in Table 2.3 has been investigated by performing X-ray Computerised Tomography Scanning (CTS) with the medical CT-scanner of the KULeuven (Prof. G. Marchal). It allowed to select for each borehole two sections of 10 cm long (which will give four samples) which were as homogeneous as possible, that is in which there was no occurrence of:

- large pyrite nodules (which appear clearly as high density areas on Figure 2.8a),
- areas with much higher porosity (which appear as low density areas),
- cracks or any damage indicators (see Figure 2.8b).

Examples of such heterogeneities as it appears on CT-scans are presented on Figure 2.8.

Based on these three criteria, the samples have been extracted from the cores at the locations reported on Figure 2.9.

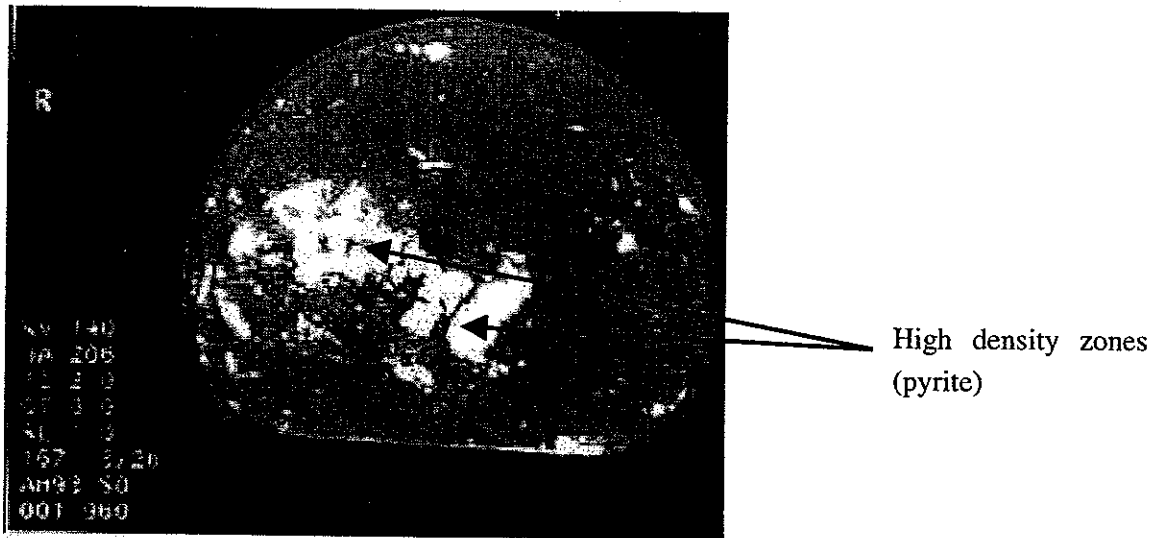


Figure 2.8a. Details of the CT-Scan of the sample from Mol: presence of large pyrite nodules (white 'spots').

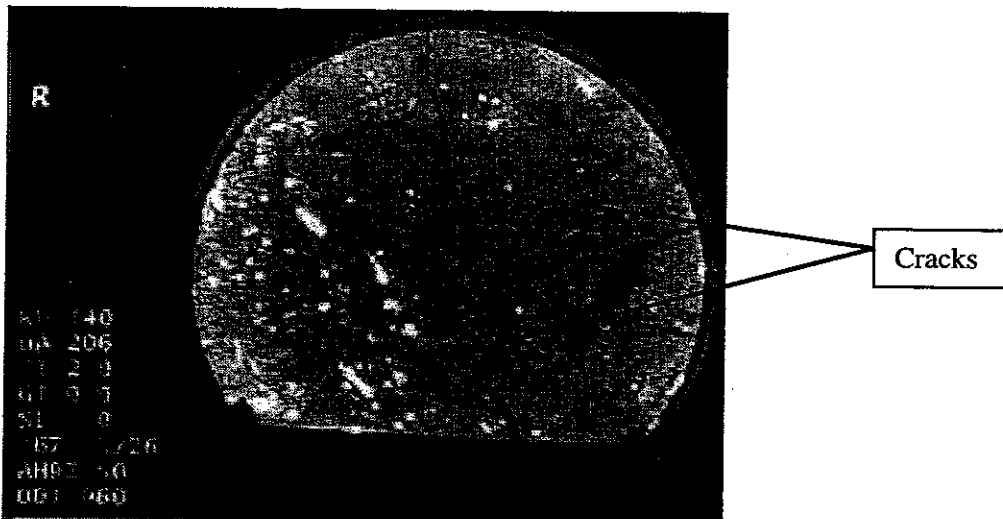
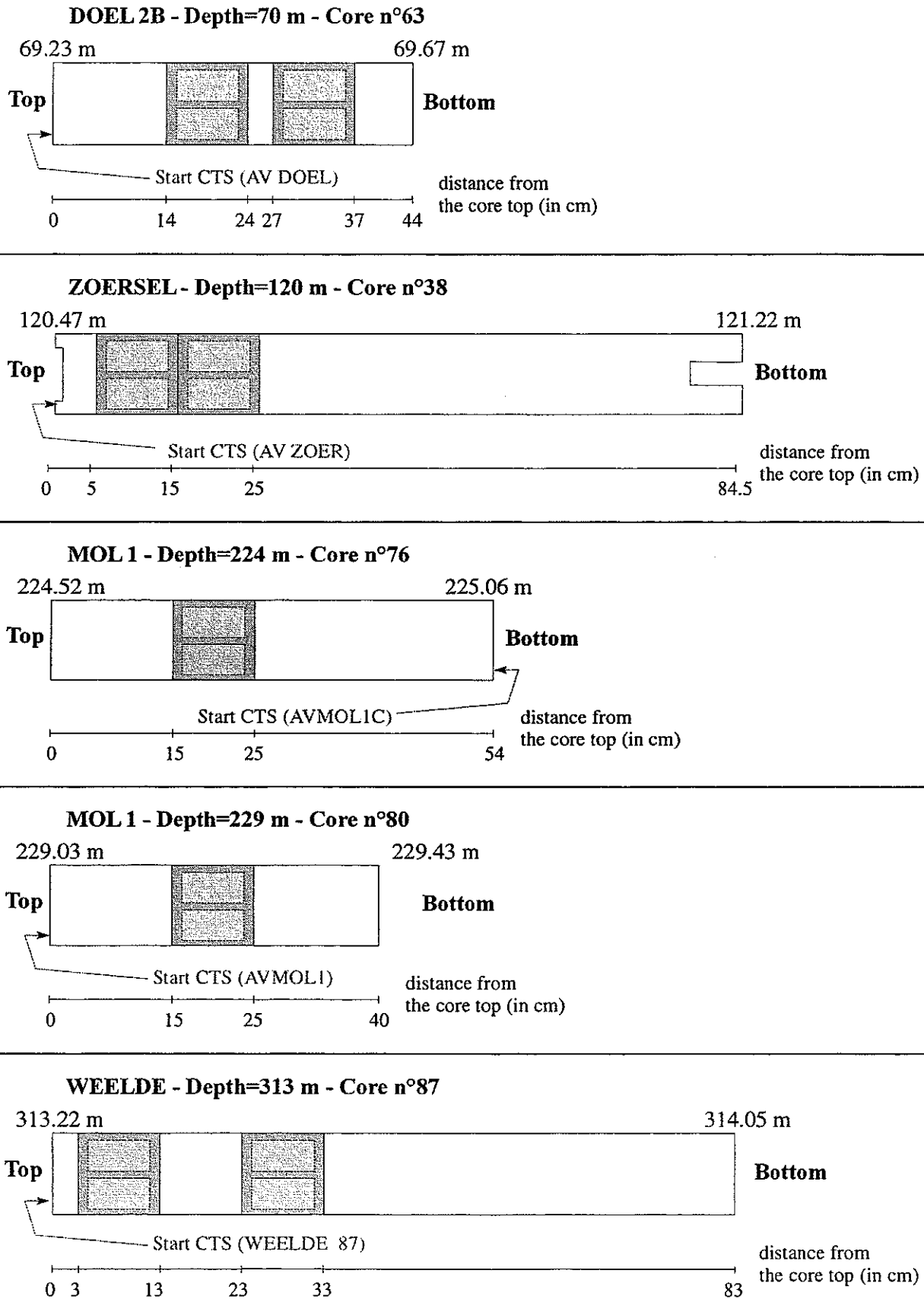


Figure 2.8b. Detail of the CT-Scan of the sample Mol: presence of cracks (in black).

2. Estimation of realistic values for mechanical properties of Boom Clay at 500 m depth



to Start by sampling in label!

Figure 2.9. Selection of geomechanical samples in the Doel, Zoersel, Mol and Weelde cores.

2.4.3. Description of the testing programme

Prior to carrying out these tests, the classical following properties of the samples have been characterised (refer to Appendix E for more details):

- the dry weight γ_d , the saturated weight γ_{sat} and the specific weight γ_s ,
- the water content w (initial and at saturation),
- the porosity n .

Main results from Appendix E show a linear variation with depth that is consistent with an increase in density as depth increases (see Figures 2.10 and 2.11).

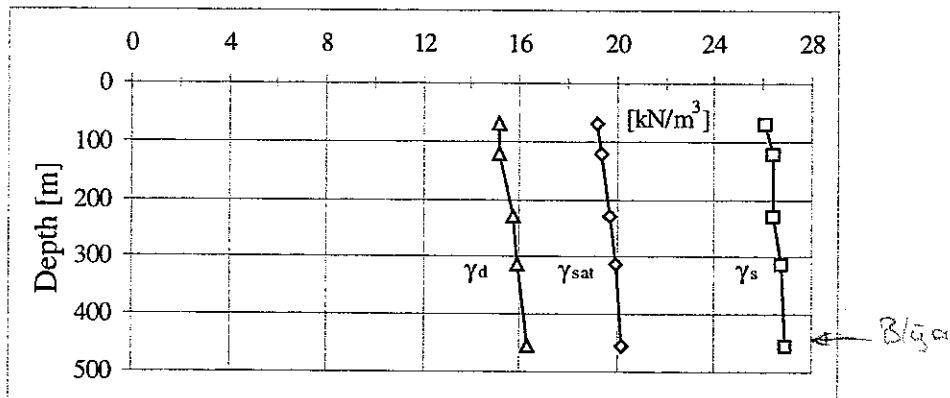


Figure 2.10. Dry, saturated and specific weights versus depth.

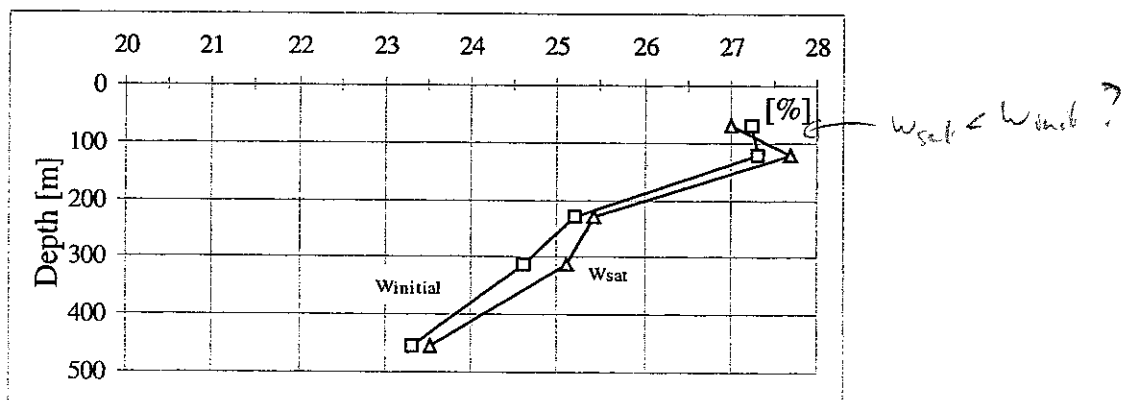


Figure 2.11. Initial and saturated water content versus depth.

However, after the first results from mechanical tests were obtained, it appeared necessary to characterise in more detail the samples, especially regarding their granulometry (by sedimentation analysis) and their mineralogy (by X-ray Diffraction). The results are presented in the Appendix E, and they do not show large heterogeneities among the samples that have been tested.

The experimental testing procedure involves a phase of saturation under a back-pressure of 0.2 MPa, and a consolidation phase (see Appendix E for more details) which consists in applying loading steps of isotropic stress until the required pressure is reached (σ_c values reported in Table 2.4).

Table 2.4. Characteristics of the test performed.

Origin	Sample	Depth [m]	Test realised	Normal soil consolidation σ_0 [MPa]	Consolidation of the samples σ_c [MPa]	Consolidation ratio [%]
Doel (B)	a	69.42	CTU	1.39	0.70	50.4
	b	69.42	CTU	1.39	1.05	75.5
	c	69.55	CTU	1.39	1.40	100.7
	d	69.55	IC	1.39	1.60	-
Zoersel (B)	a	120.57	CTU	2.41	1.20	49.8
	b	120.57	CTU	2.41	1.80	74.7
	c	120.67	CTU	2.41	2.40	99.6
	d	120.67	IC	2.41	1.60	-
Mol (B)	b	224.52	CTU	4.49	3.38	75.3
	c	224.52	CTU	4.49	4.50	100.2
Mol (B)	a	229.23	CTU	4.58	2.25	49.1
	d	229.23	IC	4.58	1.60	-
Weelde (B)	a	313.30	CTU	6.27	3.10	49.4
	b	313.30	CTU	6.27	4.70	75.0
	c	313.50	CTU	6.27	6.26	99.8
	d	313.50	IC	6.27	1.60	-
Blija (NL)	a	454.75	CTU	9.20	4.60	50.0
	b	454.75	CTU	9.20	6.90	75.0
	c	454.75	CTU	9.20	9.20	100.0
	d	478.25	IC	9.65	1.60	-

2.4.4. Consolidated Triaxial Undrained tests (CTU)

This test is a Consolidated Triaxial Undrained test (CTU) with interstitial pore pressure measurement. The confining pressure σ_3 is kept to the value σ_c while an axial loading is applied through a vertical displacement of the piston at a given velocity, which then defines the applied axial strain rate $\dot{\epsilon}_1$.

The resulting longitudinal force is measured with a load transducer outside the cell (without friction minimisation) and is converted to axial stress σ_1 , correcting by the section change of the sample. This test allows determining three parameters:

- the elastic shear modulus G (assuming a constant volume in undrained conditions)

$$\dot{q} = 3G \cdot \dot{\epsilon}_1, \text{ with } q = \sigma_1 - \sigma_3 \quad (2.29)$$

Thus, the linear part of the stress-strain curve in a q - ϵ_A plot has a slope of $3G$. In this study, we choose to define G on an unloading-reloading loop performed at about $\epsilon_1 = 1\%$. Such method is more accurate than the classical determination from the tangent at the origin;

- and the effective Mohr-Coulomb parameters ϕ' and c' obtained from the relation

$$q = M p' + C \quad (2.30)$$

where the parameters M and C define the line which fits best the ultimate soil state reached by three tests carried out at three different initial consolidation pressure p_0 . M and C are linked to ϕ' and c' through the relations

$$\sin \phi' = \frac{3M}{6+M} \quad (2.31)$$

$$c' = \frac{C}{M} \tan \phi' = \frac{3}{2} c \left\{ (2M+3)(3-M) \right\}^{-1/2} \quad (2.32)$$

2.4.5. Isotropic Consolidation tests (IC)

This test is an Isotropic ($\sigma_1 = \sigma_3$, i.e. $q = 0$) Consolidation test (IC), i.e. a test in which consolidation is performed for several isotropic loading steps. Provided the volume variation is measured at different consolidation steps, it allows determining the three Cam-clay parameters λ , κ and p_c by plotting the evolution of the specific volume as a function of mean effective pressure in a $\ln(p')$ - V plot (see Figure 2.2a).

2.5. Summary of the results

All the experimental data obtained in the TRUCK-II project are reported in the "Report on the geomechanical tests performed at UCL-LGC" that is given in Appendix E.

The main results of this report are summarised on the following Figures 2.12 to 2.16 as evolution of mechanical parameters with depth: elastic shear modulus G , cohesion c_{cu} and c' , friction angle ϕ_{cu} and ϕ' , and Cam-clay parameters λ , κ and p_c .

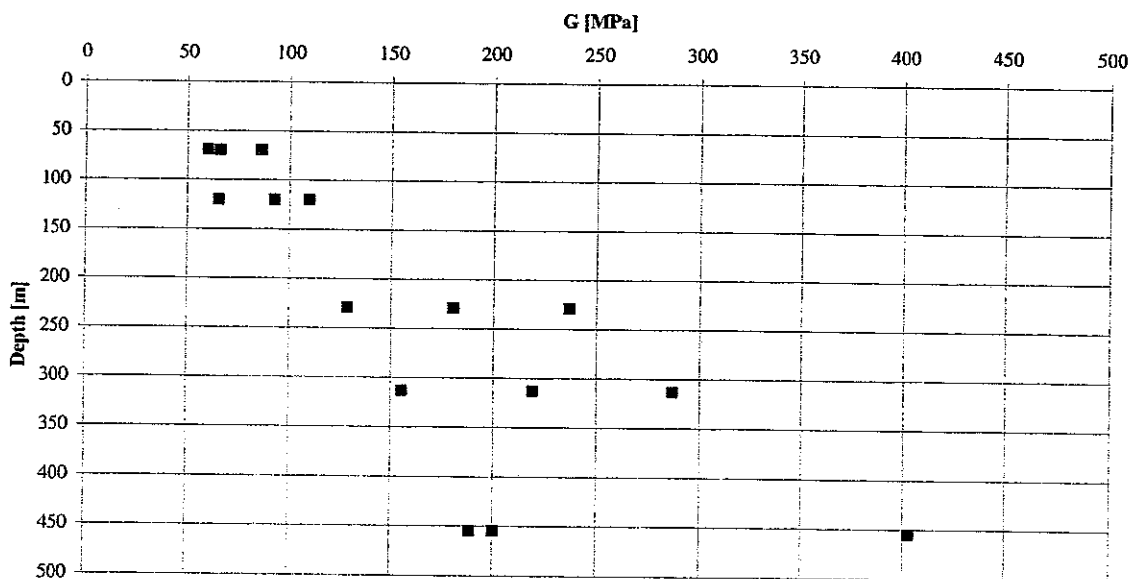
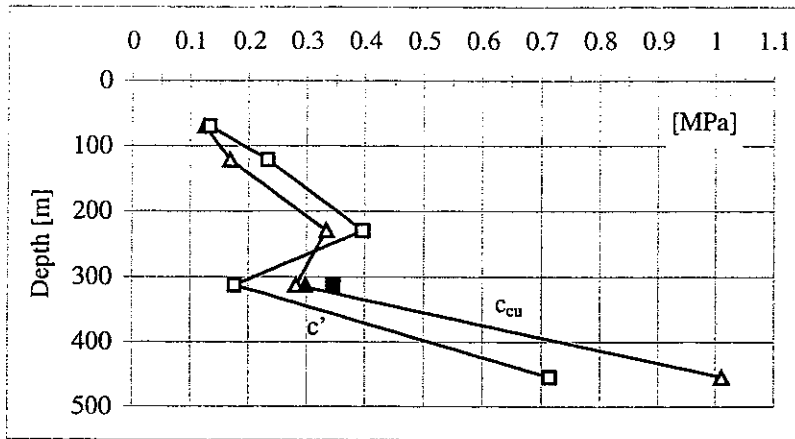


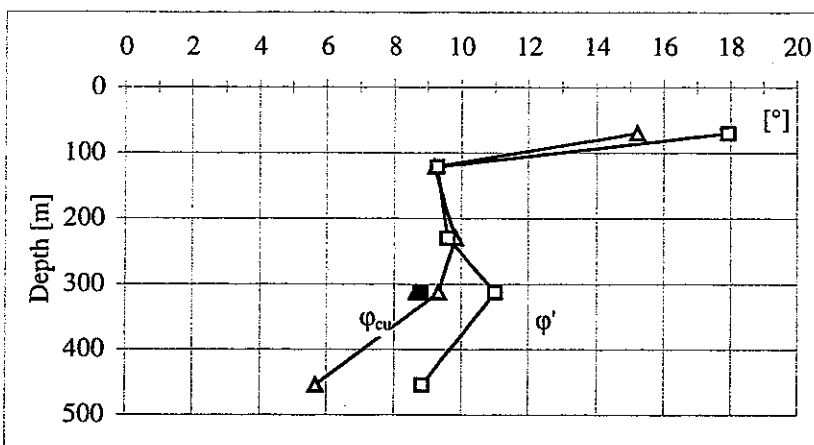
Figure 2.12. Elastic shear modulus G versus depth obtained in the TRUCK-II programme (determined on an unloading-reloading loop at about 1 % axial deformation).

2. Estimation of realistic values for mechanical properties of Boom Clay at 500 m depth



Prof. [m]	c_{cu} [MPa]	c' [MPa]
69	0.125	0.133
120	0.168	0.233
229	0.333	0.396
313	0.281	0.177
455	1.010	0.715

Figure 2.13. Undrained and effective cohesion versus depth.



Prof. [m]	ϕ_{cu} [°]	ϕ' [°]
69	15.21	17.94
120	9.20	9.31
229	9.82	9.62
313	9.35	11.01
455	5.67	8.83

Figure 2.14. Undrained and effective friction angle versus depth.

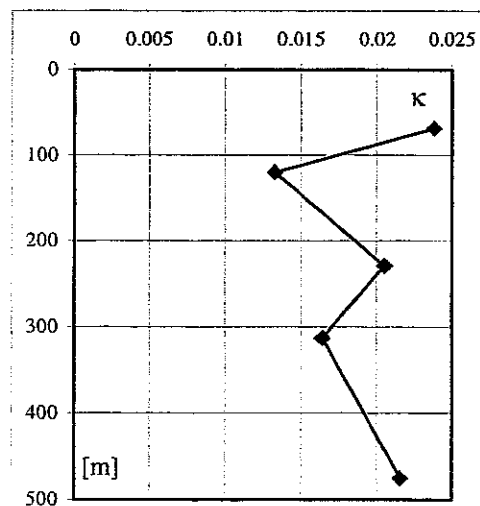
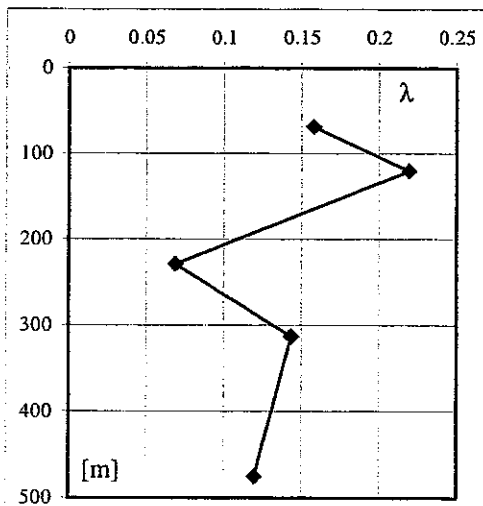


Figure 2.15. Parameters λ and κ of the Cam-Clay model versus depth.

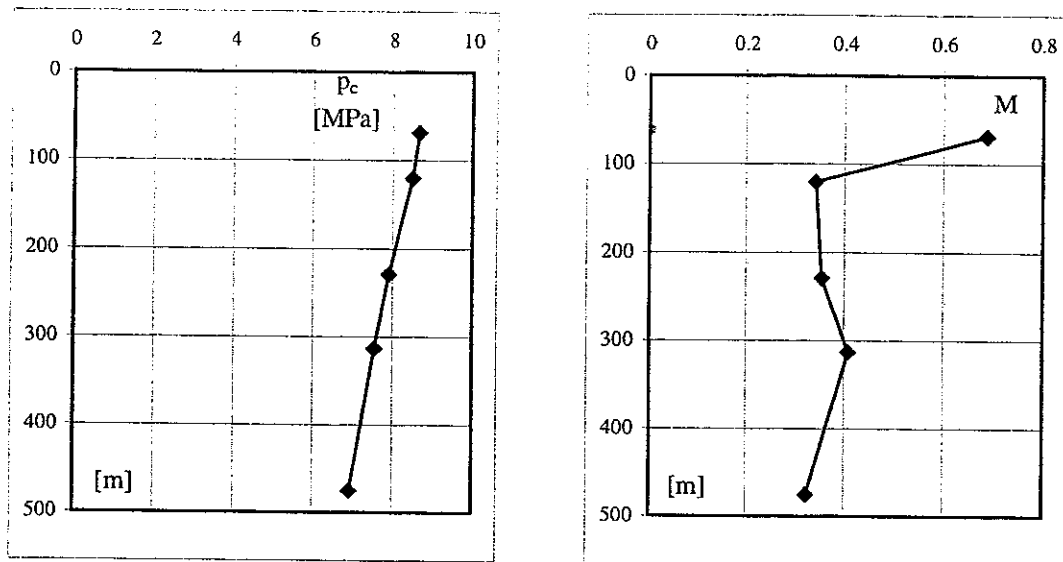


Figure 2.16. Parameters p_c and M of the Cam-Clay model versus depth.

2.6. Discussion about the experimental results

From these obtained results, several comments/questions can be formulated.

1) *There is an increase of the elastic shear modulus G with depth*, though a rather large scattering (up to 200 MPa) is observed at each given depth (see Figure 2.12). Interestingly, this scattering is reduced when G is plotted versus the effective pressure p' (mean value at which the unloading loop is performed) instead of the depth (see Figure 2.17). These results fit well non-linear elasticity (blue diamond-shape symbols on Figure 2.17) in which the moduli depend on p' (such as in critical state models, see section 2.2.2), thus they are fairly logical.

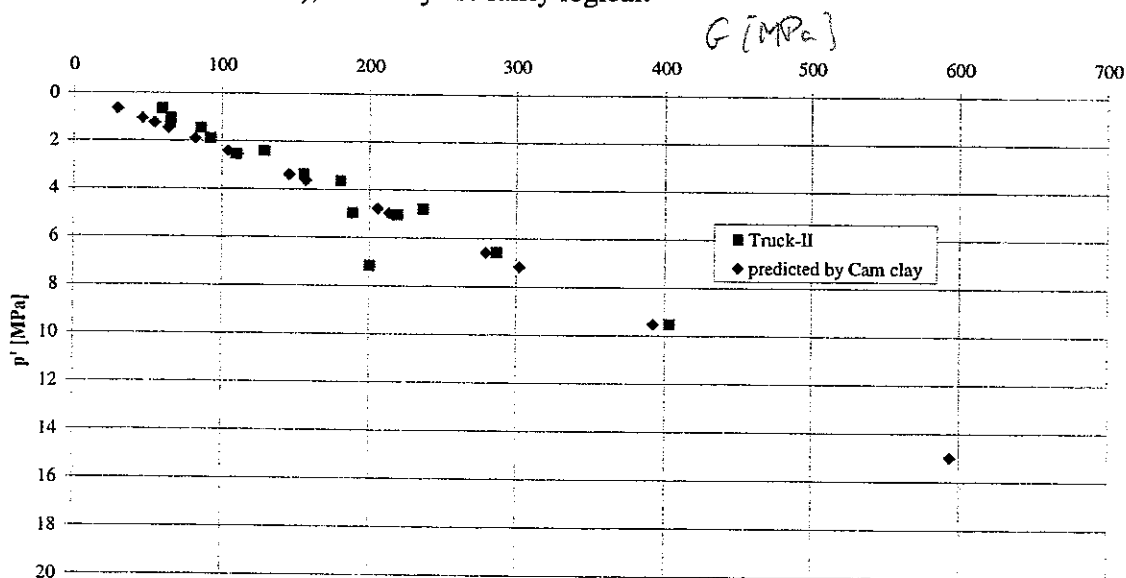


Figure 2.17. Elastic shear modulus G versus p' : a) obtained in the TRUCK-II programme determined on an unloading-reloading loop at about 1 % axial deformation and for a given p' value (squares); b) predicted by non-linear elasticity using Cam clay parameter $\kappa = 0.02$ known at Mol URL (diamond shapes).

From Figure 2.17, the elastic shear modulus G falls in the ranges:

- $180 \text{ MPa} < G < 240 \text{ MPa}$ at $p' = 5 \text{ MPa}$,
- $350 \text{ MPa} < G < 450 \text{ MPa}$ at $p' = 10 \text{ MPa}$.

Here, we have considered the highest value $G = 450 \text{ MPa}$ as it is on the safe side with respect to the gallery excavation problem (lower values of G lead to smaller extent of plastic zone). Still, the other elastic parameter (bulk modulus K) remains undetermined from the performed tests. Here we have considered an effective Poisson ratio $\nu' = 0.125$ (same value than the one considered at the Mol site). Combining the previous values of ν' and G leads to an effective Young modulus $E' \approx 1 \text{ GPa}$.

2) Regarding the undrained shear strength C_u , its values have been derived for each CTU test (using the data file provided by UCL-LGC) following the relation

$$C_u = \frac{\sigma_1 - \sigma_3}{2} \quad \text{at peak} \quad (2.33)$$

The obtained C_u values are reported on Figure 2.18 versus the depth of the sample (green triangles) and versus the depth corresponding to the effective pressure at which C_u is obtained (red circles). The other data already given in Figure 2.3 are also reported in Figure 2.18.

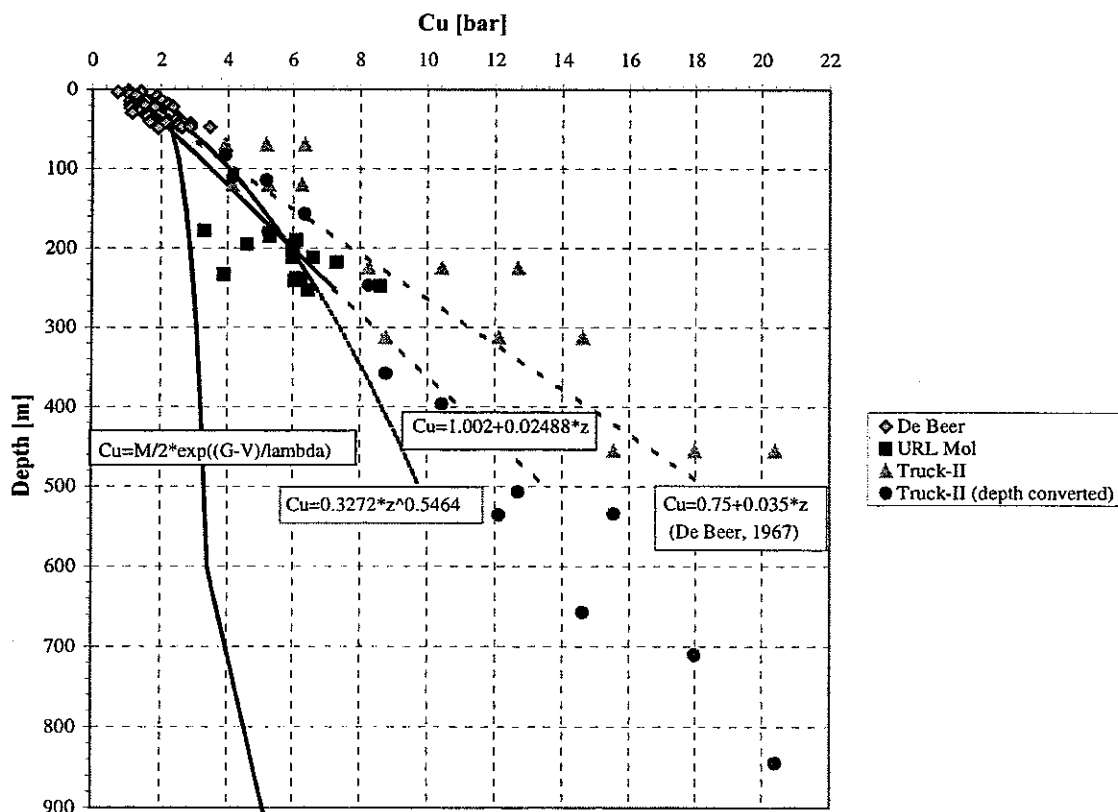


Figure 2.18. Undrained shear strength C_u obtained from consolidated undrained triaxial tests on Antwerp and Mol Boom clay samples (diamond-shaped and square points) with some proposed regressions functions (same as Figure 2.3). Data from the TRUCK-II experimental programme have been added where C_u is estimated at failure using equation (2.33): triangles represent the real depth of the cores, whereas circles represent the depth corresponding to the effective pressure at which failure occurred in the test.

3) Regarding the classical plastic properties, we must distinguish two parameters.

- The effective cohesion c' :

excepting the results from Weelde that are still unexplained (neither from mineralogy, nor from granulometry, see Appendix E), there is a rather regular increase of c' with depth from 0.13 MPa at 69 m depth to 0.72 MPa at 455 m depth (see Figure 2.13). Using such gradient, c' can be reasonably extrapolated at 500 m around the value $c' = 0.8$ MPa.

- The effective friction angle ϕ' :

the trend is here a decrease of ϕ' with depth (see Figure 2.14) from 18° at 69 m depth to about 9° at 455 m depth. *Weak! No trend! oversaturated (see) 2.11*

It is worth pointing out the good quality of the CTU tests, which then traduces by a very good alignment of the 3 peaks for each test in a p' - q diagram. This is certainly linked with the procedure of sample selection: the use of CT-scans has helped removing non-homogeneous samples.

a) Were these trends on c' and ϕ' expected?

A decrease in porosity and water content with depth has been observed on the tested samples (see Table 3 of Appendix E and Figure 2.11 of this section), which then indicates an increasing consolidation with depth (this is a normal evolution). This consolidation increase should logically translate in an increase of the elastic domain, i.e. the clay should be less plastic. Such an evolution pattern of the plastic properties was actually postulated in TRUCK-I from a conceptual point of view: "it is expected that the greater depth, from a mechanical point of view, has a beneficial effect on the clay characteristics" (Van de Steen and Vervoort, 1998).

Thus, positive trends for both c' and ϕ' were expected, whereas experimental data show that this is effectively the case for c' (see Figure 2.13), but not for ϕ' (see Figure 2.14). In other words there exists a discrepancy between what was expected and what has been obtained in term of evolution of ϕ' with depth.

b) Are these trends consistent with known data for Boom clay at Mol site (225 m depth)?

Boom clay samples from the Mol site have been tested by different laboratory teams (Baldi et al., 1987; Horseman et al., 1987; Mair et al., 1992), using either strain or stress controlled triaxial tests. Results obtained by these three laboratories are consistent between them, the obtained slope M (see Figure 2.2b) of the critical state line falling in the range $0.81 < M < 1$.

From the p' - q diagrams of these references, the following Mohr-Coulomb parameters are derived: $c' = 300$ and $\phi' = 18^\circ$. These values are considered as the reference Mohr-Coulomb parameters for Boom clay at the Mol site (they were used in the TRUCK-I project as lower bounds).

Compared to the values $c' = 396$ kPa and $\phi' = 9.6^\circ$ obtained in the present experimental program, the main inconsistency lies in the friction angle (50 % smaller in TRUCK-II compared with the reference values).

c) Is there an explanation for such a surprising result?

Such a decreasing friction angle ϕ' with depth is very difficult to explain, the main problem being that it is not coherent with:

- the consolidation that is effectively observed on the tested samples (see Table 3 of Appendix E and Figure 2.11),
- the commonly accepted concept of rock strengthening associated with consolidation process,

- the reference values prior known at the Mol site.

In order to explain such surprising results, several hypotheses can be put forward:

- the samples that have been used in TRUCK-II were more disturbed than the samples used in the references studies (although this was not evidenced by the CT-scans),
- the samples used in the references studies do not all come from the same level than the Mol samples used in TRUCK-II:
 - samples from 246 m depth were used by Baldi et al. (1987) and Horseman et al.(1987),
 - whereas Mair et al. (1992) used samples from the Hades level (223 m depth);

however, these studies did not show significant differences in terms of friction and cohesion.

- the used experimental procedure may have a strong influence on the obtained results: e.g. Bolle et al. (1995) showed that, on reconstituted clay samples, the use of small consolidation bearings results in a 40 % higher shear strength compared to the case where larger consolidation bearings are used. Such an influence of the “consolidation rate” on the shear strength should however be confirmed on a large number of tests.

In any case, such surprising results should be validated/invalidated with additional tests (other depth level, lower consolidation rates?), preferably carried out by several laboratory teams.

4) Regarding the non-classical properties (Cam clay parameters λ , κ and p_c).

Results obtained from IC tests are also quite surprising (see Figures 2.15-16 in this section and Table 5 of Appendix E):

- the κ and λ values seems quite scattered, and the value $\lambda = 0.0685$ obtained for the Mol sample differs significantly from the value $\lambda = 0.13$ obtained by (Baldi et al., 1987; Horseman et al., 1987; Mair et al., 1992). However, there has only been one test per depth level, so these results should be considered with care.
- the preconsolidation is found to decrease with depth (from 8.65 MPa at 69 m depth to 6.93 MPa at 478 m depth). This is contradicted by the evolution of the dry and saturated weights and water content that indicate an increase in consolidation with depth (see Figures 2.10-11).

When looking more carefully to the results, it appears that:

- for Doel, Zoersel and Mol samples (Figure 21-23 of Appendix E), the determination of p_c is not demonstrative at all, especially if the unloading part is taken into account. Note also that p_c decreases with depth, which is rather surprising;
- the $e-\ln(p')$ curves exhibit an unexplained trend at the beginning of the unloading loop (see Figures 21 to 25 of Appendix E): the sample volume is still decreasing substantially whereas the applied pressure decreases,
- the fixed loading rate of 10^{-4} MPa/s used in these tests (see section 3.3 page 6 of the Appendix E) means that a true consolidation has never been achieved at any moment in these tests, which explains the above mentioned unexplained trend at the beginning of the unloading loop.

Therefore, it makes it very difficult and almost meaningless to interpret the obtained results in the critical state framework.

2.7. Conclusions and implications for the TRUCK-II project

From the TRUCK-II testing programme, the main values that can be extrapolated at 500 m depth are summarised in Table 2.5. If we stick to these results, the implicit assumption made in TRUCK-I that "greater depth... should have a beneficial effect on the clay characteristics" seems refuted, although the physical characteristics (weight and water content) exhibit a correct trend.

Therefore, it seems rather unreasonable from a physical point of view to accept that the Boom clay weakens as depth increases, although experimental results show a strong decrease in friction angle with depth.

Table 2.5. Boom clay parameters: references values known at the Mol underground laboratory (225 m depth), and estimated values at 500 m depth from the TRUCK-II experimental programme.

	References values at 225 m (from Mol laboratory)	Extrapolated values at 500 m (estimated from TRUCK-II)
Elastic shear modulus G [MPa]	130	450
Effective friction angle ϕ' [°]	18	9 *
Effective cohesion c' [MPa]	0.3	0.8

* : such a low value with respect to the reference value is controversial (see text for details).

This major discrepancy, which either comes from the experimental procedure or from the samples themselves, remains unexplained.

The effect of such weak (to our opinion) parameters on the gallery excavation will be discussed in more detail in section 3.4.

2.8. References

- Baldi G., Borsetto M. & Hueckel T. 1987. Calibration of mathematical models for simulation of thermal, seepage and mechanical behaviour of Boom clay. *Report EUR-10924, Commission of the European Communities, Luxembourg.*
- Bernier F. & Neerdael B. 1996. Overview of in-situ thermomechanical experiments in clay; concept, results and interpretation. *Engineering Geology*, **41**: 51-64.
- Bolle A., Charlier R., Labiouse V., Li X.L., Huergo P., Schroeder C., Thimus J.F., Vanoverstraeten V. 1995. Etude des lois de comportement de deux types de sols en chargement statique. Fonds de la Recherche Fondamentale et Collective, rapport final de recherche, convention n° 2.9005.91F.
- Bonne A., Black J., Gera F., Gonze P., Tassoni E. & Thimus J.F. 1985. Characterization and behaviour of argillaceous rocks. *In: Radioactive waste management and disposal*. Simon, R. New York, NY: Cambridge University Press: 487-505.
- Britto A.M. & Gunn M.J. 1987. Critical state soil mechanics via finite elements. Ellis Horwood series in civil engineering.
- Cripps J.C. & Taylor R.K. 1986. Engineering characteristics of British over-consolidated clays and mudrocks. *Engineering Geology*, **22**: 349-376.
- De Beer E., Carpentier R., Manfroy P. & Heremans R. 1977. Preliminary studies of an underground facility for nuclear waste burial in a Tertiary clay formation. *Rockstore '77, Proc. 1st Int. Symp.*, Stockholm: 771-780.

- Gens A. and Potts D.M. 1988. Critical state models in computational geomechanics. *Engineering Computations*, **5**: 178-197.
- Horseman S.T., Winter M.G. & Entwistle D.C. 1987. Geotechnical characterization of Boom clay in relation to the disposal of radioactive waste. *Report EUR-10987, Commission of the European Communities*, Luxembourg.
- Horseman S.T. & McEwen T.J. 1996. Thermal constraints on disposal of heat-emitting waste in argillaceous rocks. *Engineering Geology*, **41**: 5-16.
- Knowles N.C., Jeffries R.M. & Come B. 1996. Benchmarking the thermomechanical behaviour of clays; a progress report; the CEC interclay project. *Engineering Geology*, **41**: 65-71.
- Lamoureux-Var V. 1997. Modélisation de la compaction dans les bassins sédimentaires - Approche mécanique. *Thèse de Doctorat, Ecole Polytechnique*, Palaiseau, France.
- Mair R.J., Taylor R.N. & Clarke B.G. 1992. Repository tunnel construction in deep clay formations. *Report EUR-13964, Commission of the European Communities*, Luxembourg.
- Magara K. 1980. Comparison of porosity-depth relationships of shale and sandstone. *Journal of Petroleum Geology*, **3** (2): 175-185.
- NEA. 1995. Characteristics of argillaceous rocks. Internal document NEA/SEDE.
- Neerdael B., Beaufays R., Buyens M., de Bruyn D. & Voet M. 1992. Geomechanical behaviour of boom clay under ambient and elevated temperature conditions. *Report EUR-14154, Commission of the European Communities*, Luxembourg.
- Rijkers R. 1998. Inventarisatie geomechanische, geochemische en hydrogeologische eigenschappen van Tertiaire kleipakketten - *Car Fase II. TNO Rapport*.
- Rubey W. & Hubbert M.K. 1959. Role of fluid pressure in mechanics of overthrust faulting. *Geol. Soc. Amer. Bull.*, **70**: 115-206.
- Shibuya S. & Tanaka H. 1996. Estimate of elastic shear modulus in Holocene soil deposits. *Soils and Foundations*, **36**, 4: 45-55.
- Van de Steen B. and Vervoort A. 1998. *Mine design in clay*. CORA-project TRUCK-I, K.U.Leuven.
- Wroth C.P. & Wood D.M. 1978. The correlation of index properties with some basic engineering properties of soils. *Canadian Geotechnical Journal*, **15**, 2: 137-145.
- Wood D.M. 1990. *Soil behaviour and critical state soil mechanics*, Cambridge University Press.

3. Optimisation of the design of the disposal facility

3.1. Introduction

Referring to the final design of the whole mine, it was considered worthwhile to have a look at some alternatives to this design, to get a good idea of the sensitivity of the entire project to a number of parameters (e.g. diameter and length of disposal cells, and area per canister).

For the initial design of TRUCK-I the disposal cells or the tertiary galleries had an inside diameter of 2.2 m, allowing men to access these tunnels. To obtain a final inner diameter of 2.2 m, the minimum excavation diameter was calculated to be 3.4 m. As the size of the plastic zone around an excavation is proportional to the excavated tunnel diameter, the size of the plastic zone can be reduced significantly by reducing the excavated diameter.

In TRUCK-I (Van de Steen and Vervoort, 1998), the plastic zone (diameter) was estimated to be roughly 2 to 3 times the excavated diameter. As mentioned above, the calculations were conducted for conservative values of the clay characteristics at a depth of 500 m, which means that the conclusions of TRUCK-I should always be on the safe side. If the plastic zone decreases, the area between galleries that remains entirely in the elastic zone increases (for a fixed distance between galleries, but for different diameters). In TRUCK-I, it was assumed that at least half of the area between galleries had to remain elastic. Therefore, it was concluded that a distance of 30 m between galleries was too small. However, the negative effect of plastic deformation of clay (certainly in the long term) is not well known and for the moment is still matter to debate. The general definition of the plastic deformation is that permanent deformation remains after the load has been removed. This plastic deformation can occur as macro-fractures, which in the long term could heal as a result of the clay properties. In this case, the plastic deformation should not necessarily have a negative effect on the permeability of the host rock around the disposal cells.

It was therefore decided to consider as alternative in TRUCK-II a smaller diameter for the disposal cells. A diameter of 0.75 m was selected, which is large enough to place the canisters. Excavating, supporting, positioning of a canister and filling of a disposal cell have all to be done from inside the secondary gallery. This requires larger equipment and the outside diameter of the secondary and primary galleries had to be increased to 6 m (instead of 4.6 m in TRUCK-I). Another consequence of choosing a smaller diameter for the tertiary galleries is that it would be advisable to have shorter tertiary galleries. A length of 5 m (including the 0.5 m thick concrete lining of the secondary gallery) was selected. For this length, one should be able to push the lining forward starting at the wall of the secondary gallery. In comparison to the longer holes in TRUCK-I, this should facilitate the operations, reduce costs excavation and filling and should improve the stability and safety.

As mentioned in ^{Chapter} section 2, no information was available during the project TRUCK-I on the mechanical and thermal properties of Boom clay at a depth of 500 m. It was assumed that the known characteristics for a depth of 225 m would be a safe approximation. It was also assumed in TRUCK-I

that the outside of the canisters would have a constant temperature over a long time. As will be shown by more realistic thermal calculations (see section 3.2), this approach was too conservative.

3.2. Optimisation of a repository design from a thermal point of view

In this section, we are mainly concerned in determining the maximum admissible thermal loading with respect to some predefined criteria.

3.2.1. Starting assumptions

The HLW inventory consists of 300 Cogema heat-emitting canisters. All the calculations presented in this section are based on the following assumptions:

- the generation of heat results only from the radioactivity of the fission products and actinides, and this activity globally decreases over time;
- for each individual canister, the cooling time (since reactor unloading) before final disposal ranges between 50 to 100 years; accordingly, three cooling times t_c are considered: 50, 75 and 100 years;
- the maximum increase of temperature in the aquifer located above the repository (50 m as for the Belgian concept) should verify the condition

$$\Delta T \leq 4^\circ\text{C} \text{ at 50 m above the repository mid-plane}^1 \quad (3.1)$$

The modelling of the heat generation and dissipation around a HLW disposal requires defining several parameters: the heat source term, the initial temperature field, and the thermal properties of the host rock.

3.2.2. Thermal power generated per canister

In the following, we assume that each HLW canister (vitrified waste) corresponds to the reprocessing of 1.33 tHM (ton Heavy Metal).

The heat component of HLW is directly linked to the radioactive disintegration that still occurs in this type of waste after unloading of the reactor. This is a power-controlled type problem (the heat power resulting from the activity), in which the temperature field results from the heat dissipation.

For a single canister, the thermal output P (in Watt) can be approximated by the following decreasing exponential relation (Giraud, 1993)

$$P = P_0 \cdot \exp^{-\omega t} \quad (3.2)$$

where t is the time since reactor unloading (this definition is retained throughout this section), ω is a constant factor ($\omega^{-1} = 41.7 \text{ y}$) and P_0 is the thermal power generated by one canister (equivalent to 1.33 tHM) at reactor unloading ($P_0 = 1615 \text{ W}$).

Such relation is realistic up to about 100 y, as during this period the generated thermal power is mostly controlled by the radioactivity of fission products. However, for larger time values, the generated thermal power becomes mostly controlled by the radioactivity of actinides. The heat power P generated by a canister is then better approximated by a relation which is a summation of three decreasing exponential terms (Heijdra et al., 1995)

¹ This assumption, determined in the Belgian context, would require at a latter stage to be re-considered for the Dutch framework, based on presently available information.

$$P = \sum_{j=1}^3 P_{0j} \cdot \exp^{-\omega_j t} \quad (3.3)$$

where the initial heat power values P_{0j} and the decay parameters ω_j are reported in Table 3.1.

Table 3.1. Initial heat power P_{0j} and decay parameters ω_j for the single and three exponential terms, with $t = 0$ corresponding to the reactor unloading.

Heat function	term number j	P_{0j} [W]	ω_j [y^{-1}]
Single	1	1615.35	0.024
Triple	1	9934.71	0.42006
	2	1462.76	0.02415
	3	36.64	0.00167

From relations (3.2) and (3.3), the evolution of the generated heat power versus time (since the reactor unloading) is plotted on Figure 3.1a. Clearly, relation (3.2) gives a good approximation of the generated power for time between 10 to 100 y. This is no longer true for time periods larger than 100 y, for which relation (3.2) underestimates the generated power.

The difference between relations (3.2) and (3.3) translates also in terms of total produced heat energy $E_{th}(t)$ produced by a single canister as a function of time

$$E_{th}(t) = \int_{t_1}^{t_2} P dt \quad (3.4)$$

which is plotted on Figure 3.1b both for relation (3.2) and (3.3).

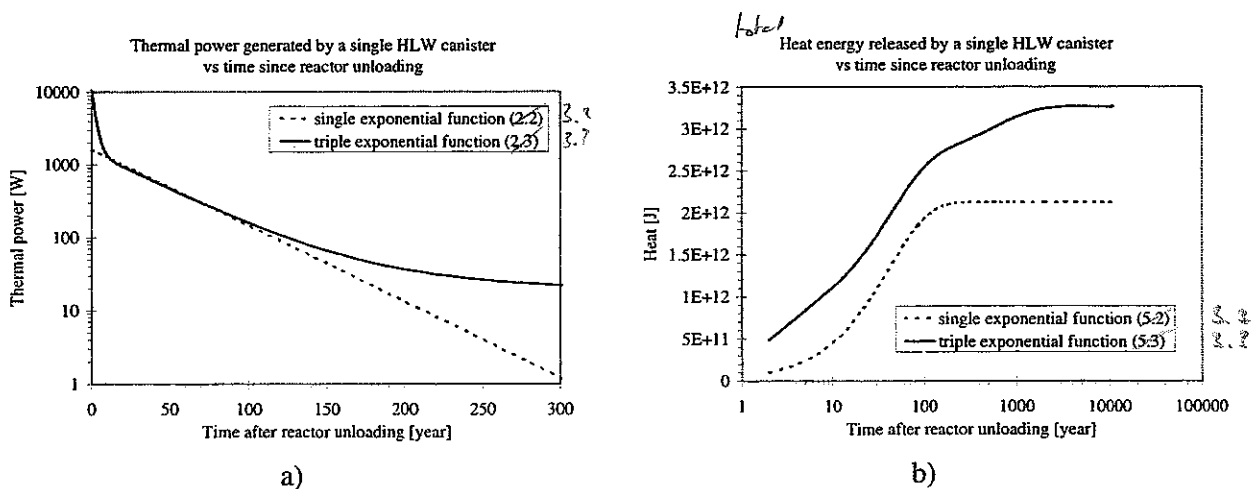


Figure 3.1. Evolution with time (from reactor unloading) of: a) thermal power generated by one HLW canister, b) heat energy produced by one HLW canister.

Obviously, the total heat released per canister (E_t) in the host formation depends on the time t_c allowed for cooling of the waste before their disposal (note that t_c is actually counted since the reactor unloading). Considering $t_c = 0$ y, the total heat released in the host rock reads $E_1 = 2.12 \cdot 10^{12}$ J from the heat generation relation (3.2), and $E_2 = 3.27 \cdot 10^{12}$ J from the heat generation (3.3), which then leads to a ratio $E_2 / E_1 = 1.54$. However, this ratio increases as $t_c > 0$ are considered (see Table 3.2), e.g. $E_2 / E_1 = 3.75$ for $t_c = 100$ y.

In other words, the difference between the single and the triple exponential heat generation functions (3.2) and (3.3) increases with t_c .

Table 3.2. Total heat E_i released per canister in the host formation considering different time of cooling before disposal.

t_c = time of cooling at surface [y]	E_1 (single exp.) [10^{12} J]	E_2 (triple exp.) [10^{12} J]	$E_2 - E_1$ [10^{12} J]	E_2 / E_1
0	2.120	3.270	1.14	1.54
50	0.640	1.170	0.53	1.83
75	0.352	0.889	0.54	2.53
100	0.193	0.724	0.53	3.75

3.2.3. Initial thermal field and canister temperatures

In the computations that are presented in the next sections, the initial temperature field is assumed to be zero everywhere, i.e.

$$T(x, y, z) = 0 \text{ } ^\circ\text{C} \quad (3.5)$$

Therefore, the obtained thermal field is actually equivalent to the field of thermal variations. As long as thermal properties remain constant (or almost) within the investigated temperature range, the superposition principle can be applied. Consequently, any initial thermal field can be added to the computed thermal variations.

In the following sections, the initial temperature of the canister is neglected, which then allows representing the thermal loading through an imposed surface heat flux (decreasing according to relations (3.2) or (3.3)). This choice does not allow obtaining the temperature field within the canister, and it does not take into account its initial temperature. The influence of the latter can be readily estimated considering that the canister is mainly made of borosilicate glass. Considering no phase changes and negligible property variations over a temperature interval ΔT , the stored energy E_c in one canister is

$$E_c = C_p \cdot m \cdot \Delta T \quad (3.6)$$

where m is the canister mass. Using a specific heat $C_p = 1000 \text{ J}\cdot\text{kg}^{-1}\cdot\text{K}^{-1}$ and a density $\rho \approx 2700 \text{ kg}\cdot\text{m}^{-3}$ for the glass, the canister geometry (1.34 m length, 43 cm diameter), and a temperature increase $\Delta T = 100 \text{ K}$, the energy stored in the canister is $E_c \approx 53 \cdot 10^6 \text{ J}$ (to be compared with the values of E_1 and E_2 given in Table 3.2).

Using the relations (3.2) and (3.3) to compute the heat generation of one canister, an amount of heat equivalent to E_c is generated in about 31 hours for $t_c = 50 \text{ y}$, 56 hours for $t_c = 75 \text{ y}$, or 102 hours for $t_c = 100 \text{ y}$. Therefore, the initial temperature of the canister has no (or a negligible) influence on the solution of the thermal conduction problem: lower than $7 \cdot 10^{-5}$ in term of error on the amount of dissipated energy, in the order of few days in term of the timing of the transient thermal phase.

3.2.4. Basic configuration

The basic configuration considers a planar type of repository, in which all the disposal cells lie in the same horizontal plane at 500 m depth below surface. Each storage gallery is filled with a single HLW canister with a decreasing heat power according to relation (3.2) or (3.3).

The basic configuration $50\text{ m} \times 50\text{ m}$ ($s_2 \times s_3$) for the thermal computation is based on the grid pattern proposed in TRUCK-I, but with some minor modifications (see Figure 3.2a):

- there is a spacing $s_2 = 50\text{ m}$ between secondary galleries,
- the tertiary galleries are blind (i.e. not continuous) and short (quarter length of s_2), and they are further referred as disposal cells,
- there is a spacing $s_3 = 50\text{ m}$ between disposal cells.

This configuration corresponds to a canister density by surface area of 1 canister / 1250 m^2 .

In addition, a second configuration $30\text{ m} \times 30\text{ m}$ is considered, with a spacing $s_2 = 30\text{ m}$ between secondary galleries (see Figure 3.2b) and a spacing $s_3 = 30\text{ m}$ between disposal cells, which then corresponds to a canister density by surface area of 1 canister / 450 m^2 .

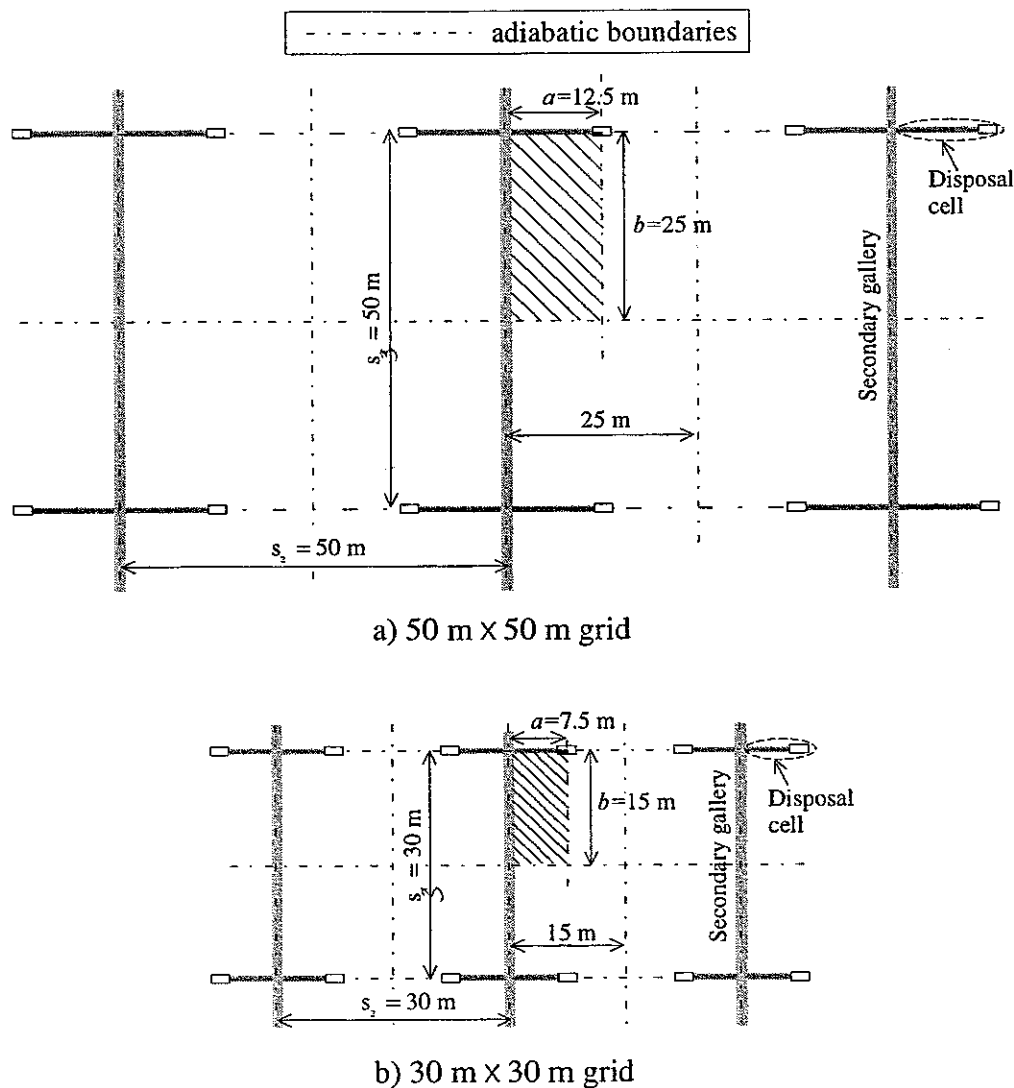


Figure 3.2. Plane view of the repository for the thermal computation.

3.2.5. Boundary conditions, properties and loading

Owing to symmetry planes (adiabatic boundaries, i.e. boundaries where there is no thermal flux) reported in Figure 3.2, the configuration can be studied considering a horizontal planar portion of area

$a \times b$ (lined areas on Figure 3.2), where $a = s_2 / 4$ and $b = s_3 / 2$. Due to the large depth of the repository mid-plane (500 m) considered here, this plane can also be approximated as an adiabatic boundary.

Therefore, around the canister and up to the top surface (ground level), the full thermal field is a true three-dimensional problem ('single canister in a finite half-medium', see Figure 3.3c) in which the dissipated power is equal to 1 / 8 of the total canister thermal power.

However, under some conditions (for points which are located far enough from the heat source), this 3-D problem can be simplified to either:

- a 2-D plane problem ('single gallery in a finite half-medium', see Figure 3.3b) in which the total dissipated power across the gallery surface is equal to 1 / 8 of the total canister thermal power,
- a 1-D plane problem ('planar repository in a finite half-medium', see Figure 3.3a) in which the total dissipated power across the repository surface is equal to 1 / 8 of the total canister thermal power.

In all the geometries reported on Figure 3.3, the three types of boundaries are the following:

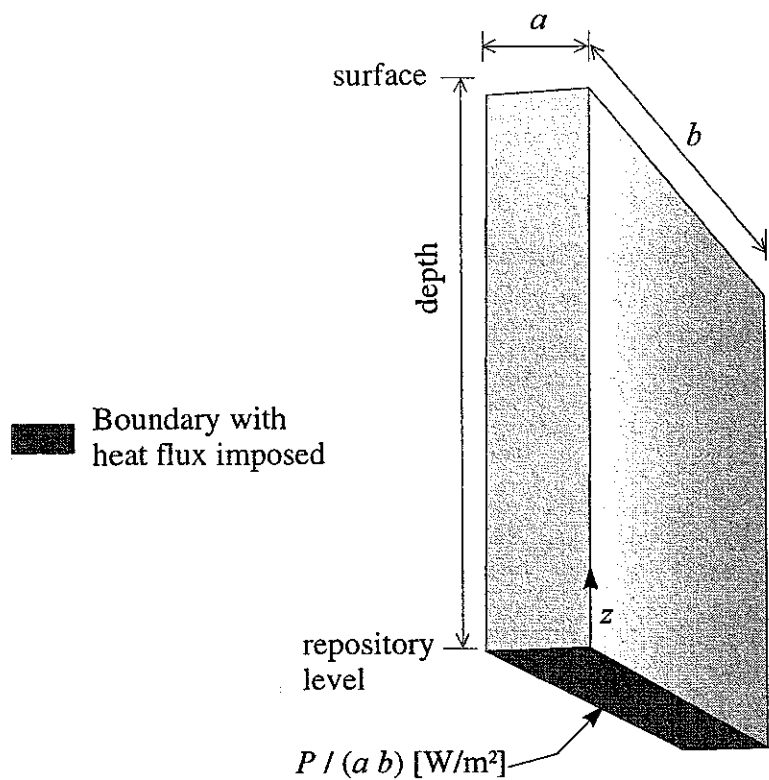
- the vertical boundaries and the bottom boundary (repository mid-plane) are adiabatic,
- the top boundary (top surface) has a prescribed temperature $T = 0$ °C,
- the heat source (1-D, 2-D or 3-D) is represented by a heat emitting boundary (plane source) in which the power is a decreasing function of time according to relations (3.2) or (3.3).

Table 3.3. Properties of the host rock considered for the thermal computations.

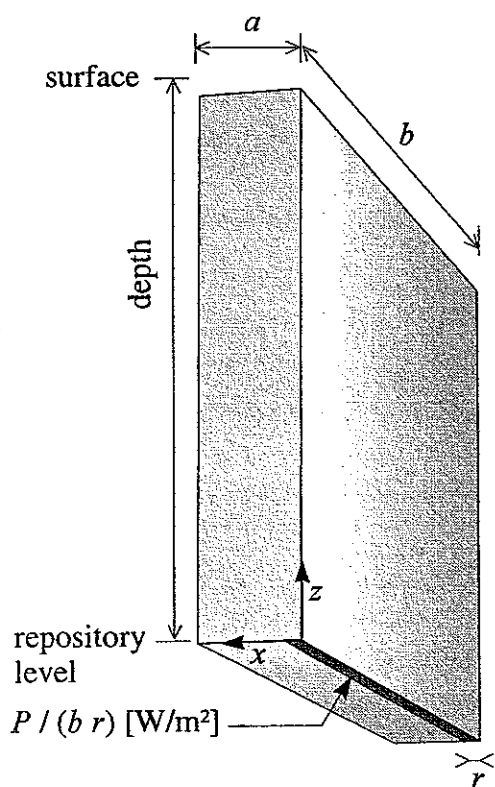
Thermal conductivity λ_T [W·m ⁻¹ ·K ⁻¹]	1.69	→ Thermal diffusivity $k_T = 6 \cdot 10^{-7}$ m ² ·s ⁻¹
Specific mass ρ [kg·m ⁻³]	1700	
Specific heat C_p [J·kg ⁻¹ ·K ⁻¹]	1647	

Table 3.4. Heat flow applied to different geometries, considering the single exponential decreasing heat generation function (3.2) and for a cooling time of 50 y.

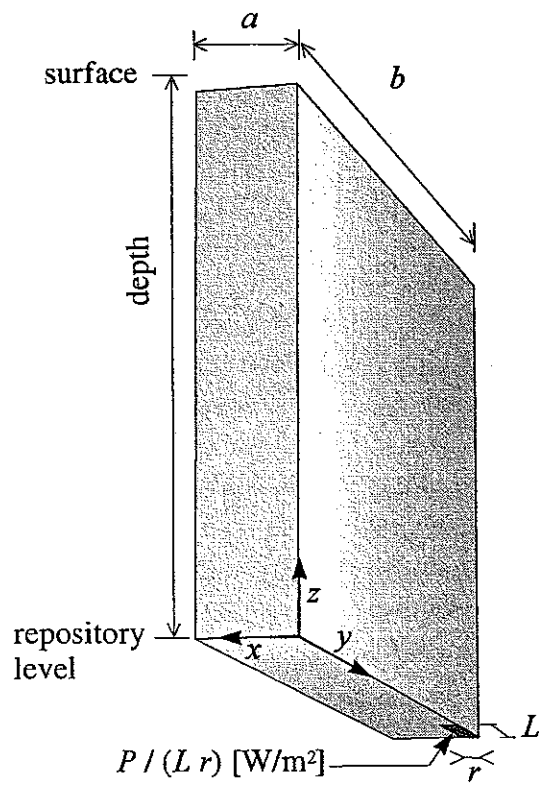
	Model type	a [m]	b [m]	r [m]	L [m]	Surface [m ²]	Applied surface heat flow [W·m ⁻²]
30 m × 30 m	1-D plane	15	7.5	—	—	112.5	0.5411
	2-D plane	15	7.5	0.25	—	1.875	32.467
	3-D	15	7.5	0.25	0.5	0.125	487
50 m × 50 m	1-D plane	25	12.5	—	—	312.5	0.1948
	2-D plane	25	12.5	0.25	—	3.125	19.48
	3-D	25	12.5	0.25	0.5	0.125	487



a) Planar repository in a finite half-medium (1-D plane)



b) Single gallery in a finite half-medium (2-D plane)



c) Single canister in a finite half-medium (3-D)

Figure 3.3. Geometries considered for the thermal computation.

3.2.6. Resolution methods

The general balance energy equation writes

$$-\frac{\partial q_i}{\partial x_i} + q_v = \frac{\partial E}{\partial t} = q \quad (3.7)$$

where q_i is the heat flux vector [$\text{W}\cdot\text{m}^{-2}$], q_v the volumetric heat source term [$\text{W}\cdot\text{m}^{-3}$], E the quantity of heat stored per unit volume [$\text{J}\cdot\text{m}^{-3}$], and q the net heat flow per unit volume [$\text{W}\cdot\text{m}^{-3}$]. Temperature changes are related to variation of stored energy (mechanical dissipation is neglected) by the relation

$$\frac{\partial T}{\partial t} = \frac{1}{C_p \rho} \frac{\partial E}{\partial t} = \frac{1}{C_p \rho} q \quad (3.8)$$

Reporting (3.7) into (3.8) for q gives

$$\frac{\partial T}{\partial t} = \frac{1}{C_p \rho} \left(-\frac{\partial q_i}{\partial x_i} + q_v \right) \quad (3.9)$$

Finally, using the heat conduction law (Fourier's law) that defines the heat flux vector q_i as

$$q_i = -\lambda_T \frac{\partial T}{\partial x_i} \quad (3.10)$$

where λ_T is the thermal conductivity [$\text{W}\cdot\text{m}^{-1}\cdot\text{K}^{-1}$], and incorporating into (3.9) yields the general diffusion equation

$$\frac{\partial T}{\partial t} = \frac{\lambda_T}{C_p \rho} \frac{\partial^2 T}{\partial x_i^2} + \frac{q_v}{C_p \rho} \quad (3.11)$$

giving the time evolution of T in solids that obey Fourier's conduction law.

The problem of interest here is the study of the thermal transient around a HLW disposal. To obtain the solution, the diffusion equation (3.11) must be combined with the present initial condition $T(x, y, z) = 0^\circ\text{C}$ and boundary conditions (adiabatic, fixed temperature, imposed heat flux, see section 3.2.5 for details). Two solutions have been used, the first one is a 1-D analytical solution and the second one is a numerical discrete solution.

3.2.6.1. Analytical solution

It is possible to derive an analytical solution of the 1-D problem such as represented on Figure 3.3a and considering a single exponential decreasing heat generation function (equation (3.2)). This 1-D solution is not valid for determining the thermal near field (around canister) due to strong 3-D effects. However, it is appropriate for determining the thermal far field in which local effects have dissipated and homogenised.

Here, we use the solution developed by Giraud (1993) that is briefly presented in the following. For the 1-D co-ordinate z (vertically oriented), $z = 0$ corresponds to the repository mid-plane, h is the repository half-thickness, and $z = d$ is the top surface. The repository (located between $-h$ and h) is emitting a volumic heat flux q_v [$\text{W}\cdot\text{m}^{-3}$] that is decreasing exponentially with t according to

$$q_v = q_{v0} \cdot \exp^{-\omega t} \quad (3.12)$$

Given the following non-dimensional variables

$$z' = \frac{z}{h}, \quad t' = \frac{4k_T}{h^2} t, \quad \omega' = \frac{h^2}{4k_T} \omega, \quad d' = \frac{d}{h} \quad (3.13)$$

where k_T is the thermal diffusivity

$$k_T = \frac{\lambda_T}{\rho C_p} \quad [\text{m}^2 \cdot \text{s}^{-1}] \quad (3.14)$$

The general solution for the thermal variation field is then given by

$$\Delta T(z', t') = T_a \cdot f_{\omega}(z', t'; d'; \omega') \quad (3.15)$$

where

$$T_a = \frac{q_{v0} h^2}{2 \lambda_T} \quad (3.16)$$

The detailed derivation of the function $f_{\omega}(z', t'; d'; \omega')$ can be found in Giraud (1993), of which only a summary is given in Appendix D, see equations (D1) to (D5). It is worth pointing out that the function $f_{\omega}(z', t'; d'; \omega')$ is written in terms of non-dimensional variables (3.13), and therefore the general solution (3.15) depends linearly on q_{v0} . Note however that this solution does not assume that the mid-plane repository is a symmetry plane, it considers that the medium has an infinite extent below the repository (infinite boundary in depth).

Here, we are interested in a solution considering a heat generation term with three exponentially decreasing terms defined by parameters ω_j and q_{v0j} in a similar way than in relation (3.3). Again, neglecting the changes of thermal properties with temperature allows using the superposition theorem. Thus, the general solution is obtained as the sum of all the individual terms computed for each single exponential separately, i.e.

$$\Delta T(z', t') = \sum_{j=1}^3 T_{aj} \cdot f_{\omega_j}(z', t'; d'; \omega_j') \quad (3.17)$$

This general solution is evaluated numerically through a FORTRAN 90 program, in which the computation of the error function of both real and complex variables is involved.

3.2.6.2. Finite difference solution

The 3-D problem such as represented in Figure 3.3c (and also the 1-D for comparison purposes) has been solved numerically using the commercial software FLAC-3D v2.0 (Itasca, 1997). Here, an approximated discrete solution is obtained using an explicit finite difference method. The main concern in computing this solution comes from the choice of an optimal spatial discretisation: fine enough to provide an accurate solution, coarse enough to require a reasonable amount of CPU time.

3.2.7. Results

In this section, the results obtained using both the analytical solution and the numerical approximation are presented.

3.2.7.1. 1-D analytical results

The input data are the following:

- $d = 500$ m (repository depth),
- $h = 0.25$ m (half the thickness of the repository),
- $k_T = 6.04 \cdot 10^{-7} \text{ m}^2 \cdot \text{s}^{-1}$ (thermal diffusivity).

It is recalled that the heat generation data P_j reported in Table 3.2 correspond to the values at reactor unloading. Thus the time t in equation (3.12) and (3.13) equals

$$t = t_C + t_{GD} \quad (3.18)$$

where t_c is the time during which the canister has cooled down at surface, and t_{GD} the time since it has been placed in the geological disposal.

Table 3.5. Stored power per unit surface for the HLW disposal considering three cooling times and a canister density equal to 1 canister / 450 m².

Cooling time t_c [y]		50	75	100
Stored power per surface unit [W·m ⁻²]	single exponential	1.0822	0.5942	0.3263
	triple exponential	1.0466	0.6031	0.3594

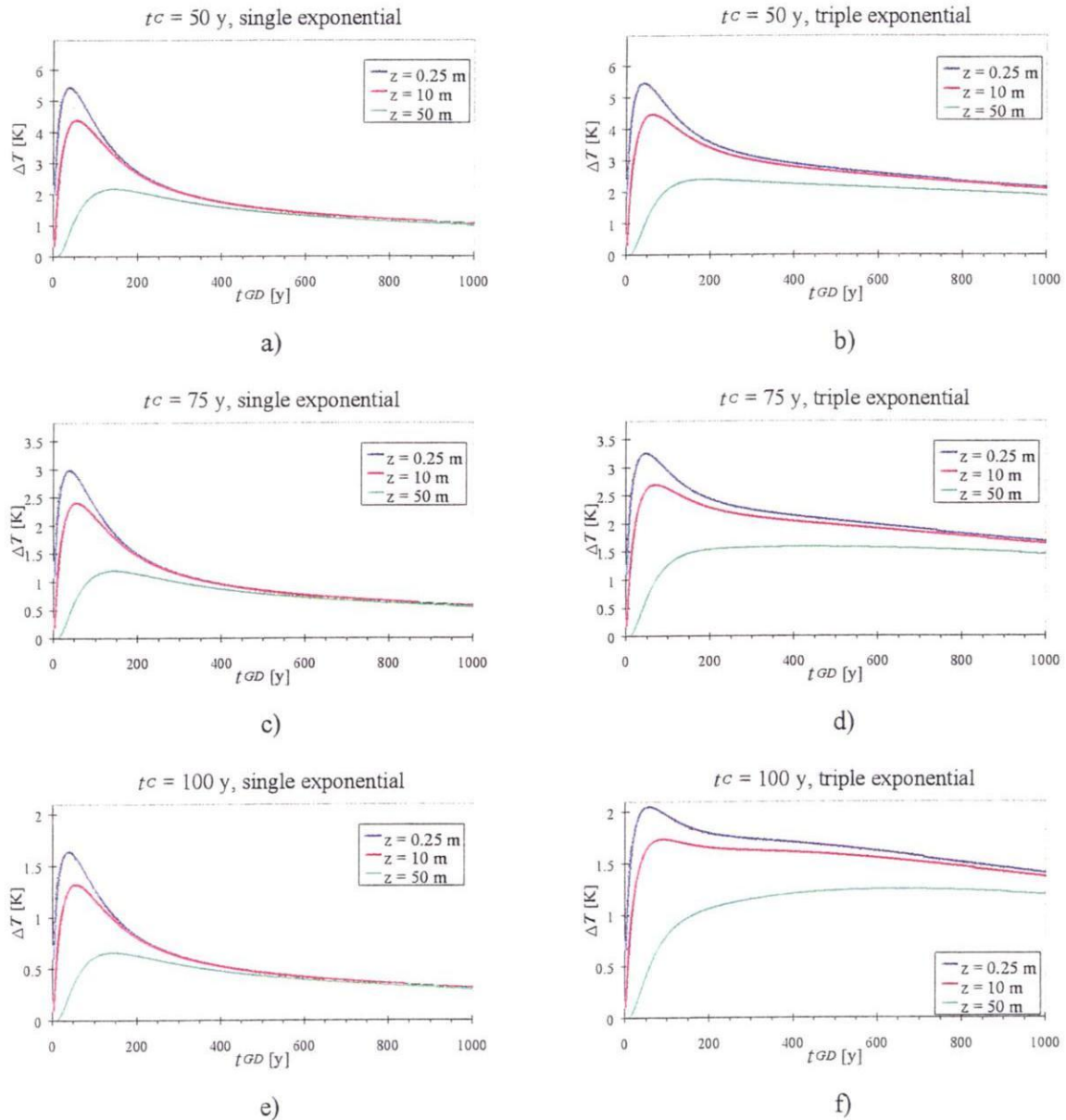


Figure 3.4. Influence of the heat generation term (decreasing single or triple exponential) and of the cooling time (t_c) on the temperature variation at several height (z) above repository for a configuration 30×30 m, i.e. 1 canister / 450 m² (1-D analytical solution).

Three values for t_c have been considered: 50, 75 and 100 years, and for these three cases both the solution with the single (see equation (3.15)) and triple (see equation (3.17)) decreasing exponential heat generation have been computed with parameters reported in Table 3.1.

The 30 m \times 30 m grid represented on Figure 3.2b corresponds to a canister density of 1 canister / 450 m². Depending on the cooling time t_c and on the exponential heat generation (single or triple), it corresponds to different values of stored power per surface unit, which are given in Table 3.5.

The variation of temperature at three locations in the host rock (0.25 m, 10 m and 50 m from the repository mid-plane) are reported on Figures 3.4a-f. Note that, at the heat source/host rock boundary ($x = 0.25$ m) and more generally the near field, the thermal variations reported in Figure 3.4 are not representative of the real variations as the local concentration of the heat source is not accounted for. This point will be investigated through the 3-D numerical solution (see section 3.2.7.2). Nevertheless, the 1-D analytical solution gives valid thermal variations for the far field, which are detailed below.

Considering the single exponential heat generation, the thermal variation field $\Delta T(x', t')$, which is given by equation (3.15), depends linearly on the imposed flux q_{v0} . Therefore, knowing the solution $\Delta T_{t_{c1}}(x', t')$ for a given value of cooling time t_{c1} , the solution $\Delta T_{t_{c2}}(x', t')$ for any other cooling time t_{c2} is given by

$$\Delta T_{t_{c2}}(x', t') = R \cdot \Delta T_{t_{c1}}(x', t') \quad (3.19)$$

where the factor R is equal to the ratio of volumic power generated at t_{c1} and t_{c2}

$$R = \frac{q_v(t_{c1})}{q_v(t_{c2})} = \frac{q_{v0} \cdot \exp^{-\omega t_{c1}}}{q_{v0} \cdot \exp^{-\omega t_{c2}}} = \exp[-\omega(t_{c1} - t_{c2})] \quad (3.20)$$

Consequently, the profiles of temperature variation are all similar independently on t_c (see Figures 3.4a, 3.4c and 3.4e), and with a scale factor R between them.

Considering the triple exponential heat generation, the thermal variation field $\Delta T(x', t')$, which is given by equation (3.17), is no longer a linear function of q_{v0} , and it incorporates three different time scales through parameters ω_j . Therefore, the profiles of temperature variation are all different dependent on the t_c value (see Figures 3.4b, 3.4d and 3.4f). Due to the third exponential term (corresponding mainly to actinides), this difference increases with the t_c value.

For $t_c = 50$ y, the difference between the single and the triple exponential heat generation is not significant up to 50 years after disposal (compare Figures 3.4a and 3.4b), but becomes markedly important as time passes. When larger t_c values are considered (75 and 100 y), the difference becomes more and more important, even for small values of time. These effects are summarised in Tables 3.6 and 3.7, in which the peak of the thermal phase is reported for the single and triple exponential heat generation, respectively.

Table 3.6. Analytical solution (1-D): characteristics of the peak of the thermal phase for single exponential generation (1 canister / 450 m²).

x [m]	$t_c = 50$ y		$t_c = 75$ y		$t_c = 100$ y	
	ΔT_{\max} [K]	time [y]	ΔT_{\max} [K]	Time [y]	ΔT_{\max} [K]	time [y]
0.25	5.44	36	2.99	36	1.64	36
10	4.38	54	2.40	54	1.32	54
50	2.19	142	1.20	142	0.66	142

Table 3.7. Analytical solution (1-D): characteristics of the peak of the thermal phase for triple exponential generation (1 canister / 450 m²).

x [m]	$t_c = 50$ y		$t_c = 75$ y		$t_c = 100$ y	
	ΔT_{\max} [K]	time [y]	ΔT_{\max} [K]	Time [y]	ΔT_{\max} [K]	time [y]
0.25	5.47	42	3.25	46	2.05	56
10	4.47	62	2.69	68	1.73	88
50	2.41	188	1.59	426	1.25	648

As there is a linear relation between the ΔT value and the canister density, it is straightforward from these results to compute the maximum canister density which can be stored per surface unit taking into account the criterion $\Delta T \leq 4$ K at 50 m above the repository. It gives a canister density of 1 canister / A (values reported in Table 3.8) where the area A is defined by

$$A = \frac{\Delta T}{4} 450 \quad (3.21)$$

Table 3.8. Minimum area (A) per canister required to fulfil the criterion $\Delta T \leq 4$ K at 50 m above the repository mid-plane for the two heat generation assumptions.

A : area [m ²] for storage of one canister			
exponential	$t_c = 50$ y	$t_c = 75$ y	$t_c = 100$ y
single	246.4	135.0	74.3
triple	271.1	178.9	140.6

Note that the A values given in the line 'single' of Table 3.8 are actually erroneous as they underestimate the heat generation (particularly the part given by actinides). If these minimum surfaces were used with a triple exponential heat generation, they would lead to ΔT values of respectively 4.41 K for $t_c = 50$ y, 5.30 K for $t_c = 75$ y, and 7.57 K for $t_c = 100$ y, which violates the required criterion $\Delta T \leq 4$ K (see section 3.2.1).

Consequently, we consider here the A values (in bold) given in the line 'triple' to be the realistic values which fulfil the criterion $\Delta T \leq 4$ K for any of the three t_c values considered. Note also that these values do not correspond to a unique thermal loading value expressed in $\text{W}\cdot\text{m}^{-2}$ (see Table 3.9).

Table 3.9. Maximum initial power which can be evacuated and which fulfils the criterion $\Delta T \leq 4$ K at 50 m above the repository mid-plane for the two heat generation assumptions.

Maximum evacuated power [$\text{W}\cdot\text{m}^{-2}$]			
exponential	$t_c = 50$ y	$t_c = 75$ y	$t_c = 100$ y
single	1.98	1.98	1.98
triple	1.74	1.52	1.15

3.2.7.2. 3-D finite difference results

The 3-D numerical solutions presented here aim to:

- confirm the conclusion/results on the thermal far field obtained from the 1-D analytical solution,
- give additional information on the thermal near field which was not available from the 1-D solution.

The geometry presented in Figure 3.3c is considered with the following geometrical properties: $a = 7.5$ m, $b = 15$ m, $depth = 500$ m, $L = 0.5$ m and $r = 0.25$ m. The heat power dissipated through the surface $r \times L$ is equal to $1/8^{\text{th}}$ of the canister power.

This geometry is discretised with 8824 zones and 10566 grid points, which are non-uniformly distributed in space (see the detail of the zone distribution on Figure 3.5). The explicit resolution in FLAC-3D is based on a time step of 0.365 d, and the solution is computed up to 200 y. This requires 200000 computing steps, which takes about 24 h CPU time on a Sun Sparc Ultra2 cadenced at 300 MHz. Results are presented in Figures 3.6, 3.7, 3.8 and 3.9 in term of the evolution of ΔT with time at different locations in the model:

- the thermal variation at points located at the canister/host rock interface ($x = 0.25$ m), at 10 m above the canister ($x = 10$ m) and at 50 m above the canister ($x = 50$ m) are presented on Figures 3.6a, 3.7a, 3.8a and 3.9a for different t_c values and for different heat generation function (single or triple exponential),
- the thermal variation at points located at the same depth as the previous ones but above the point which is at the opposite of the canister in the repository plane are presented on Figures 3.6b-c, 3.7b-c, 3.8b-c and 3.9b-c for different t_c values and for different heat generation function (single or triple exponential). *exactly the reverse*

The peak temperature increases are given in Tables 3.10 and 3.11, which can be compared directly with Table 3.6 and 3.7 obtained with the 1-D analytical solution:

- far away from the repository (e.g. at $x = 50$ m), the accordance between the 3-D and 1-D solutions is very good and we could hardly distinguish between the ΔT values above the canister and the values above its opposite; this comes from the homogenisation of ΔT as the distance from the heat source increases,
- even at $x = 10$ m, the accordance between the 3-D and 1-D solutions is still satisfactory at $x = 10$ m, although we can now distinguish between the ΔT values above the canister and the values above its opposite point,
- close to the canister/host rock interface (e.g. at $x = 0.25$ m), there is no longer concordance of the 3-D and 1-D solutions due to local heat source effect which becomes important. Note that this maximum value of ΔT , which is to be found above the canister centre, assumes that the canister is a perfect conductor, and that the full canister area is $2r \times 2L = 0.50$ m² (see Figure 3.3c). In reality the full canister area is about $2r \times \pi \times 1.33 \approx 2.09$ m², which means that the maximum temperature at the canister/host rock is overestimated in the present 3-D simulation. A more accurate temperature field close to the canister would have required a much finer grid size, which then would have required much more computing time. As it was not the primary purpose of this work to estimate the thermal near field, such model has not been considered here.

As a conclusion, results obtained from 3-D thermal modelling are fully coherent with the 1-D approximation as far as the thermal far field is concerned. Therefore, the conclusion about the

admissible thermal loading required to fulfil the criterion $\Delta T \leq 4$ K that are summarised in Tables 3.8 and 3.9 are representative and can therefore be used as a basis to define acceptable repository layouts.

Table 3.10. Numerical solution (3-D): characteristics of the peak of the thermal phase for single exponential generation (1 canister / 450 m²).

x [m]	$t_c = 50$ y	
	ΔT_{\max} [K]	time [y]
0.25	91.77	0.8
10a	4.51	51
10b	4.27	59
50	2.18	143

Table 3.11. Numerical solution (3-D): characteristics of the peak of the thermal phase for triple exponential generation (1 canister / 450 m²).

x [m]	$t_c = 50$ y		$t_c = 75$ y		$t_c = 100$ y	
	ΔT_{\max} [K]	time [y]	ΔT_{\max} [K]	Time [y]	ΔT_{\max} [K]	time [y]
0.25	88.50	0.8	50.91	0.8	30.26	0.9
10a	4.60	58	2.76	64	1.77	82
10b	4.37	65	2.63	72	1.701	93
50	2.41	189	—	—	—	—

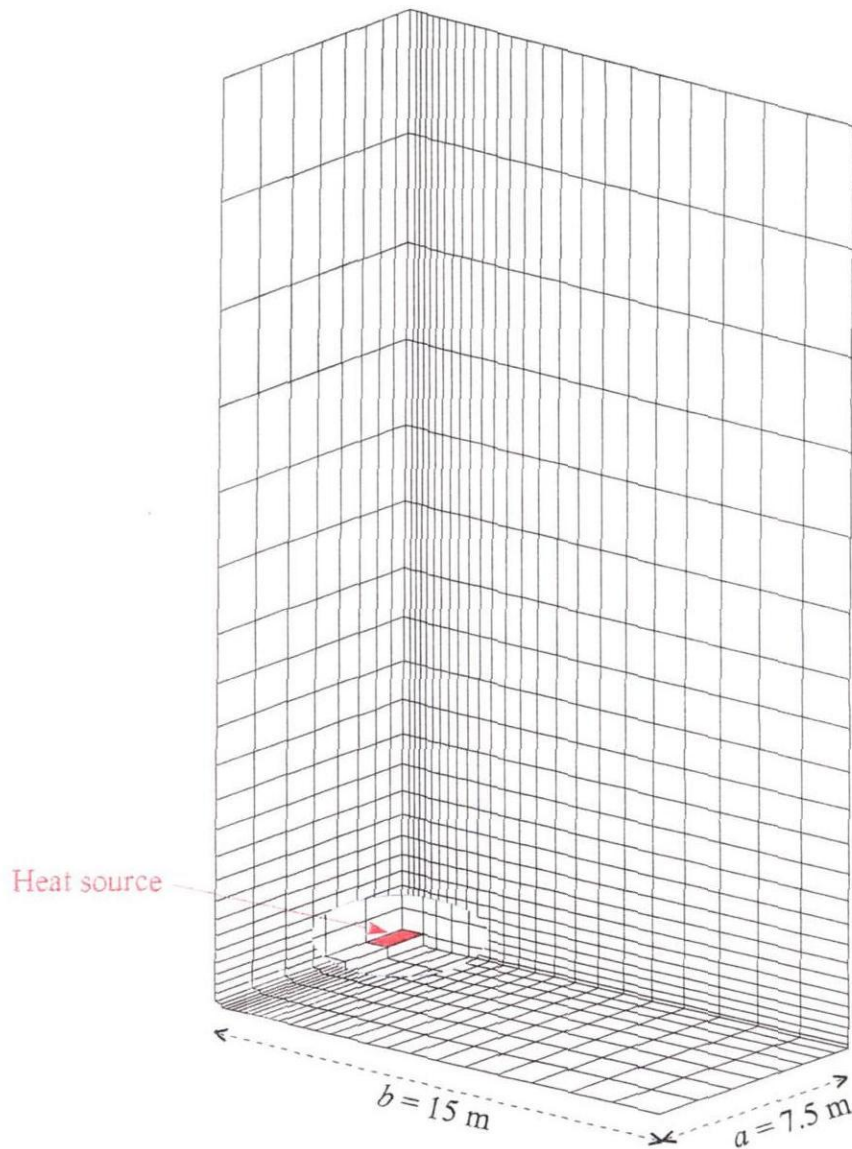


Figure 3.5. Details of the lower part of the grid: non-uniform spatial distribution of zones around the heat source (configuration $30\text{ m} \times 30\text{ m}$), with a magnification around the surface heat source (red area).

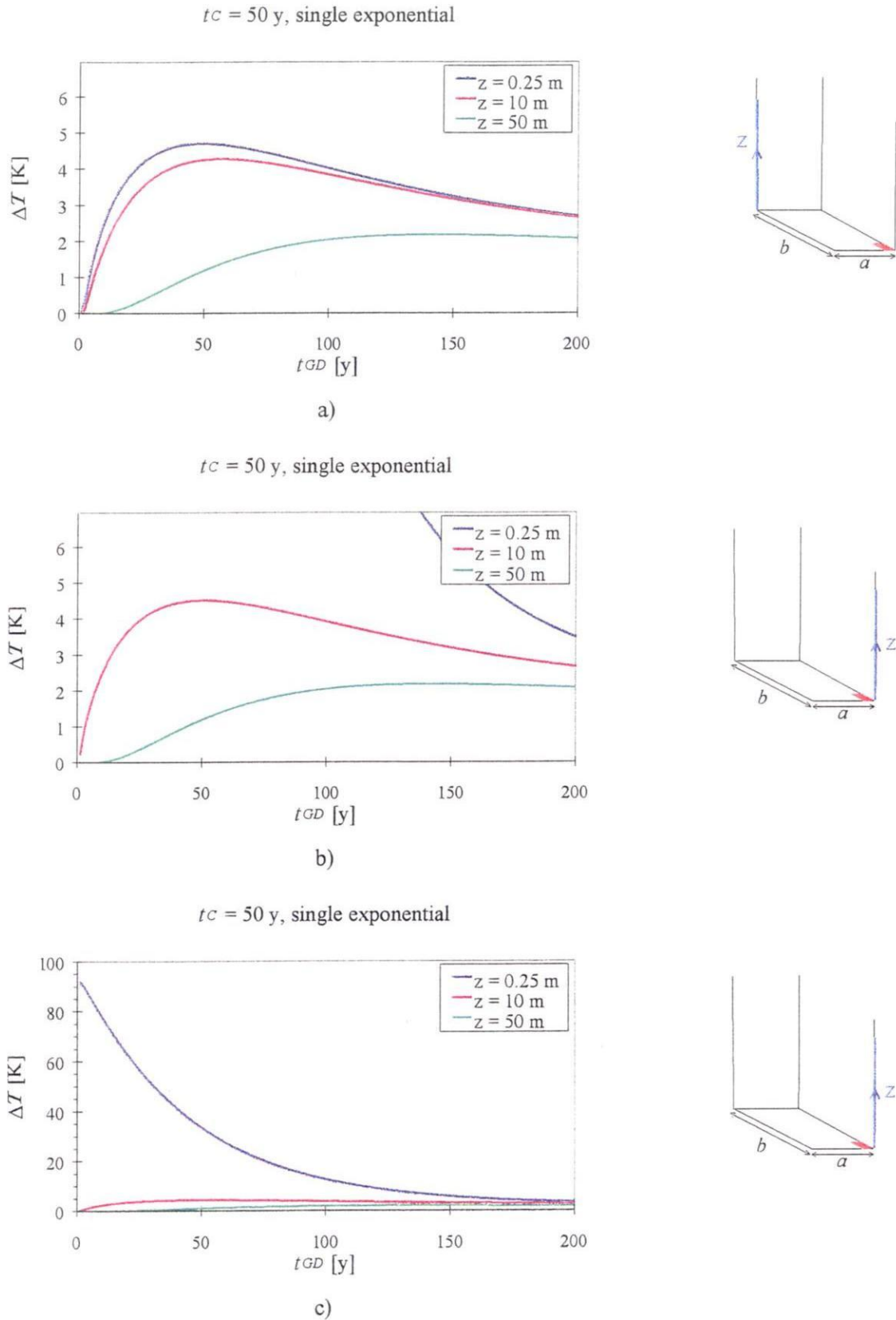


Figure 3.6. ΔT at different height (z) above the repository (heat generation term=decreasing single exponential) for $t_c=50$ y with a 30×30 m configuration (1 canister / 450 m^2), and at two locations: Fig. a gives a profile above the opposite point of the canister, Figs. b-c a profile above the canister (only the temperature scale changes between Fig. b and Fig. c).

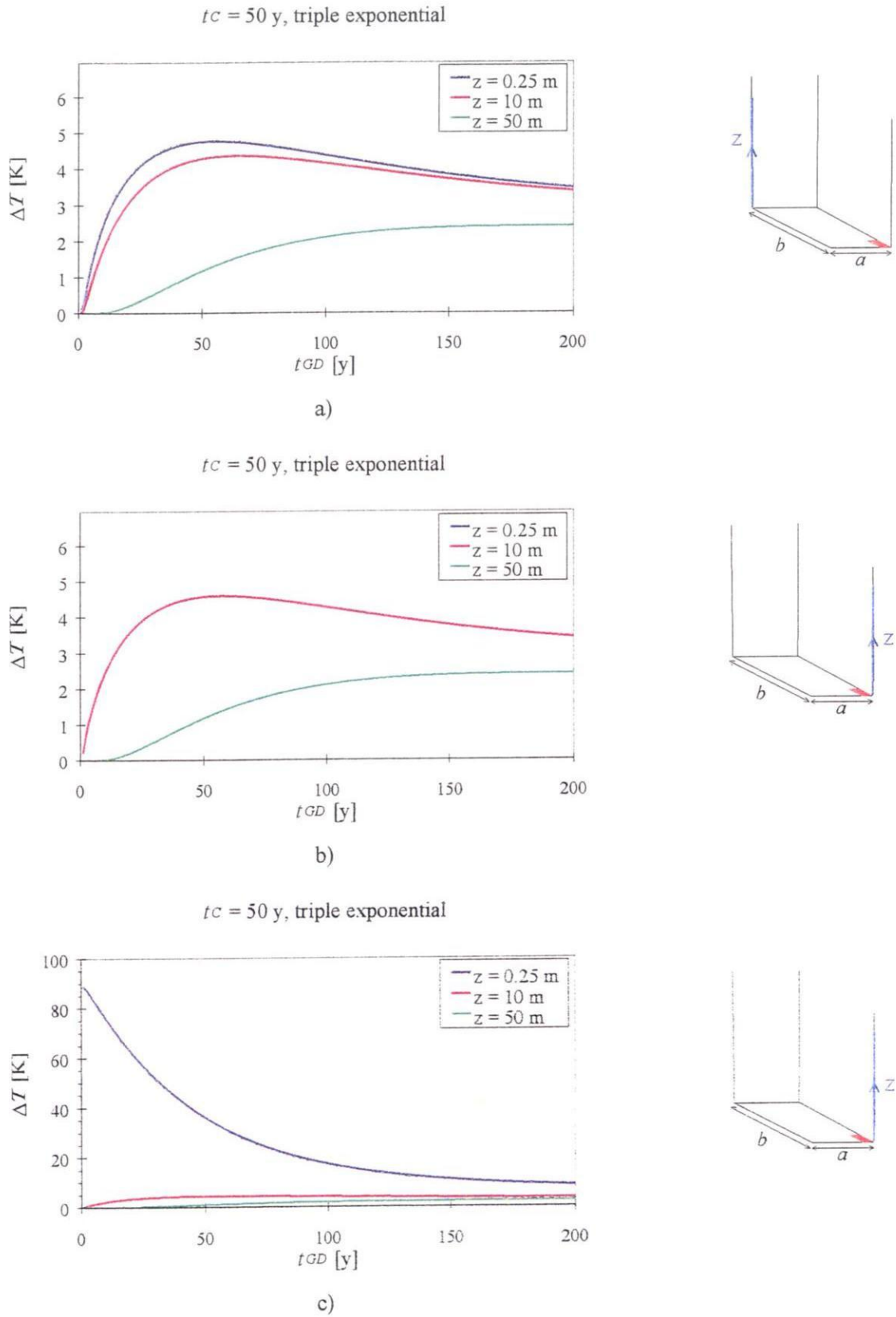


Figure 3.7. ΔT at different height (z) above the repository (heat generation term=decreasing triple exponential) for $t_c=50$ y with a 30×30 m configuration (1 canister / 450 m^2), and at two locations: Fig. a gives a profile above the opposite point of the canister, Figs. b-c a profile above the canister (only the temperature scale changes between Fig. b and Fig. c).

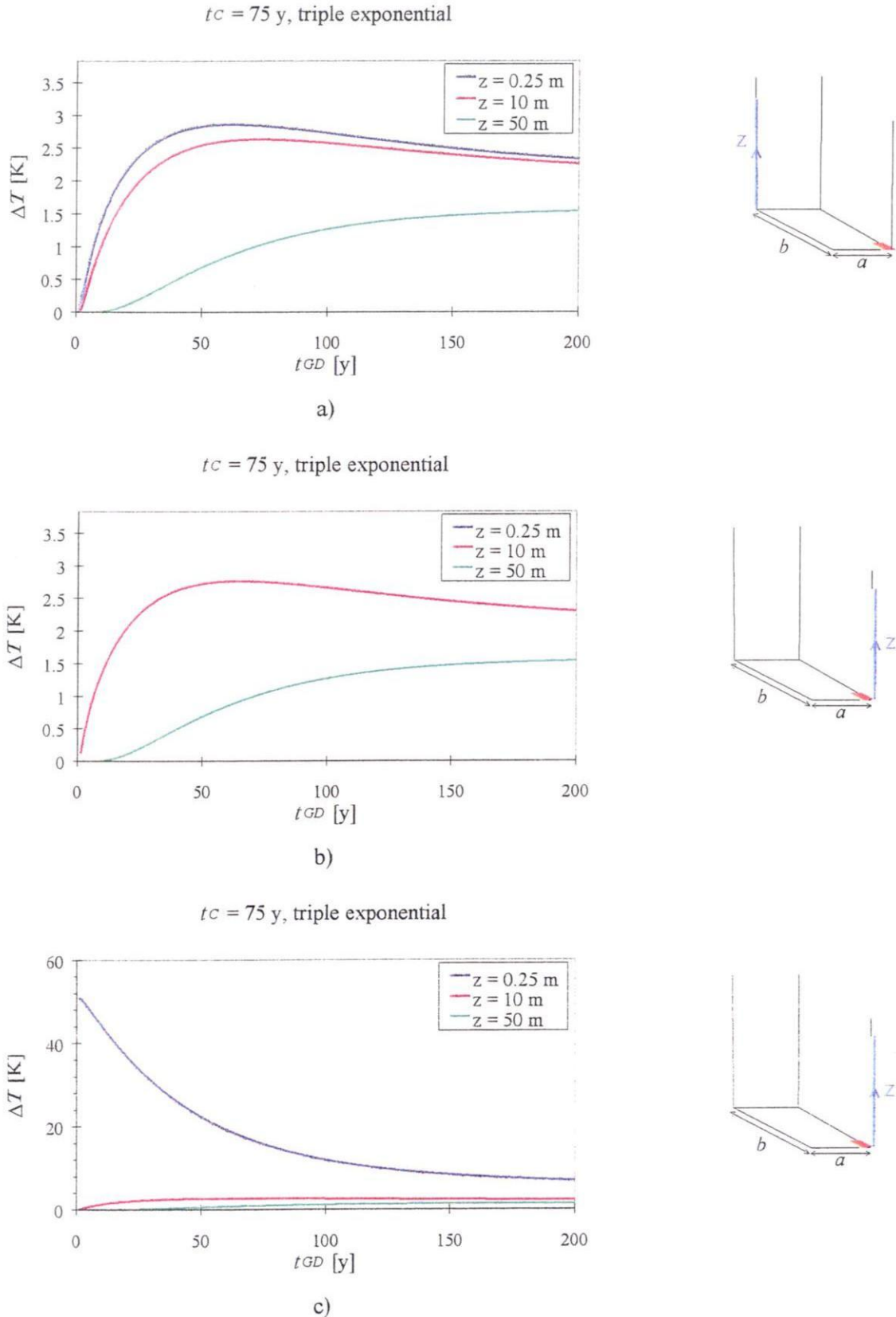


Figure 3.8. ΔT at different height (z) above the repository (heat generation term=decreasing triple exponential) for $t_c=75$ y with a 30×30 m configuration (1 canister / 450 m^2), and at two locations: Fig. a gives a profile above the opposite point of the canister, Figs. b-c a profile above the canister (only the temperature scale changes between Fig. b and Fig. c).

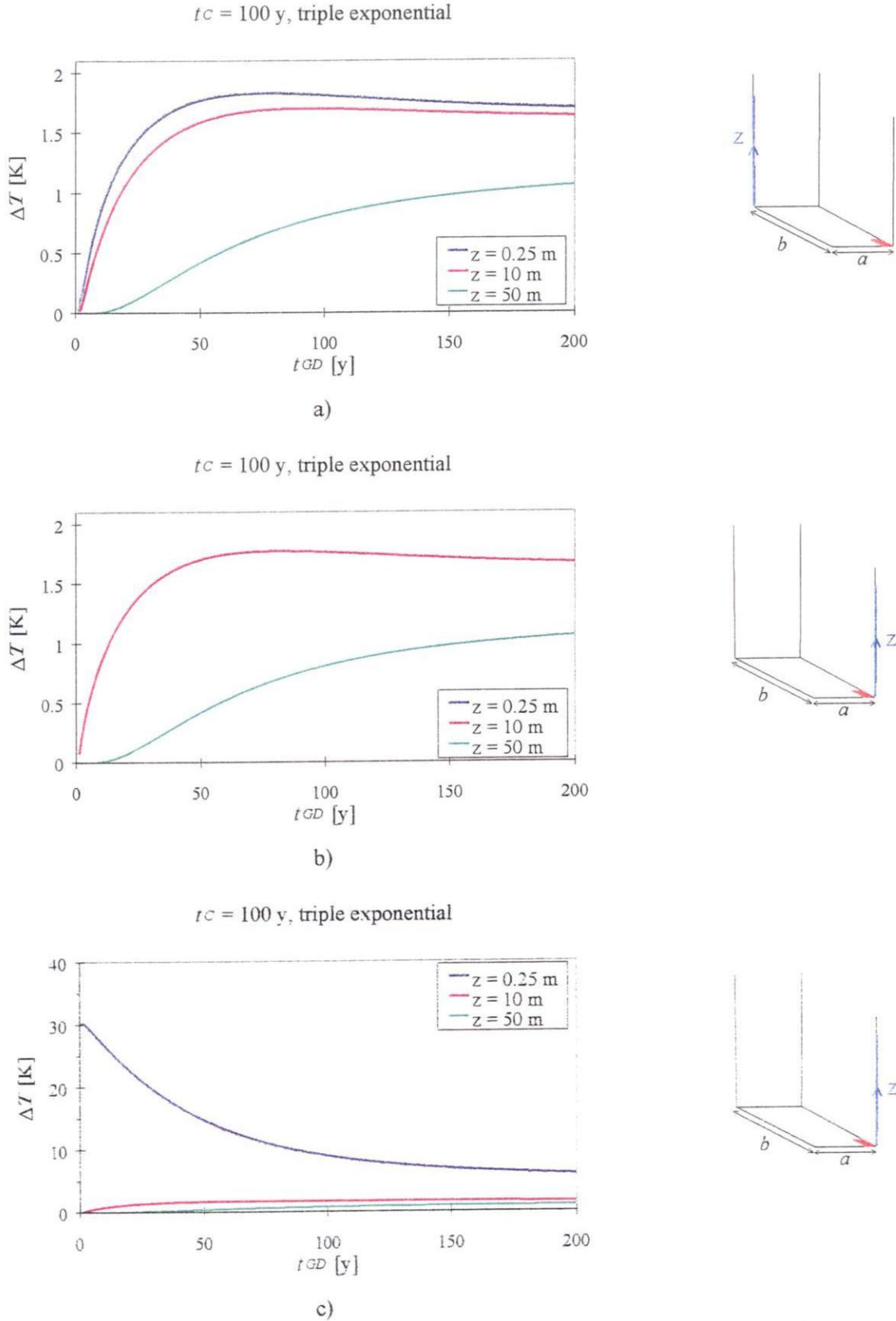


Figure 3.9. ΔT at different height (z) above the repository (heat generation term=decreasing triple exponential) for $t_c=100$ y with a 30×30 m configuration (1 canister / 450 m^2), and at two locations: Fig. a gives a profile above the opposite point of the canister, Figs. b-c a profile above the canister (only the temperature scale changes between Fig. b and Fig. c).

3.2.8. *Proposal of a repository configuration acceptable from a thermal point of view*

The initial 30 m × 30 m configuration given in Figure 3.2b is built on:

- a spacing between secondary galleries $s_2 = 30$ m,
- a spacing between disposal cells $s_3 = 30$ m,

which results in an area of 450 m² per canister.

Considering the triple exponential heat generation function (3.3), the minimum area required to store one HLW canister is 271 m² for $t_C = 50$ y, 179 m² for $t_C = 75$ y and 141 m² for $t_C = 100$ y (see Table 3.8).

From these values, the initial configuration can be modified for $t_C = 50$ y and for $t_C = 100$ y to one of the following options (or any combination with the same area/canister):

$t_C = 50$ y	→ $s_2 = 30$ m, $s_3 \approx 18.1$ m
	→ $s_2 = 50$ m, $s_3 \approx 10.9$ m
$t_C = 100$ y	→ $s_2 = 30$ m, $s_3 \approx 9.4$ m
	→ $s_2 = 50$ m, $s_3 \approx 5.6$ m

All these configurations fulfil the required criterion $\Delta T \leq 4$ K. However, they do not incorporate:

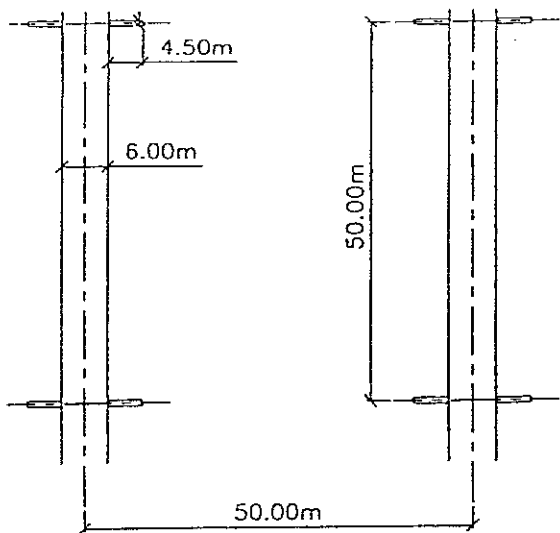
- a criterion for the maximum temperature on the canister/backfill. Such criterion would not modify the main results given in Table 3.8, but they would bring additional constraints on the s_2 and s_3 values (low values of s_2 or s_3 would certainly become unacceptable),
- real thermal properties of Boom clay at 500 m depth.

3.3. Selection of alternatives based on configuration and timing of disposal

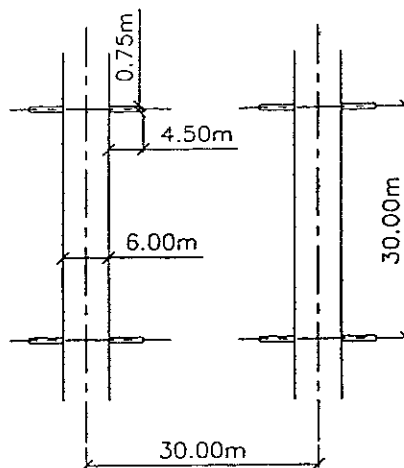
The thermal simulations showed that an area of minimum 271 m² is required per canister of high level heat generating waste, if the cooling down time t_c at the surface is 50 years. If the cooling down time is 100 years, the minimum area is reduced to 141 m². This information is used to select some alternatives to the basic layout of TRUCK-I (50 m × 50 m). However, the distance between secondary galleries was fixed at either 30 m, or 50 m, such that a barrier is created in the horizontal direction between secondary galleries.

The 6 configurations that are compared in the next paragraphs are as follows (see Figures 3.10a-f):

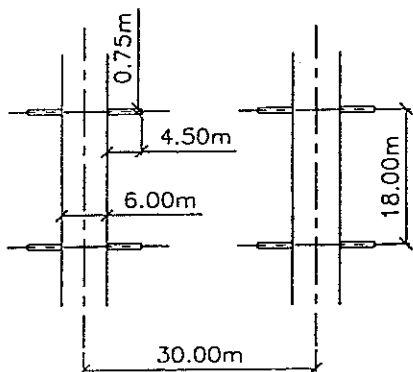
- 1) basic layout: 50 m × 50 m (same as TRUCK-I, but with smaller and shorter tertiary galleries);
- 2) grid of 30 m × 30 m (alternative to TRUCK-I),
- 3) grid of 30 m × 18 m ($t_c = 50$ years; 271 m²/canister),
- 4) grid of 50 m × 11 m ($t_c = 50$ years; 271 m²/canister),
- 5) grid of 30 m × 9.5 m ($t_c = 100$ years; 141 m²/canister),
- 6) grid of 50 m × 5.5 m ($t_c = 100$ years; 141 m²/canister).



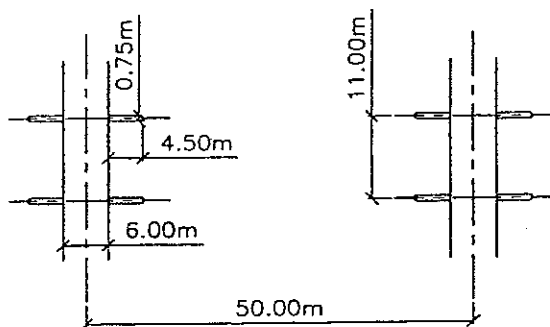
a) Basic layout: 50 m x 50 m (same as TRUCK-I, but with smaller and shorter tertiary galleries)



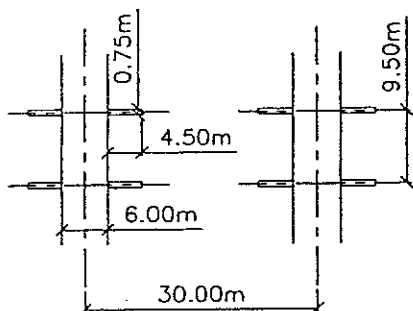
b) Grid of 30 m x 30 m (alternative to TRUCK-I)



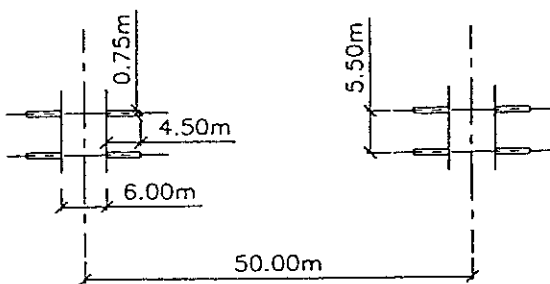
c) Grid of 30 m x 18 m
($t_c = 50$ years; $271 \text{ m}^2/\text{canister}$)



d) Grid of 50 m x 11 m
($t_c = 50$ years; $271 \text{ m}^2/\text{canister}$)



e) Grid of 30 m x 9.5 m
($t_c = 100$ years; $141 \text{ m}^2/\text{canister}$)



f) Grid of 50 m x 5.5 m
($t_c = 100$ years; $141 \text{ m}^2/\text{canister}$)

Figure 3.10. The 6 configurations studied.

3.3.1. Comparison of 6 configurations

To make the comparison easier with regards to timing, the excavation of the mine is planned in successive phases. The comparison in this report starts after both shafts have been connected (580 working days after the start of the site preparation). The same terminology is used for the successive phases as in TRUCK-I (see Tables 1.1 and 1.2 in this report and see Appendix D in Van de Steen and Vervoort, 1998).

The two differences between the 6 configurations are the distance between secondary galleries (30 m or 50 m) and the distance between tertiary galleries (ranging between 5.5 m and 50 m). For all 6 configurations discussed in this report, the excavated diameter of the tertiary galleries is 0.75 m and their length 5 m (from the sidewall of the support in the secondary gallery or 4.5 m beyond the 0.5 m thick concrete support). The outside diameter of the primary and secondary galleries is 6 m.

Similar to TRUCK-I, a barrier of at least 50 m is left between the zone of the heat generating high level waste and the adjacent zone of the middle and low level waste (MLW). Due to the position of the shaft and the size of the MLW-zone, the closest secondary gallery is at a distance of minimum 900 m from the shaft area. The distance between both shafts remains 1100 m, which implies that the length of the secondary galleries remains at 1000 m as well.

For the primary and secondary galleries, the same advance rates are taken as in TRUCK-I, even though the diameter is larger (more than 6 m instead of 4.9 m). It is assumed that the effort for cutting a larger diameter is compensated by the easier access and handling in a larger tunnel. The following advance rates are considered:

- Removal and positioning of excavation machine: 5 working days,
- Excavating a gallery in a straight line: 10 m/day.

For the tertiary galleries or the disposal cells, the same rates as in TRUCK-I are considered:

- Removal and installation of excavation machine between secondary galleries: 5 working days,
- Positioning and excavation of disposal cells at both sides of secondary galleries: 5 working days,
- Positioning and excavation of disposal cells at one side only of secondary gallery: 3 working days.

The reduction of the distance between tertiary galleries has a large effect on the number of secondary galleries required (see Table 3.12). For a centre distance of 50 m between disposal cells, 38 cells can be excavated in a secondary gallery, if at both sides disposal cells are placed (19 if only at one side disposal cells are needed). For this configuration, 9 secondary galleries are required, of which 8 are of the double type and 1 of the single. If the centre distance between disposal cells is 5.5 m (smallest considered), only one secondary gallery is required. This also means that if an accident would occur with one canister (e.g. leakage), the entire zone would immediately be affected. In other words, no sub-compartments exist and no possibilities exist for the sealing of a section of the HLW zone. In TRUCK-I, the possibility is left open to seal the mine in successive steps: e.g. first the tertiary

galleries, followed by the secondary galleries, followed by each zone. Between each step a period of monitoring can be incorporated in the planning. With only one secondary gallery, no distinction can be made between sealing the secondary gallery and the zone of HLW waste. For the 300 HLW canisters to be stored in the Netherlands the distance of 50 m between secondary galleries has for this configuration no meaning. If one would opt for this configuration, one should investigate if it is advisable to decrease the total length of the secondary galleries and hence the length of all zones (1000 m). It would increase the second dimension of the two other zones too (and for these zones an increase would probably be disadvantageous). This investigation falls however outside the scope of TRUCK-II.

Table 3.12. Available disposal cells (HLW zone only).

	# Cells per secondary gallery (double: left & right)	# Secondary galleries (double + single)	Total # cells (Required + Spare)
1. 50 m x 50 m	38	9 (8 + 1)	300 + 23
2. 30 m x 30 m	66	5 (5 + 0)	300 + 30
3. 30 m x 18 m	110	3 (3 + 0)	300 + 30
4. 50 m x 11 m	180	2 (2 + 0)	300 + 60
5. 30 m x 9.5 m	210	2 (1 + 1)	300 + 15
6. 50 m x 5.5 m	362	1 (1 + 0)	300 + 62

In Table 3.13, the total length of primary and secondary galleries for the heat generating high level waste is summarised and in Table 3.14 the total area required is presented. For both parameters the percentage in comparison to the basic layout (configuration 1, 50 m x 50 m) is calculated.

Table 3.13. Total length of primary and secondary galleries (from shaft section; HLW zone only).

	Primary (m)	Secondary (m)	Sum (m)	% CONF.1 (50 m x 50 m)
1. 50 m x 50 m	2600	9000	11600	100
2. 30 m x 30 m	2070	5000	7070	61
3. 30 m x 18 m	1950	3000	4950	43
4. 50 m x 11 m	1950	2000	3950	34
5. 30 m x 9.5 m	1860	2000	3860	33
6. 50 m x 5.5 m	1850	1000	2850	25

Table 3.14. Total area required (HLW zone).

	1000 m ²	% CONF.1 (50 m x 50 m)
1. 50 m x 50 m	425	100
2. 30 m x 30 m	150	35
3. 30 m x 18 m	90	21
4. 50 m x 11 m	100	24
5. 30 m x 9.5 m	45	11
6. 50 m x 5.5 m	50	12

The length of primary galleries (two times 900 m in TRUCK-I, see Figure 1.1a page 7) is to a great extent determined by the minimum distance between the shaft area and the HLW zone. The length of secondary galleries is a direct function of the amount of secondary galleries required (number multiplied by 1000 m). In comparison to the basic layout (50 m x 50 m), the total length of primary and secondary galleries is reduced by 39 % (configuration 2, 30 m x 30 m) to 75 % (configuration 6, 50 m x 5.5 m), which will have a direct positive effect on the cost for excavating this part of the mine.

As the basic distance to the HLW zone does not interfere with the total area required for this zone, the difference between the 6 configurations is even more significant: the reduction in area in comparison to the basic layout is 65 % for configuration 2 (30 m x 30 m) and 88 % (!) for configuration 6 (50 m x 5.5 m). For the latter configuration, the large reduction is due to the need for only one secondary gallery. As already mentioned above, this is not advisable from a sealing or safety point of view.

3.3.2. Time planning

Although the comparison of the geometry of the 6 configurations is relatively straightforward, the time planning exercise is more complex. As in TRUCK-I, all excavation phases are carried out consecutively. In this report and for comparative reasons, the excavation of the two other zones is not taken into consideration. The same advance rates as in TRUCK-I have been used (see above). Two options have been taken, namely where one and two excavation machines are available for the HLW zone. In TRUCK-I, 5 machines were used to excavate the secondary galleries in the three zones and 8 machines for the tertiary galleries. In a particular secondary gallery, it is assumed that only one machine can work to excavate the tertiary gallery. To use 2 or more machines in the same gallery would cause problems in ventilation and in transport logistics (mainly transport of excavated material and support elements)

In Table 3.15, a summary is given of the time planning. For the situation where two excavation machines can be used (Table 3.15.a), the differences between the 6 configurations are much smaller than for the geometrical parameters. Configuration 6 (50 m x 5.5 m) takes almost as long as the basic layout (50 m x 50 m), because only one excavation machine can be deployed to excavate the tertiary galleries, since there is only one secondary gallery. Considering the advance rates, this results in 910 working days instead of 462 (basic layout) for phase 5. For configuration 4 and 5, the two secondary

galleries have been excavated when phase 3 is finished and no excavation takes place in phase 4. For configuration 4, the time needed for finishing the HLW zone is the smallest, namely 62 % of the basic layout. If one would deploy one machine only, the disadvantage for excavating the tertiary galleries, associated with the single secondary gallery in configuration 6 (50 m x 5.5 m) falls away. Hence, configuration 6 is the fastest (58 % in comparison to the basic layout). The time to excavate the tertiary galleries is nearly the same for the 6 configurations

Table 3.15a. Time planning with 2 excavation machines (HLW heat generating zone only), starting at day +580 (end of phase 2.a, connection between both shafts).

	Loop (phase 2.b)	Sec. loop (phase 3)	Sec. gall. (phase 4)	Tert. gall. (phase 5)	Total	% (1.50 m x 50 m)
	days	days	days	days	days	
1. 50 m x 50 m	205	150	420	462	1237	100
2. 30 m x 30 m	206.5	122	210	510	1048.5	85
3. 30 m x 18 m	206.5	116	105	560	987.5	80
4. 50 m x 11 m	207.5	115	-	445	767.5	62
5. 30 m x 9.5 m	205	113	-	530	848	69
6. 50 m x 5.5 m	207.5	-	-	910	1117.5	90

Table 3.15b. Time planning with 1 excavation machine (HLW heat generating zone only), starting at day +580 (end of phase 2.a, connection between both shafts).

	Loop (phase 2.b)	Sec. loop (phase 3)	Sec. gall. (phase 4)	Tert. gall. (phase 5)	Total	% (1.50 m x 50 m)
	days	days	days	days	days	
1. 50 m x 50 m	295	195	735	862	2087	100
2. 30 m x 30 m	297	139	315	850	1601	77
3. 30 m x 18 m	298	127	105	840	1370	66
4. 50 m x 11 m	300	125	-	890	1315	63
5. 30 m x 9.5 m	295	121	-	850	1266	61
6. 50 m x 5.5 m	300	-	-	910	1210	58

The comparison between one and two excavation machines available is significant (except for configuration 6). For configuration 1, the time needed increases by nearly 70 % if only one excavation machine would be available. Hence, one should try to have two excavation machines available for the tertiary galleries in the HLW zone. This should not impose any major problem in the logistics nor in the budget.

The total number of working days required to excavate the HLW zone has to be compared with the total time needed for the entire project. With two excavation machines the total days for the HLW zone varies between 767 and 1237 working days. In TRUCK-I, the total time required to excavate the entire mine was estimated to be 2950 working days or about 13 years. In the fastest situation, the total time would be decreased by at most 2 years. In TRUCK-I, it was shown that if one would increase the advance rate by 50 %, the total excavation time would be 10 years instead of 13 years. Hence, one can conclude that the 6 configurations have an effect on the time required to excavate the mine, but that the choice between them is not predominant in the final planning. Other parameters are at least as important.

3.3.3. Conclusions

For the heat generating high level waste, two basic layouts were selected for comparison, namely grids of 50 m x 50 m and 30 m x 30 m (distances between respectively secondary and tertiary galleries). Four other alternatives were also considered, which take the heat dissipation into account. It was shown that after a cooling down time t_c of 50 years, an area of minimum 270 m² per canister is required. When the cooling down time is 100 years, the minimum area is 141 m² per canister. These conditions result in grids of 30 m x 18 m and 50 m x 11 m for $t_c = 50$ years and in grids of 30 m x 9.5 m and 50 m x 5.5 m for $t_c = 100$ years. For all these configurations the length of the secondary galleries is fixed at 1000 m.

The difference between these 6 configurations is mainly related to the number of secondary galleries required and to the total area of the HLW zone. For distances of 11 m or less between the centres of the tertiary galleries or the disposal cells, only 1 or 2 secondary galleries are needed for the 300 canisters to be stored in the Dutch concept.

If two excavation machines are used, the time needed to excavate the entire HLW zone is shortest for the configuration 50 m x 11 m, using two secondary galleries (768 working days). For the configurations with more than two secondary galleries, the reduction in time is maximum 20 % of the excavation time for the configuration of 50 m x 50 m (e.g. 988 working days in comparison to 1237 working days). In comparison to the total time for the entire excavation project (nearly 3000 working days or about 13 years) this time saving is relatively small and of the same order of magnitude as a change in advance rates applied. = 21% of
= 1.4% of
work

For further hydro-mechanical calculations the configurations of 30 m x 30 m and of 30 m x 18 m are selected as alternatives to the configuration of 50 m x 50 m. The configurations, where there is only 1 or 2 secondary gallery will not further be analysed. The reasons for this are twofold:

With a very small number of secondary galleries, there will be nearly no possibility to isolate a section of the HLW zone from the rest of this zone. Either the entire zone has to be sealed off, or only the individual tertiary galleries can be sealed off. In the concept of retrievable storage, one would like to leave the possibility open to seal the mine in consecutive phases, with a possible monitoring period in between two phases.

As one would probably only be working with one team in a secondary gallery at the same time for either the excavation of the tertiary galleries, the placing of the canisters, the filling of the tertiary

galleries, the possible recuperation of the waste or the cleaning up of a possible leak, it is rather disadvantageous to have all or half of the canisters in one secondary gallery. This would increase the time needed for these operations. In certain instances (e.g. the latter two), time could be crucial.

3.4. Optimisation of a repository design from a hydromechanical point of view

Following the optimisation of a repository from the thermal and from the timing point of view, the two configurations (30 m x 30 m and 30 m x 18 m) have been selected as alternatives to the TRUCK-I basic configuration (50 m x 50 m).

Here, it is aimed to:

- check if these configurations are 'acceptable' from a hydromechanical point of view considering only the excavation phase which, according to the very low hydraulic conductivity of Boom clay ($k \approx 4 \cdot 10^{-12}$ m/s), is approximated as undrained (no water flow in the media). Accordingly, short-term computations are carried out. Of course the definition of the 'acceptable' criteria is somewhat arbitrary: for instance it was postulated in TRUCK-I that at least half of the distance between secondary galleries should remain in an elastic state for the concept to be 'acceptable'. One must however keep in mind that there is a gap between the quantification of the plastic zone extent which is fairly easy to evaluate and its real effects in the field which is rather difficult to predict (diffuse deformation? localised deformation? fracturing?);
- quantify the influence of the disposal cell (tertiary gallery) excavation within the plastic zone of the secondary gallery, particularly on the modification of the plastic zone extent.

However, it is firstly necessary to check in more detail the influence of the mechanical parameters obtained from the testing programme (see sections 2.5 to 2.7). Following, a full three-dimensional hydromechanical modelling of the secondary and tertiary gallery will be presented.

3.4.1. Influence of the mechanical parameters obtained from the testing programme

Before spending much effort on careful three-dimensional hydromechanical analysis, it is important to evaluate first what are the main effects of the mechanical parameters obtained in the TRUCK-II experimental programme (see Table 2.5). For this purpose, simple one-dimensional axisymmetric computations are performed, based on an extension of the classical convergence-confinement method (Panet, 1995) to the short-term response of a saturated porous medium (Labiouse and Giraud, 1998).

Table 3.16. Fixed parameters for the 1-D axisymmetric analytical study.

Excavation radius R_i	3.1	[m]
Poisson's coefficient ν	0.125	[-]
Dilation angle ψ	0	[°]
Total pressure P_0	10	[MPa]
Pore pressure u_0	5	[MPa]
Internal pressure P_i	4	[MPa]
Porosity n	0.39	[-]
Water bulk modulus K_w	2000	[MPa]

The known parameters (geometry, initial conditions and some mechanical parameters) used are reported in Table 3.16. A³ internal pressure P_i of the same order than in the TRUCK-I study has been considered. To evaluate the impact of the new geomechanical parameters obtained in TRUCK-II, three runs are carried out:

- the first (Run 1) with the TRUCK-II parameters taken from Table 2.5,
- the second (Run 2) with parameters known at the Mol site (the ones used in TRUCK-I),
- the third (Run 3) with a mixture of TRUCK-II and Mol site parameters (actually the cohesion and elastic modulus of TRUCK-II with the friction angle known at the Mol site).

The parameters corresponding to each run are detailed in the Table 3.17.

Table 3.17. Varying parameters for the 1-D axisymmetric analytical study.

	Run 1 (lower bound set)	Run 2 (URL Mol set)	Run 3 (upper bound set)	
Young's modulus E'	1000	300	1000	[MPa]
Cohesion c'	800	300	800	[kPa]
Friction angle ϕ'	9	18	18	[°]

The results show that, for the same configuration (geometry, initial and boundary conditions), the plastic zone extends up to 13.1 m for Run 1 whereas it only extends to 9.8 m for Run 2 (see Figure 3.11a-b). Therefore, if the mechanical parameters considered in Run 1 are correct, it appears that the behaviour of Boom clay that comes from 500 m depth is less favourable than the clay from the Mol site.

As already discussed in sections 2.6 and 2.7, such conclusion is difficult to believe and is in contradiction with the observed consolidation (see Figures 2.10 and 2.11). Also, the characterisation of the samples did not show significant difference in granulometry and mineralogy between the five levels (69 m, 120 m, 229 m, 313 m and 455 m depth) at which the Boom clay has been studied.

Therefore, the Boom clay characteristics known at the Mol site (225 m depth) could be considered as lower bound values for the characteristics at 500 m depth.

The value $\phi' = 18^\circ$ could then be considered as a lower bound for the real friction angle at 500 m depth (as it was assumed in TRUCK-I). With such an assumption, the plastic zone would extend only to 7.0 m (see Run 3 on Figure 3.11c).

In conclusion, the large uncertainty existing on the frictional parameters (ϕ' and c') for Boom clay at 500 m depth results in a variation range for the plastic zone extent of order 2. It is therefore likely that:

- the 'lower bound' parameter set obtained in TRUCK-II (Run 1) gives a pessimistic R_{pe} prediction,
- the 'upper bound' parameter set of Run 3 gives a more favourable R_{pe} prediction, though experimental evidences are lacking to support this statement.

As a consequence, more detailed three-dimensional computations using both these parameter sets for Boom clay have been considered in the next section.

3. Optimisation of the design of the disposal facility

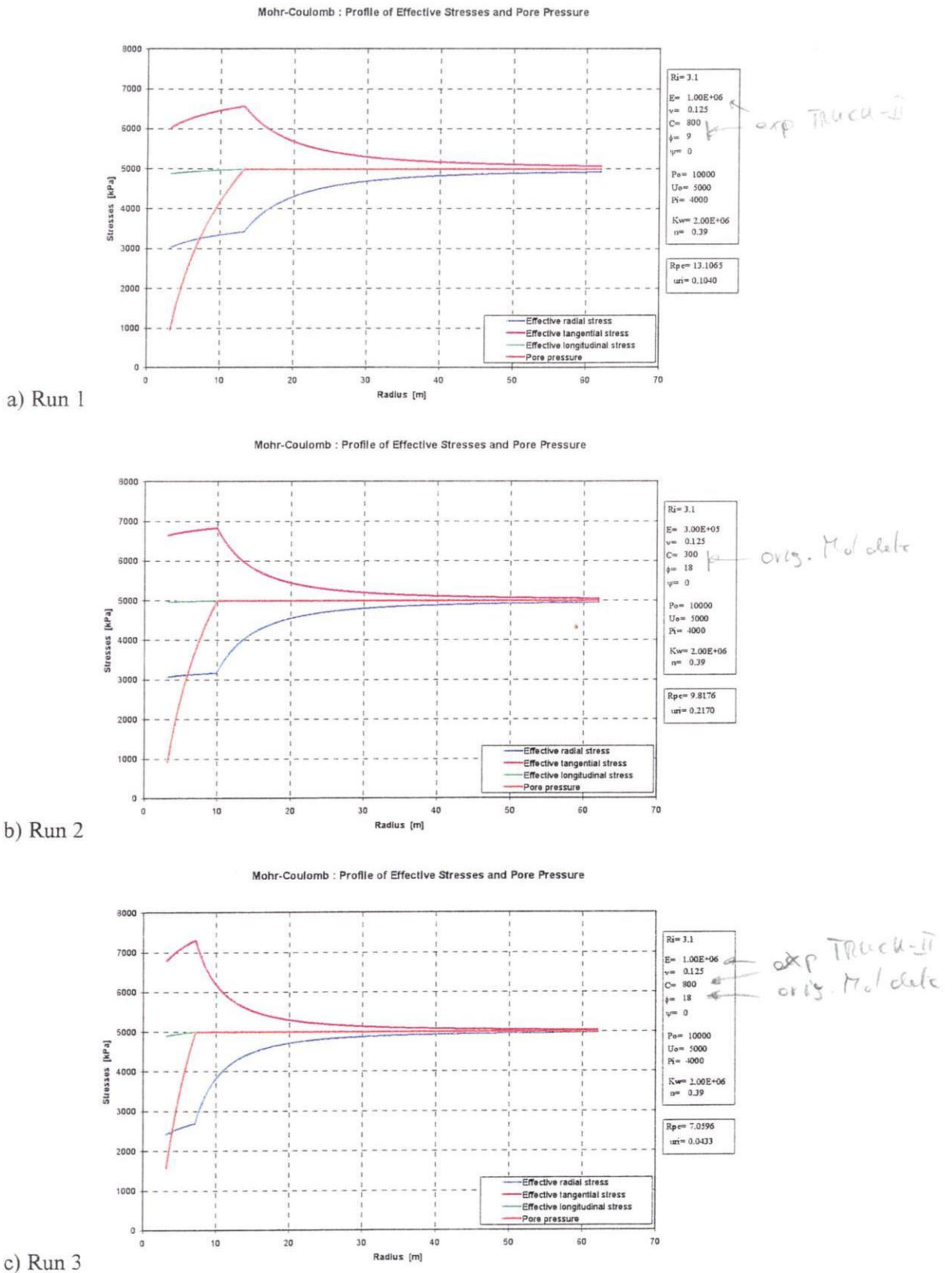


Figure 3.11. Gallery excavation (1-D analytical solution) using clay parameters from: a) the TRUCK-II experimental programme, b) the Mol site (same as in TRUCK-I), c) the TRUCK-II experimental programme with the friction value known at Mol.

3.4.2. Details about the three-dimensional models considered

Using the two parameter sets given in the previous section (see Run 1 and Run 3 in Table 3.17), three-dimensional hydromechanical computations of the excavation of the secondary and tertiary galleries have been carried out. As in the previous section, only the short-term behaviour is analysed (undrained analysis). Note that a study of time evolution has been carried out in TRUCK-I (Van de Steen and Vervoort, 1998), and that its general conclusion should remain valid though they should be attenuated here as the hydraulic conductivity is likely to be much lower than previously considered (value of $2 \cdot 4 \cdot 10^{-12}$ m/s instead of 10^{-10} m/s considered in TRUCK-I).

Geometry, initial conditions and boundary conditions

In this study, only the case with an infinite number of secondary galleries and disposal cells has been studied as it represents the most pessimistic situation. Also, the lithostatic gradient for total stress and pore pressure is not taken into account. Then, referring to the $(0,x,y,z)$ Cartesian frame depicted on Figure 3.12b, this configuration exhibits the following symmetry planes:

- $x = 0$ and $x = s_2/2$
- $y = 0$ and $y = s_3/2$
- $z = 0$

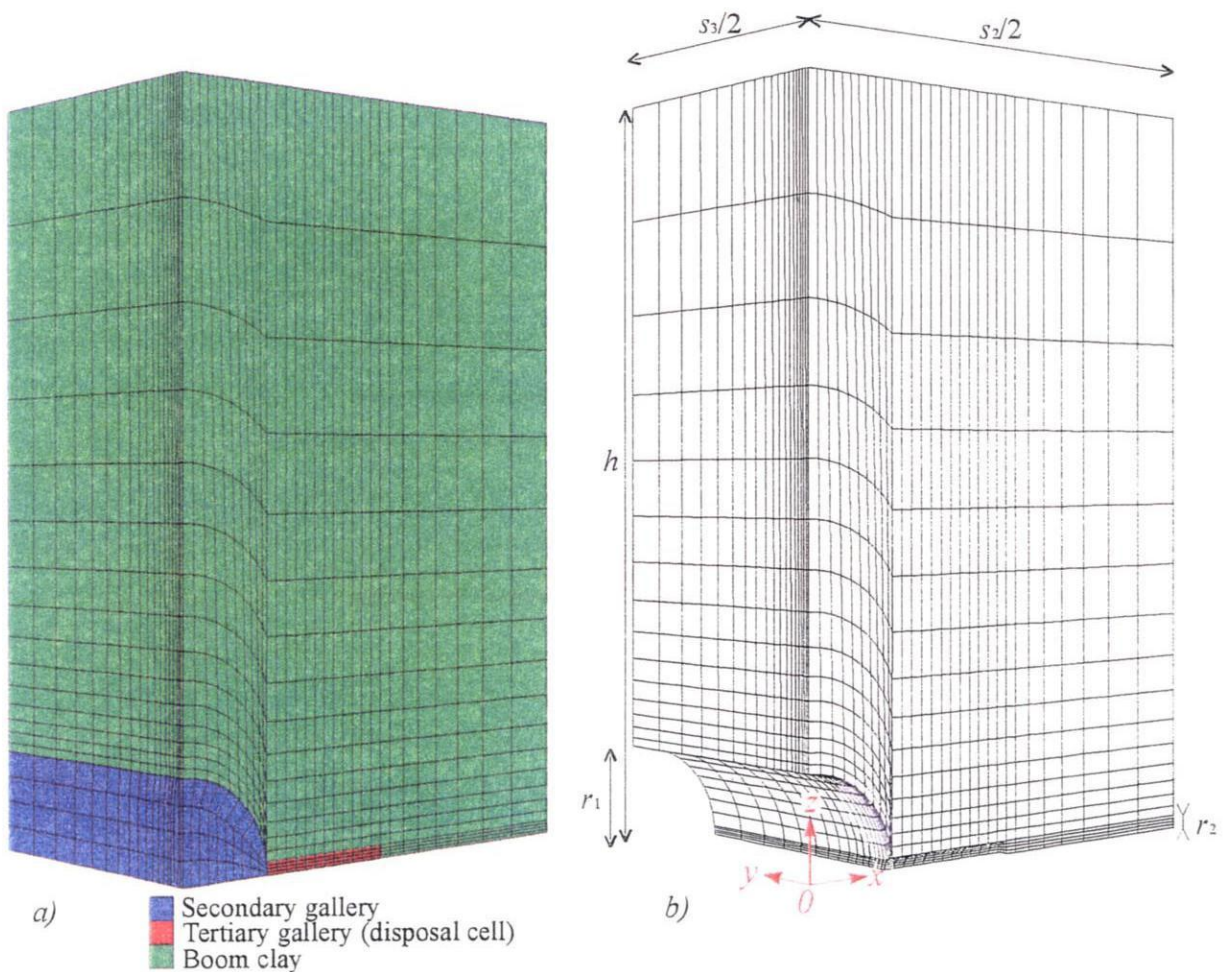


Figure 3.12. Initial 3-D model: a) the three domains (galleries and clay) with discretisation, b) reference frame, and geometry at the end of excavation.

Owing to their nature, these symmetry planes have the following boundary conditions:

- a zero normal displacement,
- and a zero water flux (i.e. impermeable).

An isotropic initial stress field is assumed with the total pressure $P_0 = 10$ MPa and the pore pressure $u_0 = 5$ MPa. These initial conditions are similar ^{to those} than in (Van de Steen and Vervoort, 1998).

The initial total pressure is fixed on the plane $z = h$, and the following model dimensions are considered:

- $s_2 = 30$ m,
- $s_3 = 30$ m or $s_3 = 18$ m,
- $h = 25$ m,
- $r_1 = 3.1$ m, which considering an overgap of 0.1 m should result in a secondary gallery of approximately 6 m in diameter,
- $r_2 = 0.4$ m, which considering an overgap of 0.025 m should result in a disposal cell of approximately 0.75 m in diameter.

This geometry and boundary conditions are discretised in the FLAC-3D finite differences code (Itasca, 1997) using the grid shown on Figure 3.12.

Features of the different considered cases

As stated in TRUCK-I (Van de Steen and Vervoort, 1998), the distance s_2 between secondary galleries is a key factor with respect to the 'acceptability' criterion considered in TRUCK-I: "at least half of the distance between secondary galleries must remain elastic". In the present study, the choice of representative parameters for Boom clay at 500 m depth is also a key factor (see section 3.4.1), especially regarding the friction angle ϕ' .

Thus, two s_2 and two ϕ' values are considered, which then results in four different models (see Table 3.18). All the other mechanical parameters correspond to the ones given in Tables 3.16 and 3.17.

Table 3.18. Differences between the four models studied.

	s_2 [m]	ϕ' [°]
Model 1	30	9
Model 2	50	9
Model 3	30	18
Model 4	50	18

($C' = 900$ kPa)
see van 1, 3 in Table 3.17

Representation of the excavation sequence and of the support method

Two different methods for simulation the excavation and support of the secondary tunnel have been used:

- A first method was foreseen, based on a progressive decrease of the total internal pressure (noted P_i) at the wall of the secondary gallery, until the contact with a 50 cm thick concrete lining is reached. It requires to define a priori an overgap value between the lining and the clay. Here a value of 10 cm has been chosen in order to correspond to an approximate support pressure of 4 MPa as in TRUCK-I, see Figure 3.13.

The advantage of this method lies in the fact that the support pressure does not need to be equal on the whole tunnel section as a result of the non-symmetrical unloading around the gallery (the lateral symmetry plane at $x = s_2/2$ whereas the upper plane $z = h$ is not a symmetry plane).

However, as a main drawback, the use of contact surface elements induces more oscillations in the explicit (pseudo-dynamic) resolution scheme used of FLAC-3D than if no interfaces are used. A key parameter for limiting these oscillations lies in an adequate definition of the interface normal stiffness, which must be a compromise between an acceptable relative penetration of both sides of the interfaces and an acceptable computing time. Moreover, we are faced here with an interface that has a variable element size along the y -direction. Therefore, the apparent stiffness is not uniform on this interface (Itasca, 1997), which leads to a non-plane strain condition along the y -axis.

Consequently, this support method has not been retained for the final computations as the results are somehow dependent on the formulation of the numerical interface.

- the retained method is based on a progressive decrease of P_i at the wall of the secondary gallery until a support value of 4 MPa, in the same spirit than the method used in the TRUCK-I study (Van de Steen and Vervoort, 1998).

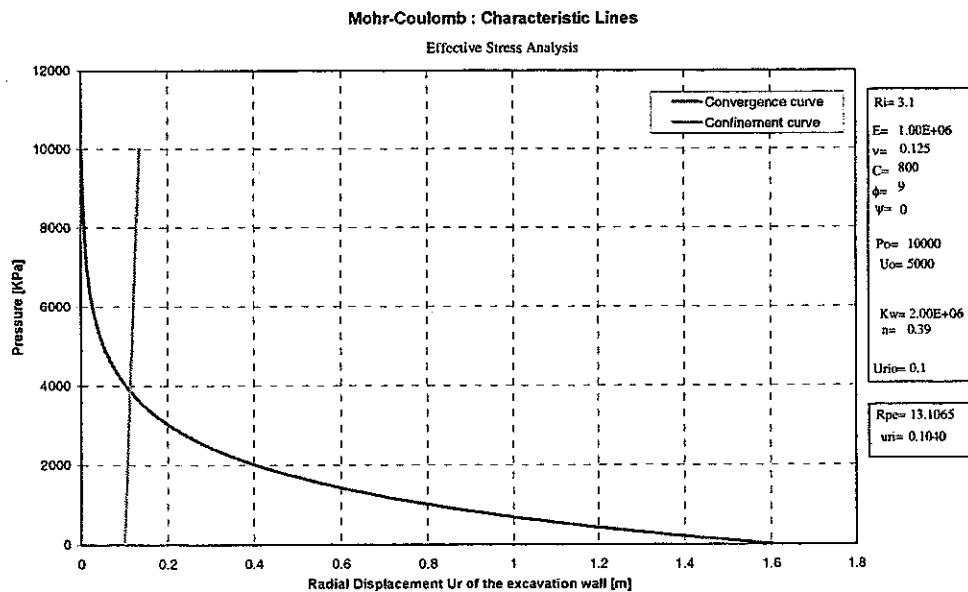


Figure 3.13. Characteristic lines obtained with the Boom clay parameters obtained in TRUCK-II for $P_i = 4$ MPa (lower bound set).

For the excavation of these disposal cell, the more pessimistic case has been considered (unlined, i.e. no support pressure).

From a numerical point of view, the modelling sequence was the following:

- a) Progressive excavation of the secondary gallery,
- b) Stepping to equilibrium,
- c) Excavation of the disposal cell,
- d) Stepping to equilibrium.

In the following section, results are presented at the end of phase b) and d).

3.4.3. Excavation of the secondary gallery

As the excavation between secondary galleries is a plane strain problem, the results presented here are valid for any s_3 value (though here the value $s_3 = 18$ m is considered).

For the four models, the plastic zone extent (see Figures C.1, C.6, C.11 and C.16) is summarised in Table 3.19.

Clearly, the lower bound friction angle $\phi' = 9^\circ$ with $s_2 = 30$ m does not fulfil the chosen criterion. However, it is unlikely that an important amount of plastic strain has occurred far from the tunnel wall, (see the pore pressure and displacement isovalues on Figures C.2 and C.5). Due to the boundary conditions (symmetry plane at $x = s_2/2$ and fixed total pressure at $z = h$), the stress gradient normal to the tunnel wall is higher in the horizontal direction than in the vertical one (compare Figures C.3 and C.4). This is consistent with a larger plastic zone extent along the horizontal direction than along the vertical direction.

The lower bound friction angle $\phi' = 9^\circ$ with $s_2 = 50$ m just fulfils the chosen criterion (see Figure C.6). It is worth pointing out that in this case the maximum displacement at tunnel wall is much higher in Model 1 ($u_{\max} \approx 40$ cm) than in Model 2 ($u_{\max} \approx 16$ cm), compare Figures C.5 with C.10.

Both models with the hypothetical upper bound friction angle $\phi' = 18^\circ$ fulfil the chosen criterion. There is almost no influence of the s_2 value on the stress and displacement fields (compare Figures C.12 & C.17, C.13 & C.18, C.14 & C.19, C.15 & C.20).

Table 3.19. Extent of the plastic zone.

	Horizontal extent [m]	Vertical extent [m]
Model 1	∞	10.0
Model 2	16.8	10.0
Model 3	8.5	6.5
Model 4	8.0	6.5

3.4.4. Excavation of the disposal cell

From the obtained results presented before, the disposal cell has been excavated without any support, thus being the more pessimistic situation (in the short term). Note that, referring to the horizontal plastic zone extents given in Table 3.19, this 4.5 m long gallery (from the lining inner radius, i.e. 8 m from the axis of the secondary gallery) falls entirely in the plastic zone of the secondary gallery.

Here, we are interested in looking at the influence of this excavation, particularly on the possible increase of the plastic zone extent and on the relevant choice of the distance s_3 (are $s_3 = 18$ m and $s_3 = 30$ m acceptable solutions for the spacing of disposal cells?).

The numerical solution for model 1 could not be achieved due to a numerical problem (a progressive relaxation procedure would have been required).

Model 2, 3 and 4 have been run successfully, all considering the value $s_3 = 18$ m (this is the more pessimistic option between the two cases $s_3 = 18$ m and $s_3 = 30$ m).

Considering the lower bound friction angle $\phi' = 9^\circ$ with $s_3 = 50$ m (Model 2), the disposal cell excavation does not induce a significant increase in the plasticity extent (compare Figures C.6 & C.21).

For Models 3 and 4, a 0.5 m increase in the horizontal extent of plastic zone is observed (compare Figures C.11 & C.25 and C.16 & C.29).

This is fairly logical as in Models 3 & 4, the open front of the disposal cell is located at 8 m from the secondary gallery axis, i.e. at the elastic-plastic boundary induced by the excavation of the secondary gallery. Inversely, for Model 2 the open front is located at the middle of the plastic zone. It translates by higher stresses in the zone where the disposal cell is to be excavated: the radial (with respect to the disposal cell) stress σ_{zz} is larger in Model 4 than in Model 2 (compare Figures C.19 & C.9).

The disturbance in pore pressure has a larger extent (following the y -direction) in the upper bound models (3 & 4, see Figure C.26 & C.30) than in the lower one (Model 2, see Figure C.22). These are consistent with the observations on the plastic zone extent.

The magnitude of displacements is directly linked to the difference in strength between the lower and upper bound models. Note that the maximum radial displacement ranges between 4.6 cm for the lower bound model (Figure C.24) and 3.0 cm for upper bound models (Figures C.28 & 32). These values have to be compared with the analytical values of 20.8 cm (lower bound) and 3.8 cm (upper bound) that would be obtained if these disposal cells were excavated far from any existing excavation. Eventually, let us point out that these values are obtained with the more pessimistic boundary conditions: infinite number of tunnels and an unlined disposal cell.

3.4.5. Conclusions

From the hydromechanical point of view, it is shown that:

- the combination of geomechanical parameters presented in the chapter 2 (referred as the lower bound set) and the value $s_2 = 30$ m does not allow verify the criterion "*half the spacing between secondary galleries must remain elastic*". This criterion requires at least $s_2 = 50$ m to be fulfilled;
- if the friction angle $\phi' = 18^\circ$ known at the Mol site is considered as the lower bound for its value at 500 m depth (which seems physical), the value $s_2 = 30$ m (and hence $s_2 = 50$ m) verifies the criterion; *fulfills*
- as far as small diameter disposal cell is concerned (75 cm in this study), the parameter s_3 is not a key factor compared to s_2 and to the friction angle ϕ' . The study with $s_3 = 18$ m showed that no

large additional plastic zone was generated by the excavation of the disposal cell. This conclusion will hold for the larger s_3 values.

3.5. Support and backfill of the galleries and disposal cells

Two methods for disposing and retrieving are considered for the disposal cells. One method relies on the lining of the disposal cell being watertight, the other method relies on the use of a watertight overpack for the waste container. At the stage of the research programme, the design is still of a generic character.

3.5.1. Initial Design of the Disposal Cell for HLW-canisters

The disposal cell designed for the TRUCK-II project is based on the geometry of the METRO-I design for vitrified high level radioactive waste (HLW). The METRO-I design concerns a disposal facility in a salt rock formation. The TRUCK-I and TRUCK-II design concerns a disposal facility in an underground clay layer.

Using conventional mining techniques a grid of circular galleries is excavated in the clay layer. There are primary and secondary galleries that provide the access to the horizontal disposal cells. The depth of each disposal cell is about 5 m (including a 0.5 m concrete wall) and the diameter is about 0.75 m. With respect to the detailed design of the disposal cell, one option is to install a watertight, corrosion resistant lining. In the other option no lining is needed because the container will be packed in an overpack. However, depending on the duration between excavation of the disposal cell and placement of the container, structural support for the void volume of the disposal cell may be necessary. In the designs described in this report it is assumed that only one container is placed in each disposal cell. However, it may be possible to place more than one container in a cell without complicating the retrieval too much.

Disposal of a HLW-canister without overpack

Figure 3.14 ~~a~~ gives a top view and a side view of the disposal cell used for containers without an overpack. A watertight lining made of stainless steel supports the wall of the disposal cell. The waste container itself is made from thin steel and is not designed to be corrosion resistant. Failure of the container and the subsequent contact of water with the waste matrix would complicate a possible retrieval operation. Therefore a lining (or an overpack) is needed.

The container is placed in the back part of the disposal cell. This part is then filled with uniformly graded fine quartz sand. Next the disposal cell is backfilled with pre-fabricated blocks. The following considerations apply to the choice of the materials:

- it must be possible to remove the backfill without too much effort,
- the backfill should provide shielding from the radiation,
- the backfill should conduct the decay heat of the radioactive waste,
- the materials should not contain (or produce) reactive substances should water intrude into the disposal cell.

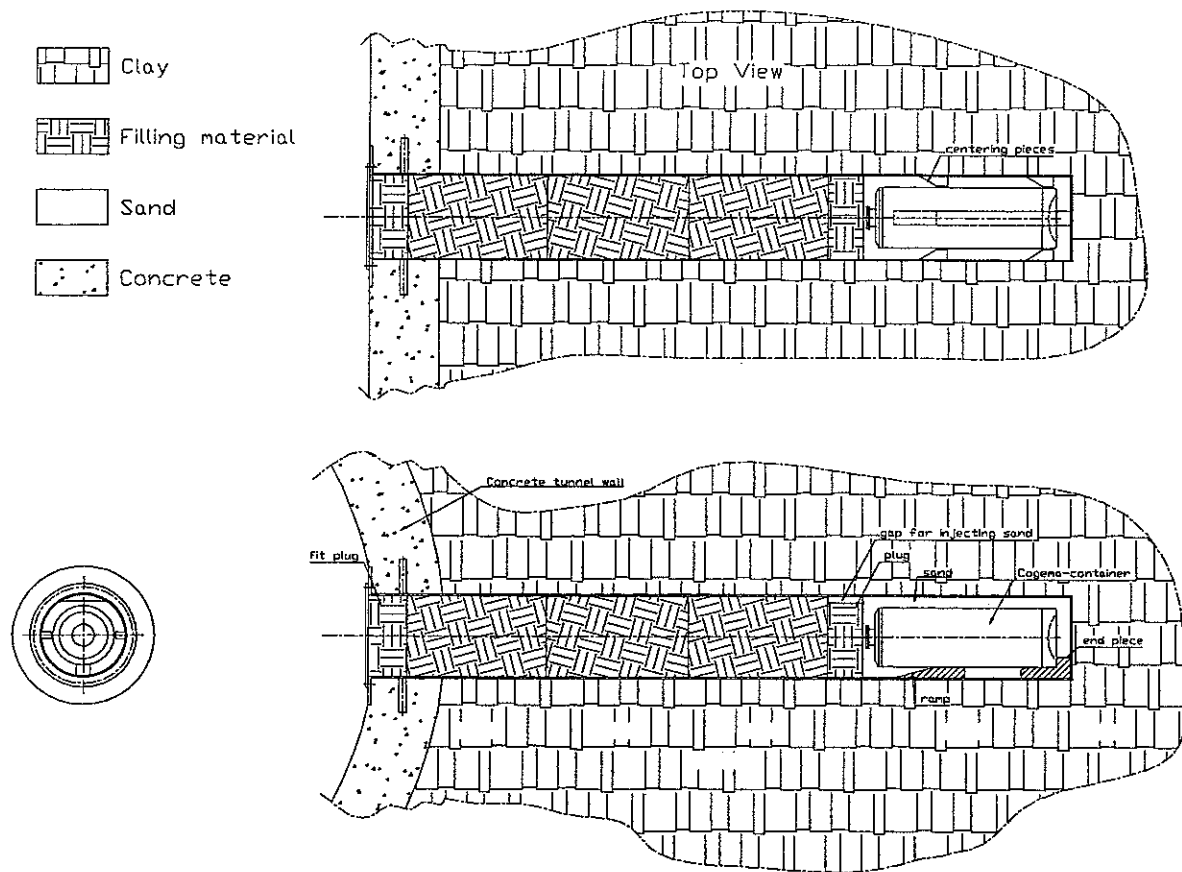


Figure 3.14. Top view and side view of a disposal cell for a canister without overpack.

Disposal of a HLW-canister with overpack

If a watertight overpack is used, the design of the disposal cell can be different. Isolation from any water present in the pores in the clay formation is provided by a second watertight 'container' - the overpack. Figure 3.15 gives an overview of the disposal cell for a HLW-canister with overpack. The overpack is watertight and is designed to resist the pressure from the surround clay formation for a long time - for this a wall thickness of about 3 cm should be sufficient. However, to provide sufficient shielding from the radiation emitted from the waste the wall would have to be at least 30 cm thick. Instead, in this design the radiation shielding is obtained from the backfill. Also, the diameter of the backfill plugs should be somewhat larger than the diameter of the overpack, to avoid radiation escaping through a possible gap between backfill and the clay.

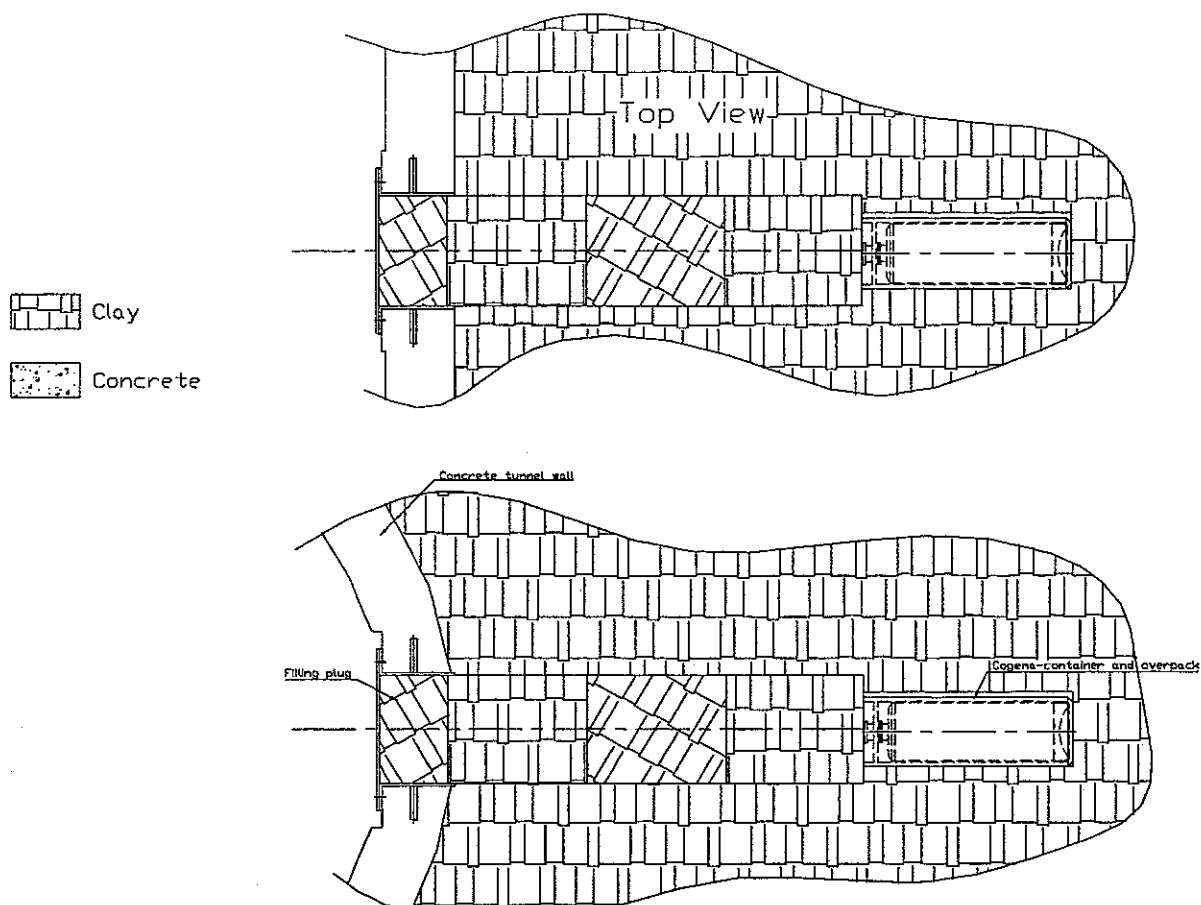


Figure 3.15. Top view and side view of a disposal cell for a HLW canister with overpack

3.5.2. Backfill

For the backfilling and sealing of radioactive waste repositories in clay, two kinds of materials have been studied, i.e. cement based and clay based materials. Cement based materials have been proposed mainly as backfilling around non-heat generating waste. Clays have been proposed because of their low hydraulic conductivity, good geochemical stability, good sorption properties and their swelling properties. Cement based materials have been proposed for their low hydraulic conductivity, good mechanical properties and creating a high pH environment that reduces the solubility of actinides and many other radionuclides.

Cement based materials cannot be used around heat generating waste because they are not chemically stable at high temperatures and because the heat of hydration of the cement in combination with the heat of the HLW could lead to such high temperatures ($> 100\text{ }^{\circ}\text{C}$) that the end product would have a very poor quality. It is also not advisable to use cement-based materials around vitrified HLW because the highly alkaline fluids from the cement will increase the dissolution rate of the glass.

Most of the clay-based materials that have been studied use bentonite either as such or mixed with sand or mixed with sand and graphite. Bentonites are clays with high swelling properties, which makes them very suitable as backfilling and sealing materials. Bentonites can show a volumetric swelling of more than 100 % and when compacted and hydrated in a confined situation they can

generate swelling pressures of up to 10 MPa and have a saturated hydraulic conductivity as low as 10^{-14} m/s. The bentonites that have been studied in most detail are: MX-80 (Wyoming bentonite, USA), FoCa clay (the French reference material) and Serrata clay (the Spanish reference material). SCK has also studied the use of Boom clay ^{residues} of underground excavations. SCK has shown that it is possible to obtain a material with a low hydraulic conductivity by compacting Boom clay, though its swelling properties are rather limited. A second problem about the use of Boom clay is that it needs to be protected from oxidation during the period between excavation and backfilling of the repository. This means that it needs to be stored dry because otherwise the finely distributed pyrite in the Boom clay oxidises what leads to a very acidic environment (pH 2 to 3).

With the above mentioned bentonites it is possible to obtain a material with a hydraulic conductivity of about 10^{-13} m/s and a swelling pressure of about 5 MPa after saturation of the material at a dry density of about 1.6 to 1.8 g/cm³. To obtain such a dry density, two techniques have been studied: the use of pre-compacted blocks and the use of a high-density pellets/powder mixture. Pre-compacted bentonite blocks can be easily produced by isostatic or uni-axial compaction. With these techniques, it is possible to obtain a dry density of even up to 2 g/cm³. The compacted blocks need to have a dry density of at least about 1.8 g/cm³ to have sufficient cohesion so that they can be handled without falling apart. The fabrication of pre-compacted blocks however requires the use of a large high force press and their production is thus rather expensive. The second technique has been developed by CEA in co-operation with SCK and consists in producing high density (> 2 g/cm³) bentonite pellets and mixing them with bentonite powder. The pellets (2.5 x 2.5 x 1.5 cm) are made with a pelletizer such as used for the compaction of coal powder or ore powders from flotation processes (Volckaert et al., 1996). With a pilot size facility it is possible to produce 1 to 2 ton/h of this material. So it is possible to produce in a very cost effective way large quantities of this material. The pellets are mixed with powder in a 50/50 ratio and in this way a material with a mean dry density of 1.5 to 1.6 g/cm³ can be obtained. The mixture can be further densified by vibro-compaction techniques as used in road construction. This makes this technique interesting for backfilling of large volumes. This technique will be applied in the RESEAL project to seal the 'experimental shaft' in the HADES underground research facility (Volckaert et al., 1998) in Mol.

Also mixtures of bentonite with sand and/or graphite have been proposed. Sand is in general added to reduce the swelling pressure (or to make the product cheaper), while graphite is added to increase the thermal conductivity, which is of prime importance for a buffer material to be used around heat generating HLW. A mixture of 60 % FoCa clay with 35 % sand and 5 % graphite is currently being tested in the PRACLAY mock-up experiment (Van Caueren et al., 1998).

For the backfilling and sealing of the TRUCK II concept proposal, the following materials could be used in the different parts of the repository:

- The disposal cell

For backfilling and sealing the disposal cell, bentonite based materials are probably the most suitable because if water infiltrates through the cell liner, the bentonite will swell and seal the cell. One needs however to study carefully the hydrothermal conditions that will govern in the disposal cell close the HLW canisters. It is well known that unsaturated bentonite in the presence of steam can lose quickly most of its favourable properties i.e. swelling, permeability, specific surface (Couture, 1985a&b; Oscarson and Dixon, 1989; Push, 1987). Therefore it might be necessary to add graphite to the

bentonite to increase the thermal conductivity and thus ^{decrease} the maximum temperature, and to use bentonite block with a high initial degree of saturation.

Another possibility could be to install temporary plugs made of barite concrete cast in stainless steel drums that are removed at the end of the retrievability period when the whole repository has to be sealed. At that time the heat output of the HLW will have diminished and thus the temperatures around the HLW will be much lower and thus bentonite can be used in a much safer way.

- The secondary galleries

As these galleries are still rather close to the waste, it is not advisable to use a cement-based material for backfilling because the alkaline plume of the backfill might reach the vitrified HLW. Therefore clay-based materials would be a better choice. It would also be possible to backfill the galleries with any inert, geomechanical and geochemical stable material (e.g. sand, gravel) and to install clay based seals at the connection with the primary galleries.

- The primary galleries

As they are at a rather large distance from the waste, cement based materials could be used as well as any inert, geomechanical and geochemical stable material (e.g. sand, gravel). Also in this case, clay seals could be installed at the interconnection with the shafts.

- The shafts

The shafts could be backfilled in the same way as the primary galleries.

3.6. References

- Couture R.A. 1985a. Steam rapidly reduces the swelling capacity of bentonite. *Nature*, **318**: 50-52.
- Couture R.A. 1985b. Rapid increases in permeability and porosity of bentonite-sand mixtures due to alteration by water vapor. *Mat. Res. Soc. Symp. Proc.*, **44**: 515-522.
- Giraud A. 1993. Couplages thermo-hydro-mécaniques dans les milieux poreux peu perméables : application aux argiles profondes. *Thèse de doctorat de l'Ecole Nationale des Ponts et Chaussées*.
- Heijdra J.J., Bekkering J., Gaag J.V.D., Kleyn P.H.V.D & Prij J. 1995. Retrievability of radioactive waste from a deep underground disposal facility. *Report EUR-16197, Commission of the European Communities*, Luxembourg.
- Itasca, 1997. *FLAC 3D Users's Manual*. Itasca Consulting Group, Inc.
- Labiouse V. and Giraud A. 1998. Analytical solutions for undrained response of a poro-elasto-plastic medium around a cylindrical opening. *Poromechanics, Thimus et al. (eds)*, Balkema, Rotterdam: 439-444.
- Oscarson D.W. and Dixon D.A. 1989. The effect of steam on montmorillonite. *Applied Clay Science*, **4**: 279-292.
- Panet M. 1995. Le calcul des tunnels par la méthode convergence-confinement. *Presses de l'Ecole Nationales des Ponts et Chaussées*, Paris.
- Push R. 1987. Permanent crystal lattice contraction, a primary mechanism in thermally induced alteration of Na-bentonite. *Mat. Res. Soc. Symp. Proc.*, **84**: 791-802.

- Van Cauteren L., De Bruyn D., Verstricht J. 1998. PRACLAY: Preliminary demonstration of disposal in clay, Mock-up and shaft sinking. *European Commission, Nuclear science and technology, In situ testing in underground research laboratories for radioactive waste disposal*, Proc. Of a Cluster seminar held in Alden Biesen, Belgium, 10 and 11 December 1997, Luxembourg, EUR 18323.
- Van de Steen B. and Vervoort A. 1998. *Mine design in clay*. CORA-project TRUCK-I, K.U.Leuven.
- Volckaert G., Bernier F., Dardaine M. 1996. Demonstration of the in situ application of an industrial clay-based backfill material (BACCHUS 2). *European Commission, Nuclear science and technology*, Luxembourg, EUR 16860.
- Volckaert G. et al. 1998. RESEAL: A large scale in situ demonstration for Repository SEALing in an argillaceous host rock. *European Commission, Nuclear science and technology, In situ testing in underground research laboratories for radioactive waste disposal*, Proc. Of a Cluster seminar held in Alden Biesen, Belgium, 10 and 11 December 1997, Luxembourg, EUR 18323.

4. Procedure for retrieval of a HLW canister

4.1. Disposal and retrieval of a HLW-canister without overpack

Before the HLW-canister is placed in the disposal cell, the lining should be checked for leakage. A shutter system is installed at the entrance of the disposal cell. This shutter system provides shielding during the disposal operation. The transport vehicle carrying the HLW-canister (in a transport container) is positioned in front of the disposal cell. The bolt of the transport container and the bolt of the shutter system are connected. This situation is shown in the upper part of Figure 4.1.

The shutters of the transport container and the disposal cell are opened. The HLW-canister is pushed into the disposal cell, and is placed on the ramps at the end of the cell. This operation is shown in the lower part of Figure 4.1. Once the container is in place, and the telescopic arm of the transport vehicle is retracted, the shutter to the disposal cell is closed, and new equipment is positioned in front of the disposal cell.

In the same way as described above for the container, a plug with a gap for injecting the quartz sand is placed in the disposal cell. The quartz sand is injected using a hollow pipe, and the voids surrounding the canister are filled. This is shown in the upper part of Figure 4.2. The air expelled during this operation should be monitored for possible radioactive contamination.

The remaining void space in the disposal cell has to be filled with backfill plugs. Bentonite could be used as it meets the requirements given in Chapter 3.5.1. However, other possibilities should be investigated. The last plug should be made to fit. This is shown in the lower part of Figure 4.2. The shutter system can then be removed and the disposal cell sealed with a steel plate. The situation is then as shown as in Figure 3.14.

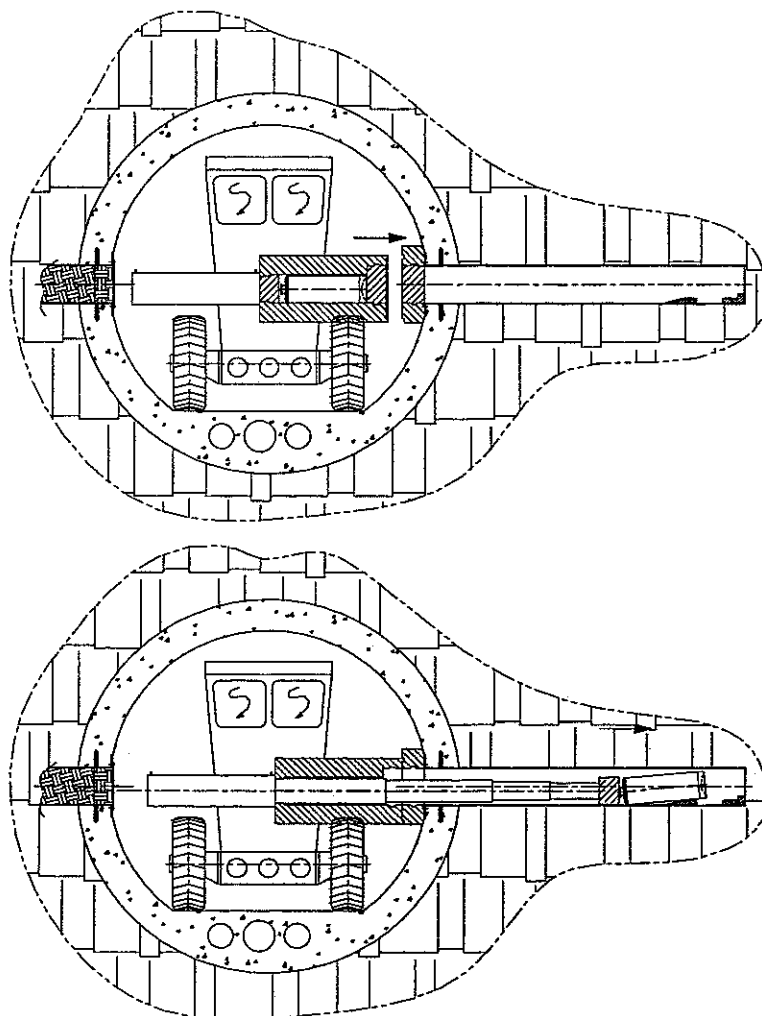


Figure 4.1. Disposal of a HLW-canister without overpack.

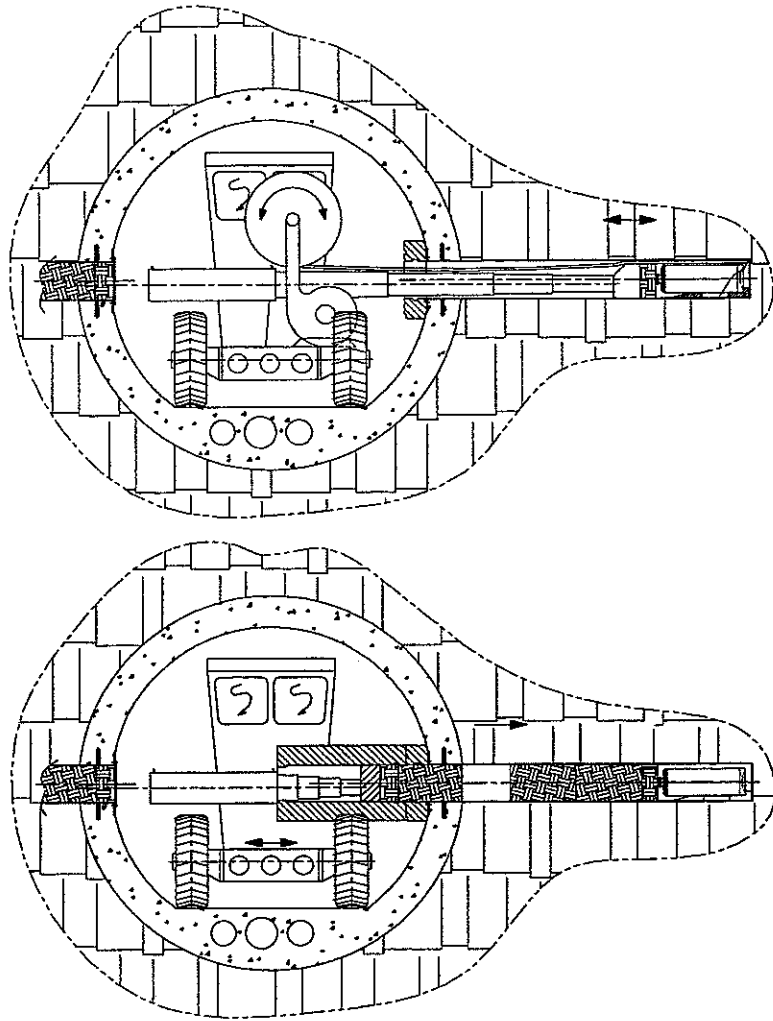


Figure 4.2. Disposal of a HLW-canister without overpack.

The retrieval of the HLW-canister starts with the removal of the steel plate from the disposal cell. The shutter system is then re-installed at the entrance of the disposal cell. The backfill is removed as shown in the upper part of Figure 4.3, until only about 20 cm of the backfill and the quartz sand remains. These materials are removed using a ring shaped high pressure hose, as shown in the lower part of Figure 4.3.

The transport vehicle with the transport container is placed in front of the disposal cell. A hydraulic telescopic arm, fitted with an appropriate end-piece, is used to grab the HLW-container and pull it into the transport container. This is shown in Figure 4.4.

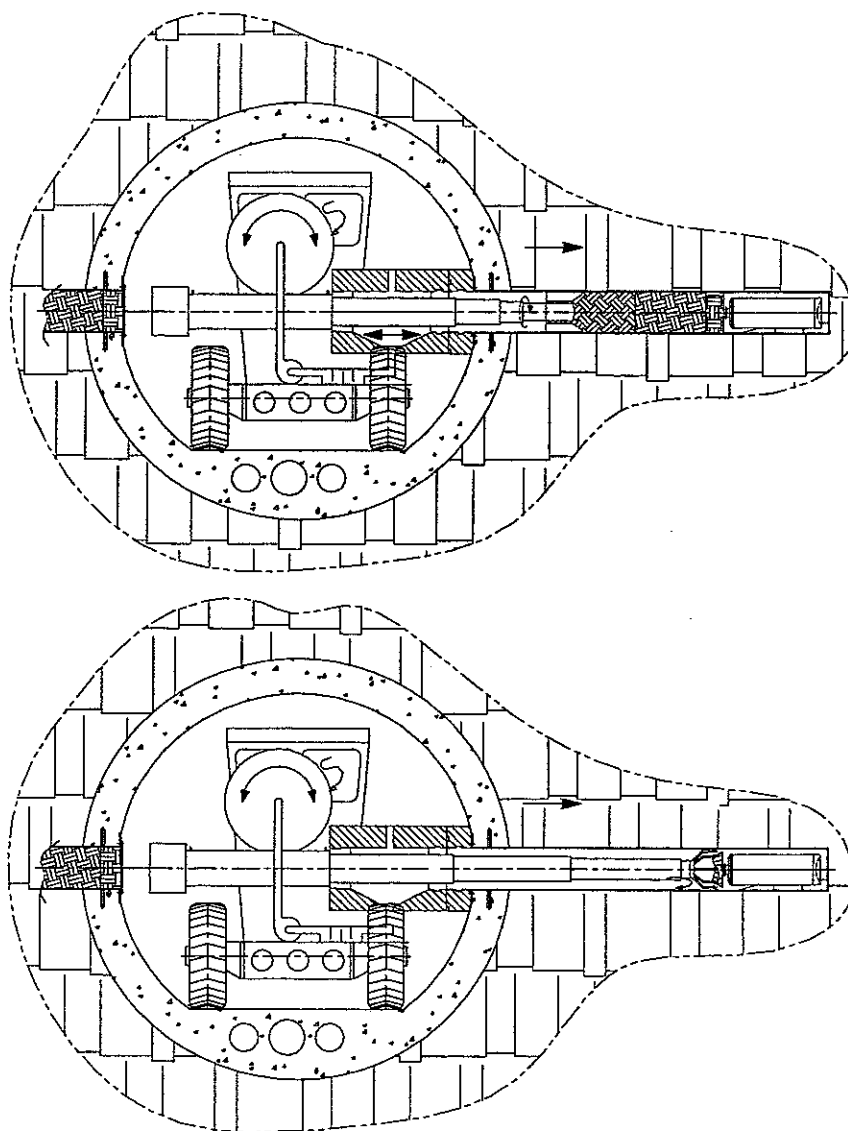


Figure 4.3. Retrieval of the HLW container without overpack.

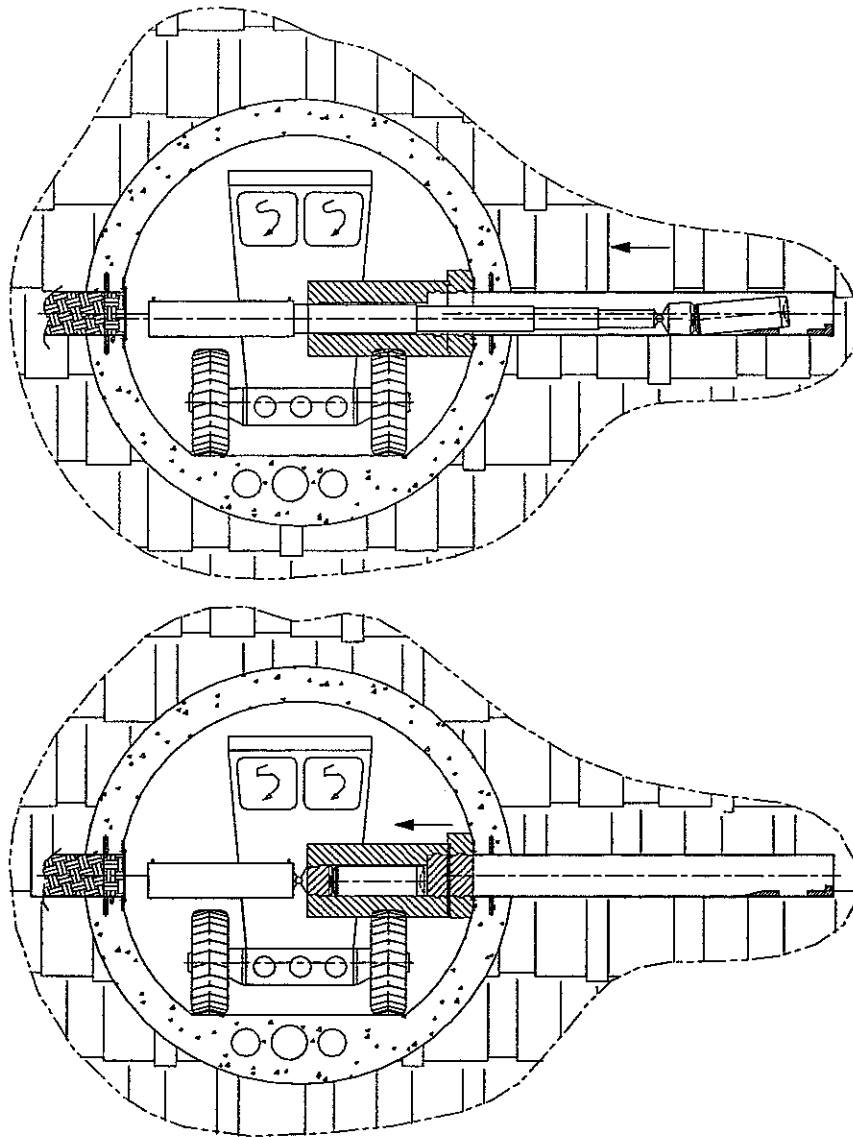


Figure 4.4. Retrieval of a HLW container without overpack.

4.2. Disposal and retrieval of a HLW-canister with overpack

The construction of a watertight lining in the disposal cell can be avoided if the canister is placed in an overpack. The wall thickness of the overpack should be at least 3 cm, and the material used should be resistant to corrosion caused by contact with the pore water in the clay. In addition, the overpack can be equipped with a grip for handling the container, just like the HLW-canister.

Before placing the container, possible support constructions used to preserve the integrity of the disposal cell are removed and a shutter system is installed at the entrance to the cell. The transport container, containing the overpacked HLW-canister, is positioned in front of the disposal cell. The shutters are opened, and the container is pushed into the disposal cell, using a kind of 'sledge' to

ensure that the container does not get stuck at the of the raised edge near the back of the disposal cell. This is shown in Figure 4.5.

Once the container is in place, and the telescopic arm of the transport vehicle is retracted, the shutter to the disposal cell is closed, and new equipment is positioned in front of the disposal cell. In a similar fashion as for the container, the backfill plugs are pushed into the disposal cell. This is shown in the upper part of Figure 4.6. Finally the shutter system is removed and the disposal cell is closed with a steel plate. This is shown in the lower part of Figure 4.6.

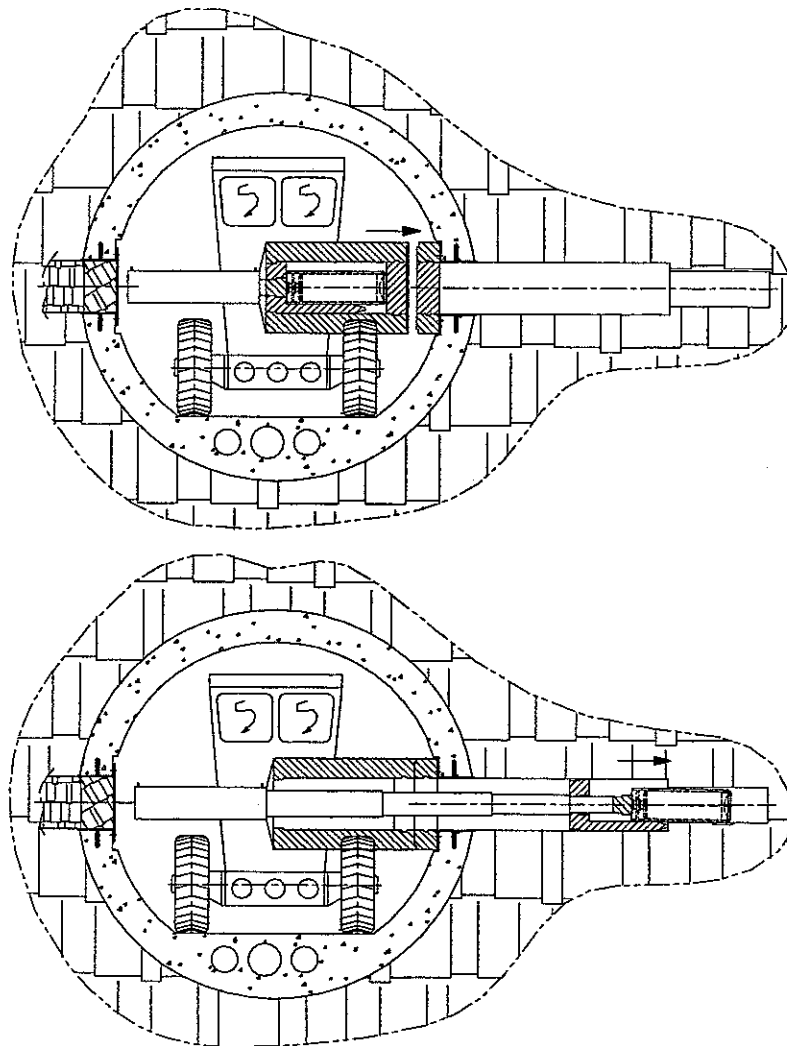


Figure 4.5. Disposal of a HLW-canister with overpack.

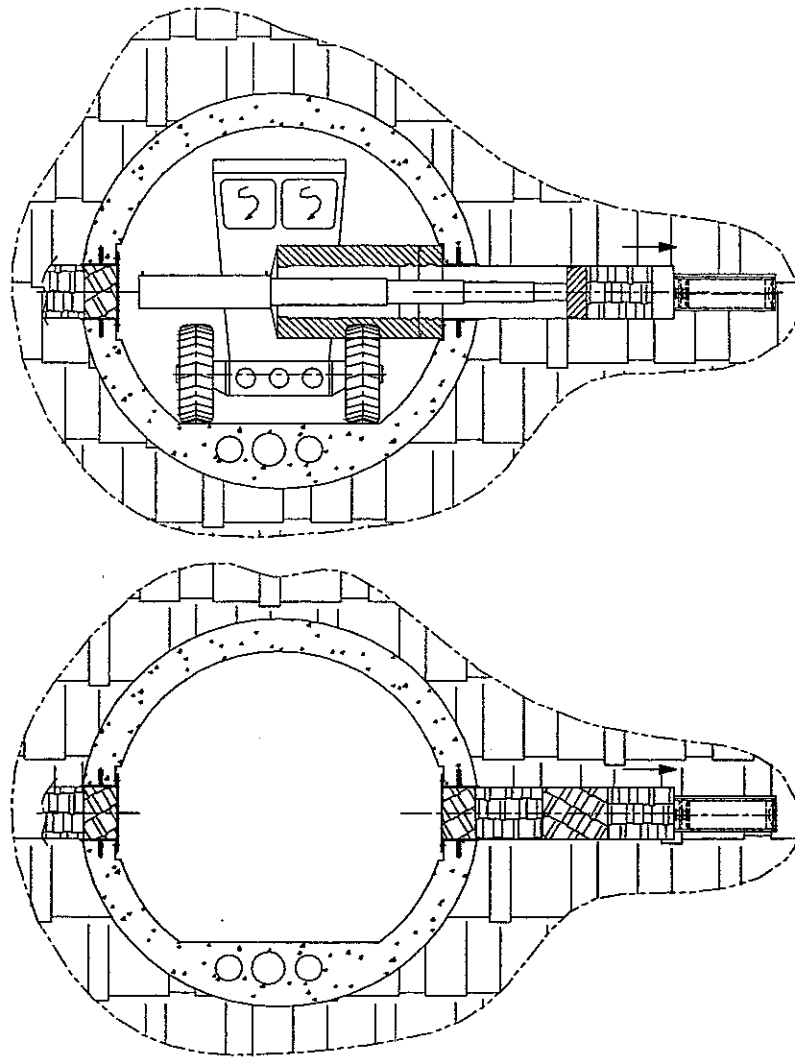


Figure 4.6. Disposal of a HLW-canister with overpack.

Removal of the HLW-canister with overpack starts with removing the steel plate from the disposal cell, and re-installing a shutter system. A vehicle with the machinery to remove the backfill is located in front of the disposal cell. The backfill is removed by jacking forward a steel pipe into the clay, and then pull out this pipe and its contents. It is difficult to guide the pipe during jacking in the proper direction. Some provisions to better guide the pipe may be needed, e.g. a ring of small bore holes that will guide the pipe.

The pipe jacking technique is shown in Figure 4.7. It is not necessary to put the backfill so removed into a shielded transport container. However, the same device is used to retrieve the container with the HLW-canister, as shown in Figure 4.8. For this, the shielding transport container is necessary.

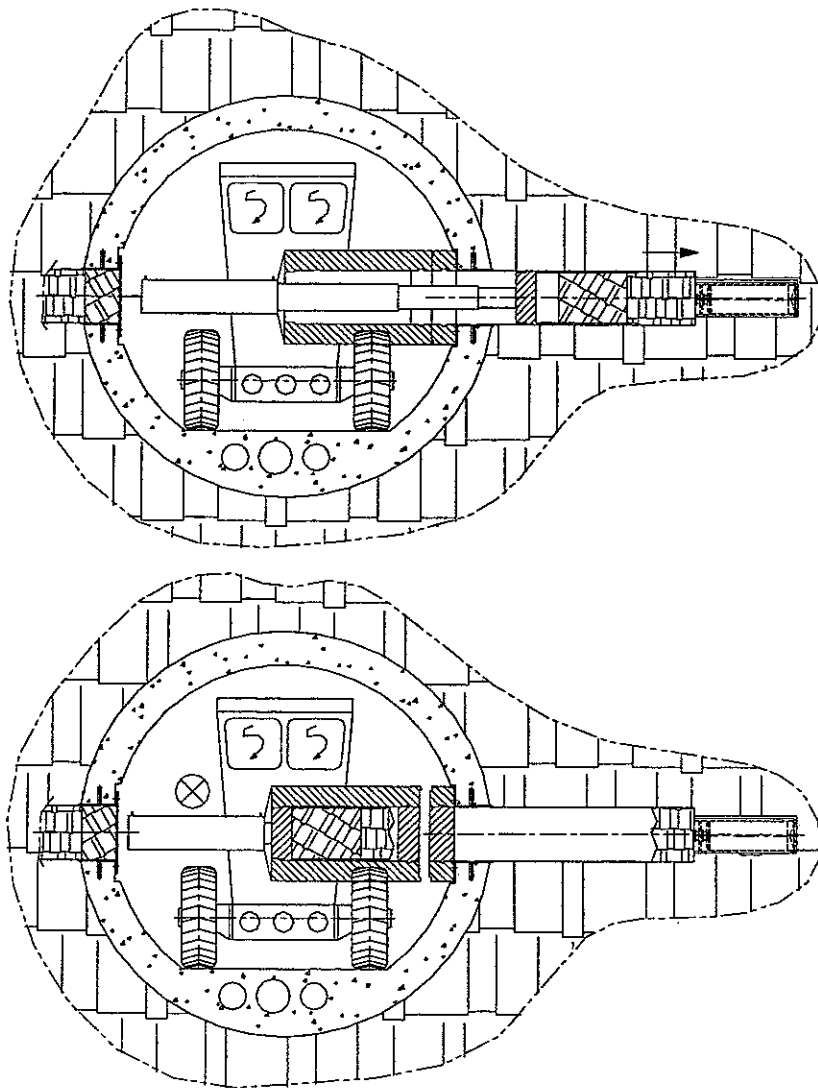


Figure 4.7. Retrieval of a HLW-canister with overpack.

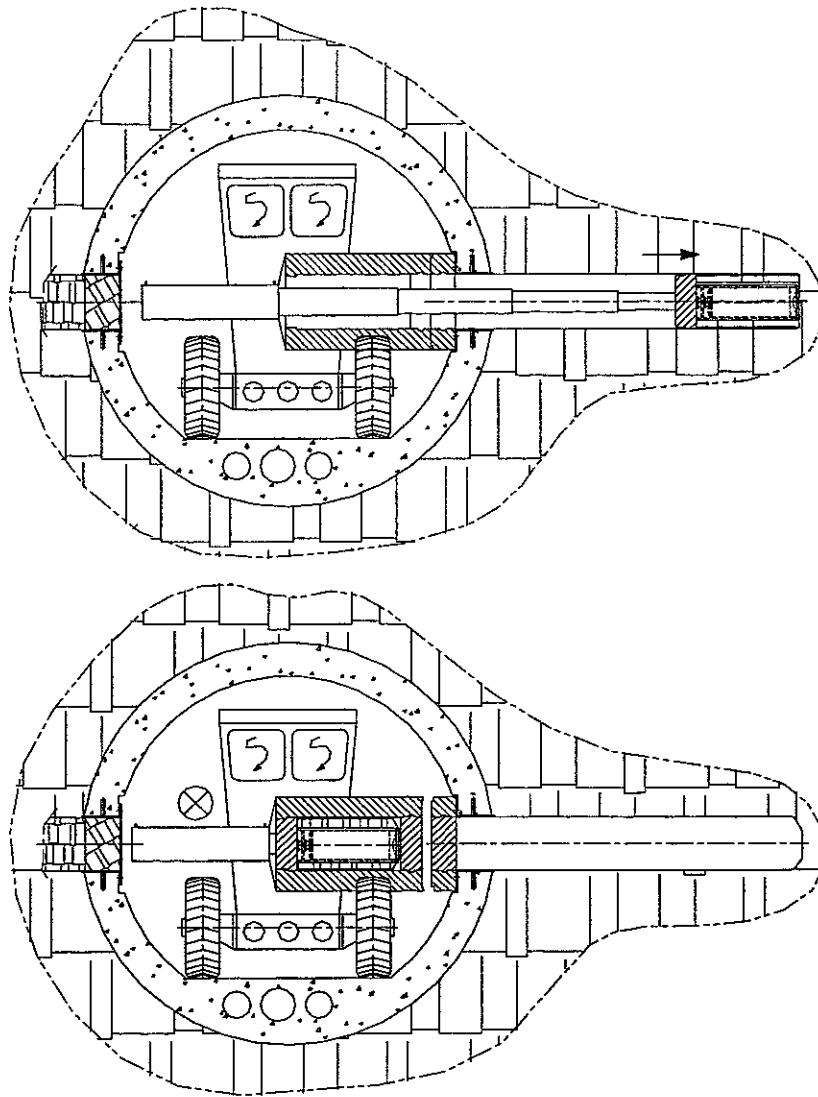


Figure 4.8. Retrieval of a HLW-canister with overpack.

4.3. Further considerations

4.3.1. Radiation protection

The radiation level from the HLW-canisters is very high. Shielding is therefore needed at all times to provide protection for the workers. Therefore, remote control of some devices is foreseen. For example the shutter system and the telescopic devices need remote control. In addition, facilities must be available for decontamination of liquids, gases and tools that have been in contact with the HLW-canister.

The level of radiation should be monitored continuously. Further, emergency procedures must be developed for this design. These procedures prescribe any action that must be performed in case of an emergency. In such a situation it must be possible to restore the situation to normal, without exposing workers to unacceptable levels of radiation. Such emergency procedure will probably be similar to procedures developed for surface (interim) storage, transport of canisters, and packaging of the waste. If the repository design is developed further, such procedures have to be accounted for, and provisions have to be incorporated in the final design.

4.3.2. *Generic designs*

The proposed designs should be regarded as initial, generic designs. It is anticipated that, in a future research programme, the designs will be modified or even dismissed. The main purpose was to develop a design that in principle allows retrieval of the waste.

4.3.3. *Damage to the overpack or to the lining of the disposal cell*

The HLW-container should be isolated by a watertight construction from any water present in the clay. However, it cannot be excluded that the integrity of the watertight construction will be violated and that leakage will occur. A large variety of events could cause such damage, e.g. the lithostatic pressure, corrosion, a seismic event, construction defects, or a design error.

In complement to the information already provided in section 3.5, some other considerations should be taken into account:

- All voids inside the watertight lining or inside the overpack should be filled (for example with quartz sand) to increase the resistance to the lithostatic pressure.
- The use of buffer materials inside the disposal cell or overpack should be considered. For instance, the backfill plugs placed inside the lining could contain bentonite. This material absorbs water and swells up, and could decrease the leakage rate.
- The dimensions of the disposal cells and the tools to retrieve the HLW-container should allow for some degree of deformation without unduly complicating the retrieval.
- There should be a backup procedure for retrieval if the normal procedure fails; for example should the handling grip on the waste container break.

4.3.4. *Monitoring*

The development of sensors that can be placed inside the disposal cell (for example to detect water intrusion) should be considered. Information from these sensors could be important in a possible future decision on whether measures must be taken to ensure continuing the option of retrieving the waste. This is an important subject for further study.

5. Cost estimate of a disposal facility in clay

5.1. Introduction

In the framework of the OPLA program, generic designs for disposal facilities have been developed. The cost estimates for these designs were published in (Van Hattum and Blankevoort, 1986): "Locatie-onafhankelijke studie inzake de aanleg, bedrijfsvoering en afsluiting van mogelijke faciliteiten voor de definitieve opberging van radioactief afval in steenzoutformaties in Nederland". These designs were developed for disposal in a salt formation, and retrievability was not explicitly accounted for in the design. However, a large part of the generic design is similar to the TRUCK-II design. For these parts the cost estimates published in (Van Hattum and Blankevoort, 1986) are used, only accounting for the devaluation of the value of the Dutch guilder between 1986 and 1994.

Another source of data is (Heijdra et al., 1995): "Retrievability of radioactive waste from a deep underground disposal facility". This report gives generic cost estimates for large-scale disposal facilities for disposal in salt, in clay, and in granite formations.

The NEA report *The cost of high-level waste disposal in geological repositories* (NEA, 1993) is used as a guideline for presenting the results of the cost analysis. There are two important recommendations in this NEA report:

- present the cost estimates in a breakdown of the disposal project into five separate activities:
 1. Research and development,
 2. Site screening and evaluation,
 3. Construction of the facility,
 4. Operation of the facility,
 5. Decommissioning and closure,
- to avoid complications with (unknown) future inflation and interest rates, use only undiscounted costs in price value of a given year and a given currency.

In the present TRUCK-II study, this breakdown in cost estimates has been used and all costs have been presented in Dutch guilders, price value 1994. Undiscounted (future) costs have been calculated by assuming an inflation rate of 0 % per year and a real interest rate of 0 % per year: i.e. a constant money value of the year 1994.

5.2. Cost estimates per phase in the disposal process

5.2.1. Costs of research and development

This activity starts at the same time as the site screening and evaluation. However, differently ^{ing s-} than the other activities that are more or less subsequent, research and development continues until the facility is decommissioned and closed.

The costs of this activity depend on the policy, the legal system and social factors. An inventarisation of these costs in (NEA, 1993) shows large variations for different countries. The summarised costs of 'research and development' and 'site screening and evaluation' vary from 100 M\$ to 8100 M\$ (price value 1994).

These activities have not been incorporated in previous cost estimates for The Netherlands (Van Hattum and Blankevoort, 1986; Heijdra et al., 1995).

5.2.2. Costs of site screening and evaluation

This activity comprises the identification of potential sites (site screening) followed by detailed investigation at one or more preferred sites. The costs of this activity are very much depending on legal, political and societal factors. As stated in section 5.2.1, no cost estimate is available for the Dutch concepts for a disposal facility.

5.2.3. Costs of construction of the facility

5.2.3.1. Surface constructions

For the generic designs it is reasonable to assume that the costs of the surface constructions are equal for a disposal facility in clay or in salt. The costs of the surface constructions for disposal in a salt rock formation is estimated in (Van Hattum and Blankevoort, 1986). Table 5.1 gives the cost estimate for surface constructions as in (Van Hattum and Blankevoort, 1986).

The total cost (value 1985) is Mfl 43.8. Expressed in the value for 1994 this is about Mfl 60 (inflation rate of 3 % per year).

Table 5.1. Costs of surface constructions (from Van Hattum and Blankevoort, 1986).

Activity	breakdown	Costs (Mfl), value 1985
Preparing the site for construction		9
Storage facilities for waste		6
	Waste treatment; hot cells	
	Waste administration system	
	Radiation control 'dienst'	
	Monitor stations	
	Decontamination facilities	
	Research stations	
Equipment for business administration		7
Facilities for electrical supply		2.5
	'transformator station'	
	emergency supply	
Water supply		0.2
Means of transport		1
Means of communication		2.5
Miscellaneous		15.3
	Security	
	Waste reception facility	
	Workshops	
	Offices	
	Restaurant	
	First aid	
	Public information	
	Fire brigade	
	Storage rooms for oil, clay, etc.	

5.2.3.2. Shafts

The cost estimates contain sinking of the shafts, constructing the shaft foundation and the lining, furnishing the shafts and installing the hoist system and buildings. The shafts are built by a private company, and the personnel costs are included in the price of the shafts.

Cost estimate in (Van Hattum and Blankevoort, 1986)

The costs of one shaft with a diameter of 5 m to a depth of 850 m are estimated as Mfl 50 (value 1985): for value 1994 this is about Mfl 65. In (Van Hattum and Blankevoort, 1986) the shafts are only partly built in unconsolidated rock (the salt rock is consolidated). However, construction of the shafts to a clay layer encompasses sinking in unconsolidated rock only, which is likely to be more expensive.

Cost estimate in (Heijdra et al., 1995)

The costs of sinking one shaft (diameter 5 m) to a clay layer at a depth of 250 m are estimated Mfl 61. The underlying calculation in (Heijdra et al., 1995) can be summarised by a fixed amount of Mfl 12, and an amount that depends on the depth of the shaft: kfl 196 per meter. For the TRUCK-II design the facility is at 500 m depth, so the costs of one shaft are Mfl 110.

In (Heijdra et al., 1995) the cost is almost linear with the depth. However, another source (van de Gaag, 1990) refers to a rule of thumb that claims that the costs of the shafts grow with the depth to the (at least) third power. If the cost of a shaft to 250 m is about Mfl 60 (estimate from Van Hattum and Blankevoort, 1986, and from Heijdra et al., 1995), the cost of a shaft with a depth of 500 m is Mfl 480.

In the TRUCK-II design two shafts are foreseen, so the total costs of the shafts is estimated between Mfl 220 and Mfl 1000. *→ Cost: 2nd HANCOCK-1-10?*

5.2.3.3. Underground infrastructure; tunnelling

The underground infrastructure largely exists of tunnels. These tunnels are excavated, e.g. by a tunnelling machine, and have to be supported by a lining. The most cost effective is a concrete lining. As a rule of thumb the thickness of a concrete lining should be 10 % of the internal diameter to obtain sufficient support. In the TRUCK-I design (Van de Steen and Vervoort, 1998), the wall thickness is larger than 10 % of the internal diameter.

Since underground constructions in clay are a priori more expensive, no special excavations for workshops, etc. are foreseen; it is assumed that most of the repair and maintenance work can be done at the surface.

A starting point for the cost estimate is given in (Heijdra et al., 1995). Sheet 5.1.3 (page 203 in Heijdra et al., 1995) gives the cost for tunnelling of galleries with internal diameters 3 m and 3.5 m. Using this estimation strategy, the costs for tunnelling a gallery with an internal diameter of 5 m has been determined. The cost estimates are shown in Table 5.2, based on a tunnelling rate of 0.5 m/h.

Table 5.2. Cost estimates of tunnelling taken from (Heijdra et al., 1995).

internal diameter	3 m	3.5 m	5 m
labour	550	550	550
lining (concrete)	2400	3200	6400
machine	50 ₊	50 ₊	50 ₊
Cost/metre (Hfl/metre)	3000	3800	7000

Further, the cost of each junction in the galleries is estimated Hfl 165 000 (sheet 5.1.5 in Heijdra et al., 1995).

In the following paragraphs the breakdown of the costs is discussed in some detail.

Tunnelling machine

The estimated cost of the tunnelling machine in (Heijdra et al., 1995) is Hfl 1 140 000, based on information of James Howden and Company. Normally a tunnelling machine is customised, and the price is agreed through negotiations with the manufacturer.

Prices of used tunnelling machines have been obtained from TBM Exchange International (www.tbmexchange.com). An overview of the asked prices (used machine) and the estimated new prices is given in Table 5.3.

Table 5.3. Estimated price of various tunnelling machines.

Manufacturer	Diameter (m)	Price (second hand machine)	Estimated new price
American Auger (1994)	2.42	\$ 200 000	\$ 300 000 - 400 000
RLM (1993)	2.79	\$ 350 000	\$ 400 000 - 700 000
Lovat (<1985)	2.9	\$ 285 000	\$ 500 000 - 800 000
James Holden (Backhoe)	3 - 3.5		\$ 500 000
Lovat (1974)	3.34	\$ 250 000	\$ 750 000 - 1 250 000
(Backhoe digger)	3.4	\$ 174 000	\$ 750 000 - 1 250 000
Akkerman (1993)	4.26	\$ 525 000	\$ 750 000 - 1 500 000

The estimate in (Heijdra et al., 1995) of the price of the tunnelling machine seems relatively low. Intuitive extrapolation of Table 5.3 to tunnelling machines of diameter of 6 m results in an estimate from \$ 1 250 000 to \$ 2 500 000, i.e. Hfl 2 000 000 to Hfl 6 000 000. Note that the machine probably would have to be designed specifically for this task. Such design would take about 3 man-years, in costs about Hfl 1 000 000.

The cost estimate for the machine in Table 5.2 includes the price of the machine and fuel and maintenance when it is operated. However, even if the machine costs in Table 5.2 is multiplied by 6 (extrapolated from Table 5.3 the tunnelling machine could be 6 times more expensive than estimated in Heijdra et al., 1995) this still gives only a small contribution to the total costs of tunnelling.

Labour costs

Labour costs are estimated Hfl 275 per hour in (Heijdra et al., 1995). These are the labour costs for about two workmen. We expect that about 5 to 10 workmen are needed for operating a tunnelling machine. This would result in estimated labour costs of Hfl 800 to Hfl 1600 per hour. The progress rate of tunnelling is estimated as 0.5 m per hour (as in Heijdra et al., 1995). The estimated labour costs per meter are Hfl 1600 to Hfl 3200.

Lining

The estimate of the costs of the lining are based on the cost of 1 m³ concrete blocks: in (Heijdra et al., 1995), this is Hfl 750 per m³. Plain concrete grout would cost about Hfl 100 per m³. However, concrete blocks for supporting constructions are much more expensive: these would cost Hfl 1300 to Hfl 1600 per m³ (DACE, 1994: 'betonwanden, stabiliteitswanden').

In Table 5.4, the resulting cost estimates for the tunnel diameters used in the TRUCK-I and TRUCK-II design are listed. If the length of the tunnels is taken into account (at least a few hundreds of meters for each tunnel dimension), it is obvious that the cost of the concrete lining dominates in the cost estimate.

Table 5.4. Lower and upper cost estimates for various tunnel dimensions.

type	diameter (m)		concrete costs (kfl/m)		labour costs (kfl/m)		tunnelling machine (kfl)	
	internal	external	lower	upper	lower	upper	lower	upper
S1	5	6	11	14	1.6	3.2	2000	6000
P1	4.3	5.4	11	13	1.6	3.2	2000	6000
P/S	3.5	4.6	9	11	1.6	3.2	1500	3000
T	2.2	3.2	6	7	1.6	3.2	750	1250

Length of the tunnels

The underground disposal facility is divided in a shaft area and three disposal fields: a disposal field for high level vitrified waste, a disposal field for medium level waste and a disposal field for other high level waste. For the cost calculation, the layout of the high level field presented in TRUCK-II is used, and the other parts of the facility are taken from TRUCK-I (Van de Steen and Vervoort, 1998).

In TRUCK-I four sections have been distinguished: the primary layout, the heat-generating-HLW (vitrified waste) field, a field for the non-heat-generating-HLW, and a field for MLW. The characteristics of these sections are summarised in Table 5.5. Further, the costs of each junction in the galleries is estimated Hfl 165 000 (sheet 5.1.5 in Heijdra et al., 1995).

Table 5.5. Length of the tunnels and number of junctions per section of the facility.

	canisters	S1	P1	P	S	T	junctions
primary layout			388	5086			4
heat generating HLW field	300	1000 to 3000		0 to 300			2 to 6
non-heat generating HLW	1260			2700	27000	32400	648
MLW field	56288			1600	16000	19200	384

For the heat generating vitrified waste, 4 different layouts have been considered. The option with the smallest length (1000 m) of the tunnels of type S1 can be used for vitrified waste that has been in interim storage for at least 100 years. The largest length (3000 m) is found for waste that has been in interim storage for 50 years. However, this length can be reduced to 2000 m in another layout option.

Cost estimate for the underground infrastructure

Table 5.6 shows the estimated costs of the underground infrastructure. The costs of the junctions and tunnelling machines are included in the estimate, although their contribution is negligible. The cost of the concrete lining of the tunnels is dominating the cost estimate. Therefore, the total tunnel length of each section is included in the Table 5.6.

Table 5.6. Cost estimates for the underground infrastructure.

	total tunnel length (km; rounded)	lower cost estimate (Mfl)	upper cost estimate (Mfl)
primary layout	5	59	80
heat generating HLW	1 - 3	13	55
non heat generating HLW	62	530	720
MLW field	37	310	430
Total	107	912	1285

Note that the disposal field for heat generating HLW has been optimised in TRUCK-II, while the other sections are equal to the concept presented in TRUCK-I and have not been optimised.

5.2.3.4. Personnel costs during operation and construction

In (Van Hattum and Blankevoort, 1986) the personnel costs (personnel and management costs plus all incidental expenditures) of the waste management organisation in this phase is estimated Mfl 121. This is based on an estimated need of manpower of 840 worker-years.

5.2.4. Costs of operation of the facility

'Operation' is the packaging and disposal of the waste. Special attention has been given to the packaging of the heat generating HLW. It was anticipated that the cost of the disposal cell increases significantly if the waste package without overpack was placed in a disposal cell, because this would require a watertight lining. Because the watertight lining in principle can replace the overpack, these costs have been incorporated in the 'operation' activity.

5.2.4.1. Cost of a watertight lining of a disposal cell

The disposal cell should allow reasonably easy retrieval of the canister. An option is to construct a disposal cell with a watertight lining. The lining should have a wall thickness of at least 25.4 mm to be able to resist the lithostatic pressure at 500 m depth. Further, stainless steel should be used because of the clay water and the concrete lining.

Cost estimate of lining for heat generating HLW

Cost element	Estimated cost
Cost of the stainless steel pipe (24", w=25.4, L=4500 mm RVS316L)	kfl 21.5
Other materials (lids, etc)	kfl 15
Labour costs for assembling the materials (welding etc.)	kfl 3
Labour cost of underground installing the lining	kfl 7.5
Total per disposal cell	kfl 47
Total: disposal cells for 300 HLW canisters	Mfl 14

5.2.4.2. *Packaging and disposal of the waste*

If no watertight lining is constructed, the container may be packed in an overpack.

Cost estimate of overpack for heat generating HLW.

Cost element	Estimated cost
Pipe (D=510mm; w=30mm; L=1300 mm; RVS 316L)	kfl 5.5
Other materials	kfl 10
Assembling labour costs	kfl 19.5
Total cost per canister	kfl 35
Overpack for 300 canisters	Mfl 10.5

The assembling costs are relatively large, because the overpack does not provide sufficient shielding from the radiation. Part of the assembling must be done by remote control, which is more expensive.

The labour costs of placing the HLW container in the disposal cell and backfilling/sealing the cells are estimated as kfl 10. Therefore, the total cost for placing 300 HLW canisters are estimated to be Mfl 3.

No detailed design for the disposal cells for the non-heat generating HLW (1260 canisters) and the MLW (approximately 56000 canisters) has been developed in TRUCK-II. Therefore it is not known what the costs for a possible overpack are. These costs have not been included in the estimate.

5.2.4.3. *Personnel costs during disposal operation*

In (Van Hattum and Blankevoort, 1986), the personnel costs (personnel and management costs plus all incidental expenditures) of the waste management organisation in this phase is estimated Mfl 89. These costs include the personnel costs for disposal of the HLW and MLW waste. The amount is based on an estimated need of manpower of 600 worker-years.

5.2.4.4. *Prolonged operation without disposal*

In (Grupa and Jansma, 1999) the costs of prolonged operation of a disposal facility in salt rock have been estimated. The estimated costs were the costs of an organisation that takes care of the technical maintenance of the facility to keep the underground structures accessible. We assume that these costs are the same for clay. The costs are summarised in Table 5.7.

Table 5.7. Yearly costs for prolonged operation without disposal.

Cost breakdown	Cost estimate (kfl/year)
Personnel (14)	1460
Ventilation (electricity)	120
Maintenance (shafts and tunnels)	160
Depreciation (buildings, machinery, equipment)	1500
General costs (office, etc)	186
Monitoring (environmental) and inspections	260
Total	3700

The yearly costs for prolonged operation without disposal are (rounded) Mfl 4 (considering that pumping activities have been neglected). However, this is an estimate of the costs of an organisation for minimal technical maintenance. It is reasonable to expect that social and political demands (e.g. extensive test- and monitoring programs) may increase these costs significantly.

5.2.5. *Costs of decommissioning and closure*

In (Van Hattum and Blankevoort, 1986) these cost are estimated Mfl 79, excluding personnel costs of the waste management organisation in this phase. The activities in this task are backfilling and sealing of the tunnels and shafts, and decommissioning and clearing of the surface constructions. This is not (much) host rock dependent, so this estimate is also used for the TRUCK designs.

In (Van Hattum and Blankevoort, 1986), the personnel costs (personnel and management costs plus all incidental expenditures) of the waste management organisation in this phase is estimated to be Mfl 29. This is based on an estimated need of manpower of 200 worker-years.

5.3. **Results**

An overview of the results of the cost estimate is presented in Table 5.8. The breakdown of the disposal project into five activities is in accordance with guidelines provided by the Nuclear Energy Agency (NEA, 1993). Further, each activity is broken down in sub-activities in accordance with the corresponding sections in this report.

It is recalled that, to avoid complications with (unknown) future inflation and interest rates, only undiscounted costs in price value of a given year (1994) and a given currency (Dutch guilders) have been used.

5. Cost estimate of a disposal facility in clay

Table 5.8. Overview of the estimated costs.

Activities in the project	Cost estimate (value 1994)	
	Total	breakdown
Research and development	no cost estimate	
Site surveillance and evaluation	no cost estimate	
Construction of the facility	Total: Mfl 1320 - Mfl 2480	
Surface constructions		Mfl 60
Construction of two shafts		Mfl 220 - Mfl 1000
Construction infrastructure (several variants)		Mfl 920 - Mfl 1300
<i>primary layout:</i>	Mfl 59 - 80	
<i>heat generating HLW:</i>	Mfl 13 - 55	
<i>non-heat-generating HLW:</i>	Mfl 530 - 720	
<i>MLW field:</i>	Mfl 310 - 430	
Personnel costs waste management organisation		Mfl 121
Operation of the facility	Total: Mfl 100 - Mfl 115	
Watertight lining of 300 disposal cells (optional)		Mfl 14
Overpack for 300 canisters (optional)		Mfl 10.5
Cost for placing 300 HLW canisters		Mfl 3
Personnel costs waste management organisation disposal		Mfl 87
Prolonged operation without disposal	at minimum Mfl 4 per year	
Decommissioning and closure	Total: Mfl 108	
Backfill, sealing, clear site		Mfl 79
Personnel costs waste management organisation		Mfl 29
Total	Mfl 1530 - Mfl 2700 plus at minimum: Mfl 4 per year of prolonged operation	

5.4. Comparison with the cost estimate provided by Belgium (SCK•CEN and ONDRAF)

To evaluate the result of the cost estimate, a comparison is made (see Table 5.9) with the cost estimates in (NEA, 1993) for disposal in clay. The design in (NEA, 1993) can accommodate 52 000 canisters using about 38 km of tunnels, while the TRUCK-II design can accommodate about 57 000 canisters, but uses about 110 km of tunnels. The estimate in (NEA, 1993) has been provided by SCK•CEN and ONDRAF.

Table 5.9. Cost estimates for TRUCK-II and from NEA.

	TRUCK-II	From (NEA, 1993)
R&D and siting	no estimate	Mfl 375 (MECU 150)
Construction	Mfl 1320 - Mfl 2480	Mfl 1125 (MECU 450)
Operation	Mfl 100 - Mfl 115 plus Mfl 4 per year	Mfl 488 (MECU 195)
Decommissioning and closure	Mfl 108	Mfl 75 (MECU 30)
Total	Mfl 1530 - Mfl 2700; Mfl 4 per year	Mfl 2062 (MECU 825)

Assumed conversion: 1 MECU (1990) = 2.5 Mfl (1994)

Construction costs

In the TRUCK-II design, the costs are dominated by the construction costs (85 % - 90 %). In (NEA, 1993) the costs are also dominated by the construction costs, but to a smaller extent (54 %). To study this difference, a reconstruction of the cost estimate in (NEA, 1993) is presented in Table 5.10 using the information that has also been used for the cost estimate of TRUCK-II.

Table 5.10. Construction costs estimated using TRUCK-II data.

Construction as in (NEA, 1993)	Cost estimate based on TRUCK-II data
Two shafts to 250 m	Mfl 120
12 km of tunnels internal diameter 3.5 m	Mfl 130 - Mfl 170 (tunnel type P or S)
26 km of tunnels internal diameter 2 m	Mfl 185 - Mfl 260 (tunnel type T)
Personnel costs	Mfl 121
Total construction	Mfl 556 - Mfl 671

So, the estimate for the construction costs that has been provided by SCK•CEN and ONDRAF in (NEA, 1993), Mfl 1125, is almost two times larger than the estimate obtained with the TRUCK-II data: about Mfl 600. The NEA report (NEA, 1993) does not give sufficient detail information to explain this difference.

It can be seen from the previous that the tunnel costs are dominating the construction costs of the facility: in (NEA, 1993) (probably) about 55 % to 65 % of the construction costs; in TRUCK-II 50 % to 60 % of the construction costs. However, when compared to the total costs, there is a difference between the two studies: in (NEA, 1993) the costs of the tunnels are about 30 % of the total costs (assuming that tunnel costs are 60 % of the construction costs in Table 5.9), while in TRUCK-II the tunnel costs are 50 % to 60 % of the total costs (see Table 5.8).

Operation costs

The costs of operation of the facility (packaging and disposal of the waste) are estimated about Mfl 300 larger in (NEA, 1993) than for TRUCK-II, while the number of canisters considered is about the same. The NEA report (NEA, 1993) does not give sufficient detail information to explain this difference.

5.5. Conclusions

The estimated cost for the TRUCK design, which has not been optimised with respect to costs, ranges between Mfl 1500-2700. These are undiscounted costs in Dutch guilders, price value 1994. Undiscounted costs were obtained by assuming an inflation rate of 0 % per year and a real interest rate of 0 % per year: i.e. a constant money value of the year 1994.

Reconstruction of a cost estimated published by NEA in (NEA, 1993) shows that the data used for the TRUCK-II cost estimate may lead to an underestimation of about 50 %.

The dominant cost component is the cost of the underground construction: the tunnels cost represents between 48 % to 60 % of the total cost, and the shafts cost between 14 % to 37 % of the total cost.

Optimisation of the section for non-heat generating HLW and MLW is possible. The design in (NEA, 1993) uses about 70 % less tunnel length to dispose the same amount of canisters. So the estimated cost range decreases to Mfl 900-1900 for an optimised design. However, attention has to be paid to retrievability of the waste when optimising the TRUCK design.

Uncertainties in the estimate

The cost of the tunnels varies between kfl 7 per meter (lower estimate for internal diameter 2.2 m) and kfl 17 per meter (upper estimate for internal diameter 5 m). More than 80 % of these costs are the costs of supporting concrete blocks in the lining. As most of the prices of building components depend on negotiations, the uncertainty in the cost estimate depends a lot on the price negotiations for the supporting concrete blocks.

In literature, a few different documents give estimates for shafts to a depth of about 250 m through unconsolidated rock. In TRUCK-II, the assumed depth of the facility is 500 m. One source (Heijdra et al., 1995) assumes that these costs are largely linear with the depth, while another source gives as a rule of thumb that the cost increases with the depth to (at least) the third power (van de Gaag, 1990). This causes an uncertainty of a factor 4 in the cost of the shafts.

As no detailed design was available for the disposal of non-heat generating HLW and MLW, possible costs of overpacks for these waste types have not been included.

5.6. References

- DACE, Mei 1994. 17e editie. Prijzenboekje Dutch Association of Cost Engineers.
- Grupa J. and Jansma R. 1999. De kosten van het terughaalbaar opbergen van afval in de diepe ondergrond. Opberging in zoutgesteente. ECN-C--98-094.
- Heijdra J.J., Bekkering J., Gaag J.V.D., Kleyn P.H.V.D & Prij J. 1995. Retrievability of radioactive waste from a deep underground disposal facility. Report EUR-16197, Commission of the European Communities, Luxembourg.
- NEA. 1993. *The cost of high-level waste disposal in geological repositories: an analysis of factors affecting cost estimates*. Nuclear Energy Agency OECD.
- van de Gaag P. 1990. Erop of eronder? : Verkenning van aardwetenschappelijke mogelijkheden tot herroepelijk opbergen van chemisch afval in de Nederlandse ondergrond [RMNO-43].
- Van de Steen B. and Vervoort A. 1998. Mine Design in Clay. CORA-project TRUCK-I, K.U.Leuven.
- Van Hattum and Blankevoort. 1986. *Locatie-onafhankelijke studie inzake de aanleg, bedrijfsvoering en afsluiting van mogelijke faciliteiten voor de definitieve opberging van radioactief afval in steenzoutformaties in Nederland*. Koninkl. Volker Stevin, Rotterdam.

6. Conclusions and recommendations

The main conclusions of each chapter are recalled, and when relevant, some recommendations are given.

Chapter 2 aimed at determining representative geomechanical parameters for Boom clay at 500 m depth. The laboratory testing programme (Appendix E) showed:

- a decrease in water content and an increase in specific weight with depth. These results are consistent with what could be expected, i.e. that the clay at 500 m depth is more consolidated than for the Mol site at 225 m depth,
- an increase in elastic shear modulus G with depth, which could even better be represented in term of mean effective pressure. Such variation of G could be fitted with the non-linear elasticity of the modified Cam clay model.

However, the results obtained on the frictional behaviour (plastic parameters) are much more controversial:

- the effective cohesion increases with depth following a reasonable trend,
- but the friction angle decreases with depth to very low values of 8-9°. This trend was not expected, it is neither consistent with the observed water content and specific weight trends, nor with the Mol references values known at the Mol site (225 m depth).

Eventually, the attempt to determine the additional Cam clay parameters through isotropic consolidation tests was not demonstrative, mainly due to a lack of true consolidation steps (or a far too high loading rate) in the experimental procedure. It must however be pointed out that such tests, if performed correctly, would have required several weeks or months.

In the future, a new testing campaign would certainly be required in order to validate/invalidate the very low friction angle estimated at 500 m depth, and also to obtain reliable parameters for the Cam clay model.

Optimisation of the repository design has been studied in **Chapter 3**, based on several approaches:

- the thermal study is based on the fulfilment of the same criterion than for the Belgian concept, i.e. *"the temperature variation must be lower or equal to 4°C at 50 m above the repository mid-plane"* (i.e. at the base of the overlying aquifer). It shows that, taking into account an exponential heat decay for three source terms, the minimum area required was 271 m² for 50 years cooling time (at surface), 179 m² for 75 years cooling time and a 141 m² for 100 year cooling time;
- in addition to the basic TRUCK-I configuration (50 m × 50 m), five alternative configurations that all verify the assumed thermal criterion have been studied from the mining and timing aspects. As a main conclusion, only two of the five alternatives are realistic both from an operational and constructional point of view: 30 m × 30 m and 30 m × 18 m;
- the hydromechanical modelling only considered the short-term mine 'stability' problem, using the same criterion as in TRUCK-I: *"at least half of the distance between secondary galleries (referred as s_2) should remain elastic"*. It is found that the key parameters are the s_2 value and the

Boom clay friction angle. When the friction angle estimated from the tests is considered ($\phi' = 9^\circ$), the criterion is only verified for $s_2 = 50$ m. Due to the controversy about the friction angle value, if the value known from the Mol laboratory is used ($\phi' = 18^\circ$, which seems more realistic though not experimentally proven), then the criterion is verified for both $s_2 = 30$ m and $s_2 = 50$ m. In any case, the excavation of the disposal cell (80 cm excavated diameter and 5 m length) does not have any significant influence on the 'stability' criterion for $s_3 = 18$ m, and a fortiori for larger s_3 values;

- The design of the disposal cells and of the secondary galleries has been modified substantially compared with the TRUCK-I features. The diameter of secondary galleries has been increased to 6 m, and the dimension of the tertiary galleries (disposal cells) has been reduced (5 m in length and 75 cm in diameter). Two designs of the disposal cells have been proposed: the disposal of a canister with and without overpack, with their respective impact on the lining and on the backfill design.

Clearly, the mine design is pretty much dependent on the 'stability' criterion considered for the mine. This criterion could be refined in further studies, but more important is the crucial influence of the mechanical parameters, especially regarding the friction angle. Therefore, its value (or range of values) should be better assessed through a new testing campaign. This would also allow using more sophisticated and realistic models, such as the modified Cam clay one.

On the other hand, the impact of the disturbed zone around secondary galleries in a further optimisation of the design would require to pay more attention to the possible reduction of the diameter to its original value (4.6 m), assuming new handling technologies for disposing the canister would become available.

Procedures for disposal and retrieval of a Cogema canister have been proposed in **Chapter 4**, both for the option of a canister without and with overpack. Some comments on safety and monitoring aspects are also given. However, the proposed design would need to be confirmed and refined, the type of backfill sealing material would need also to be characterised. Further, some considerations on the use of barite concrete in the operational phase could be addressed in more detail.

The cost estimation of such disposal facility in Boom clay at 500 m has been presented in **Chapter 5**. However, this cost study applied to the storage of all the wastes (HLW+MLW+LLW), whereas only the disposal of HLW (300 canisters on 57000) has been optimised in the TRUCK-II project. This activity should certainly be refined in the future, which could lead to a substantial decrease in costs. Further studies are, to our opinion, a prerequisite before a definitive statement can be taken between clay and salt host rock.

Finally, the following items should certainly require to be considered in future activities:

Monitoring aspects

- The development of sensors that can be placed inside the disposal cell (e.g. to detect water intrusion) should be considered. Information from these sensors could be important in a possible future decision on whether measures must be taken to ensure continuing the option of retrievability of the waste.

- This is an important subject for further study, which is also of interest for other agencies, and can therefore be tackled within an international framework.

Long term study

- Long term evolution of the storage, especially from the coupled thermohydromechanical point of view.

- The effect of time on the Boom clay behaviour (i.e. its viscous component) should be quantified, which is particularly important during the monitoring (retrievability) period of the repository.

Study of other types of wastes

- A similar study could be made for the MLW and LLW.

Appendixes A to E

Appendix A – Dose rate calculations

Assumptions

Clay and backfill

The vitrified waste is supposed to be buried in a mine excavated in the Boom-clay. This is a mineral of the type of a 3-layered clay which can be represented as the typical mineral Phlogopite, an alteration product of Mica, which has the general form $\text{KMg}_3(\text{AlSi}_3)\text{O}_{10}(\text{OH})_2 + \text{water}$. The specific density is 2.0 g/cm^3 and has a water content of 20 % by weight (Cadelli, 1988; Pannekoek and van Straaten, 1984). To be conservative, the lightest version of Phlogopite has been chosen as the Mg can be replaced by Al, Ti or Fe, depending on the origin of the mineral (higher Z- or atomic-number means better shielding).

For the backfill, Bentonite (dried Phlogopite) has been considered having a specific density of 1.8 g/cm^3 and no inter-layered water. The diameter of the backfill cylinder has been taken 75 cm, it is oversized compared to the canister to reduce radiative streaming through the seams of the backfill.

Canister

The dimensions of a canister are: height = 135 cm, inner/outer diameter = 42.0/43.0 cm, bottom and top wall thickness = 0.5 cm and it is made of stainless steel AISI 316 with density 7.85 g/cm^3 .

A canister will be filled to a level of 110 cm or with 150 litres of glass (80 % filling fraction). The remaining volume is supposed to be atmospheric air.

Glass and radioactive source

The composition of the vitrified waste the content has been taken from from (Heijboer et al., 1988). The composition of the glass frit has been specified by COGEMA. The amount of oxides of the fission products, minor actinides and the remaining amount of the uranium- and plutonium content, after reprocessing, has been calculated. It has been assumed that this amount is limited by the molybdenum in the waste, that should not precipitate after the melt. The result was that the waste from initially 1.33 ton heavy metal (tHM) with a burn-up of 33 GWd/tHM can be stored in the glass in one canister. The resulting glass has a specific density of 2.73 g/cm^3 .

Burn-up calculations have been performed with the ORIGEN-S code (Hermann and Westfall, 1981) to calculate the content of fission products and actinides of LWR-fuel. It has been assumed that the fuel was enriched to 3.3 % in ^{235}U , and that the burn-up after unloading is 33 GWd/tHM. A representative neutron spectrum for an LWR has been assumed. Three years after unloading from the reactor, the fuel assemblies are assumed to be reprocessed. It has been assumed that after reprocessing, 0.5 % of the actual uranium and plutonium content is left in the waste. This waste is vitrified in steel canisters and stored for another 50 years in an interim storage, to “cool down”.

Sand

The sand surrounding the canister, used to fill the gap between the canister and the oversized storage hole, is supposed to be quartz sand and has been taken as pure SiO_2 with a specific density of 1.60 g/cm^3 .

Concrete

A concrete liner supports the mine gallery. The thickness of this liner is assumed 50 cm, and the composition is assumed equal to ordinary concrete (Portland, sand and gravel) with a density of 2.33 g/cm^3 .

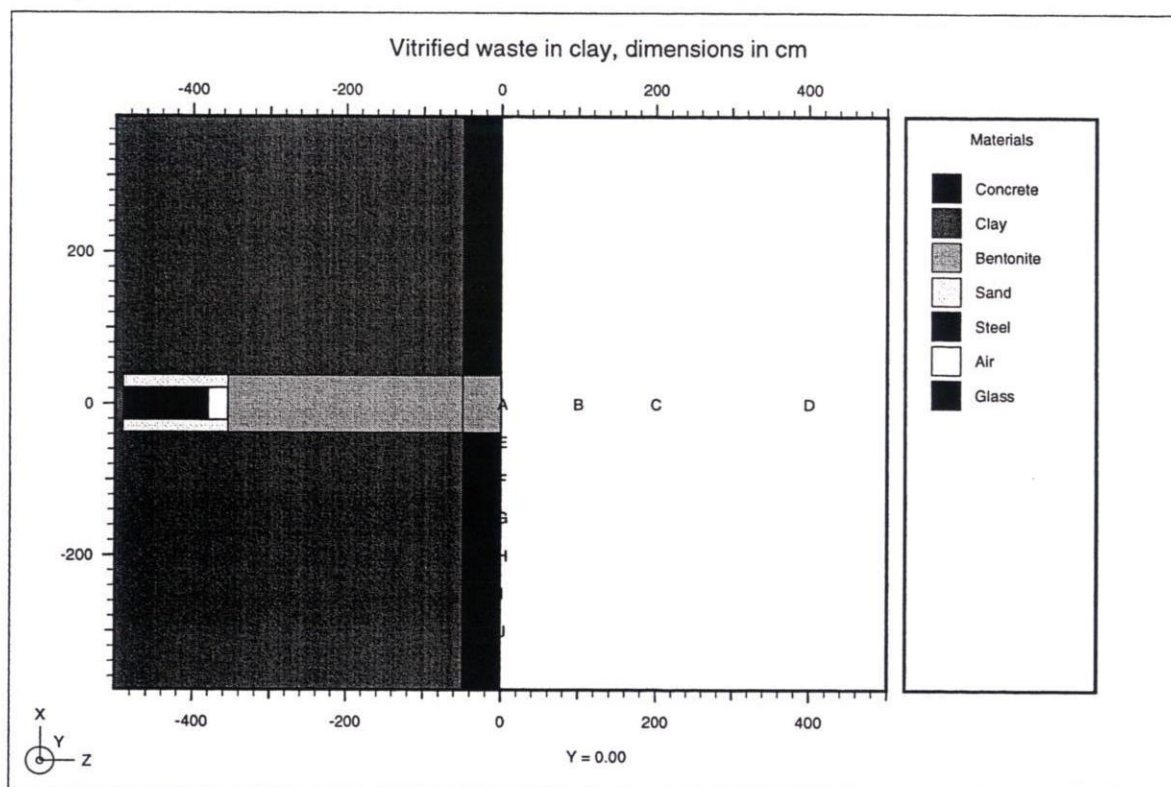


Figure A.1. Configuration assumed for the dose rate calculation.

Dose rate calculations

For the configuration shown in Figure A.1, dose rates have been calculated for different points in the gallery by means of the shielding code MARMER (Kloosterman, 1990). Two sets of calculations have been performed: one with a burial depth (length of backfill cylinder) of 3.5 meter and one for a depth of 1.5 m, both with 4 points along the axis of the cylinders away from the gallery wall and 6 points along the wall with distances from the axis.

The results are given in Table A.1.

Table A.1. Dose rates in the gallery.

Dose point in Figure A.1	Distance on axis (cm)	Dose rate in $\mu\text{Sv/h}$ at various depths	
		Depth 3.5 m	Depth 1.5 m
A	1.0	$\ll 1 \text{ e-6}$	1.1 e-01
B	100	$\ll 1 \text{ e-6}$	4.9 e-02
C	200	$\ll 1 \text{ e-6}$	2.6 e-02
D	400	$\ll 1 \text{ e-6}$	1.2 e-02
	Distance along wall (cm)		
E	50	$\ll 1 \text{ e-6}$	1.0 e-02
F	100	$\ll 1 \text{ e-6}$	4.8 e-04
G	150	$\ll 1 \text{ e-6}$	1.6 e-05
H	200	$\ll 1 \text{ e-6}$	4.8 e-07
I	250	$\ll 1 \text{ e-6}$	1.0 e-08
J	300	$\ll 1 \text{ e-6}$	2.2 e-10

For the depth of 1.5 m the main contribution is from the decay of ^{137}Cs and its daughter ^{137}Ba . For the depth of 3.5 m the dose rates calculated with MARMER are about $10^{-9} \mu\text{Sv/hr}$. At this very low dose rate, "Bremsstrahlung" and capture gamma's may give a significant contribution to the dose rate. These types of radiation are not accounted for in the MARMER calculations. A separate analysis has shown that the contribution from capture gamma's (generated in the vicinity of the canister, from the absorbed neutrons produced by the decay of some of the actinides) is negligible. The contribution to the dose rate of the "Bremsstrahlung" (induced by the slowing down of β -particles) increases with the burial depth from about $1/10^{\text{th}}$ at 1.5 m till it is about equal to the gamma dose rate as calculated with MARMER at 3.5 m. The Bremsstrahlung is mainly caused by β -particles originating from the decay of ^{90}Y (daughter of ^{90}Sr).

References

- Cadelli N. 1988. PAGIS. Performance Assessment of Geological Isolation Systems for Radioactive Waste. Report EUR 11775, Commission of the European Communities, Luxembourg.
- Heijboer R.J., de Haas J.B.M., van Dalen A. en Benneker P.B.J.M. March 1988. Nuclide Inventaris, Warmteproductie en Gammastraling van Kernsplijtingsafval. VEOS Eindrapportage: Deelrapport 11, ECN-Petten.
- Hermann O.W. and Westfall R.M. October 1981. ORIGEN-S - Scale System Module to calculate Fuel Depletion, Actinide Transmutation, Fission Product Build-up and Decay and Associated Radiation Source Terms. ORNL.
- Kloosterman J.L. June 1990. MARMER a Flexible Point-Kernel Shielding Code, User Manual, Version 2, II-131-89-03/2, Delft.
- Pannekoek A.J. and van Straaten L.M.J.U. 1984. Algemene Geologie. Wolters-Noordhoff, Groningen.

Appendix B - Mechanical analysis

To check whether the proposed disposal designs are viable, a screening mechanical analysis has been performed, to determine the structural integrity of the disposal cell for given dimensions and characteristics of all parts. The equations to determine the strength of a given construction are taken from (Roark and Young, 1975).

- The thickness of the stainless steel lining of the disposal cell

Assumed is that the outside radius of the lining is 304.8 mm and the thickness of the wall is 25.4 mm. The lithostatic pressure is estimated about 10 MPa.

This wall thickness should be sufficient to resist the pressure: the calculated safety factor to resist the pressure (using Roark and Young, 1975) is 1.7; engineering practise requires a minimal safety factor of 1.5.

The form of the pipe should be stable and must resist buckling. For the given wall thickness, radius and length of the lining, the stability is only treathened for pressures larger than 36 MPa.

- The thickness of the lids on both sides of the lining

If the assumed thickness is 70 mm, the safety factor is 1.8. The thickness of the lids is larger than the wall thickness of the lining, because of the flat shape of the lids. Special attention must be given to the design of the weld between lid and lining.

- The connection of the stainless steel lining with the concrete lining of the gallery

It is possible to weld a 'collar' on the lining that anchors the lining in the concrete lining of the gallery, that is sufficiently strong.

- The strength of the lid (and connection) if the pressure inside the disposal cell increases in case of water intrusion

It is anticipated that in case of water intrusion the internal pressure inside the disposal cell could increase to 5 MPa. The lid that closes the disposal cell at the side of he gallery should resist the pressure. If the lid is connected to the lining with 24 bolts M36 the safety factor is 1.88.

- The thickness of the overpack

The thickness of the overpack is assumed 30 mm. The calculated safety factor for external pressure of 10 MPa is 2.5. The form of the overpack is stable (against buckling) as long as the pressure is lower than 134 MPa.

Reference

R.J. Roark, W.C. Young *Formulas For Stress and Strain* New York, McGraw-Hill, 1975.

Appendix C - Hydromechanical computations

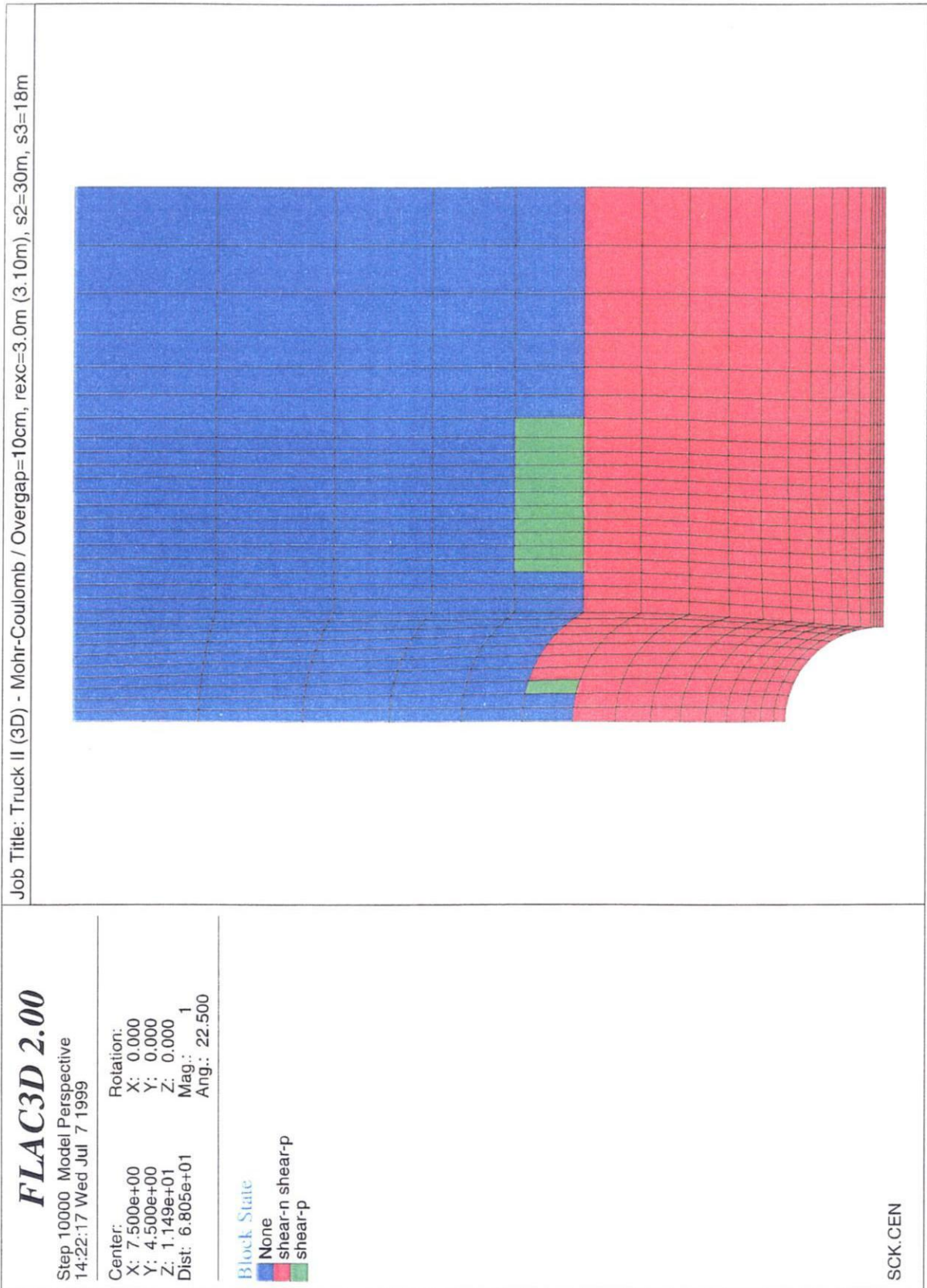


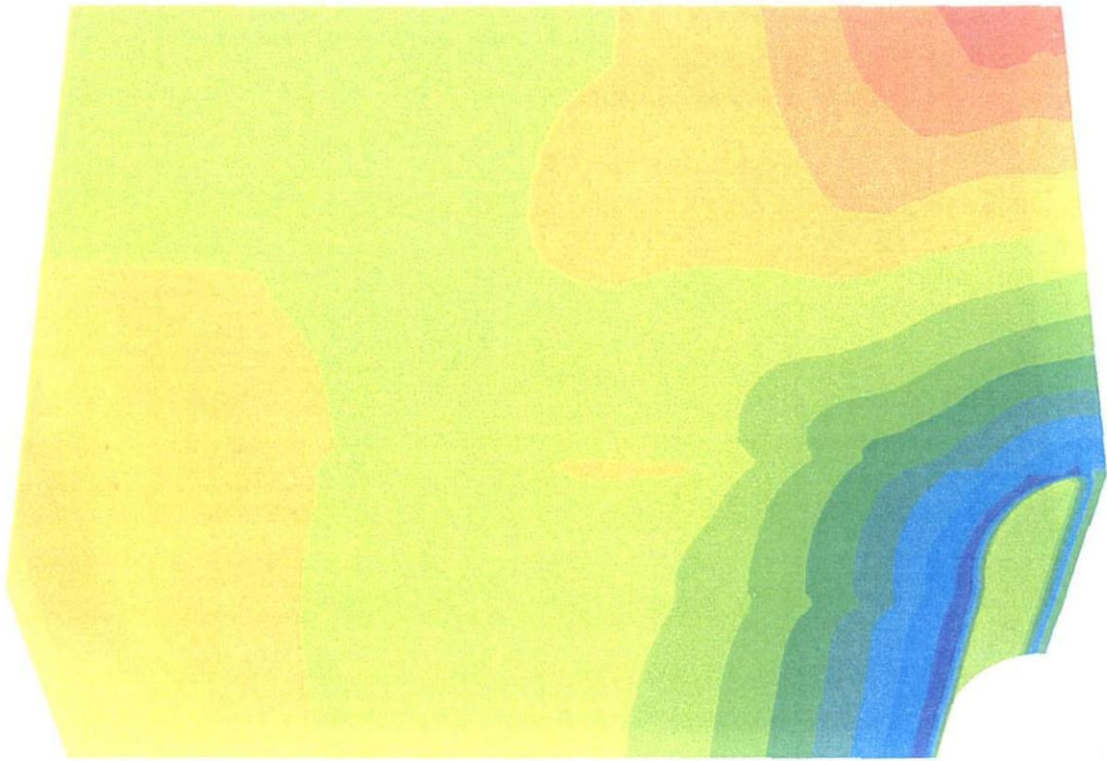
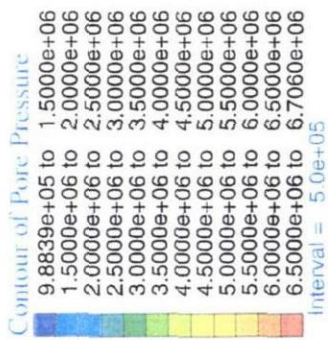
Figure C.1. Model 30 m × 18 m (lower bound) after the excavation of the secondary gallery with $P_1 = 4$ MPa: plastic state indicator.

Job Title: Truck II (3D) - Mohr-Coulomb / Overgap=10cm, rexc=3.0m (3.10m), s2=30m, s3=18m

FLAC3D 2.00

Step 10000 Model Perspective
14:39:56 Wed Jul 7 1999

Center: Rotation:
X: 7.500e+00 X: 0.000
Y: 4.500e+00 Y: 0.000
Z: 1.149e+01 Z: 30.000
Dist: 6.805e+01 Mag.: 1
 Ang.: 22.500



SCK.CEN

Figure C.2. Model 30 m × 18 m (lower bound) after the excavation of the secondary gallery with $P_i = 4$ MPa: pore pressure isovalues.

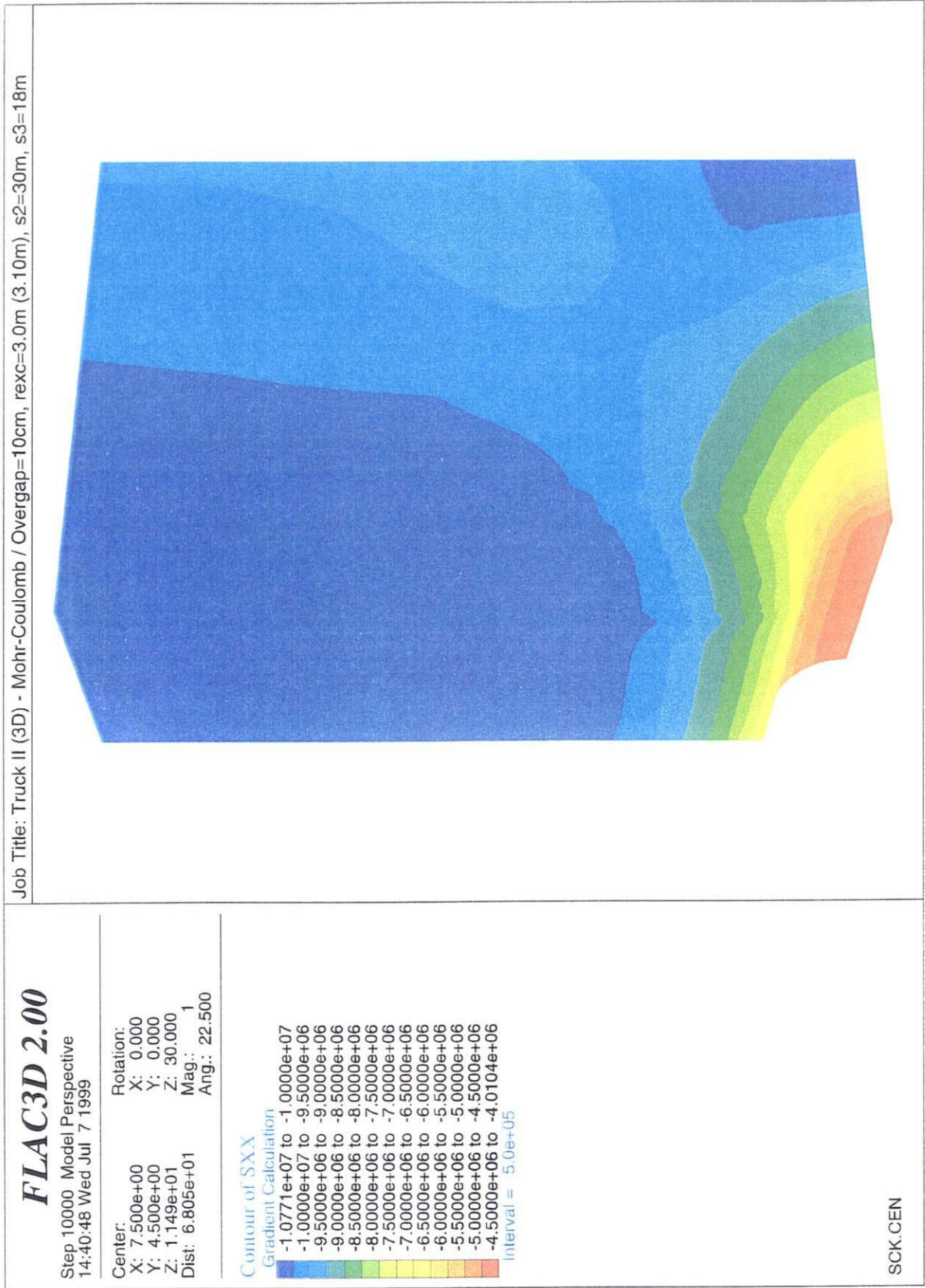


Figure C.3. Model 30 m × 18 m (lower bound) after the excavation of the secondary gallery with $P_1 = 4 \text{ MPa}$: σ_{xx} isovalues.

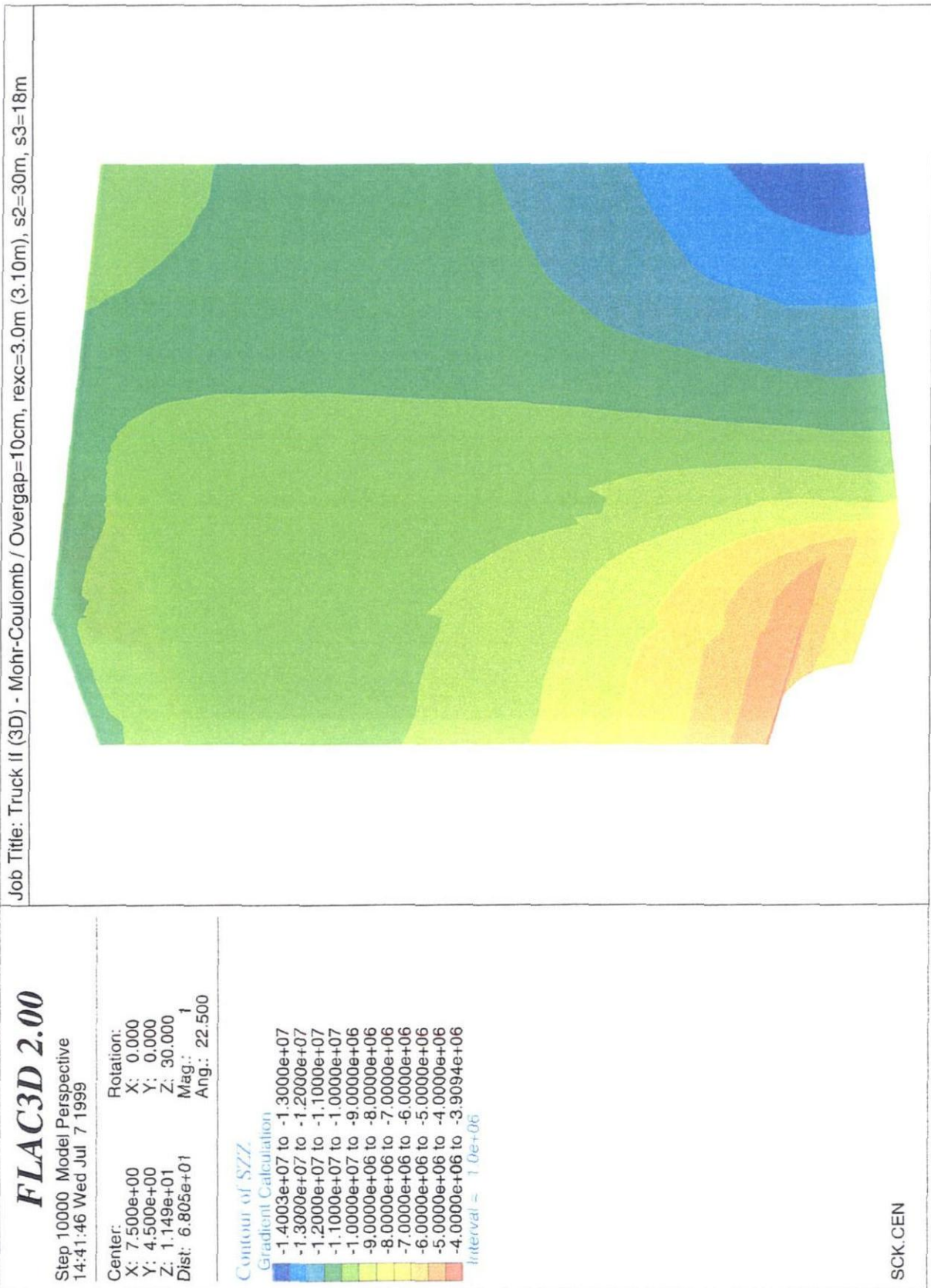


Figure C.4. Model 30 m × 18 m (lower bound) after the excavation of the secondary gallery with $P_i = 4 \text{ MPa}$: σ_{zz} isovalues.

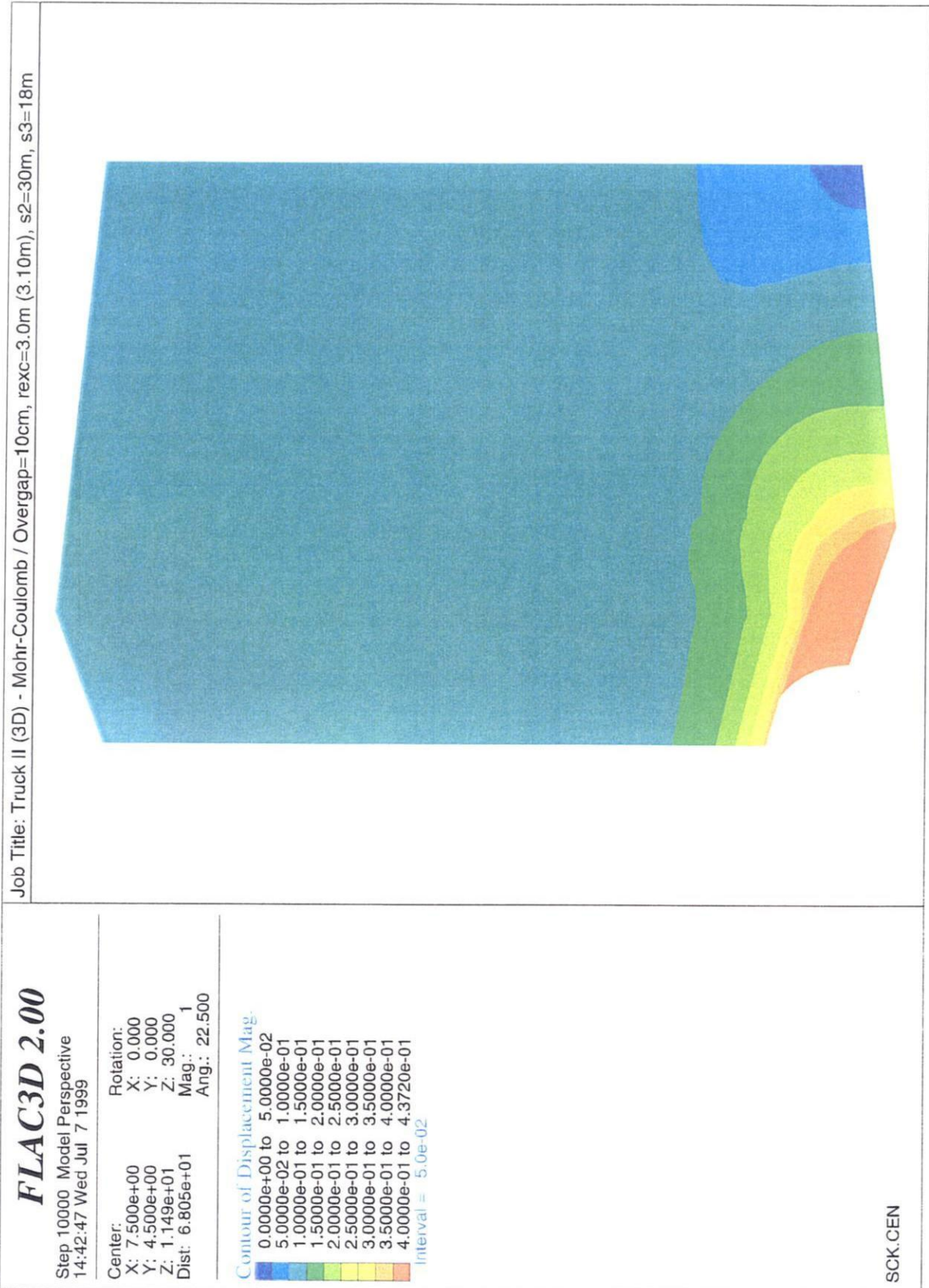
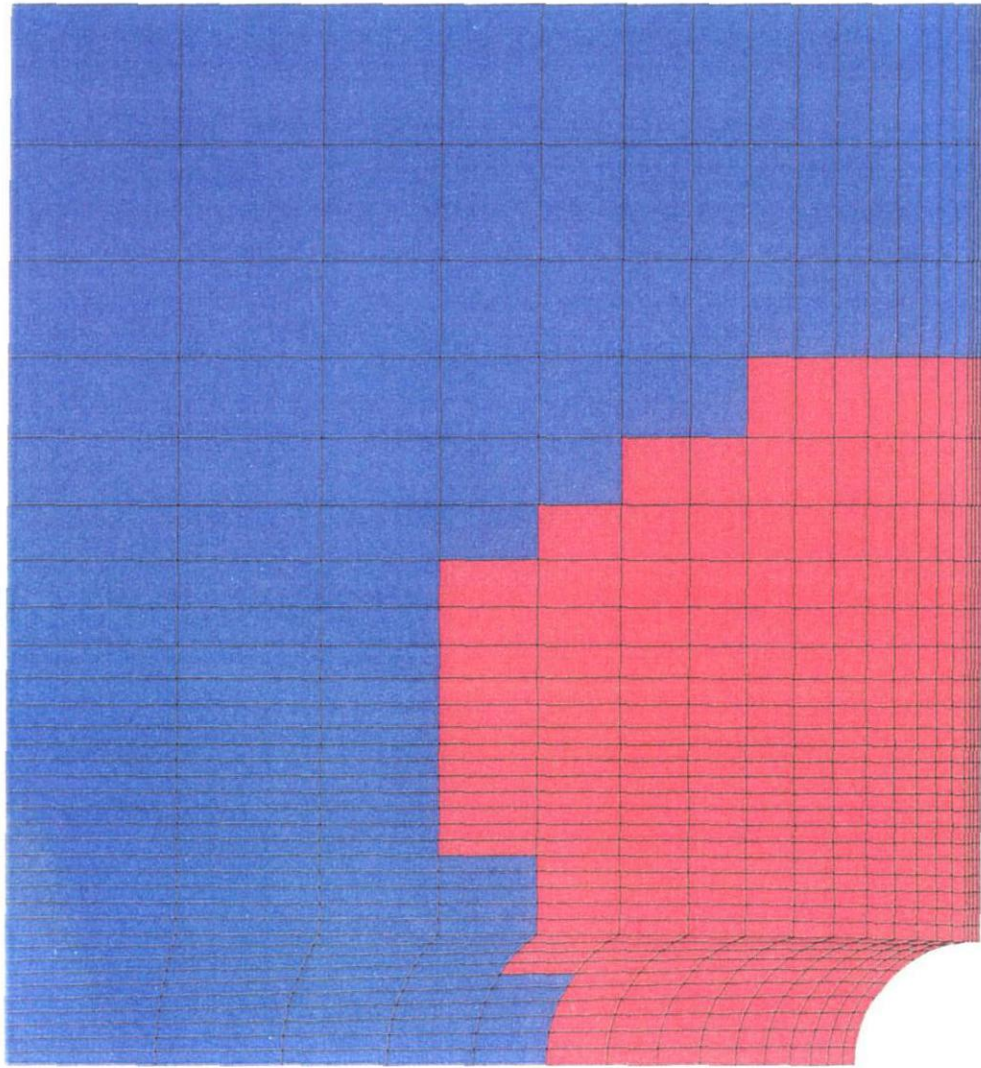


Figure C.5. Model 30 m × 18 m (lower bound) after the excavation of the secondary gallery with $P_i = 4$ MPa: displacement magnitude isovalues.

Job Title: Truck II (3D) - Mohr-Coulomb / Overgap=10cm, rexc=3.0m (3.10m), s2=50m, s3=18m



FLAC3D 2.00

Step 10000 Model Perspective
14:24:17 Wed Jul 7 1999

Center: X: 1.250e+01 Y: 4.500e+00 Z: 1.154e+01
Dist: 7.363e+01
Rotation: X: 0.000 Y: 0.000 Z: 0.000
Mag.: 1
Ang.: 22.500

Block State
■ None
■ shear-p

SCK.CEN

Figure C.6. Model 50 m × 18 m (lower bound) after the excavation of the secondary gallery with $P_1 = 4$ MPa: plastic state indicator.

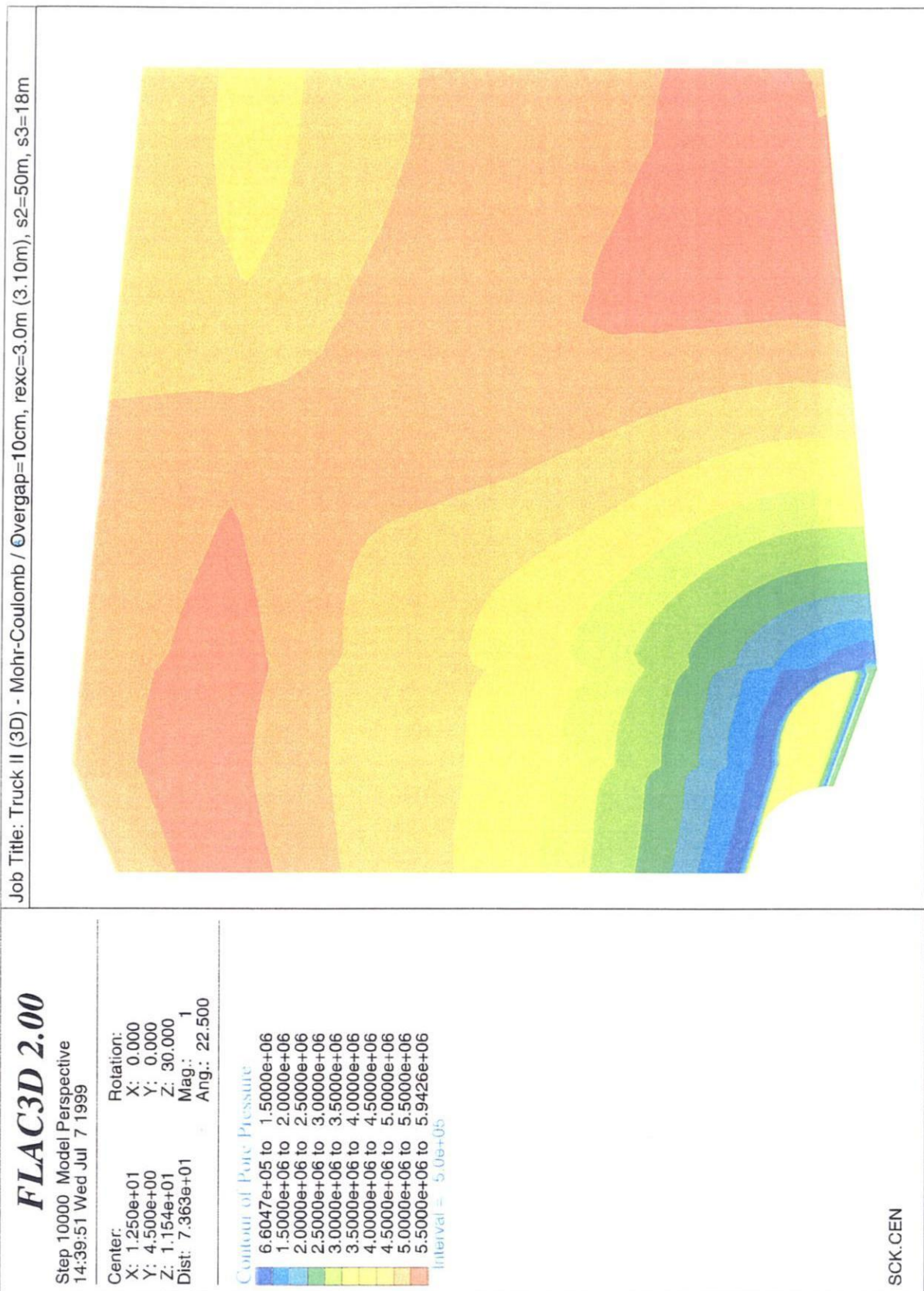


Figure C.7. Model 50 m × 18 m (lower bound) after the excavation of the secondary gallery with $P_i = 4$ MPa: pore pressure isovalues.

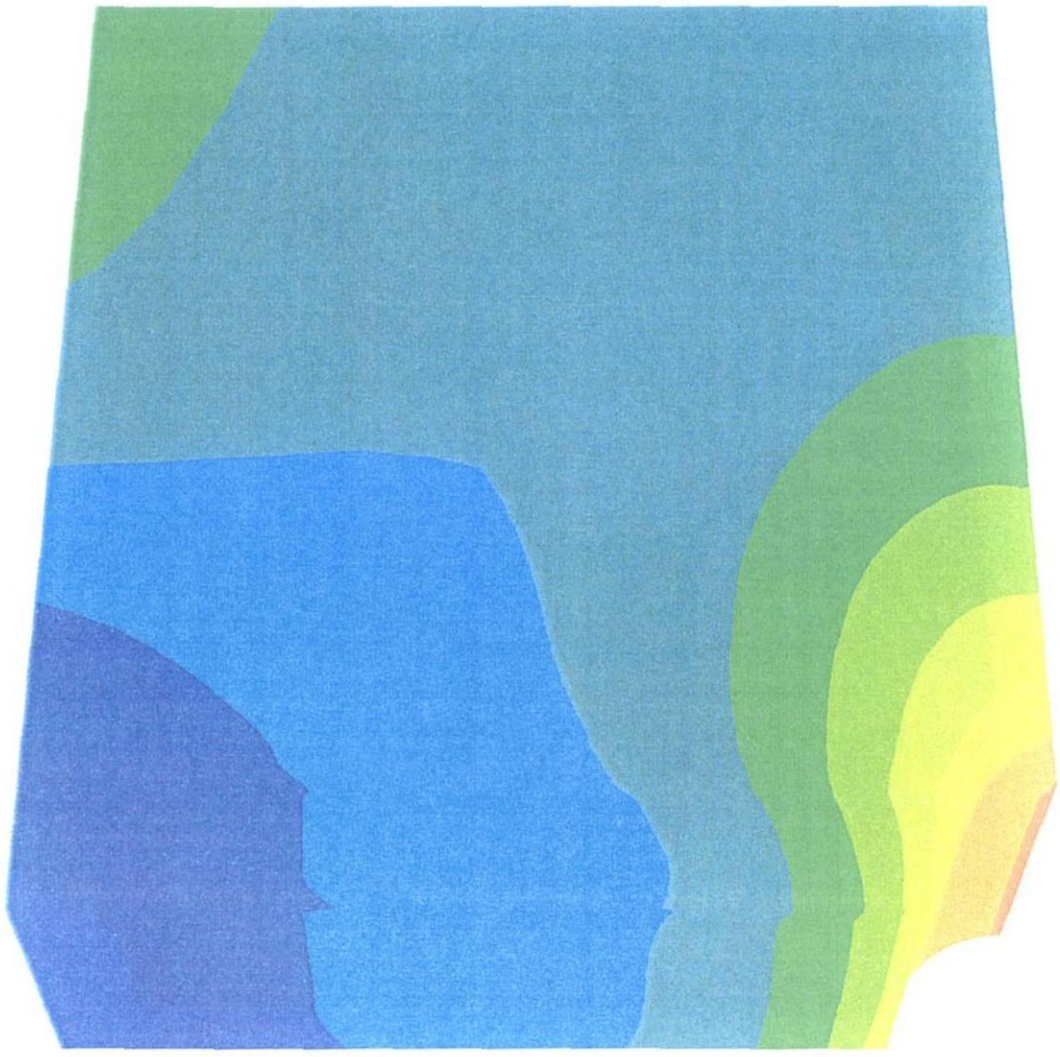
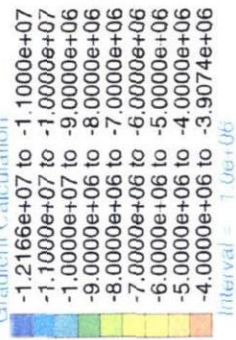
Job Title: Truck II (3D) - Mohr-Coulomb / Overgap=10cm, rexc=3.0m (3.10m), s2=50m, s3=18m

FLAC3D 2.00

Step 10000 Model Perspective
14:41:56 Wed Jul 7 1999

Center: X: 1.250e+01 Y: 4.500e+00 Z: 1.154e+01
Dist: 7.363e+01
Rotation: X: 0.000 Y: 0.000 Z: 30.000
Mag.: 1
Ang.: 22.500

Contour of σ_{xx}



SCK.CEN

Figure C.8. Model 50 m × 18 m (lower bound) after the excavation of the secondary gallery with $P_1 = 4$ MPa: σ_{xx} isovalues.

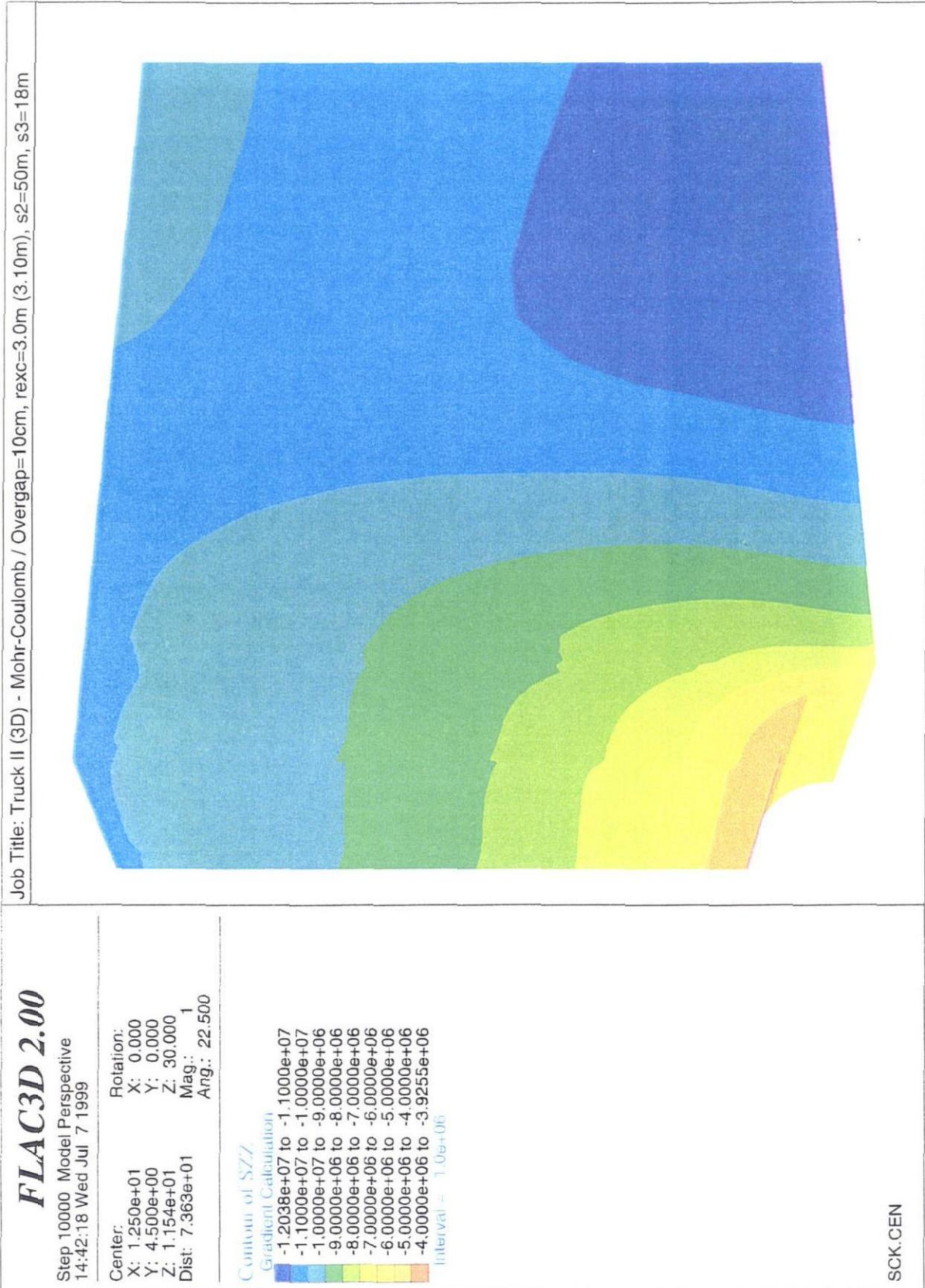


Figure C.9. Model 50 m × 18 m (lower bound) after the excavation of the secondary gallery with $P_1 = 4 \text{ MPa}$: σ_{zz} isovalues.

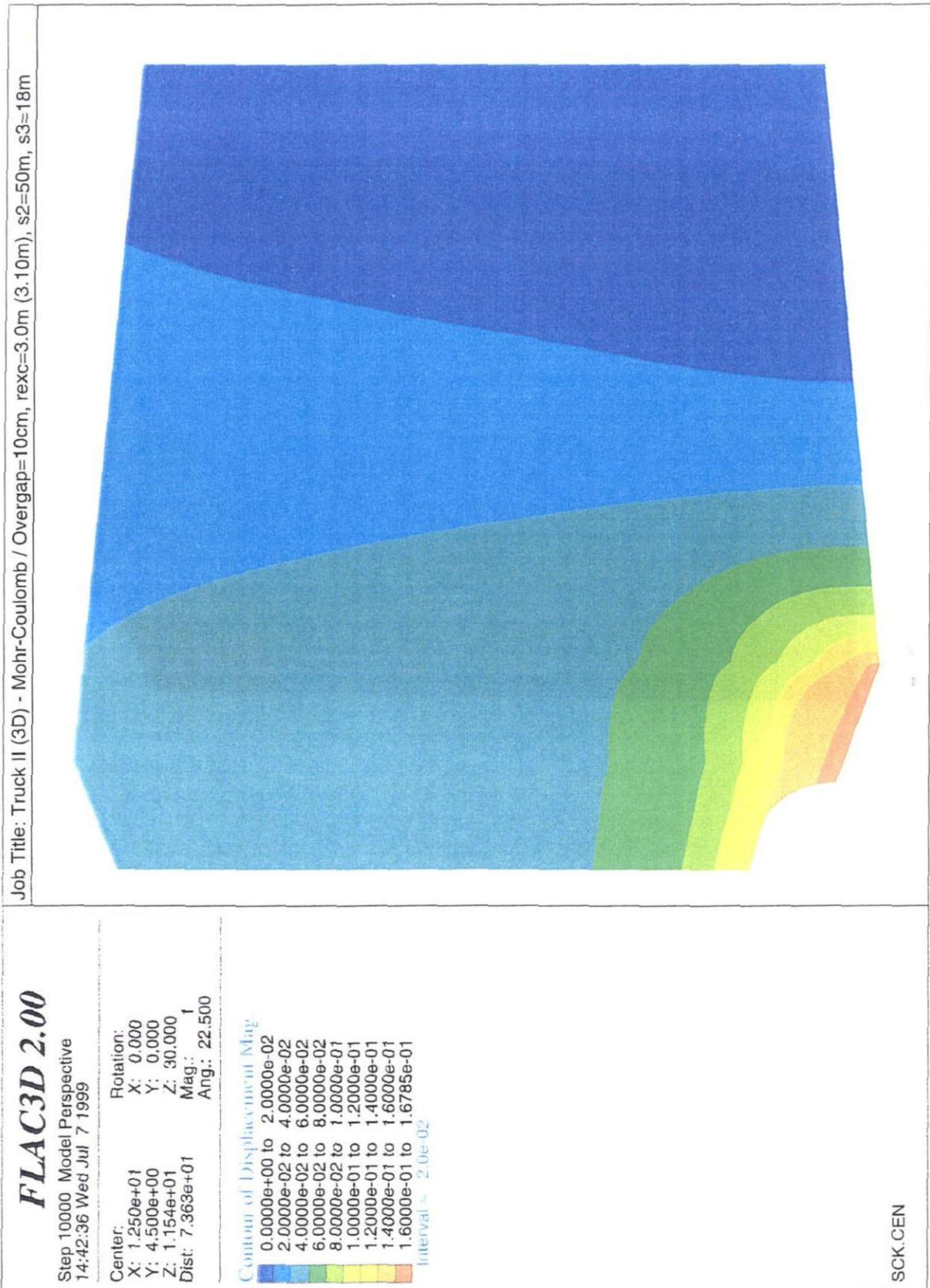
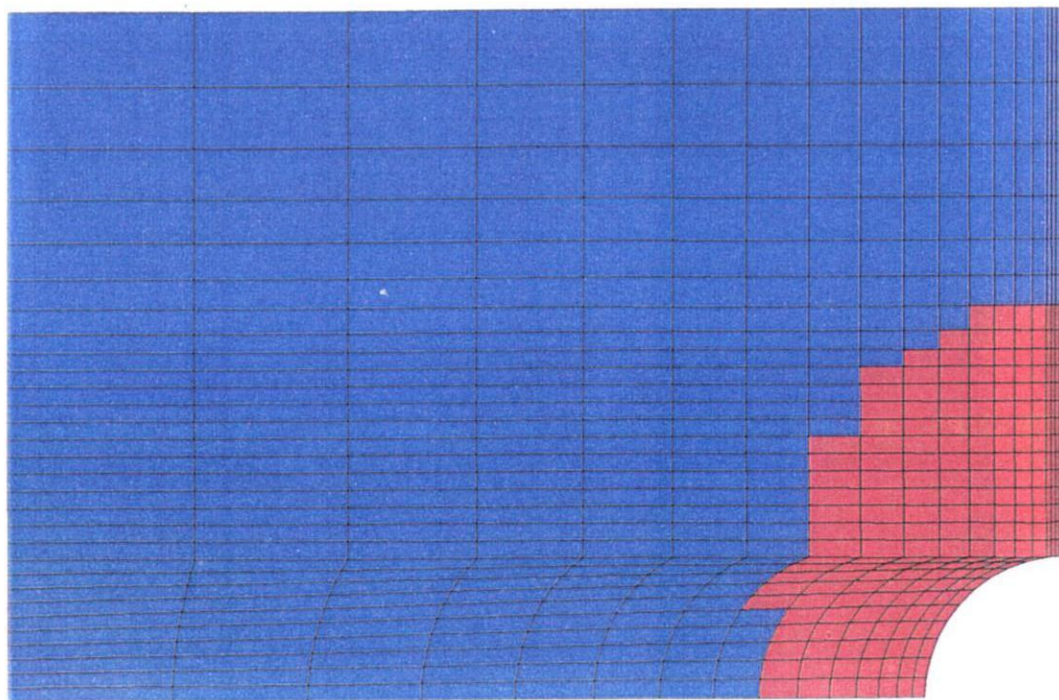


Figure C.10. Model 50 m × 18 m (lower bound) after the excavation of the secondary gallery with $P_i = 4$ MPa: displacement magnitude isovalues.

Job Title: Truck II (3D) - Mohr-Coulomb(strong) / Overgap=10cm, 3.10m, s2=30m, s3=18m



FLAC3D 2.00

Step 10000 Model Perspective
18:42:34 Wed Jul 7 1999

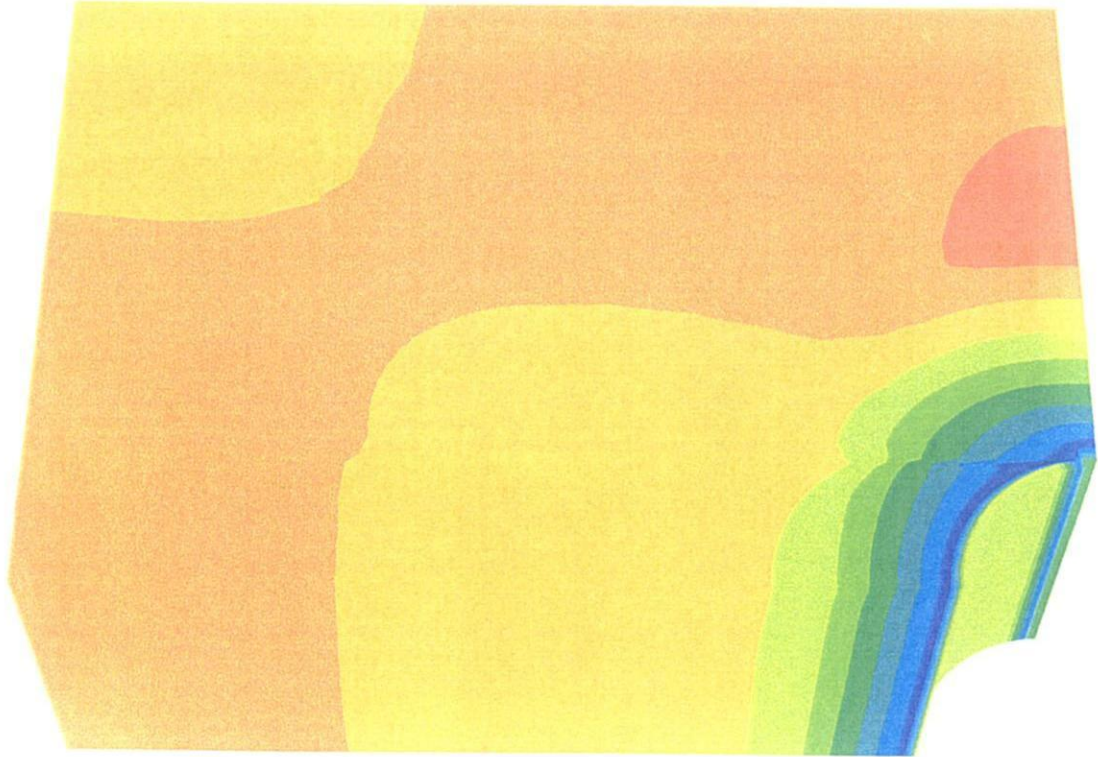
Center: X: 7.500e+00 Y: 4.500e+00 Z: 1.154e+01
Dist: 6.833e+01
Rotation: X: 0.000 Y: 0.000 Z: 0.000
Mag.: 1
Ang.: 22.500

Block State
None
shear-p

SCK.CEN

Figure C.11. Model 30 m × 18 m (upper bound) after the excavation of the secondary gallery with $P_i = 4$ MPa: plastic state indicator.

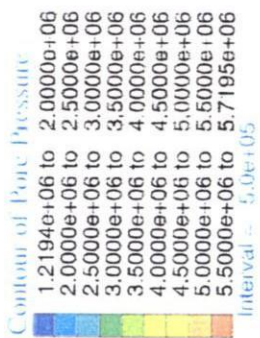
Job Title: Truck II (3D) - Mohr-Coulomb(strong) / Overgap=10cm, 3.10m, s2=30m, s3=18m



FLAC3D 2.00

Step 10000 Model Perspective
18:43:39 Wed Jul 7 1999

Center: X: 7.500e+00 Y: 4.500e+00 Z: 1.154e+01
Rotation: X: 0.000 Y: 0.000 Z: 30.000
Dist: 6.833e+01 Mag.: 1
Ang.: 22.500



SCK.CEN

Figure C.12. Model 30 m × 18 m (upper bound) after the excavation of the secondary gallery with $P_i = 4 \text{ MPa}$: pore pressure isovalues.

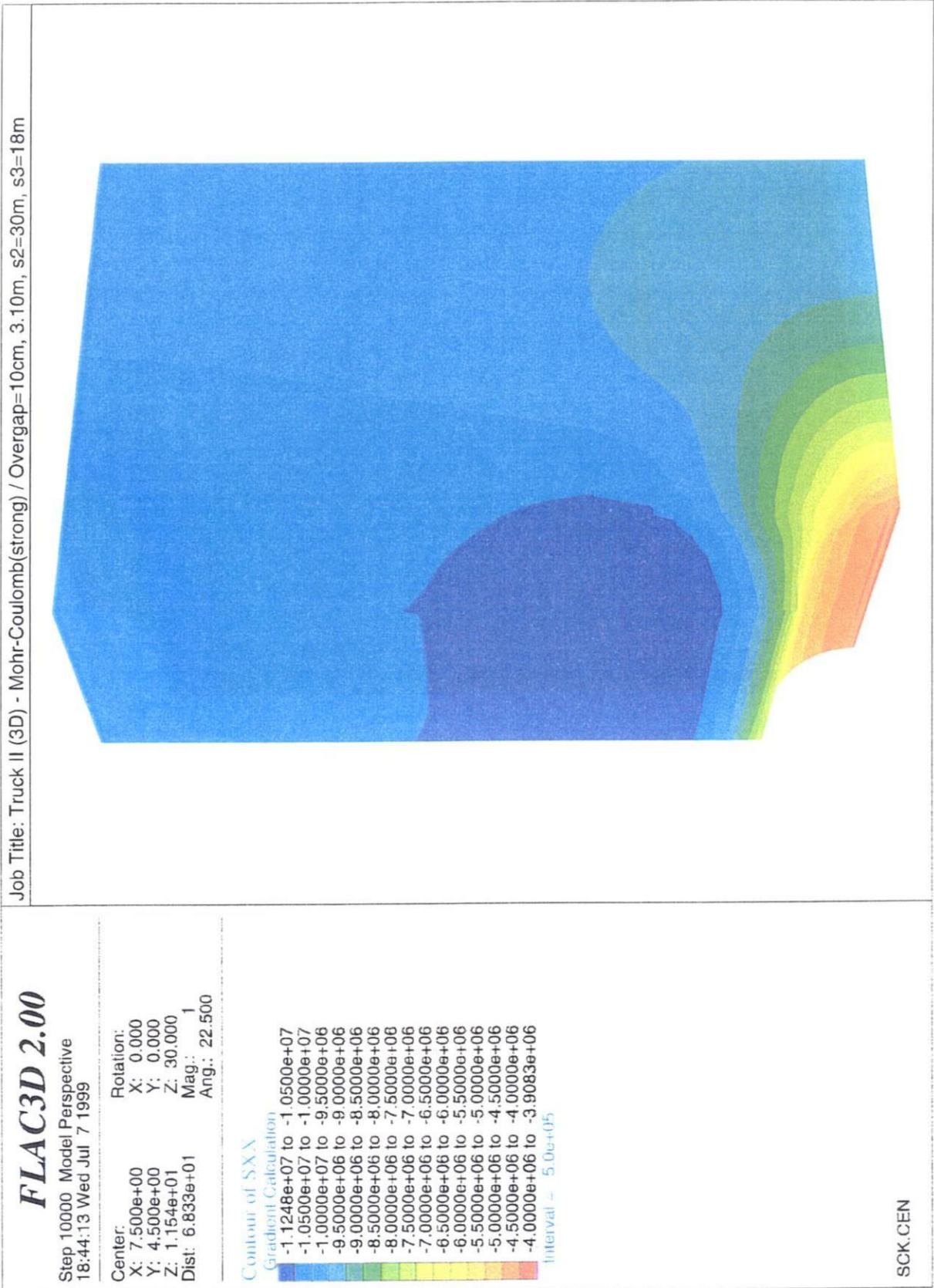


Figure C.13. Model 30 m x 18 m (upper bound) after the excavation of the secondary gallery with $P_1 = 4 \text{ MPa}$: σ_{xx} isovalues.

Job Title: Truck II (3D) - Mohr-Coulomb(strong) / Overgap=10cm, 3.10m, s2=30m, s3=18m



FLAC3D 2.00

Step 10000 Model Perspective
18:44:46 Wed Jul 7 1999

Center: X: 7.500e+00 Y: 4.500e+00 Z: 1.154e+01
Dist: 6.833e+01
Rotation: X: 0.000 Y: 0.000 Z: 30.000
Mag.: 1
Ang.: 22.500



SCK-CEN

Figure C.14. Model 30 m x 18 m (upper bound) after the excavation of the secondary gallery with $P_i = 4 \text{ MPa}$: σ_{zz} isovalues.

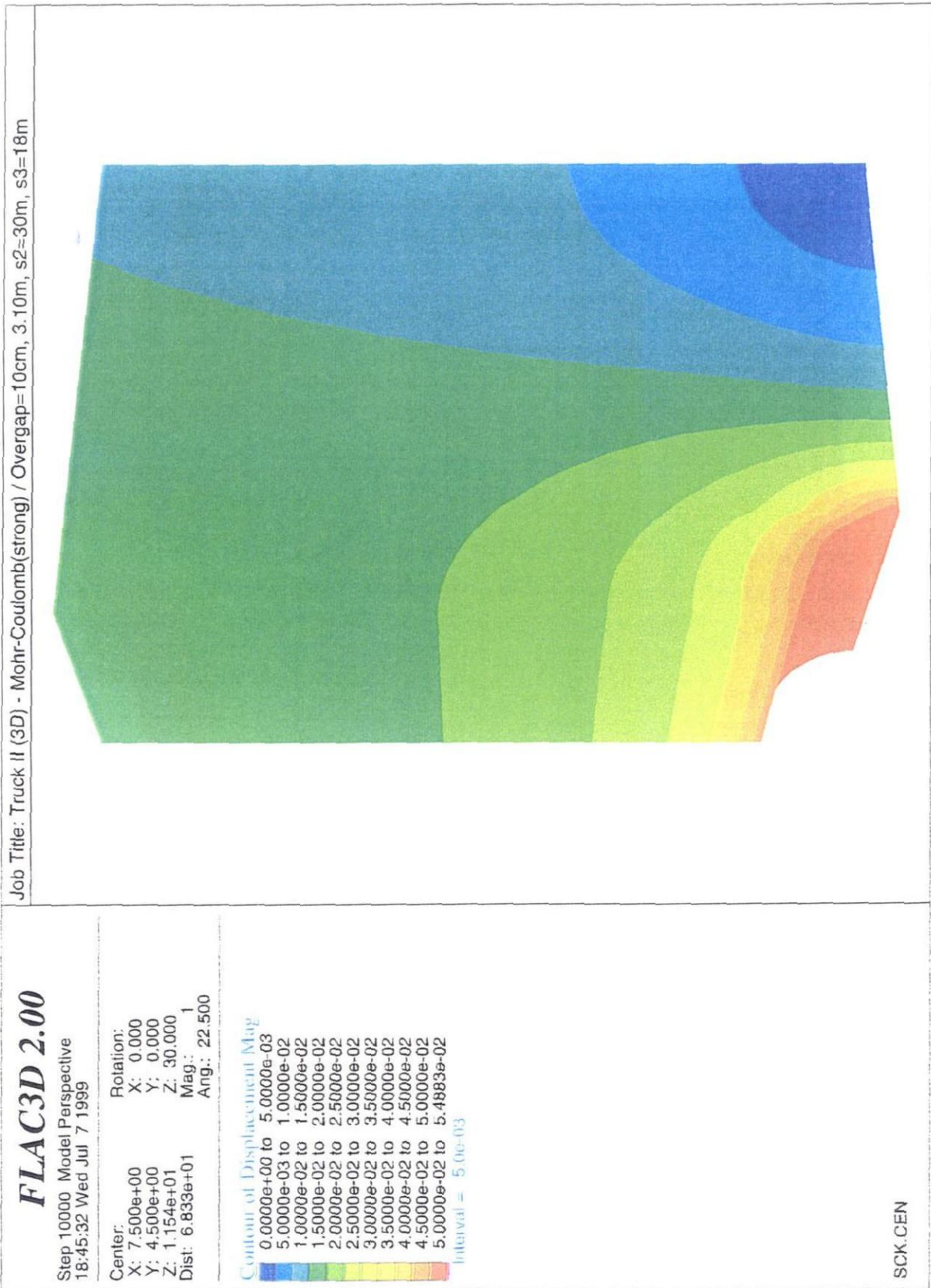


Figure C.15. Model 30 m × 18 m (upper bound) after the excavation of the secondary gallery with $P_i = 4$ MPa: displacement magnitude isovalues.

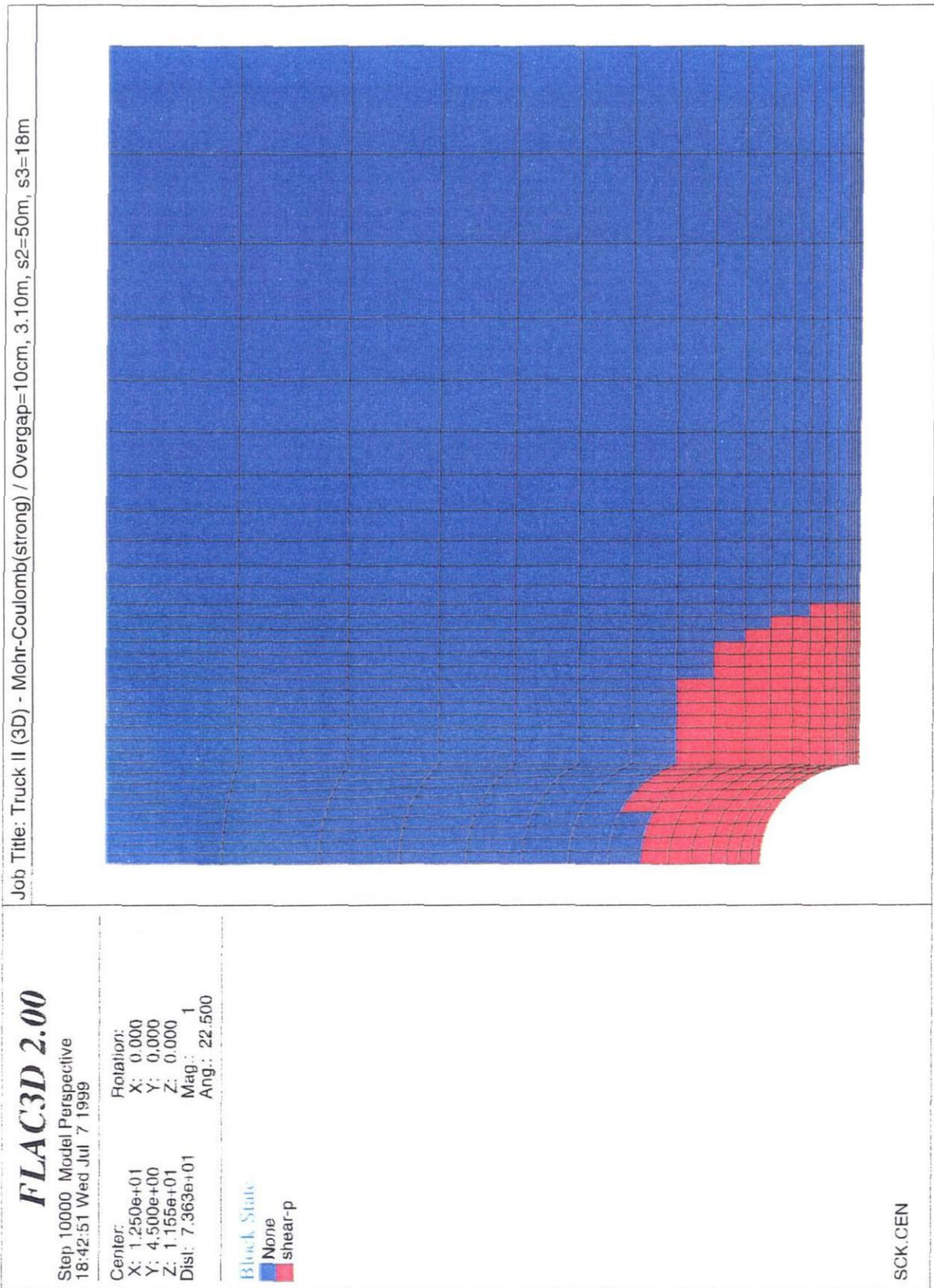


Figure C.16. Model 50 m × 18 m (upper bound) after the excavation of the secondary gallery with $P_1 = 4 \text{ MPa}$: plastic state indicator.

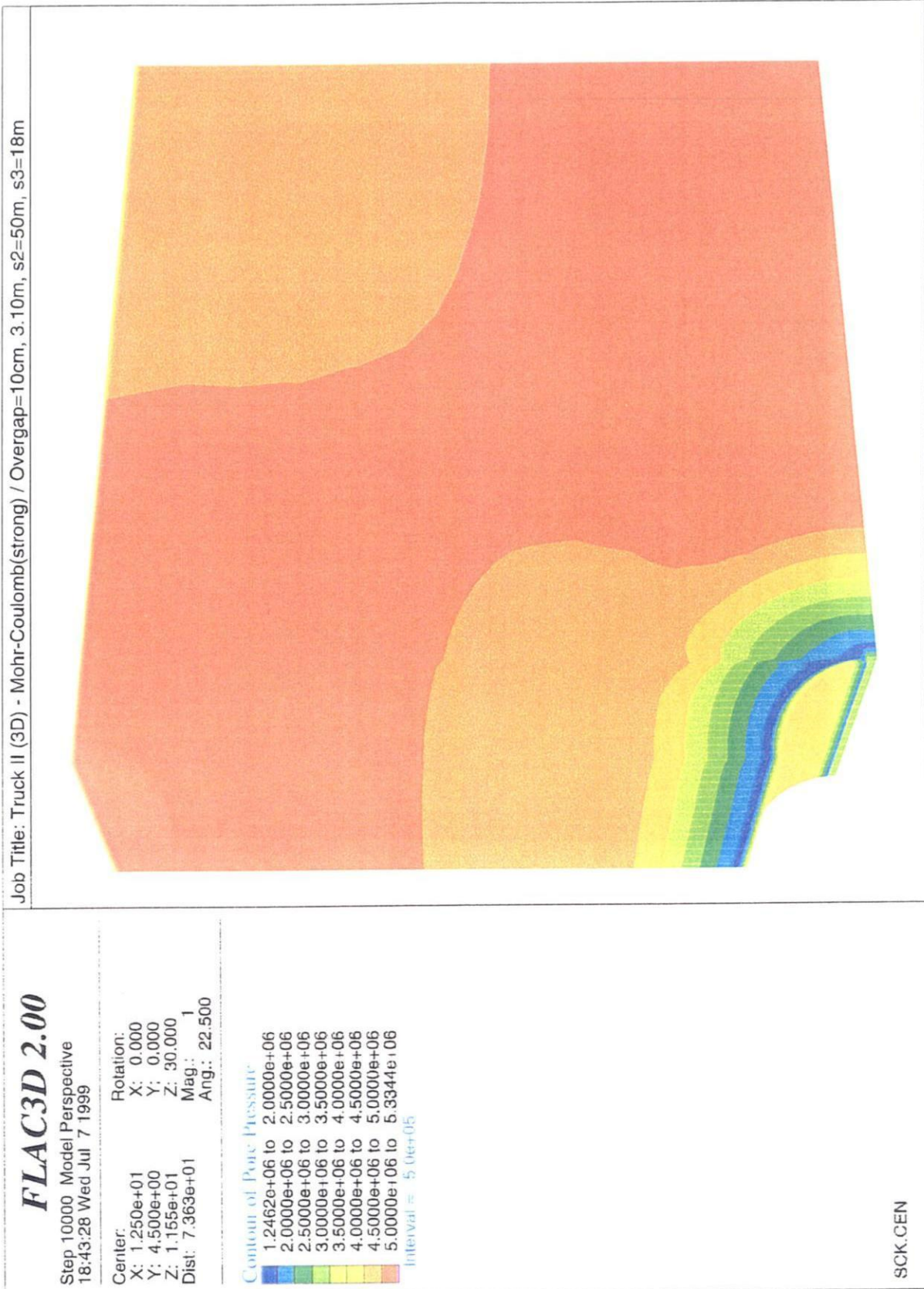


Figure C.17. Model 50 m × 18 m (upper bound) after the excavation of the secondary gallery with $P_i = 4$ MPa: pore pressure isovalues.

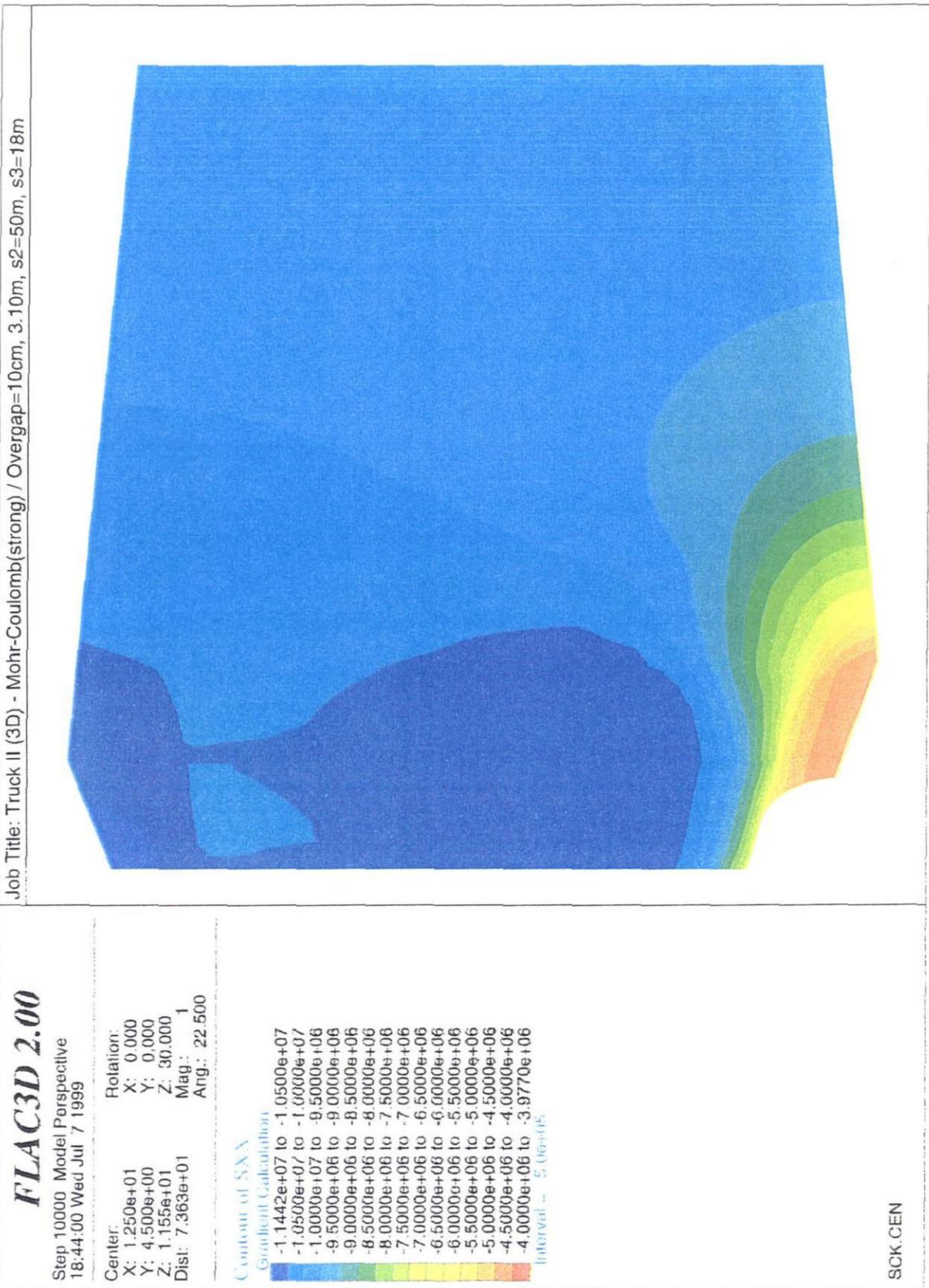


Figure C.18. Model 50 m × 18 m (upper bound) after the excavation of the secondary gallery with $P_1 = 4 \text{ MPa}$; σ_{xx} isovalues.

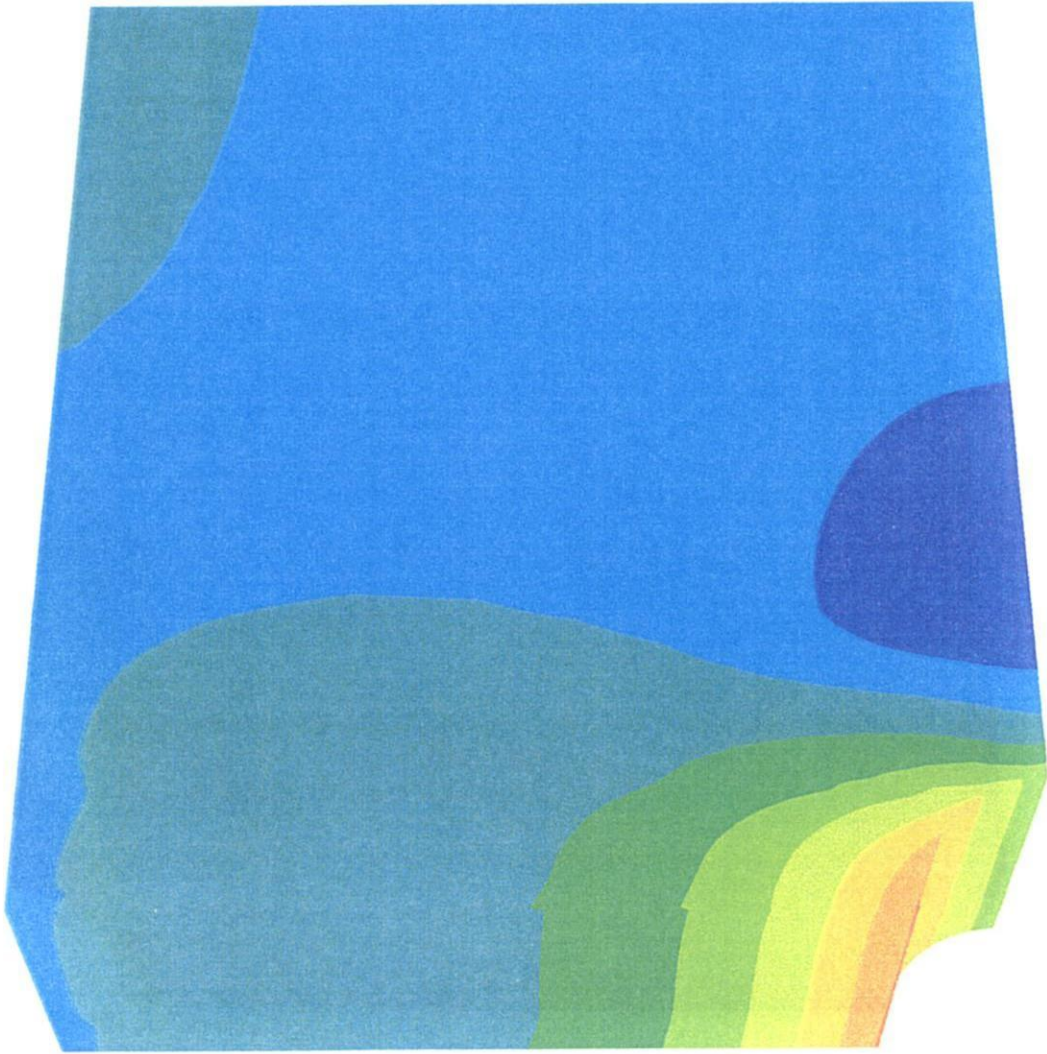
Job Title: Truck II (3D) - Mohr-Coulomb(strong) / Overgap=10cm, 3.10m, s2=50m, s3=18m

FLAC3D 2.00

Step 10000 Model Perspective
18:44:52 Wed Jul 7 1999

Center: X: 1.250e+01 Y: 4.500e+00 Z: 1.155e+01
Dist: 7.363e+01
Rotation: X: 0.000 Y: 0.000 Z: 30.000
Mag.: 1 Ang.: 22.500

Contour of SZZ



SCK.CEN

Figure C.19. Model 50 m x 18 m (upper bound) after the excavation of the secondary gallery with $P_1 = 4 \text{ MPa}$: σ_{zz} isovalues.

Job Title: Truck II (3D) - Mohr-Coulomb(strong) / Overgap=10cm, 3.10m, s2=50m, s3=18m

FLAC3D 2.00

Step 10000 Model Perspective
18:45:14 Wed Jul 7 1999

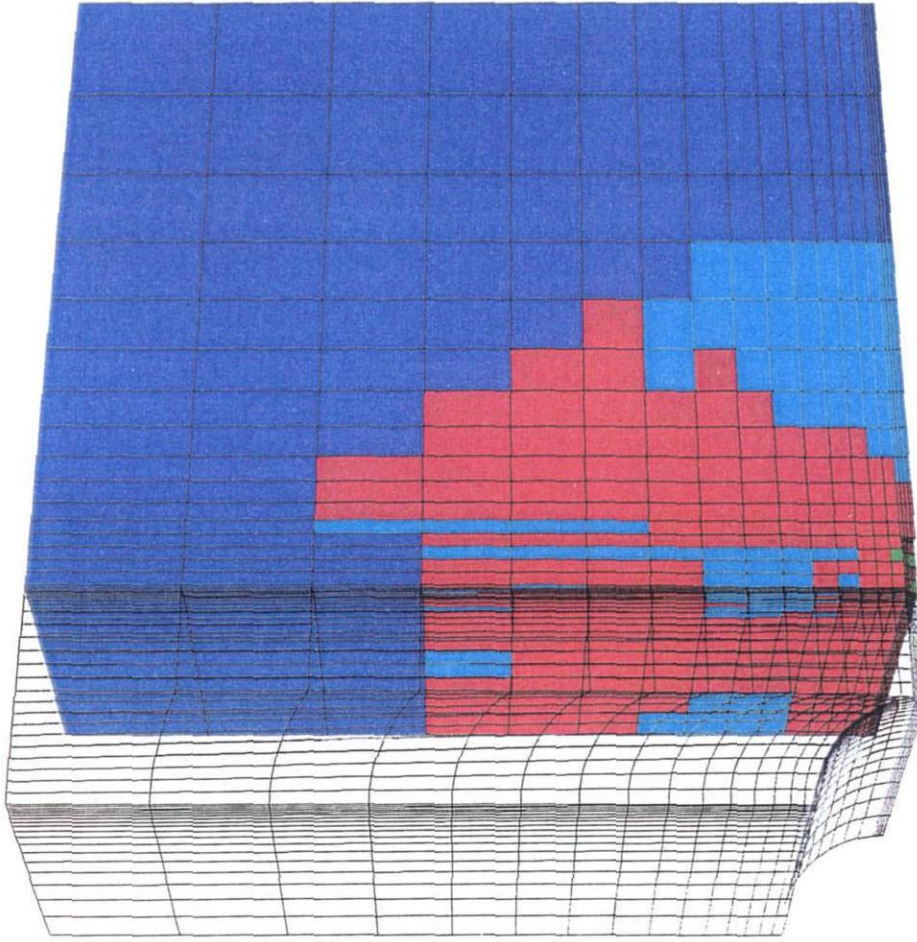
Center: Rotation:
X: 1.250e+01 X: 0.000
Y: 4.500e+00 Y: 0.000
Z: 1.155e+01 Z: 30.000
Dist: 7.363e+01 Mag.: 1
Ang.: 22.500



SCK.CEN

Figure C.20. Model 50 m × 18 m (upper bound) after the excavation of the secondary gallery with $P_i = 4$ MPa: displacement magnitude isovalues.

Job Title: Truck II (3D) - Mohr-Coulomb / Overgap=10cm, rexc=3.0m (3.10m), s2=50m, s3=18m



FLAC3D 2.00

Step 20000 Model Perspective
20:37:15 Wed Jul 7 1999

Center:
X: 1.250e+01
Y: 4.500e+00
Z: 1.154e+01
Dist: 8.245e+01
Rotation:
X: 0.000
Y: 0.000
Z: 30.000
Mag.: 1
Ang.: 22.500

Plane Origin:
X: 6.000e+00
Y: 0.000e+00
Z: 0.000e+00
Plane Normal:
X: 1.000e+00
Y: 0.000e+00
Z: 0.000e+00

Block State

Plane: on behind

- None
- shear-n shear-p
- shear-n shear-p tension-p
- shear-p

Sketch

LineStyle

SCK.CEN

Figure C.21. Model 50 m × 18 m (lower bound) after the excavation of the secondary gallery with $P_1 = 4$ MPa, and of the disposal cell without support: plastic state indicator on planes located at $x=6$ m and $y=0$ m.

Job Title: Truck II (3D) - Mohr-Coulomb / Overgap=10cm, rexc=3.0m (3.10m), s2=50m, s3=18m

FLAC3D 2.00

Step: 20000 Model Perspective
20:37:20 Wed Jul 7 1999

Center: X: 1.250e+01 Y: 4.500e+00 Z: 1.154e+01
Rotation: X: 0.000 Y: 0.000 Z: 30.000
Dist: 8.245e+01 Mag.: 1
Ang.: 22.500

Plane Origin: X: 6.000e+00 Y: 0.000e+00 Z: 0.000e+00
Plane Normal: X: 1.000e+00 Y: 0.000e+00 Z: 0.000e+00

Contour of Pore Pressure



Sketch
Linestyle

SCK.CEN

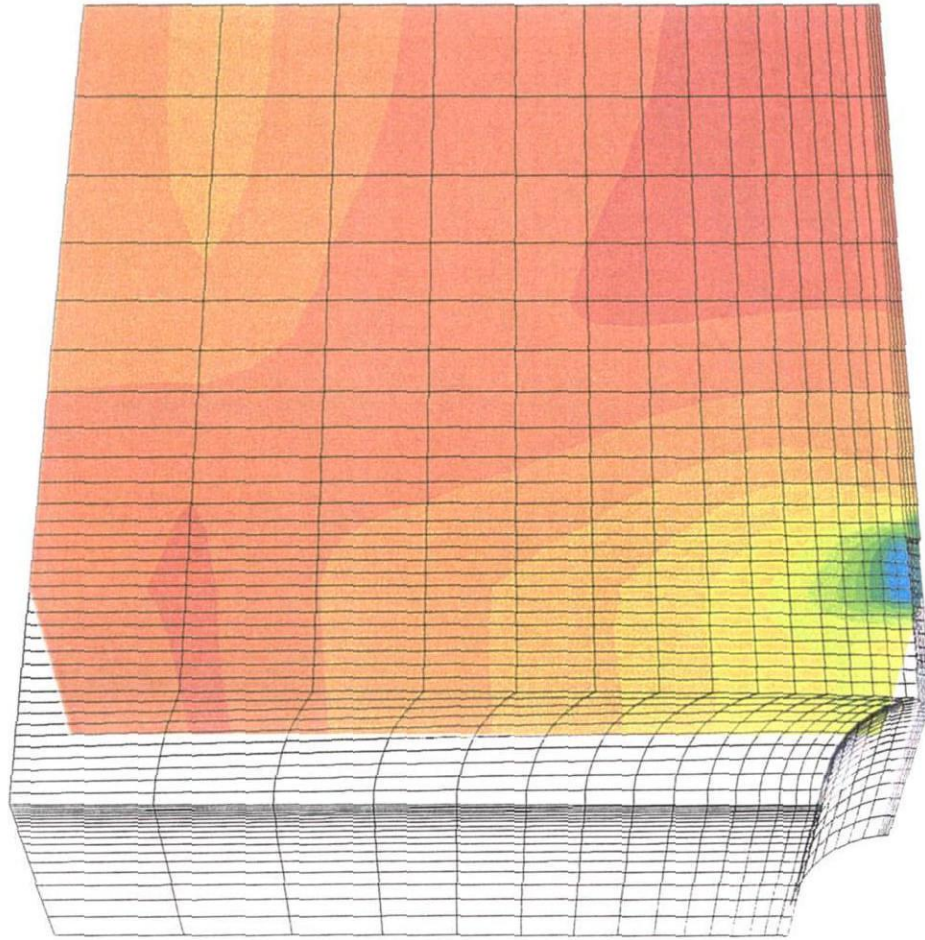


Figure C.22. Model 50 m × 18 m (lower bound) after the excavation of the secondary gallery with $P_1 = 4$ MPa, and of the disposal cell without support: pore pressure isovalues on planes located at $x=6$ m and $y=0$ m.

Job Title: Truck II (3D) - Mohr-Coulomb / Overgap=10cm, rexc=3.0m (3.10m), s2=50m, s3=18m

FLAC3D 2.00

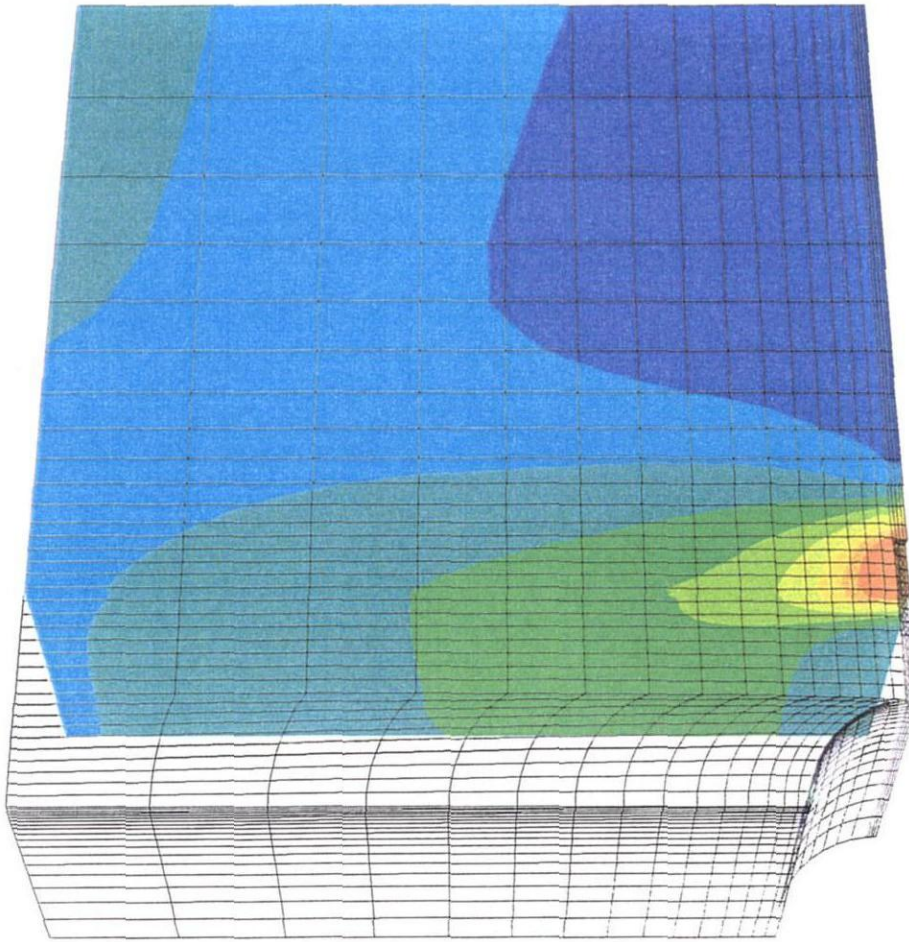
Step 20000 Model Perspective
20:38:06 Wed Jul 7 1999

Center: X: 1.250e+01 Y: 4.500e+00 Z: 1.154e+01
Dist: 8.245e+01
Rotation: X: 0.000 Y: 0.000 Z: 30.000
Mag.: 1
Ang.: 22.500

Plane Origin: X: 6.000e+00 Y: 0.000e+00 Z: 0.000e+00
Plane Normal: X: 1.000e+00 Y: 0.000e+00 Z: 0.000e+00

Contour of SZZ

Plane: on behind
Gradient Calculation
-1.2094e+07 to -1.1000e+07
-1.1000e+07 to -1.0000e+07
-1.0000e+07 to -9.0000e+06
-9.0000e+06 to -8.0000e+06
-8.0000e+06 to -7.0000e+06
-7.0000e+06 to -6.0000e+06
-6.0000e+06 to -5.0000e+06
-5.0000e+06 to -4.0000e+06
-4.0000e+06 to -4.0000e+06
Interval = 1.0e+06



Sketch
LineStyle

SCK.CEN

Figure C.23. Model 50 m × 18 m (lower bound) after the excavation of the secondary gallery with $P_i = 4$ MPa, and of the disposal cell without support: σ_{zz} isovalues on planes located at $x=6$ m and $y=0$ m.

Job Title: Truck II (3D) - Mohr-Coulomb / Overgap=10cm, rexc=3.0m (3.10m), s2=50m, s3=18m

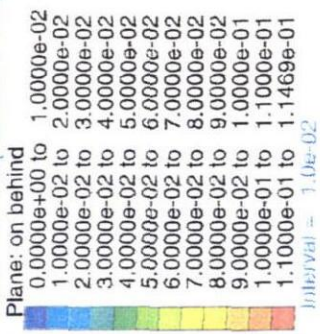
FLAC3D 2.00

Step 20000 Model Perspective
20:38:11 Wed Jul 7 1999

Center: Rotation:
X: 1.250e+01 X: 0.000
Y: 4.500e+00 Y: 0.000
Z: 1.154e+01 Z: 30.000
Dist: 8.245e+01 Mag.: 1
Ang.: 22.500

Plane Origin: Plane Normal:
X: 6.000e+00 X: 1.000e+00
Y: 0.000e+00 Y: 0.000e+00
Z: 0.000e+00 Z: 0.000e+00

Contour of Displacement Mag.



Sketch
Linestyle

SCK.CEN

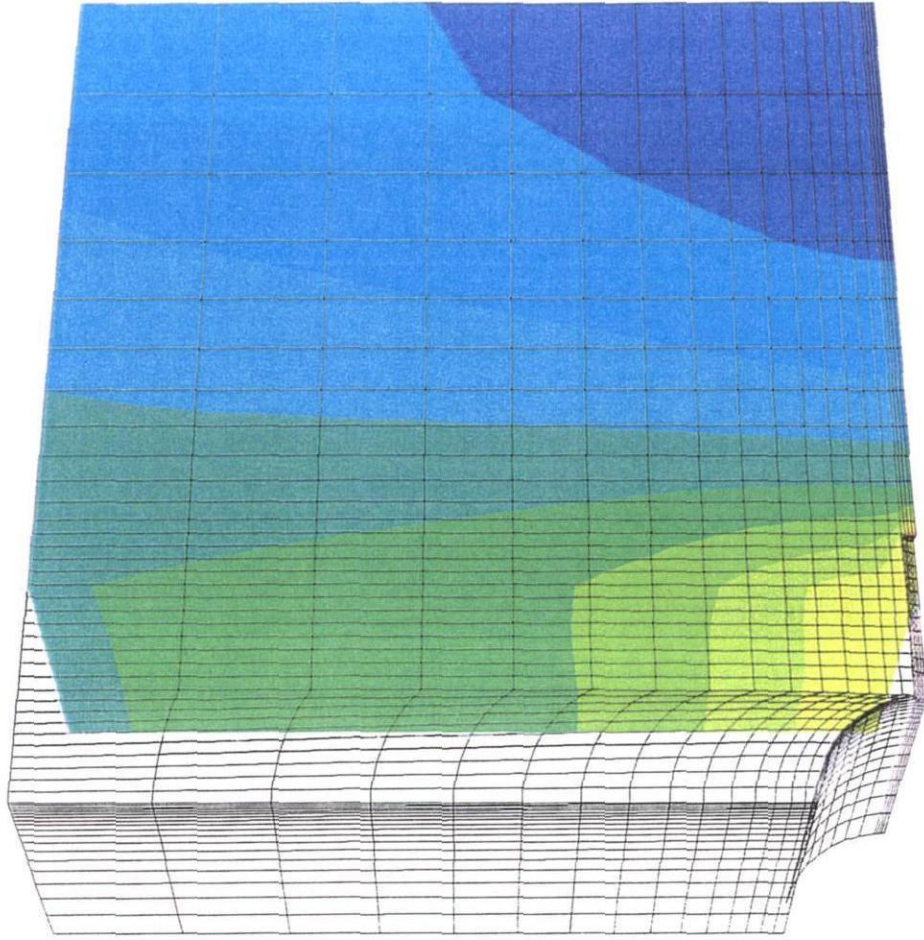


Figure C.24. Model 50 m × 18 m (lower bound) after the excavation of the secondary gallery with $P_1 = 4 \text{ MPa}$, and of the disposal cell without support: displacement magnitude isovalues on planes located at $x=6\text{m}$ and $y=0 \text{ m}$.

Job Title: Truck II (3D) - Mohr-Coulomb(strong) / Overgap=10cm, 3.10m, s2=30m, s3=18m

FLAC3D 2.00

Step 20000 Model Perspective
20:43:22 Wed Jul 7 1999

Center: X: 7.500e+00 Y: 4.500e+00 Z: 1.154e+01
Dist: 7.148e+01
Rotation: X: 0.000 Y: 0.000 Z: 30.000
Mag.: 1
Ang.: 22.500

Plane Origin: X: 6.000e+00 Y: 0.000e+00 Z: 0.000e+00
Plane Normal: X: 1.000e+00 Y: 0.000e+00 Z: 0.000e+00

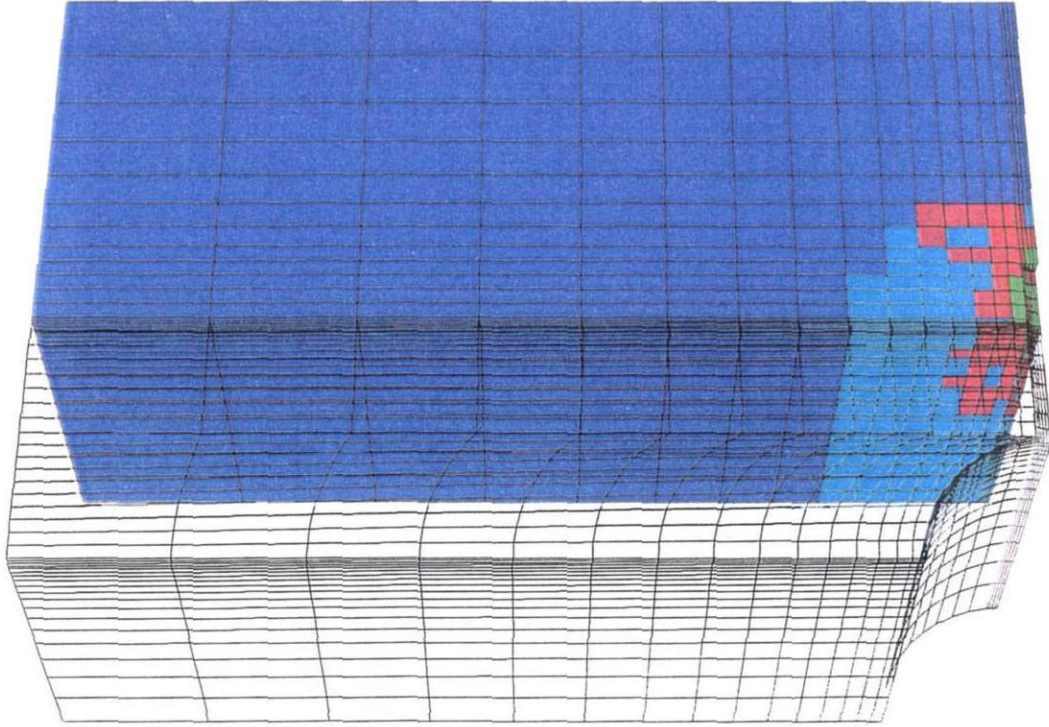
Block State

Plane: on behind

- None
- shear-n shear-p
- shear-n shear-p tension-p
- shear-p

Sketch

LineStyle



SCK.CEN

Figure C.25. Model 30 m × 18 m (upper bound) after the excavation of the secondary gallery with $P_i = 4$ MPa, and of the disposal cell without support: plastic state indicator on planes located at $x=6$ m and $y=0$ m.

Job Title: Truck II (3D) - Mohr-Coulomb(strong) / Overgap=10cm, 3.10m, s2=30m, s3=18m

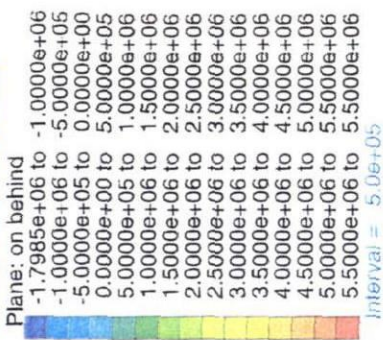
FLAC3D 2.00

Step 20000 Model Perspective
20:43:26 Wed Jul 7 1999

Center: X: 7.500e+00 Y: 4.500e+00 Z: 1.154e+01
Dist: 7.148e+01
Rotation: X: 0.000 Y: 0.000 Z: 30.000
Mag.: 1
Ang.: 22.500

Plane Origin: X: 6.000e+00 Y: 0.000e+00 Z: 0.000e+00
Plane Normal: X: 1.000e+00 Y: 0.000e+00 Z: 0.000e+00

Contour of Pore Pressure



Sketch
Linestyle

SCK.CEN

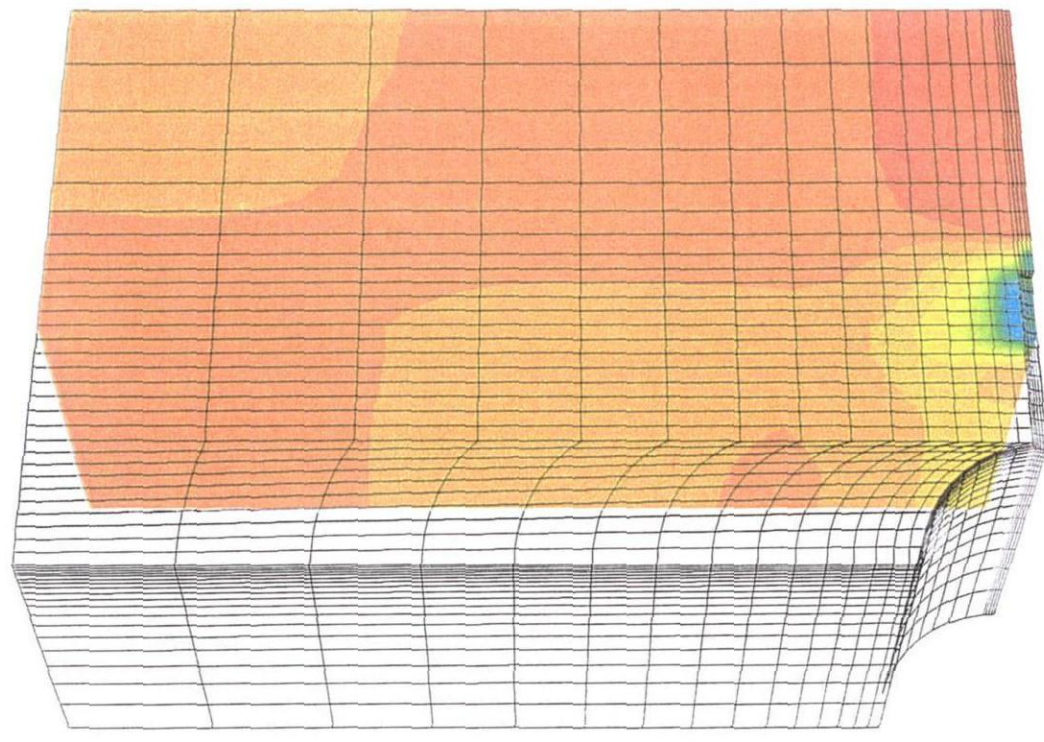


Figure C.26. Model 30 m × 18 m (upper bound) after the excavation of the secondary gallery with $P_i = 4 \text{ MPa}$, and of the disposal cell without support: pore pressure isovalues on planes located at $x=6\text{m}$ and $y=0 \text{ m}$.

Job Title: Truck II (3D) - Mohr-Coulomb(strong) / Overgap=10cm, 3.10m, s2=30m, s3=18m

FLAC3D 2.00

Step 20000 Model Perspective
20:43:32 Wed Jul 7 1999

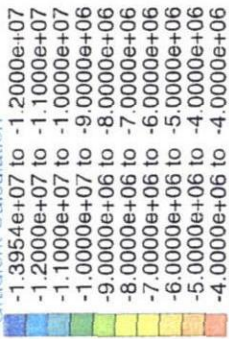
Center: Rotation:
X: 7.500e+00 X: 0.000
Y: 4.500e+00 Y: 0.000
Z: 1.154e+01 Z: 30.000
Dist: 7.148e+01 Mag.: 1
Ang.: 22.500

Plane Origin: Plane Normal:
X: 6.000e+00 X: 1.000e+00
Y: 0.000e+00 Y: 0.000e+00
Z: 0.000e+00 Z: 0.000e+00

Contour of σ_{zz}

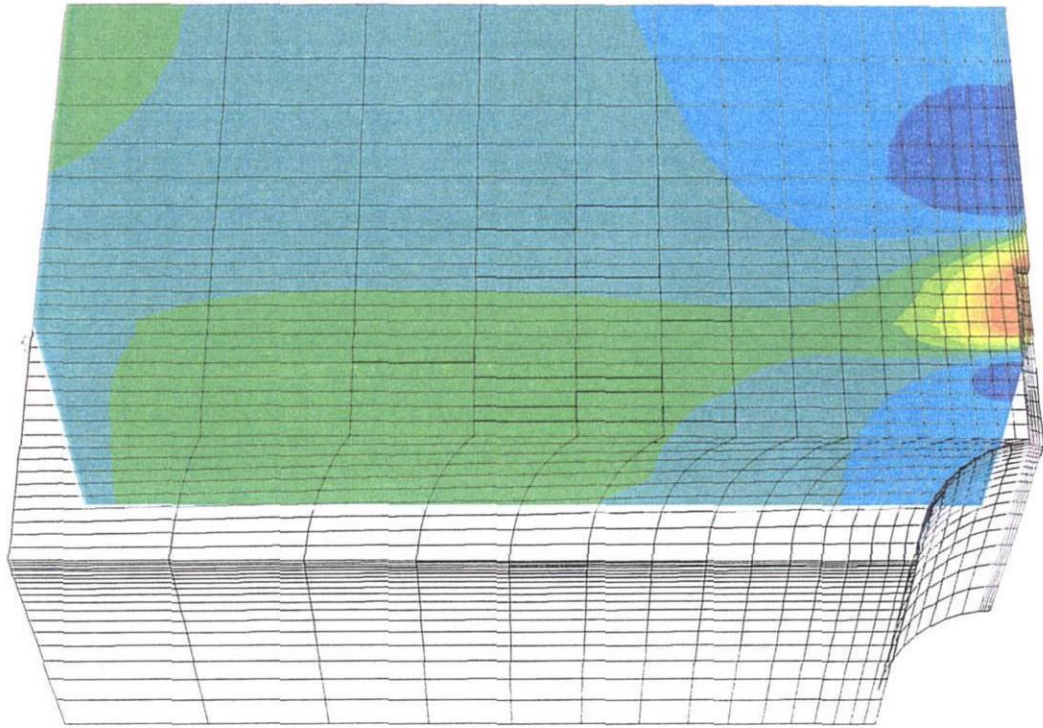
Plane: on behind

Gradient Calculation



Interval = 1.0e+06

Sketch
Linestyle



SCK.CEN

Figure C.27. Model 30 m × 18 m (upper bound) after the excavation of the secondary gallery with $P_i = 4$ MPa, and of the disposal cell without support: σ_{zz} isovalues on planes located at $x=6$ m and $y=0$ m.

Job Title: Truck II (3D) - Mohr-Coulomb(strong) / Overgap=10cm, 3.10m, s2=30m, s3=18m

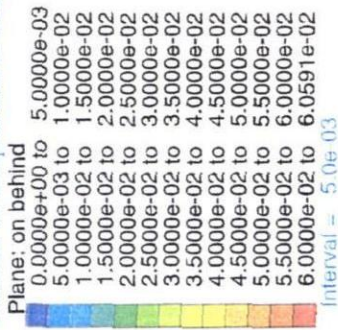
FLAC3D 2.00

Step 20000 Model Perspective
20:43:37 Wed Jul 7 1999

Center: X: 7.500e+00 Y: 4.500e+00 Z: 1.154e+01
Dist: 7.148e+01
Rotation: X: 0.000 Y: 0.000 Z: 30.000
Mag.: 1
Ang.: 22.500

Plane Origin: X: 6.000e+00 Y: 0.000e+00 Z: 0.000e+00
Plane Normal: X: 1.000e+00 Y: 0.000e+00 Z: 0.000e+00

Contour of Displacement Mag.



Sketch
LineStyle

SCK.CEN

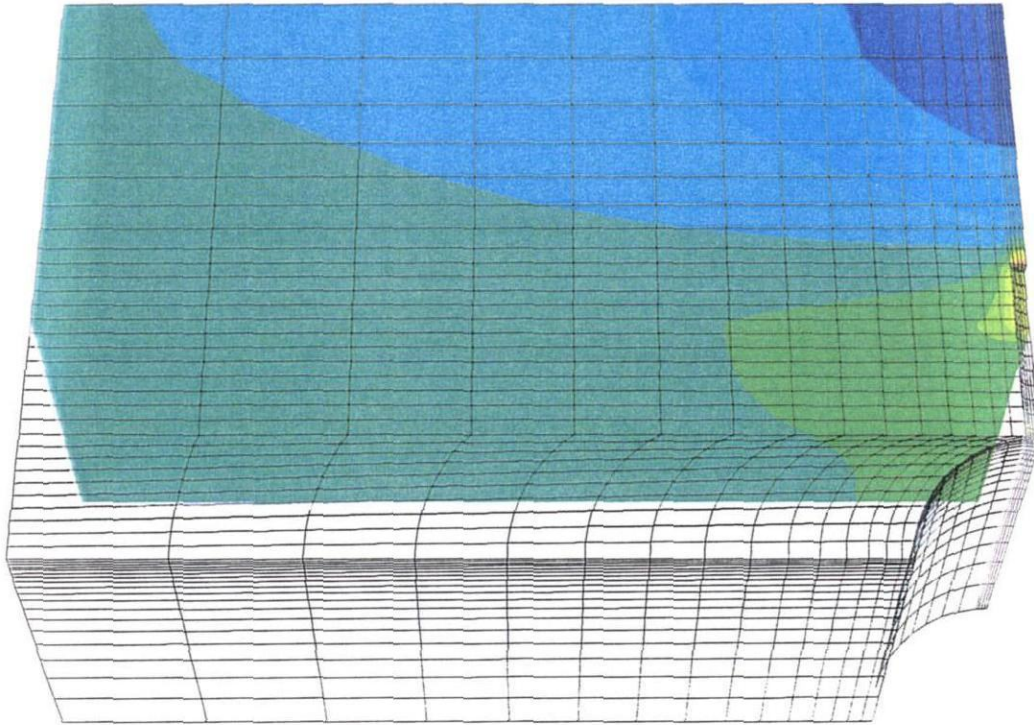


Figure C.28. Model 30 m × 18 m (upper bound) after the excavation of the secondary gallery with $P_i = 4$ MPa, and of the disposal cell without support: displacement magnitude isovalues on planes located at $x=6$ m and $y=0$ m.

Job Title: Truck II (3D) - Mohr-Coulomb(strong) / Overgap=10cm, 3.10m, s2=50m, s3=18m

FLAC3D 2.00

Step 20000 Model Perspective
20:41:24 Wed Jul 7 1999

Center: X: 1.250e+01 Y: 4.500e+00 Z: 1.155e+01
Dist: 8.245e+01
Rotation: X: 0.000 Y: 0.000 Z: 30.000
Mag.: 1
Ang.: 22.500

Plane Origin: X: 6.000e+00 Y: 0.000e+00 Z: 0.000e+00
Plane Normal: X: 1.000e+00 Y: 0.000e+00 Z: 0.000e+00

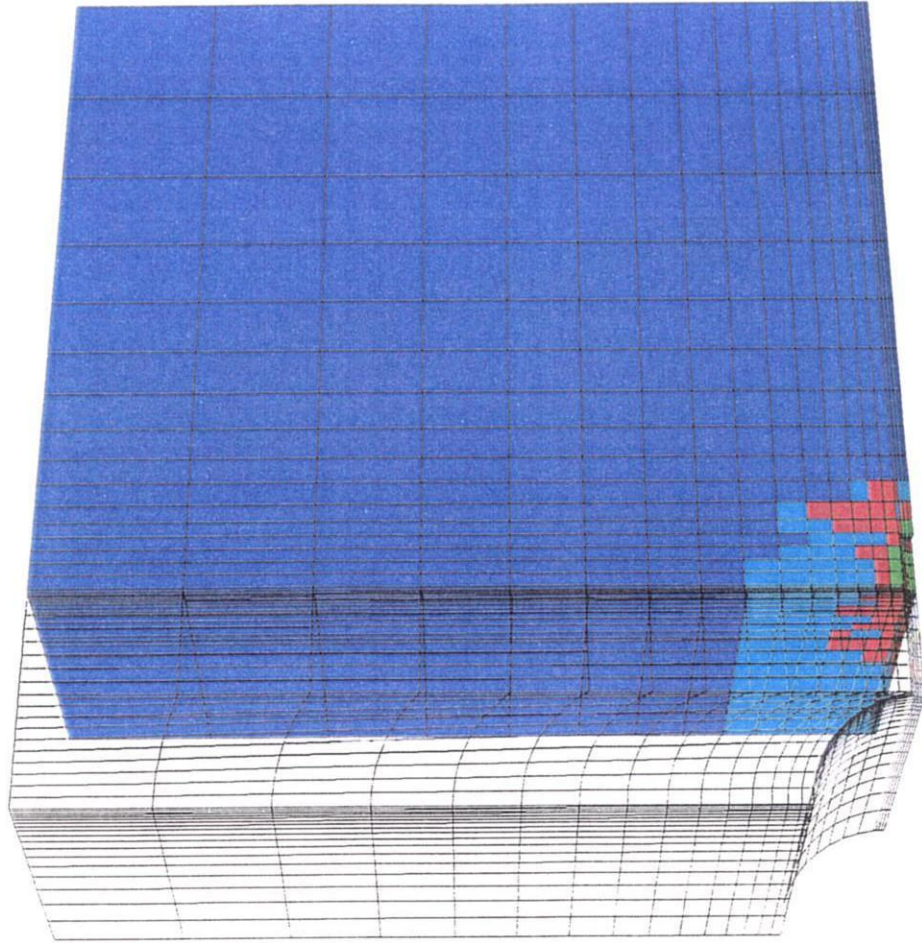
Block State

Plane: on behind

- None
- shear-n shear-p
- shear-n shear-p tension-p
- shear-p

Sketch

Linestyle



SCK.CEN

Figure C.29. Model 50 m × 18 m (upper bound) after the excavation of the secondary gallery with $P_1 = 4$ MPa, and of the disposal cell without support: plastic state indicator on planes located at $x=6$ m and $y=0$ m.

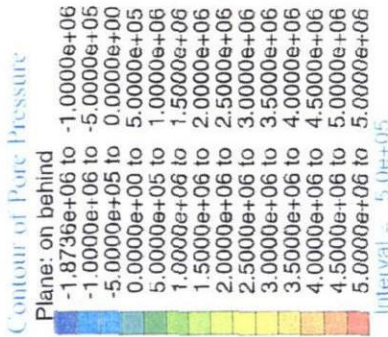
Job Title: Truck II (3D) - Mohr-Coulomb(strong) / Overgap=10cm, 3.10m, s2=50m, s3=18m

FLAC3D 2.00

Step 20000 Model Perspective
20:41:31 Wed Jul 7 1999

Center: Rotation:
X: 1.250e+01 X: 0.000
Y: 4.500e+00 Y: 0.000
Z: 1.155e+01 Z: 30.000
Dist: 8.245e+01 Mag.: 1
 Ang.: 22.500

Plane Origin: Plane Normal:
X: 6.000e+00 X: 1.000e+00
Y: 0.000e+00 Y: 0.000e+00
Z: 0.000e+00 Z: 0.000e+00



Sketch
Linestyle

SCK.CEN

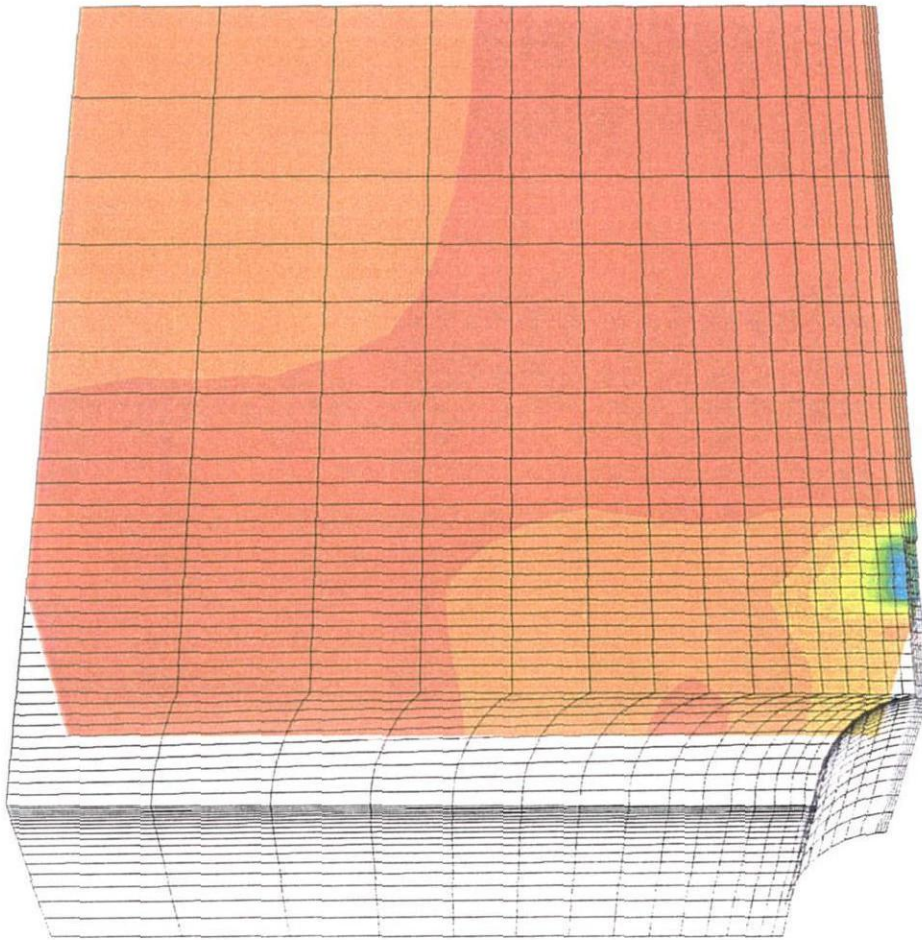
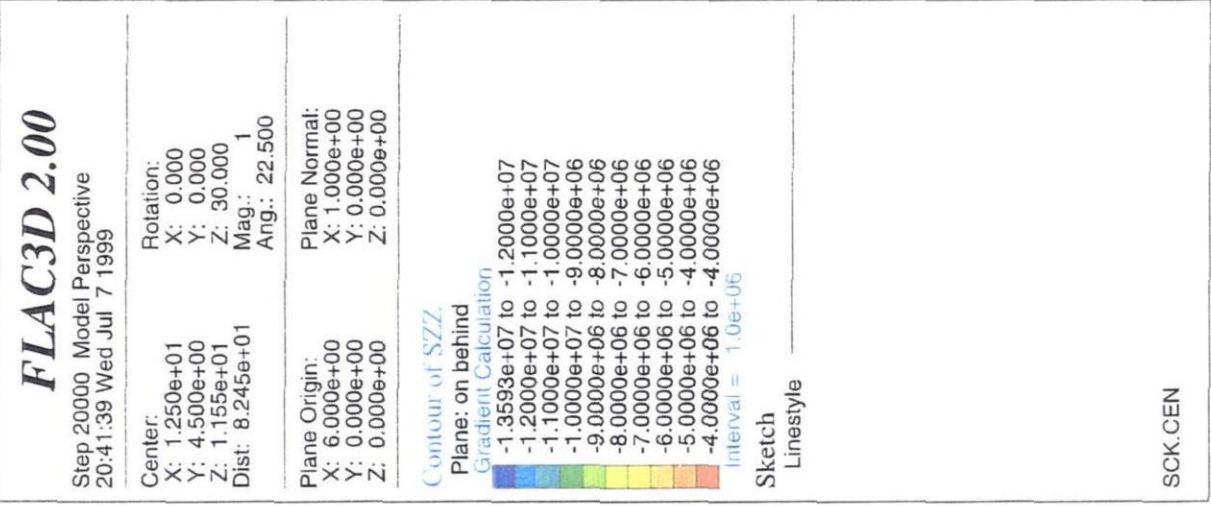


Figure C.30. Model 50 m × 18 m (upper bound) after the excavation of the secondary gallery with $P_i = 4$ MPa, and of the disposal cell without support: pore pressure isovahues on planes located at $x=6m$ and $y=0$ m.

Job Title: Truck II (3D) - Mohr-Coulomb(strong) / Overgap=10cm, 3.10m, s2=50m, s3=18m



SCK.CEN

Figure C.31. Model 50 m × 18 m (upper bound) after the excavation of the secondary gallery with $P_1 = 4$ MPa, and of the disposal cell without support: σ_{zz} isovalues on planes located at $x=6$ m and $y=0$ m.

Job Title: Truck II (3D) - Mohr-Coulomb(strong) / Overgap=10cm, 3.10m, s2=50m, s3=18m

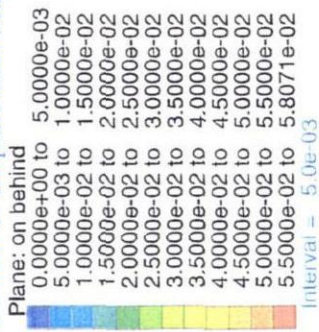
FLAC3D 2.00

Step 20000 Model Perspective
20:41:45 Wed Jul 7 1999

Center: X: 1.250e+01 Y: 4.500e+00 Z: 1.155e+01
Dist: 8.245e+01
Rotation: X: 0.000 Y: 0.000 Z: 30.000
Mag.: 1
Ang.: 22.500

Plane Origin: X: 6.000e+00 Y: 0.000e+00 Z: 0.000e+00
Plane Normal: X: 1.000e+00 Y: 0.000e+00 Z: 0.000e+00

Contour of Displacement Mag.



Sketch
Linstyle

SCK.CEN

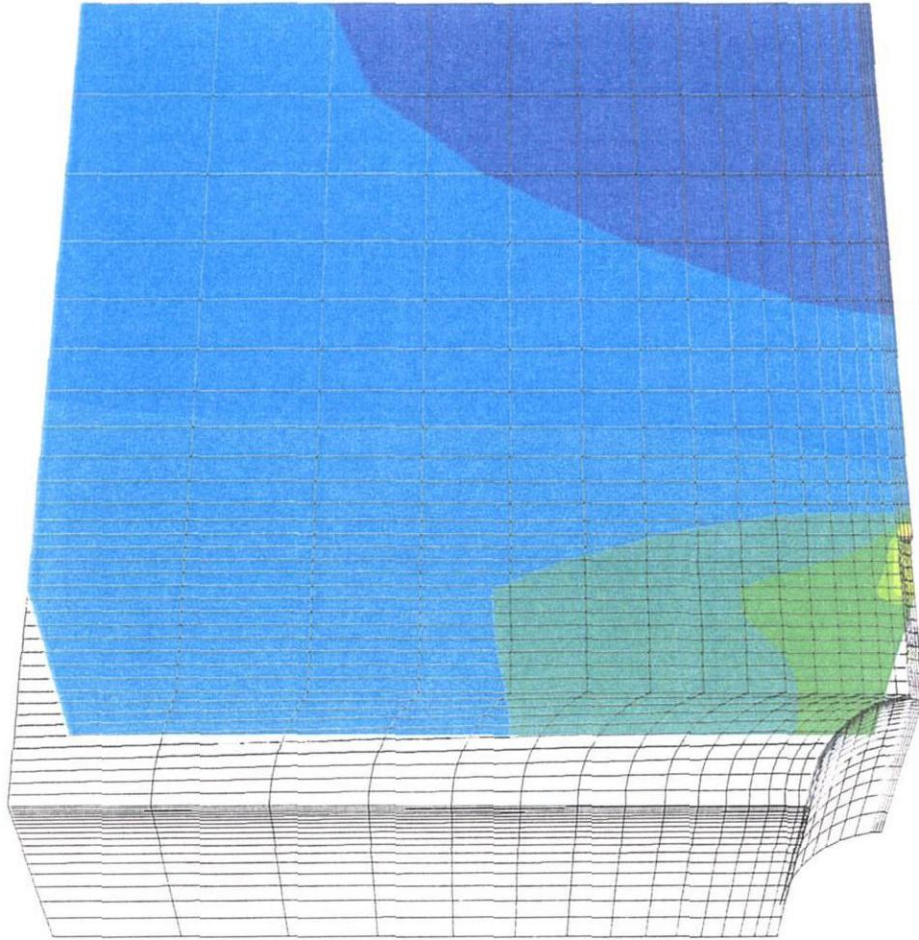


Figure C.32. Model 50 m × 18 m (upper bound) after the excavation of the secondary gallery with $P_1 = 4$ MPa, and of the disposal cell without support: displacement magnitude isovalues on planes located at $x=6m$ and $y=0$ m.

Appendix D - Analytical solution for the function f_ω

The general solution for the thermal variation field $\Delta T(x', t')$

$$\Delta T(x', t') = T_a \cdot f_\omega(x', t'; d'; \omega') \quad (3.15)$$

depends on T_a (given by equation (3.16)) and on the function $f_\omega(z', t'; d'; \omega')$. Here, only the final expression for $f_\omega(z', t'; d'; \omega')$ is given; for the full derivation of $f_\omega(z', t'; d'; \omega')$, the reader is referred to Giraud (1993).

Depending on the value of the 1-D co-ordinates z , three cases are distinguished to compute the function $f_\omega(z', t'; d'; \omega')$:

$$(1) \quad 1 \leq z' \leq d'$$

$$f_\omega(z', t'; d'; \omega') = -\{f_{T\omega}(z_1', t'; \omega') - f_{T\omega}(z_2', t'; \omega') - f_{T\omega}(z_3', t'; \omega') + f_{T\omega}(z_4', t'; \omega')\}$$

$$(2) \quad -1 \leq z' \leq 1$$

$$f_\omega(z', t'; d'; \omega') = \left\{ \begin{array}{l} f_{T\omega}(z_1', t'; \omega') - f_{T\omega}(z_2', t'; \omega') + f_{T\omega}(z_3', t'; \omega') + f_{T\omega}(z_4', t'; \omega') \\ -\frac{1}{2\omega'}(1 - e^{-\omega' t'}) \end{array} \right\} \quad (D.1)$$

$$(3) \quad -\infty \leq z' \leq -1$$

$$f_\omega(z', t'; d'; \omega') = -\{f_{T\omega}(z_1', t'; \omega') - f_{T\omega}(z_2', t'; \omega') + f_{T\omega}(z_3', t'; \omega') - f_{T\omega}(z_4', t'; \omega')\}$$

This general solution (D.1) depends on the adimensional functions

$$\begin{array}{ll} z_1' = -1 + 2d' - z' & z_2' = 1 + 2d' - z' \\ z_3' = -1 + z' & z_4' = 1 + z' \end{array} \quad (D.2)$$

and on a sum of the function $f_{T\omega}(z', t'; \omega')$ computed for z_1', z_2', z_3', z_4' that is defined by

$$f_{T\omega}(z', t'; \omega') = \frac{1}{4\omega'} \left(\operatorname{erfc} \left[\frac{z'}{t'^{1/2}} \right] - e^{-\omega' t'} \operatorname{Re} \left[e^{2z' i \omega'^{1/2}} \operatorname{erfc}[u(z)] \right] \right) \quad (D.3)$$

where the complex variable $u(z)$ is defined by

$$u(z) = \frac{z'}{t'^{1/2}} + i(\omega' t')^{1/2} \quad (D.4)$$

In (D.3), the complementary error function erfc of the complex variable $u(z)$ is evaluated from the infinite serie approximation given in the Handbook of Mathematical Functions (Abramowitz and Stegun, 1964), see formula 7.1.29 p.299

$$\operatorname{erf}(x + iy) = \operatorname{erf}(x) + \frac{e^{-x^2}}{2\pi x} [1 - 2\cos(2xy) + i\sin(2xy)] + \frac{2}{\pi} e^{-x^2} \sum_{n=1}^{\infty} [f_n(x, y) + i g_n(x, y)] \quad (D.5a)$$

with

$$\begin{array}{l} f_n(x, y) = 2x - 2x \cosh(ny) \cos(2xy) + n \sinh(ny) \sin(2xy) \\ g_n(x, y) = 2x \cosh(ny) \sin(2xy) + n \sinh(ny) \cos(2xy) \end{array} \quad (D.5b)$$

The infinite serie in (D.5a) is evaluated numerically such that the error $e(\Delta T)$ on the temperature field $\Delta T(x',t')$ verifies

$$|e(\Delta T)| \leq 10^{-5} \text{ K}, \quad (\text{D.6})$$

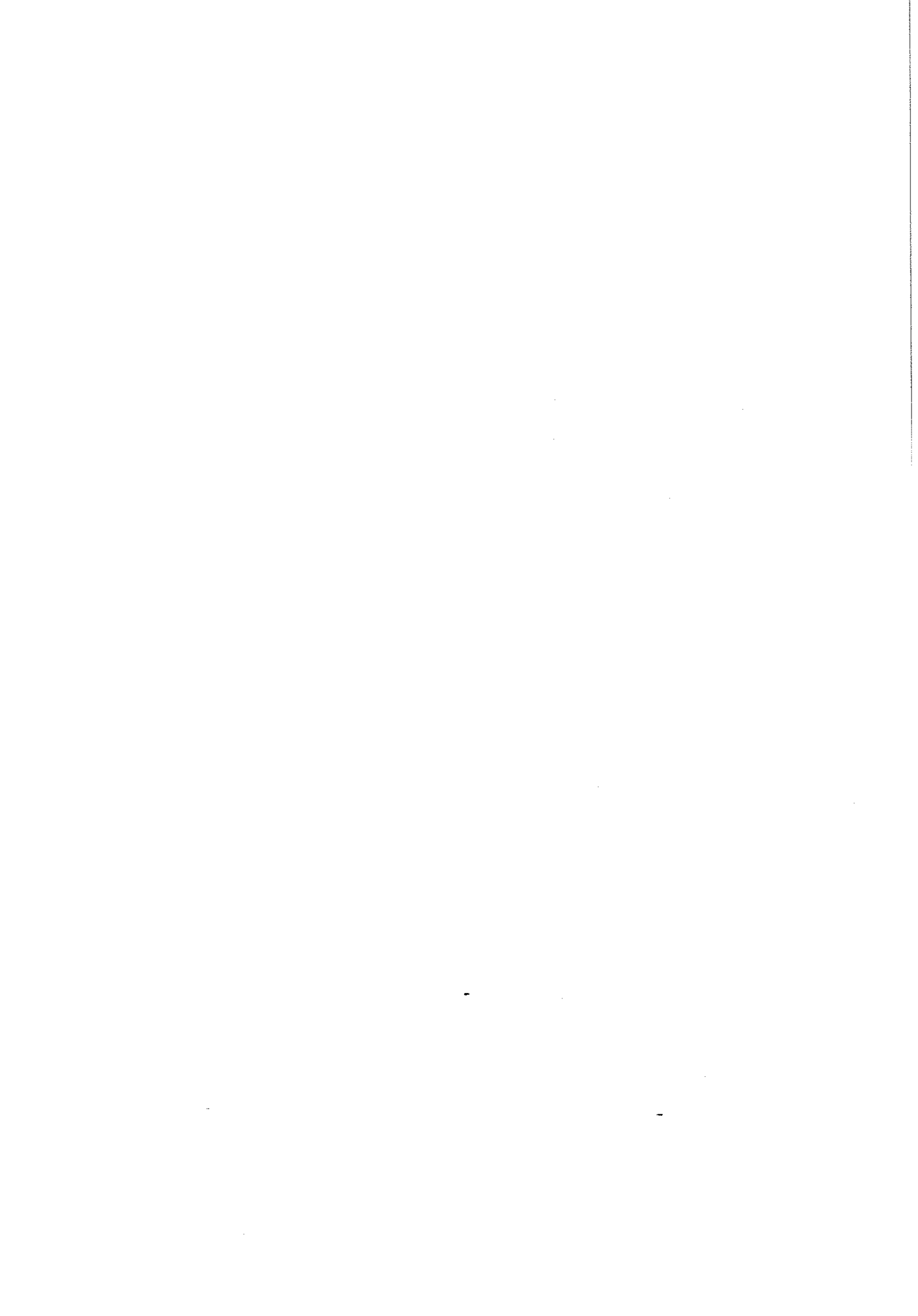
which then require to evaluate each individual function $f_{T_\omega}(z',t';\omega')$ with an error $e(f_{T_\omega})$ such that

$$|e(f_{T_\omega})| \leq \frac{10^{-5}}{4T_a} \quad (\text{D.7})$$

References

- Giraud A. 1993. Couplages thermo-hydro-mécaniques dans les milieux poreux peu perméables : application aux argiles profondes. *Thèse de doctorat de l'Ecole Nationale des Ponts et Chaussées*.
- Handbook of Mathematical Functions. 1964. A.M.S. 55, Abramowitz M. and Stegun J.A (Eds).

Appendix E - Report on the geomechanical tests performed at UCL-LGC





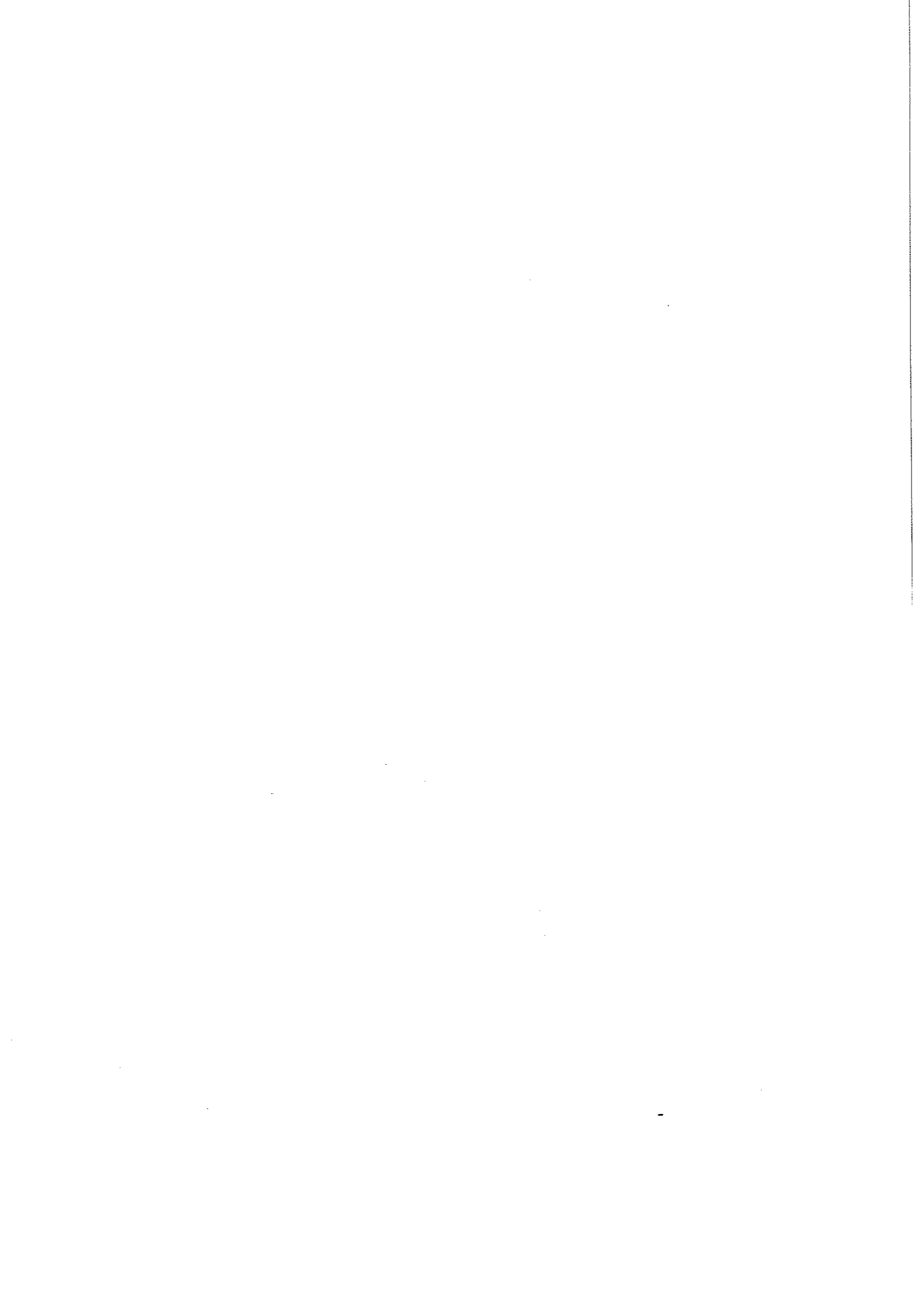
PROJECT TRUCK II

TEST RESULTS

Louvain-la-Neuve July 8, 1999

ir. S. DE COCK
Research Assistant

Prof. Dr. ir. J.F. THIMUS
Promoter





Contents

0. The project TRUCK II	3
1. Origin of the samples	4
2. Types of tests to realize on the sample	4
3. Methods and techniques used for testing	4
3.1 Preparation of the samples	4
3.2 CTU test	5
3.3 HCD test	6
4. The samples	6
4.1 Characteristics of the samples	6
4.2 Sedimentation analysis	7
4.3 Mineralogical analysis	7
5. Results	9
5.1 Consolidation	9
5.2 CTU tests	9
5.2.1 <i>Stress paths</i>	9
5.2.2 <i>Shear strength parameters</i>	19
5.2.3 <i>Modulus of shear deformation</i>	24
5.2.4 <i>Numerical values for each test</i>	25
5.3 HCD tests	25
5.3.1 <i>Results</i>	25
5.3.2 <i>Parameters of the Cam-Clay model</i>	30
6. Conclusions	32
6.1 Characteristics of the samples	32
6.2 CTU tests	32
6.3 HCD tests	32
7. Appendix	33



0. The project TRUCK II

The project TRUCK II contains an experimental programme on the hydromechanical behaviour of the Boom Clay.

By request of the Netherlands Institute of Applied Geoscience TNO, the Université catholique de Louvain has carried out hydromechanical tests on sample material from Belgium and the Netherlands.

The individual tests were defined in agreement with Mr. A.F.B. Wildenborg and Mr. G. de Lange from NITG-TNO, and Mr. B. Neerdael from SCK/CEN at Mol.

The test programme is composed of 5 triaxial tests over samples from 5 different depths to estimate the Mohr-Coulomb and Cam-Clay model parameters.



1. Origin of the samples

The samples come from five different places, four situated in Belgium and one in the Netherlands. Each site corresponds to a different depth :

Table 1 : Origin of the samples

Doel 2b	(B)	69.23 - 69.68 m
Zoersel	(B)	120.47 - 121.22 m
Mol	(B)	224.52 - 225.06 m 229.18 - 229.28 m
Weelde	(B)	313.22 - 313.55 m
Blija	(NL)	454.50 - 455.00 m 478.00 - 478.50 m

2. Types of tests to realize on the sample

The tests to realize on the clay samples consist of consolidated undrained or drained triaxial tests. For each depth, four triaxial tests must be realized :

- 3 CTU tests (consolidated and undrained test) where the lateral pressure is fixed while the axial pressure increases with the deformation of the sample
- 1 HCD test (hydrostatic, consolidated and drained test) where the axial and lateral pressures are identical.

For a same depth, the difference between the 3 CTU tests consists of the value of the initial stress state of the isotropic consolidation and of lateral stress during the test.

3. Methods and techniques used for testing

3.1 Preparation of the samples

The test sample should be large enough to represent adequately the material whose properties are to be determined. For the triaxial tests, samples should be of a length/diameter ratio of at least 2/1, but not greater than about 2.5/1. In our case, the samples are about 76 mm height and 38 mm diameter.

The saturation of the samples with de-aired water is done by application of a pore water pressure of 0.2 MPa in the sample so the air as a separate phase in the void spaces is eliminated. Due to the high degree of saturation of the samples, this saturation is almost instantaneous.



In the consolidation stage the sample is isotropically consolidated under a confining pressure by allowing water to drain out. Drainage of water results in a decrease in volume and an increase in the effective stress, which after consolidation is equal to the difference between the confining pressure and the mean pore pressure remaining in the sample. The consolidation is complete when the sample is stabilised and does not expel water. The consolidation bearings are 1 MPa and each bearing last seven days at least.

The characteristics of the realized tests are given in the table 2.

Table 2 : Tests realized on the samples

Origin	Sample	Depth [m]	Test realised	Normal soil consolidation s_0 [MPa]	Consolidation of the samples σ_c [MPa]	Consolidation ratio [%]
Doel (B)	a	69.42	CTU	1.39	0.70	50.4
	b	69.42	CTU	1.39	1.05	75.5
	c	69.55	CTU	1.39	1.40	100.7
	d	69.55	HCD	1.39	1.60	-
Zoersel (B)	a	120.57	CTU	2.41	1.20	49.8
	b	120.57	CTU	2.41	1.80	74.7
	c	120.67	CTU	2.41	2.40	99.6
	d	120.67	HCD	2.41	1.60	-
Mol (B)	b	224.52	CTU	4.49	3.38	75.3
	c	224.52	CTU	4.49	4.50	100.2
Mol (B)	a	229.23	CTU	4.58	2.25	49.1
	d	229.23	HCD	4.58	1.60	-
Weelde (B)	a	313.30	CTU	6.27	3.10	49.4
	b	313.30	CTU	6.27	4.70	75.0
	c	313.50	CTU	6.27	6.26	99.8
	d	313.50	HCD	6.27	1.60	-
Blija (NL)	a	454.75	CTU	9.20	4.60	50.0
	b	454.75	CTU	9.20	6.90	75.0
	c	454.75	CTU	9.20	9.20	100.0
	d	478.25	HCD	9.65	1.60	-

3.2 CTU test

After the consolidation, the sample is placed in the cell and the axial load increases gradually while the total confining pressure remains constant, until failure occurs due to the overcome of the maximum available shear strength of the sample.

In this test no change of water content of the sample is allowed while it is being compressed. The undrained conditions mean that there is no change in sample volume during the test. To allow pore



pressure changes to equalise throughout the sample, compression is applied slowly enough. The displacement rate is fixed at 10^{-2} mm/min, except during a loading-unloading cycle where it is fixed at $2 \cdot 10^{-3}$ mm/min.

$$\bar{\gamma} = \frac{\dot{\gamma}}{\dot{\epsilon}} = 0.19 / \text{day}$$

During the test, the following parameters are continuously measured :

- the axial stress
- the lateral stress
- the pore pressure
- the axial strain.

The results allow to estimate the shear strength parameters for the soil and the parameter M of the Cam-Clay model. These parameters are computed at the peak deviator stress.

3.3 HCD test

In this test, the axial and lateral pressures remain identical. These two pressures increase (and decrease) from 1.6 MPa to 10 MPa at the rate of 10^{-4} MPa/s. The maximum shear strength of the sample is not overcome.

This test allows to calculate the parameters of the Cam-Clay model : p_c , λ and k .

4. The samples

4.1 Characteristics of the samples

The selection of the geomechanical samples in the Doel, Zoersel, Mol, Weelde and Blija cores has been done owing to the scanners realized on the cores.

The table 3 summarizes the dry, saturated and specific weights and the initial and saturated water contents of the samples. The figures 1 and 2 represent respectively the evolution of the dry, saturated and specific weights and the evolution of the initial and saturated water contents versus the depth.

Table 3 : Characteristics of the samples

Origin	γ_d [kN/m ³]	γ_{sat} [kN/m ³]	γ_s [kN/m ³]	$w_{initial}$ [%]	w_{sat} [%]	S_r [%]	n [%]
Doel (B)	15.11	19.19	26.07	27.25	27.00	100.93	42.03
Zoersel (B)	15.11	19.30	26.41	27.30	27.70	98.56	42.76
Mol (B)	15.69	19.68	26.43	25.20	25.42	99.12	40.64
Weelde (B)	15.90	19.89	26.70	24.62	25.12	98.01	40.47
Blija (NL)	16.34	20.15	26.89	23.31	23.52	99.09	39.23

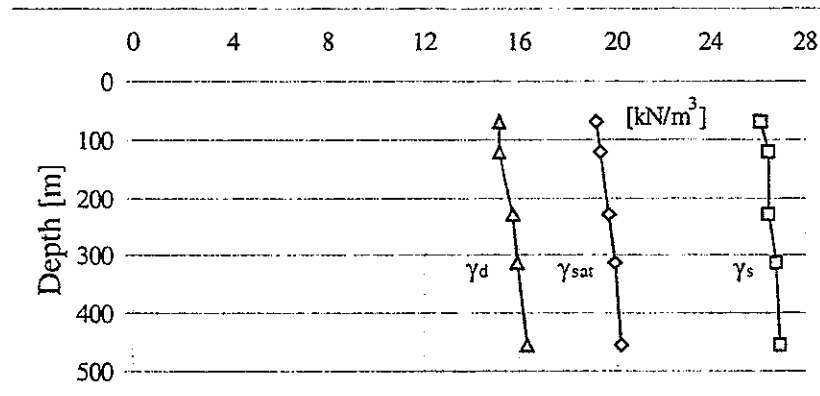


Fig. 1 : Dry, saturated and specific weights versus depth

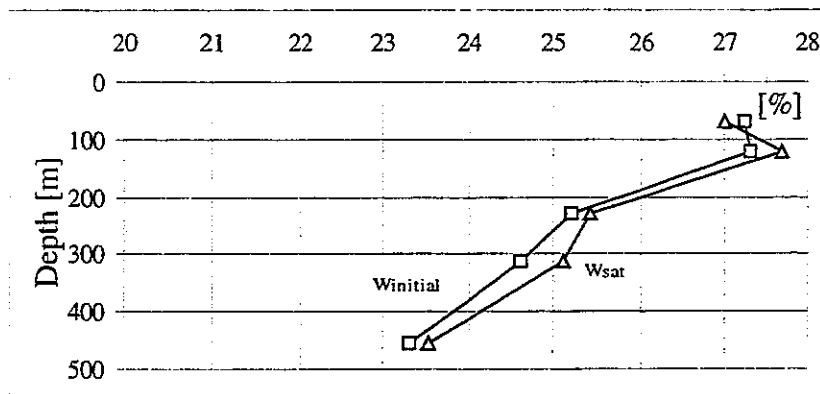


Fig. 2 : Initial and saturated water content versus depth

4.2 Sedimentation analysis

To verify the homogeneity of the samples, a sedimentation analysis was done for each site, one for Doel, Zoersel, Weelde and Blija, but two for Mol, due to the 5 meter depth difference between the samples. These analyses are given in the figure 3.

4.3 Mineralogical analysis

In the same purpose, a mineralogical analysis was done too for Doel, Zoersel, Weelde and 2 for Mol. The results of such analysis consist of 4 curves given in 2 different graphics.

The first curves (Appendix 1 to 5) represent the total spectra realized with the initial samples. These spectra indicate the presence of large amounts of quartz and feldspar, and there is no significant difference between all the samples.

For the other curves (Appendix 6 to 10), the clay ($d \leq 2\mu m$) is separated from the sample with sedimentation. The black curve corresponds to the unprocessed clay, the red one to the clay saturated by an atmosphere of glycol (it increases the heaving of the clay), and the blue one to the clay after a 500 °C burning.

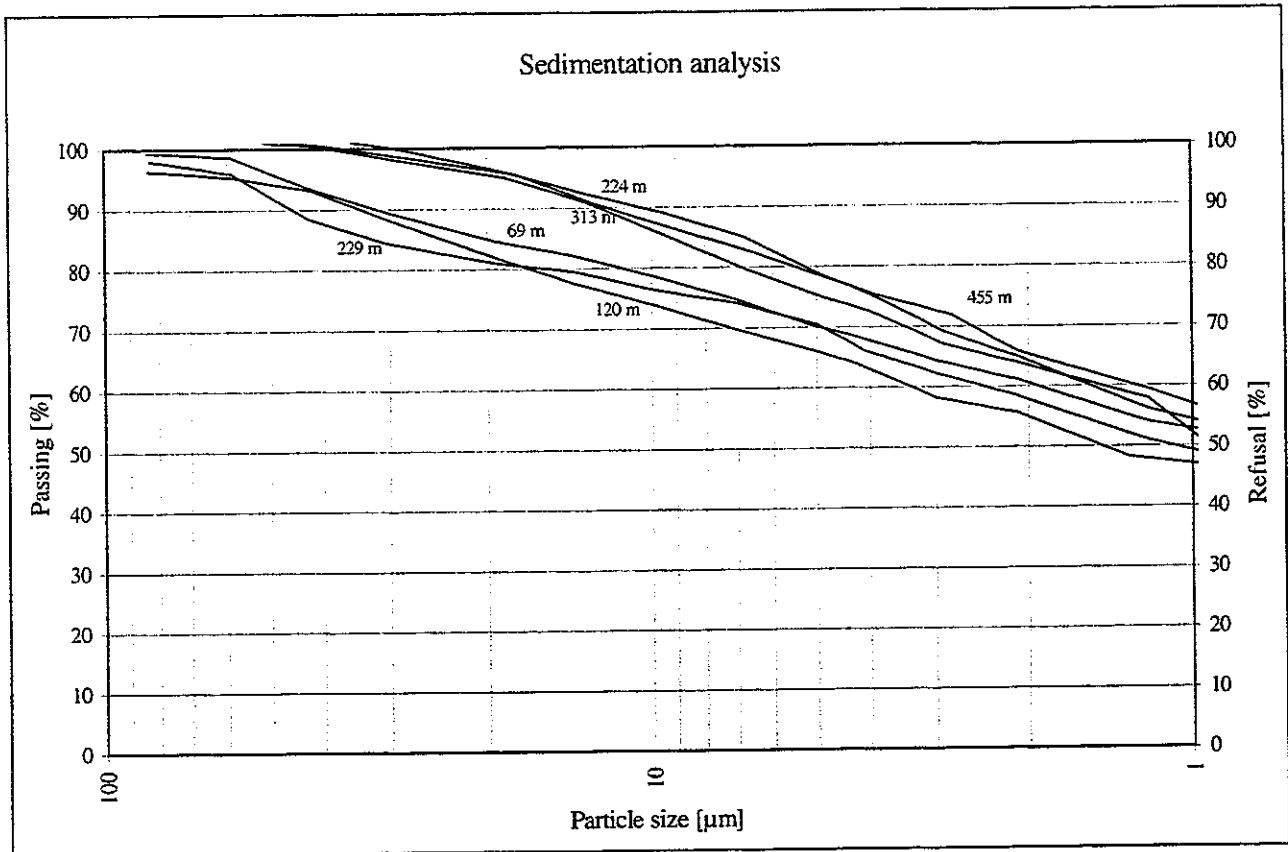


Fig. 3 : Sedimentation analysis for Doel (69 m), Zoersel (120 m), Mol (224 and 229 m), Weelde (313 m) and Blija (455 m)

Several remarks can be made over the analysis of the clay :

- For each sample, there are 3 different peaks :
 - 6 ° Smectite (Montmorillonite)
 - 8.5 ° Illite
 - 12 ° Kaolinite

Between 6 ° and 8.5 °, there are the interstratifieds of Montmorillonite and Illite. There is no difference between the samples, except about the Montmorillonite for the one from Doel (B).

- The glycol acts on the swelling sheets (montmorillonite principally) : the thickness of the sheets increases and its peak moves to the left of the graphics.
- The 500 °C burning eliminates the kaolinite. (12°)
- The clay is constituted for third to half of smectite. With regard to the initial sample, there is approximately between 20 and 30 % of smectite.



5. Results

5.1 Consolidation

The consolidation curves are done for each sample and are given in the appendix 11 to 28.

5.2 CTU tests

5.2.1 Stress paths

The next figures give, for each test, the deviator stress versus the mean effective stress (Fig. 4 to 8) and the deviatoric stress versus the mean total stress (Fig. 9 to 13).

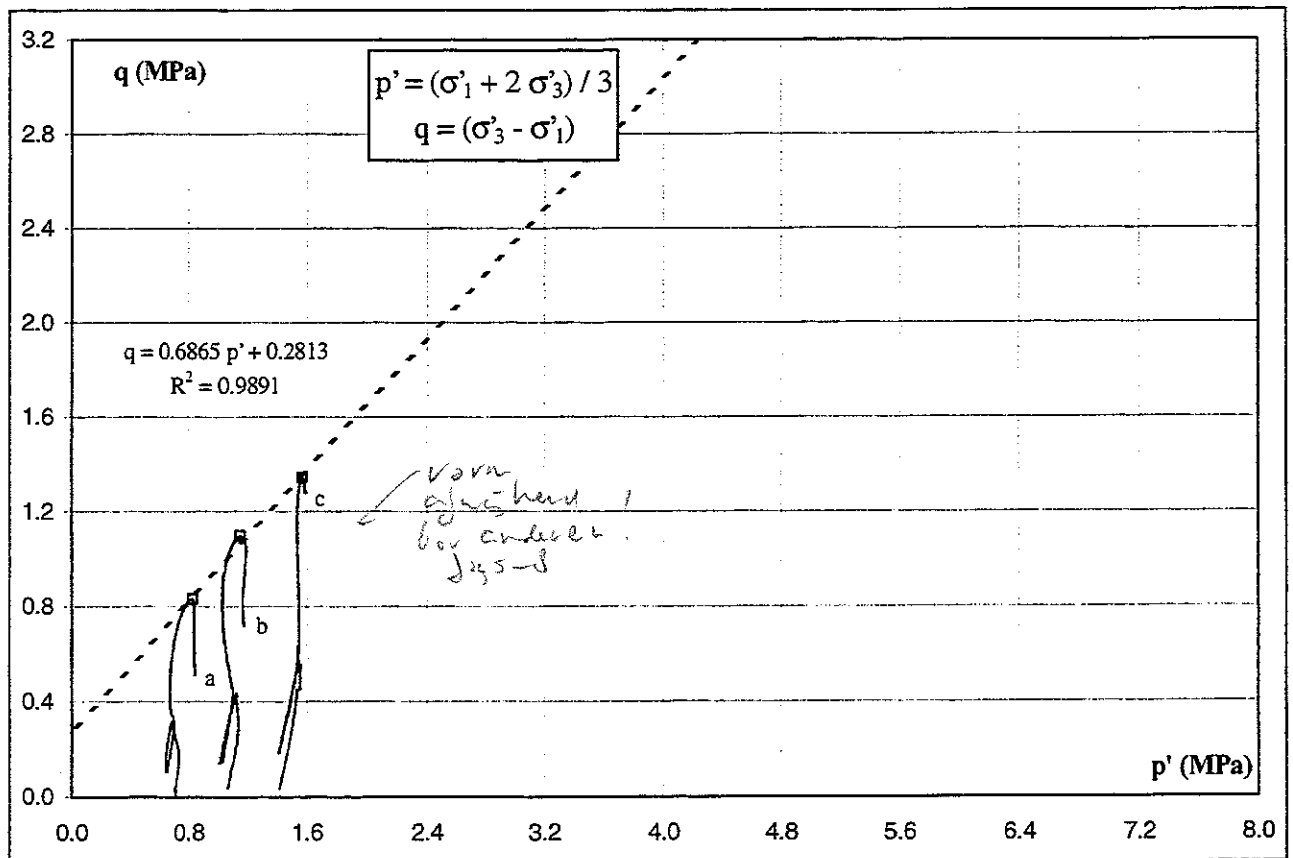


Fig. 4 : Deviator stress versus the mean effective stress for Doel (B) 69.23 - 69.68 m

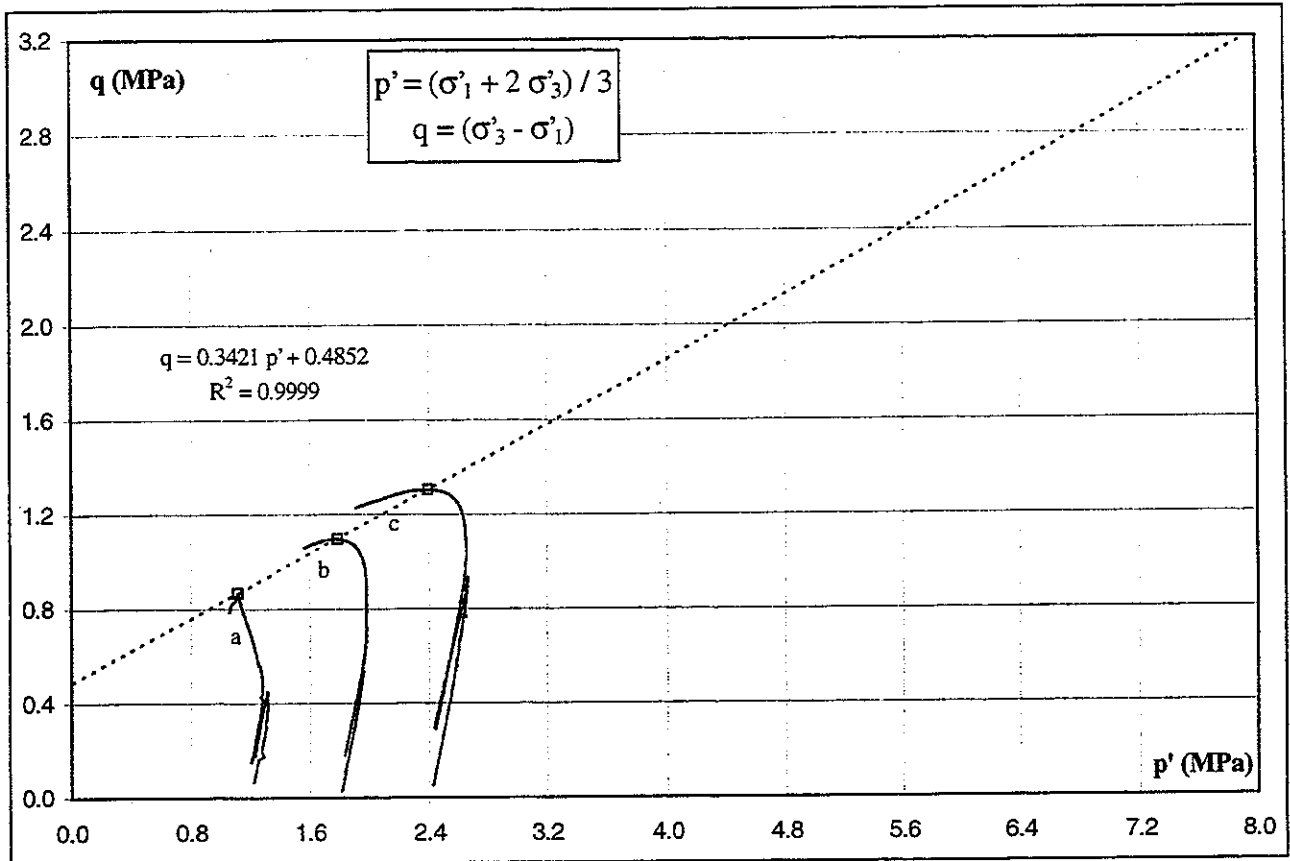


Fig. 5 : Deviator stress versus the mean effective stress for Zoersel (B) 120.47 - 121.22 m

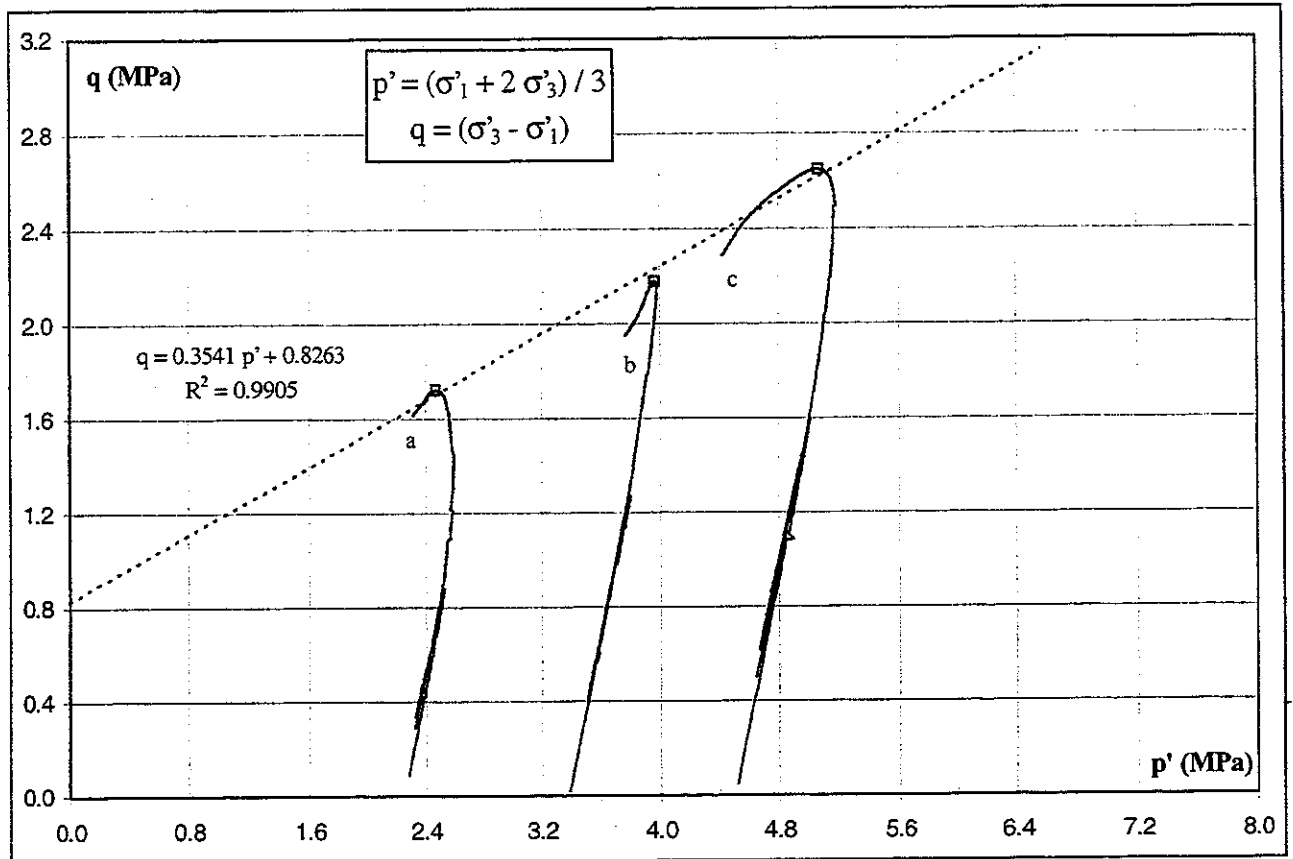


Fig. 6 : Deviator stress versus the mean effective stress for Mol (B) 229.18 - 229.28 m

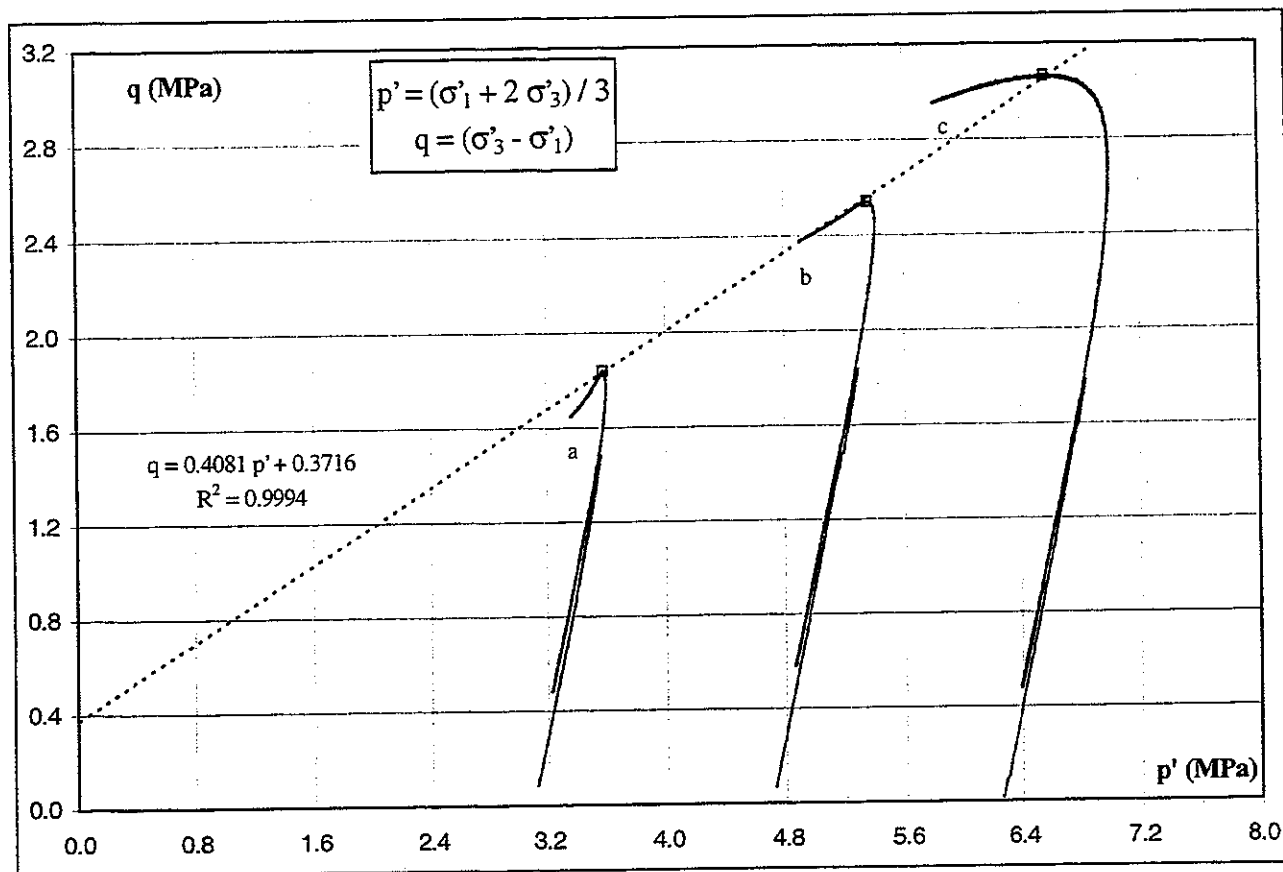


Fig. 7 : Deviator stress versus the mean effective stress for Weelde (B) 313.22 - 313.55 m

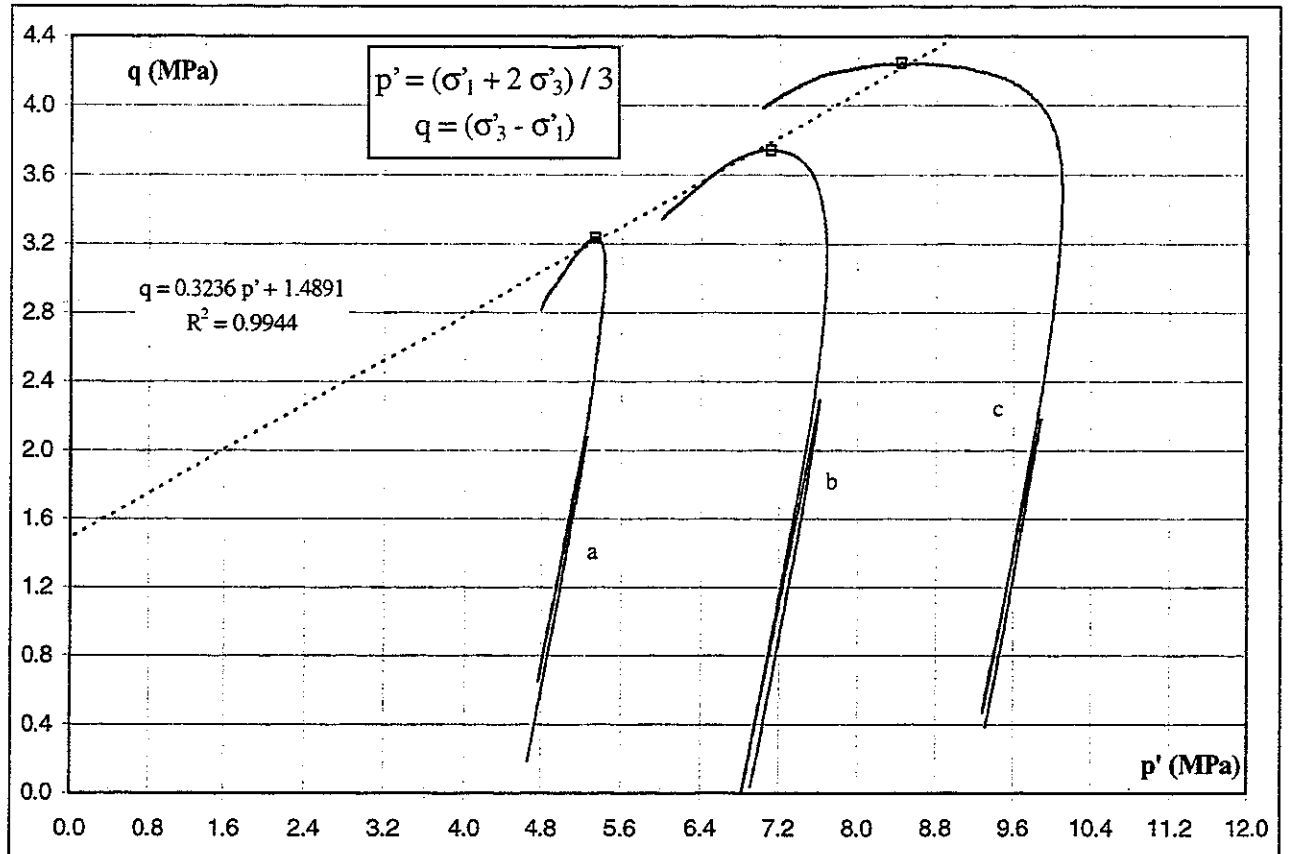


Fig. 8 : Deviator stress versus the mean effective stress for Blija (NL) 454.50 - 455.00 m

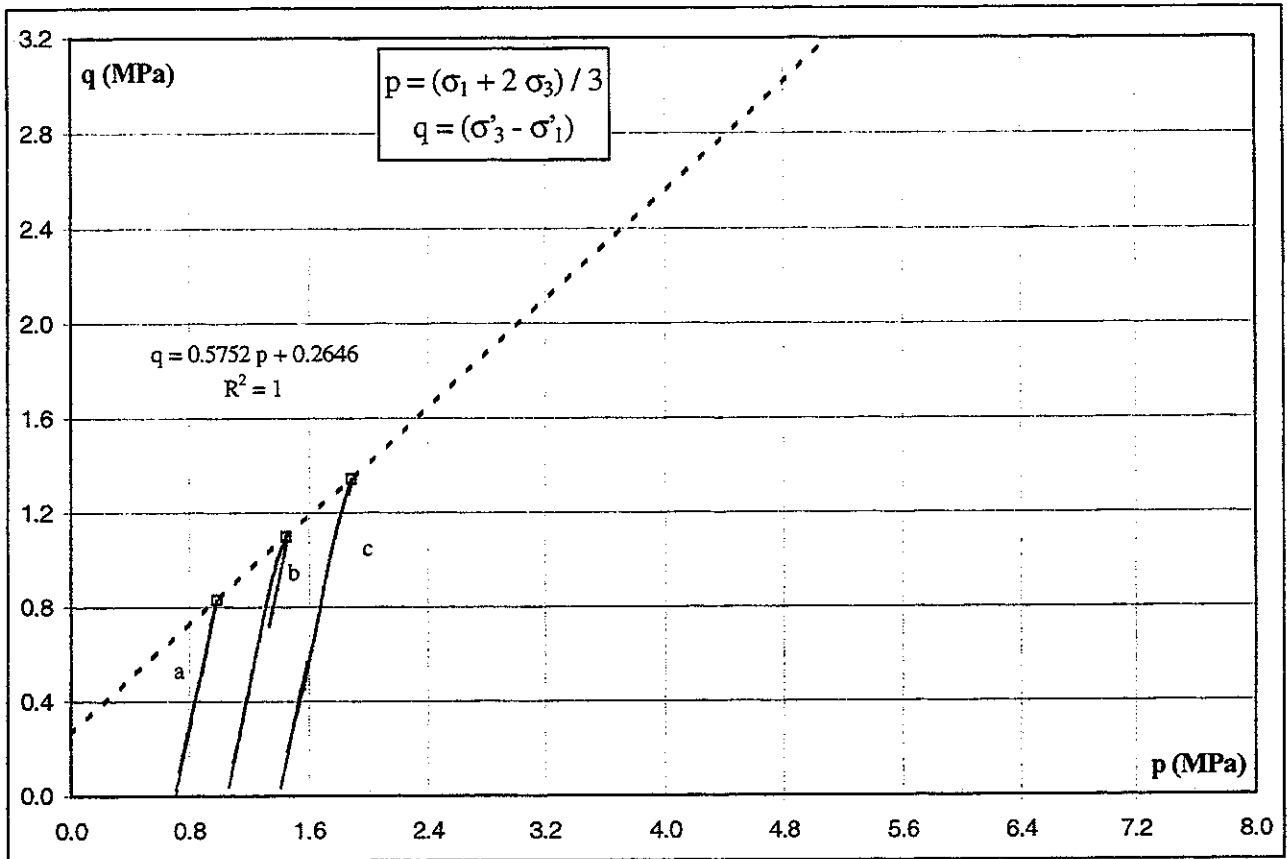


Fig. 9 : Deviator stress versus the mean total stress for Doel (B) 69.23 - 69.68 m

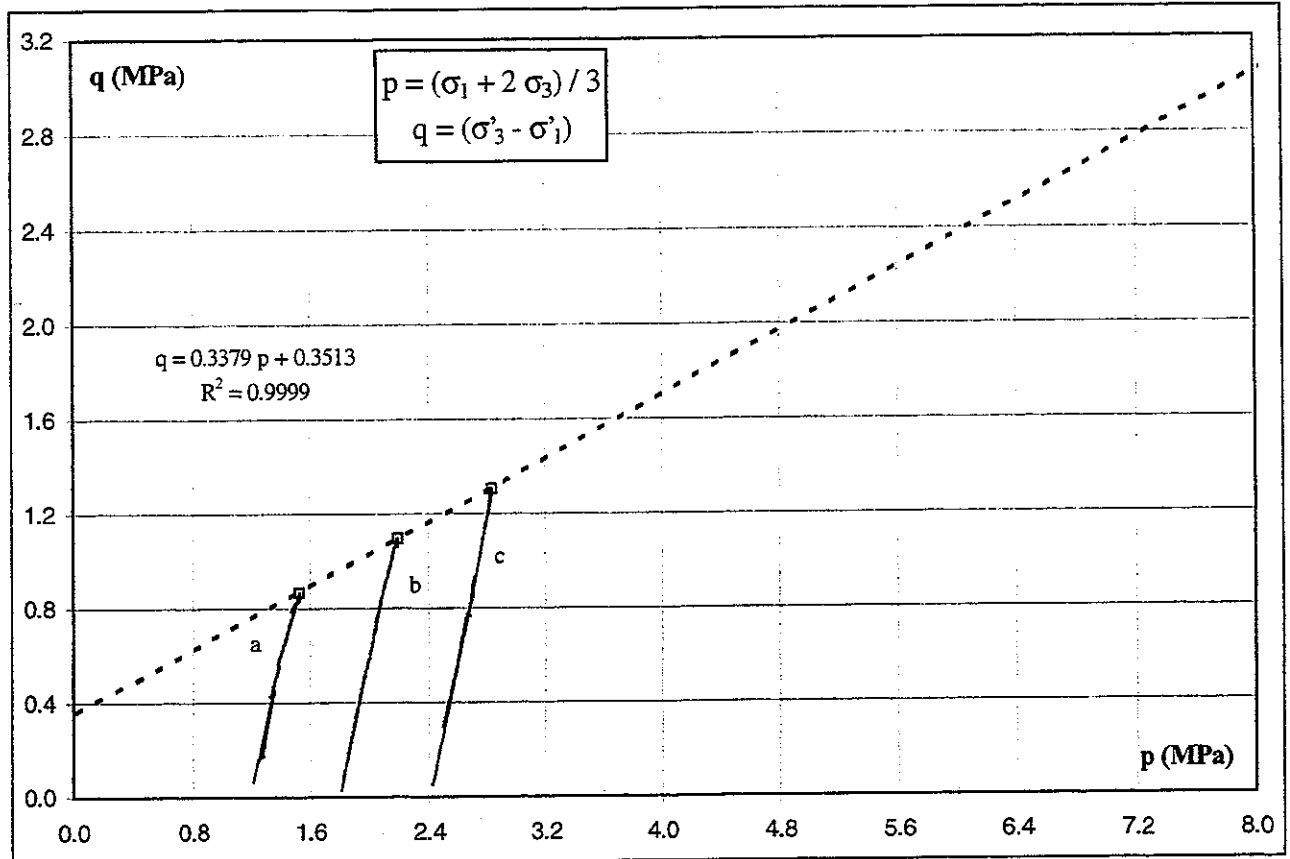


Fig. 10 : Deviator stress versus the mean total stress for Zoersel (B) 120.47 - 121.22 m

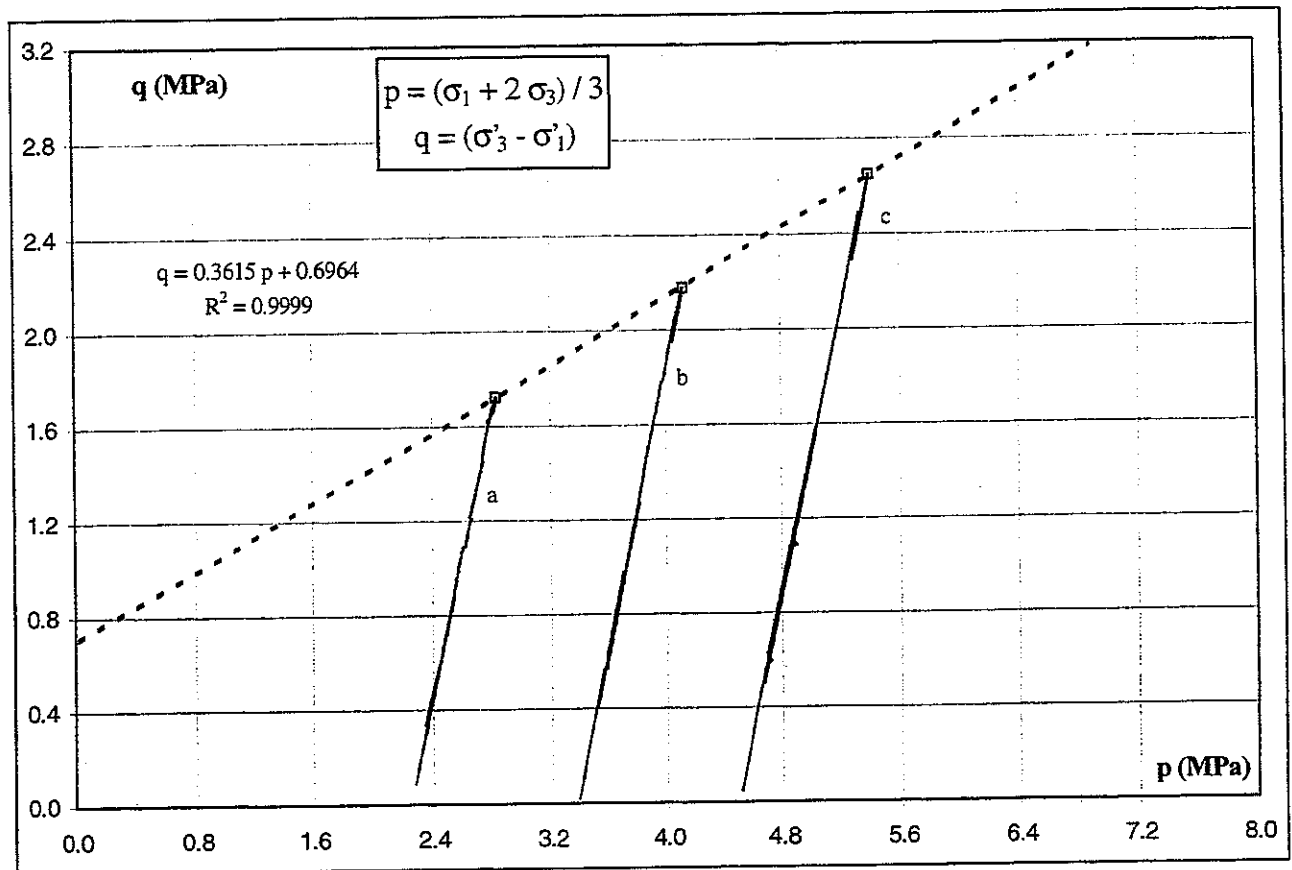


Fig. 11 : Deviator stress versus the mean total stress for Mol (B) 229.18 - 229.28 m

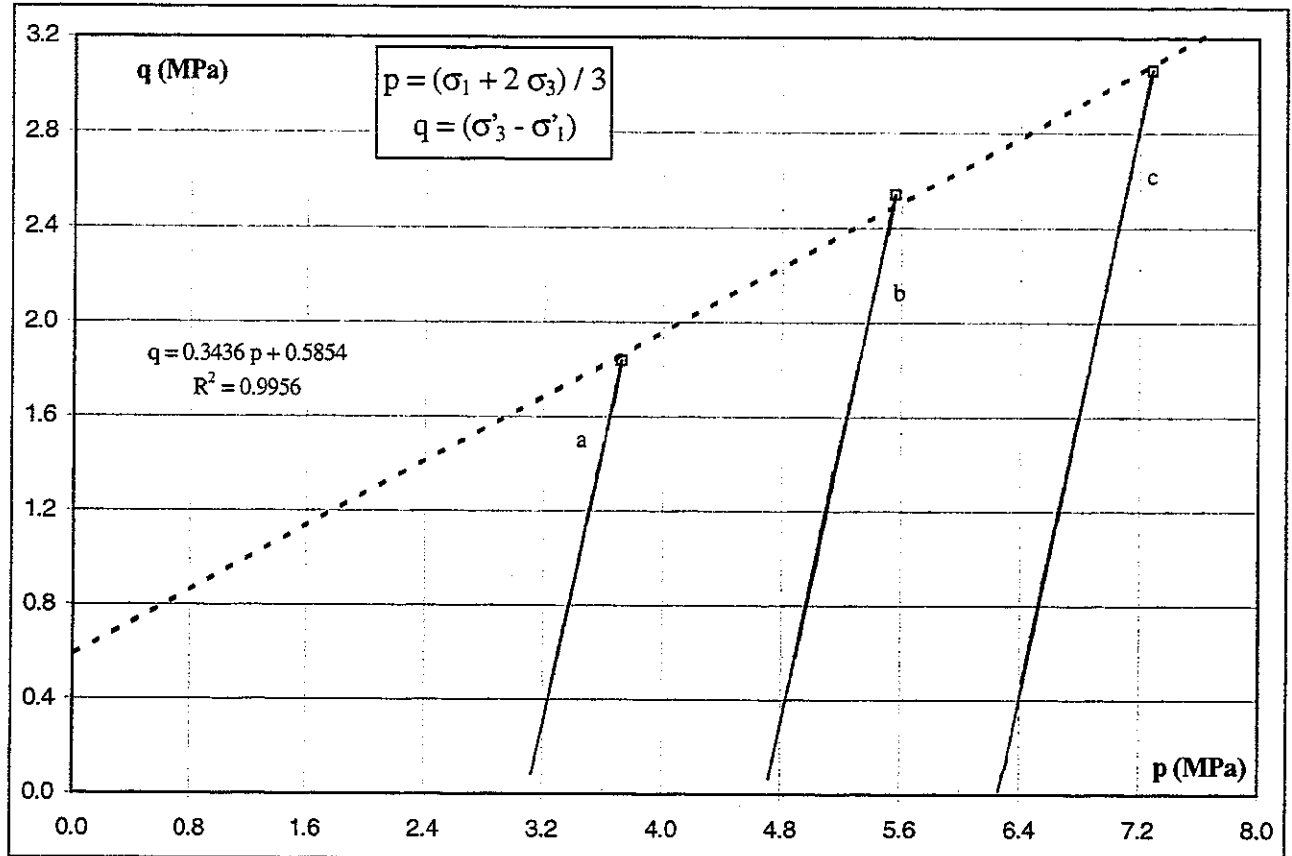


Fig. 12 : Deviator stress versus the mean total stress for Weelde (B) 313.22 - 313.55 m

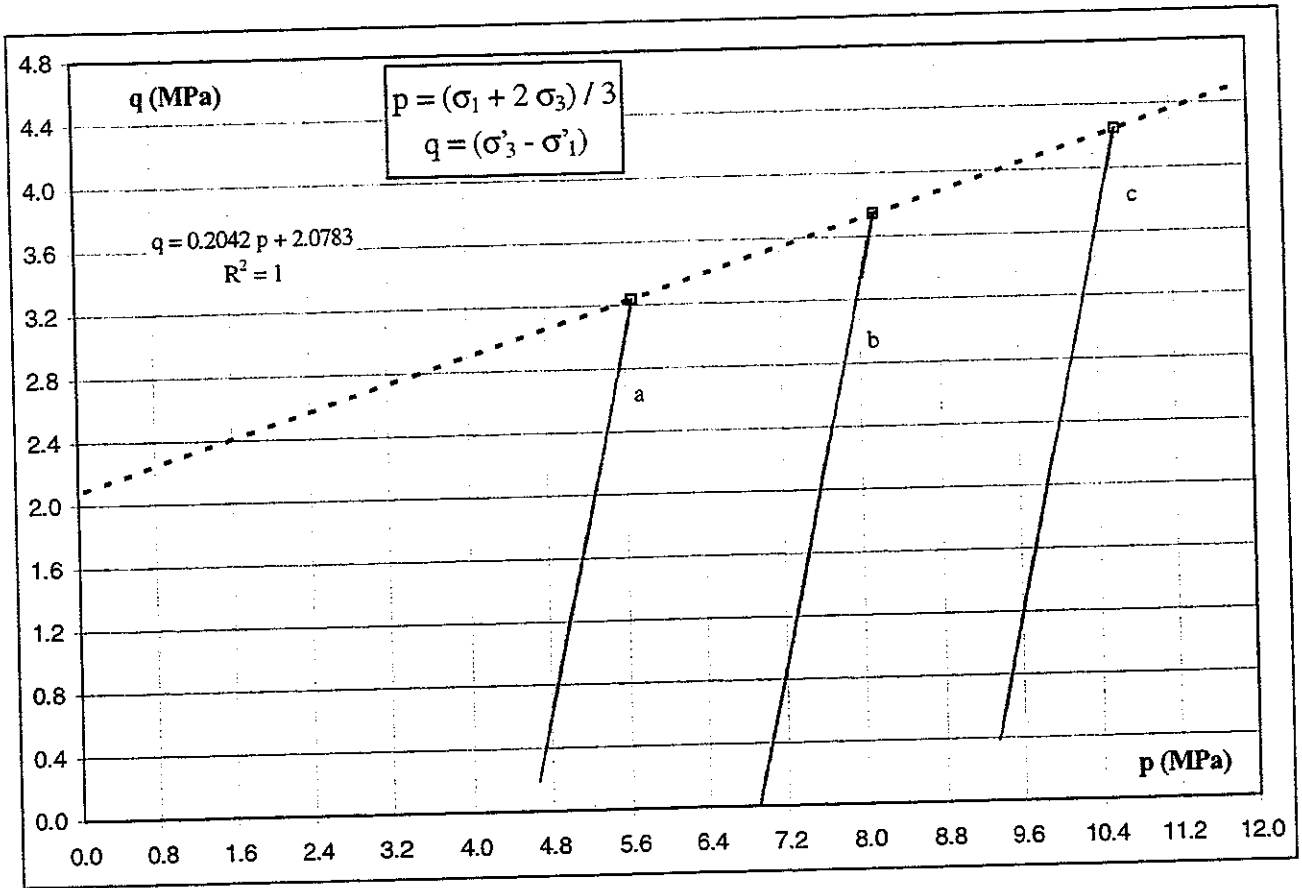


Fig. 13 : Deviator stress versus the mean total stress for Blija (NL) 454.50 - 455.00 m



5.2.2 Shear strength parameters

The values of the shear strength parameters for the soil are calculated from the linear regression coefficients in the p'-q and p-q diagrams (Fig.4 to 8 and Fig. 9 to 13) and are given in the next 2 figures (Fig. 14 and 15).

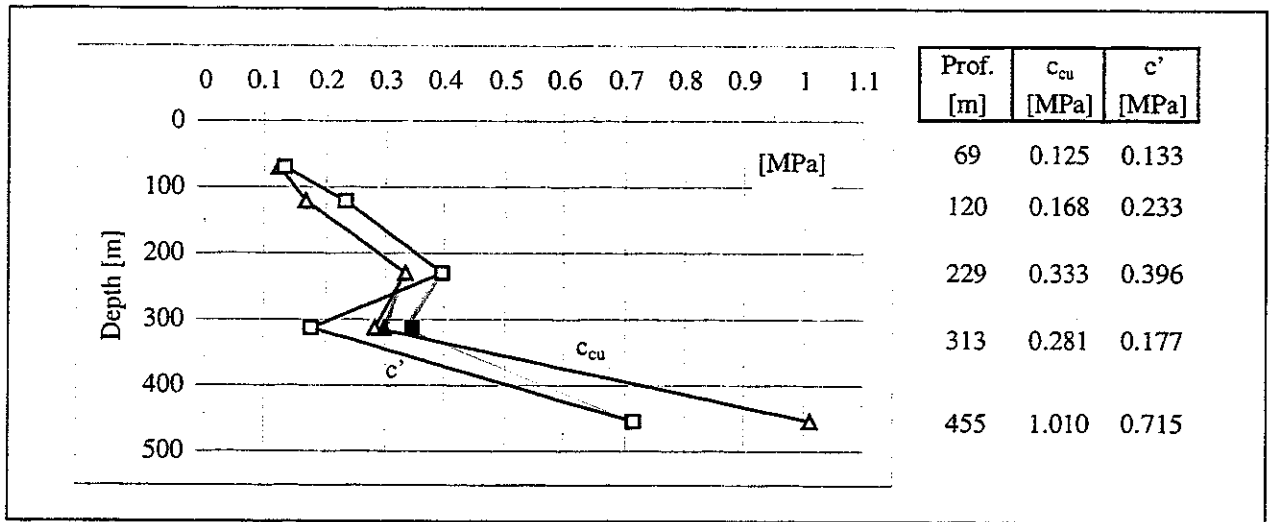


Fig 14 : Cohesions versus depth

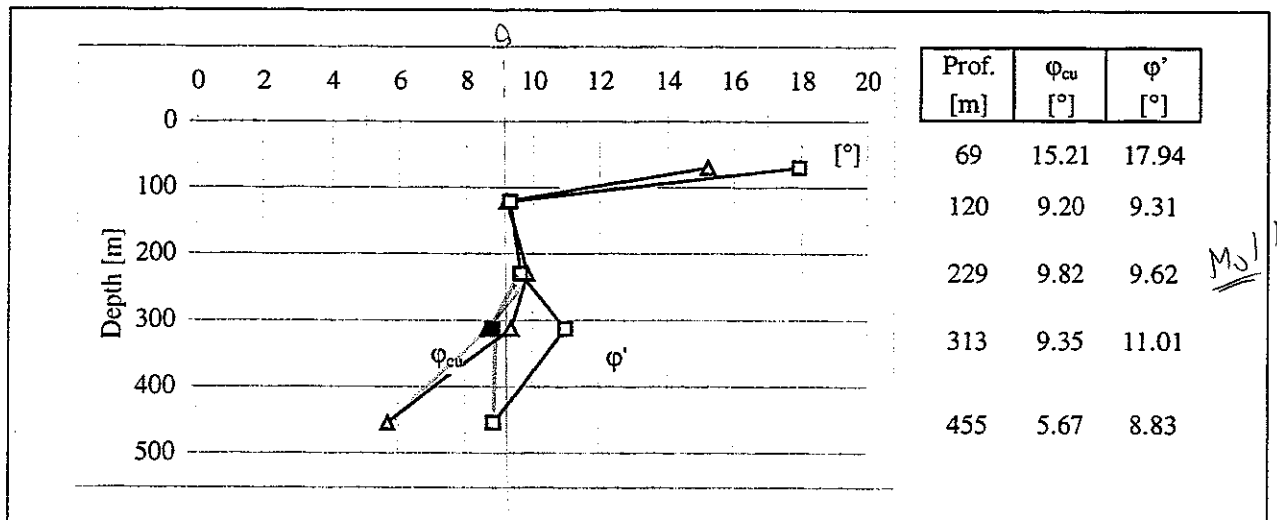


Fig. 15 : Friction angles versus depth

Due to the difference in terms of cohesion between the results of Weelde (313 m) and the others, we have realized a second serie of test over samples from Weelde (Fig. 16 and 17). These new values are plotted with ■ and ▲ in the figures 14 and 15.

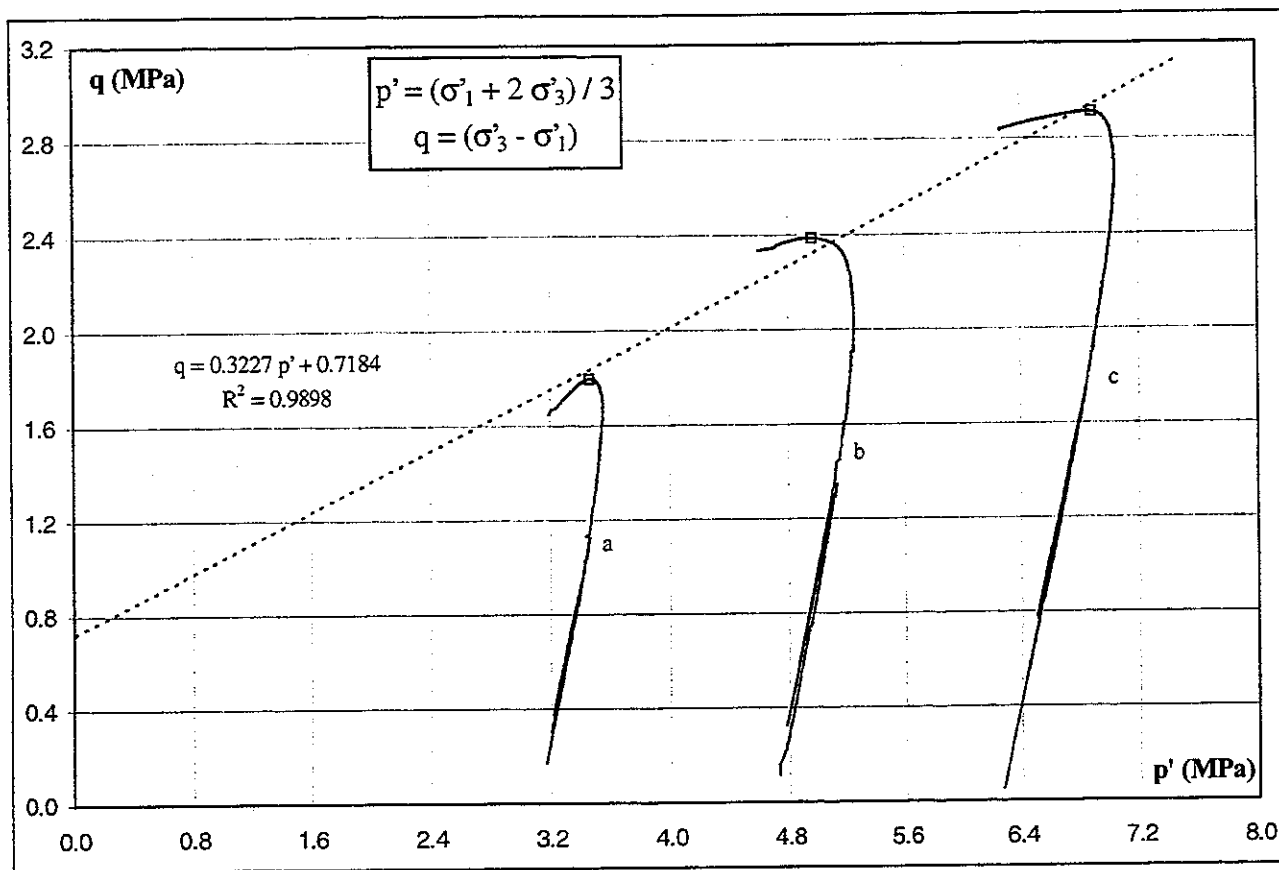


Fig 16 : Deviator stress versus the mean effective stress for Weelde (B) 313.22 - 313.55 m (Second serie)

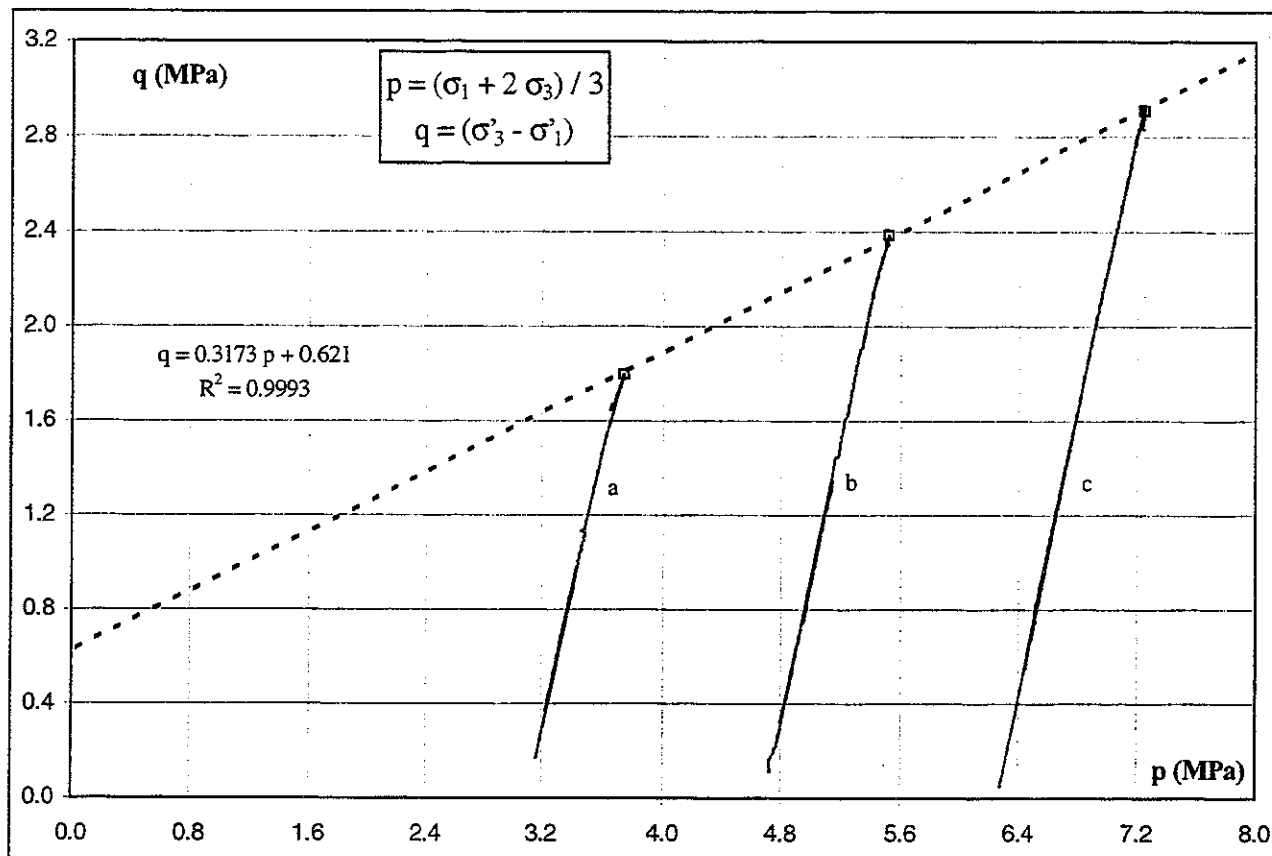
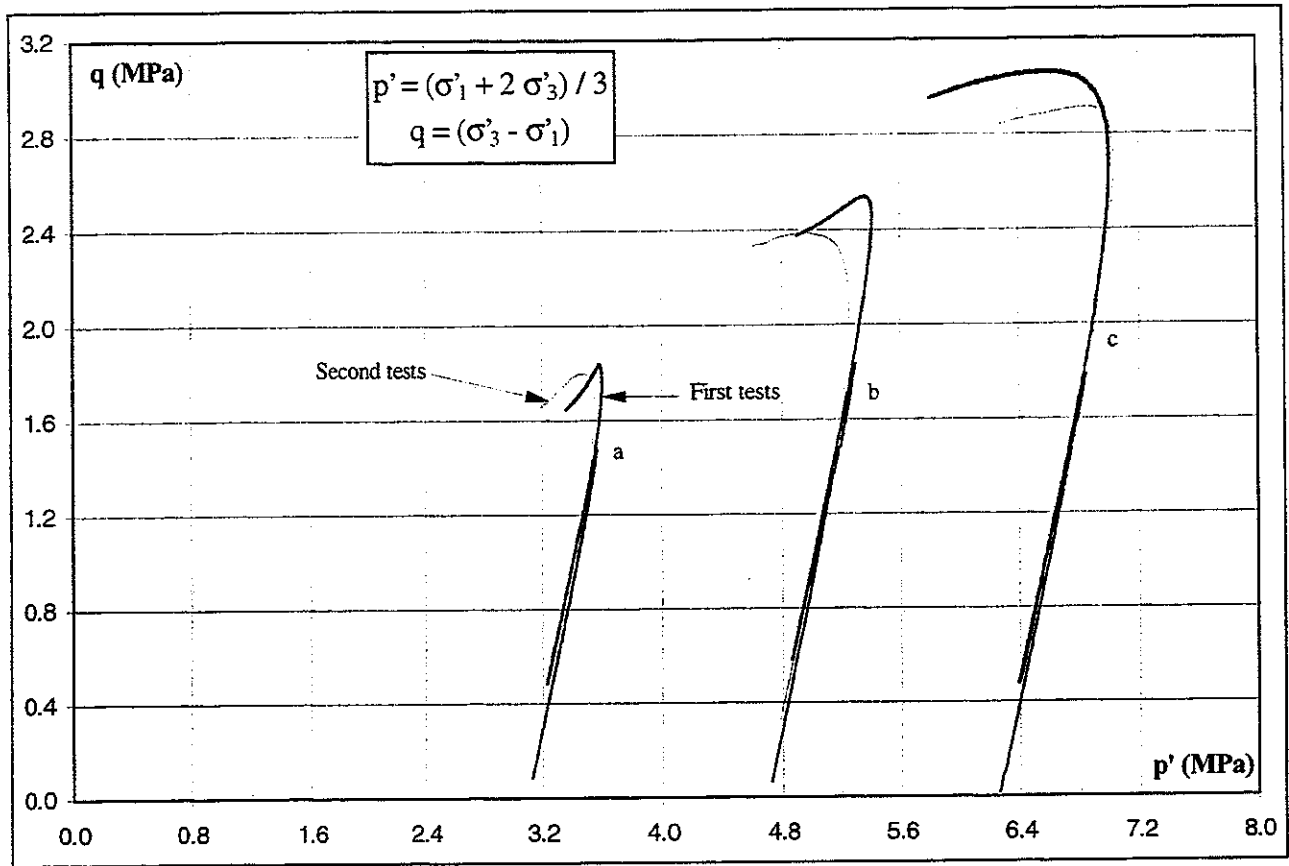


Fig 17 : Deviator stress versus the mean total stress for Weelde (B) 313.22 - 313.55 m (Second serie)

This second serie allows to re-estimate the shear strength parameters for Weelde (B) :

- c_{cu} 0.298 MPa (First serie : 0.281 MPa)
- φ_{cu} 8.67 ° (First serie : 9.35 °)
- c' 0.345 MPa (First serie : 0.177 MPa)
- φ' 8.81 ° (First serie : 11.01 °)

The two series of tests realized over the samples from Weelde give quite similar results (Fig 18 and Fig. 19).



*Fig 18 : Deviator stress versus the mean effective stress for Weelde (B) 313.22 - 313.55 m
Comparison of the results of the two series of tests*

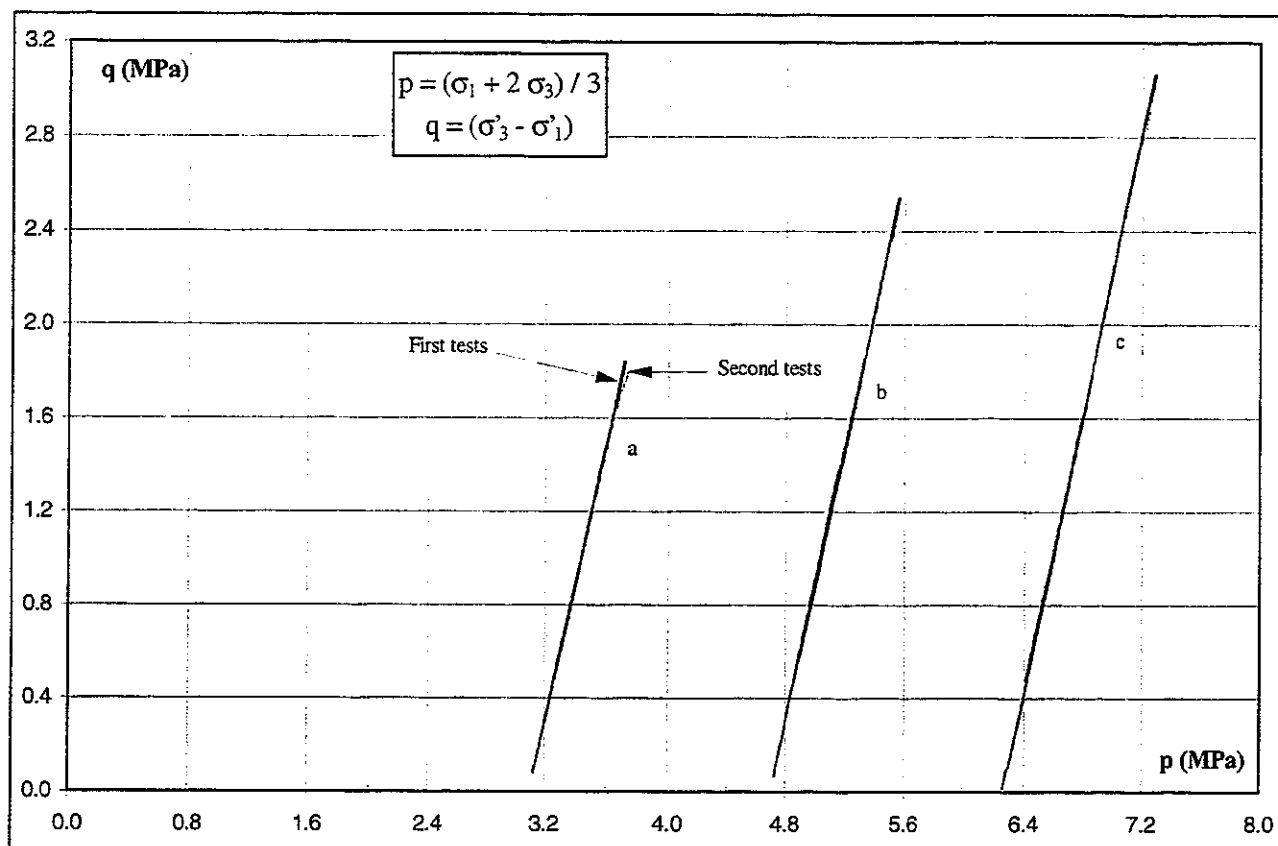


*Fig 19 : Deviator stress versus the mean total stress for Weelde (B) 313.22 - 313.55 m
Comparison of the results of the two series of tests*



5.2.3 Modulus of shear deformation

The shear modulus (G) is the ratio between a given shear stress change and the corresponding shear strain change. We can estimate its value owing to the loading-unloading cycle realized during the CTU test : G is the third of the mean slope of the cycle in the p - q' diagram. Then we have 18 values of this modulus (Fig. 20), and the table 4 gives the numerical values of this modulus.

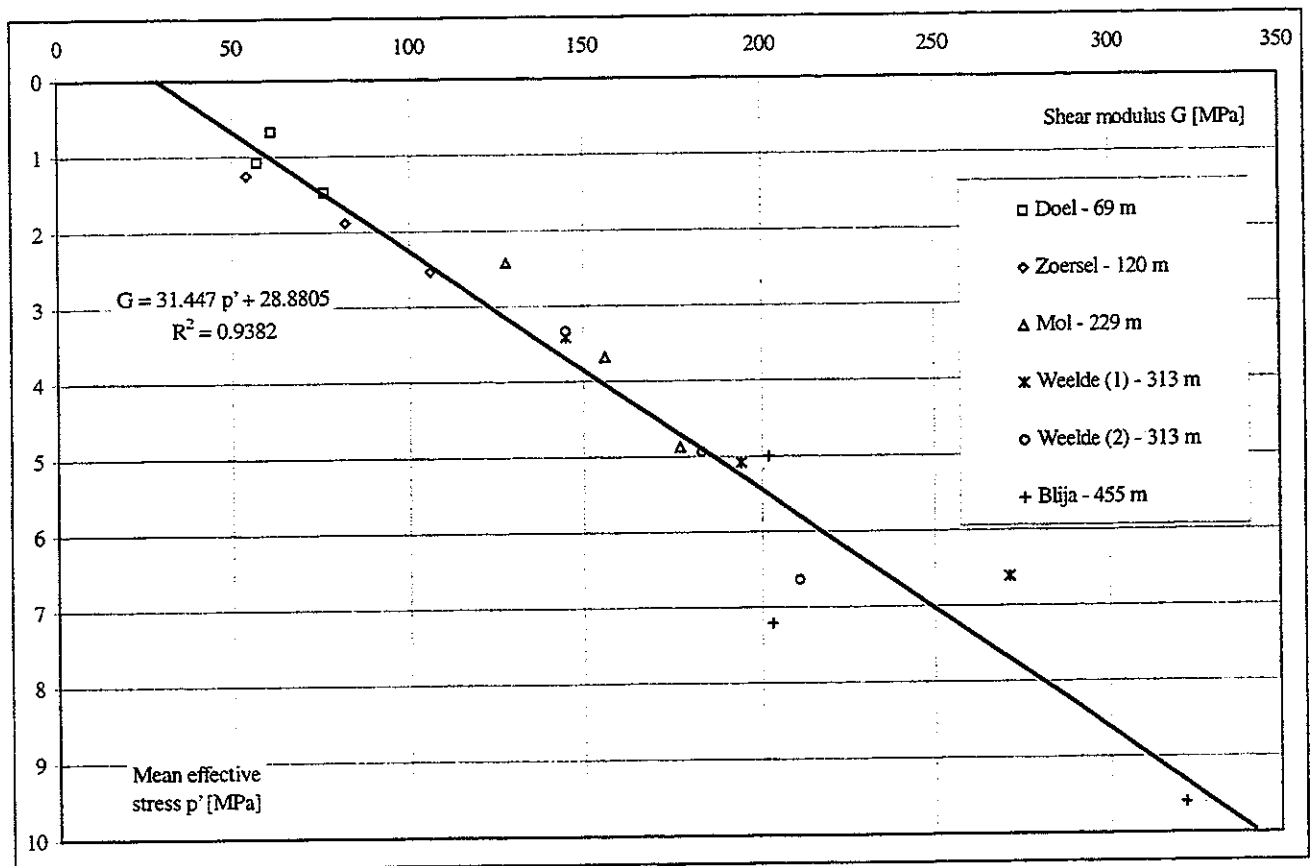


Fig. 20 : Shear modulus (G) versus the mean effective stress

The numerical values corresponding are given in the table 4.

*Table 4 : Numerical values for the shear modulus G*

Origin	Sample	Depth [m]	Mean effective stress p' [MPa]	Shear modulus G [MPa]
Doel (B)	a	69.42	0.674	61
	b	69.42	1.068	57
	c	69.42	1.477	76
Zoersel (B)	a	120.57	1.254	54
	b	120.57	1.884	82
	c	120.67	2.535	106
Mol (B)	a	229.23	2.421	128
	b	224.52	3.678	156
	c	224.52	4.873	177
Weelde (B)	a	313.30	3.417	145
	b	313.30	5.088	194
	c	313.30	6.616	271
Weelde (B)	a	313.30	3.334	145
	b	313.30	4.945	183
	c	313.30	6.640	211
Blija (NL)	a	454.75	5.001	202
	b	454.75	7.212	203
	c	454.75	9.599	322

5.2.4 Numerical values for each test

The numerical values and the other curves ($q - \varepsilon$, $\sigma'_1/\sigma'_3 - \varepsilon$ and $u - \varepsilon$) obtained from the results of the CTU tests are given in the appendix 29 to 40.

By request of NITG-TNO, the evolution of the 'shear strength parameters' versus the deformation and the depth is given in the appendix 41 to 52 with the corresponding p' - q and p - q diagrams.

5.3 HCD tests

5.3.1 Results

During these drained tests, the measure of the variation of the volume of the samples allows to calculate the void ratio versus the effective stress.

The evolution of the void ratio is given in the next 5 figures (Fig.21 to 25).

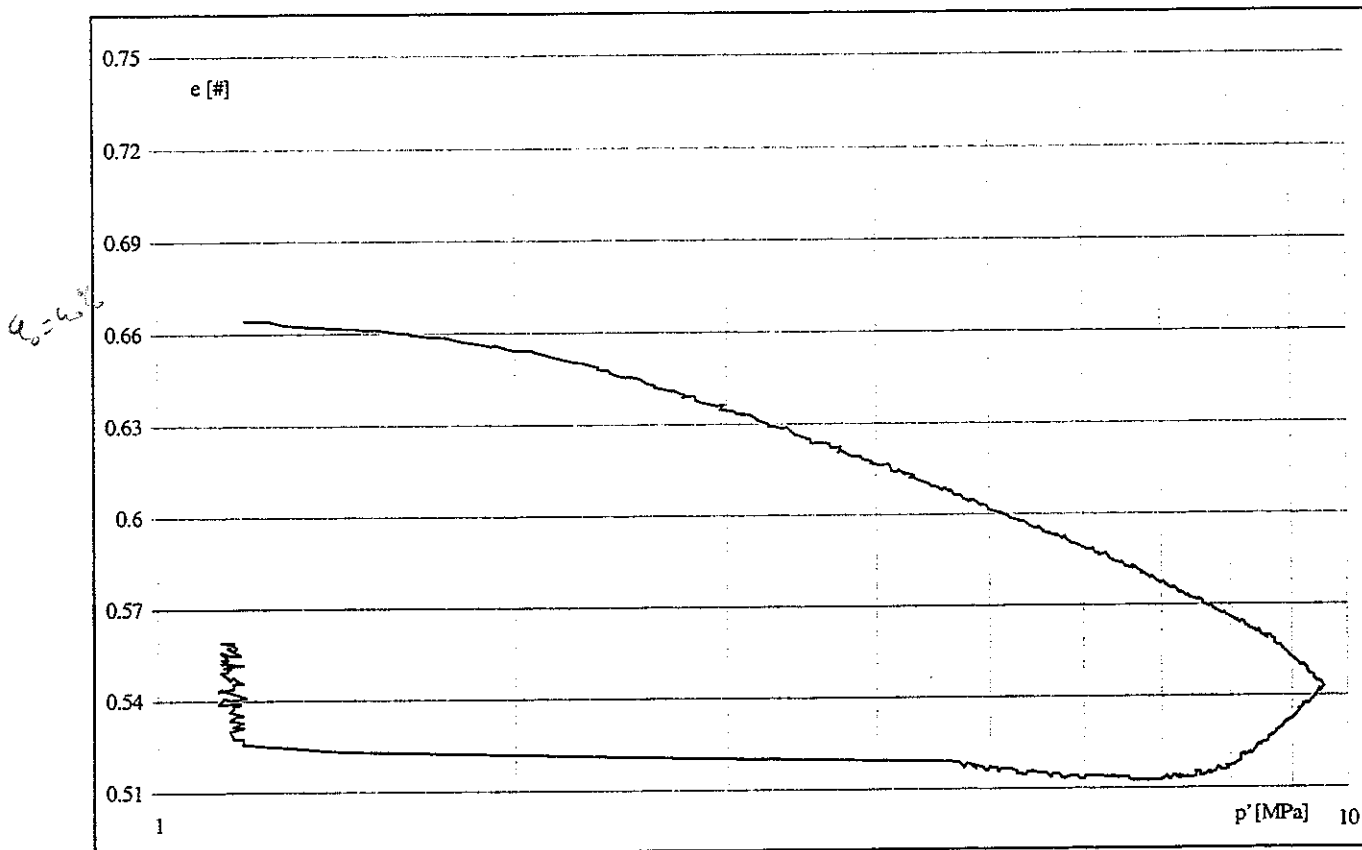


Fig. 21 : Void ratio versus the effective stress - Doel (B) 69 m

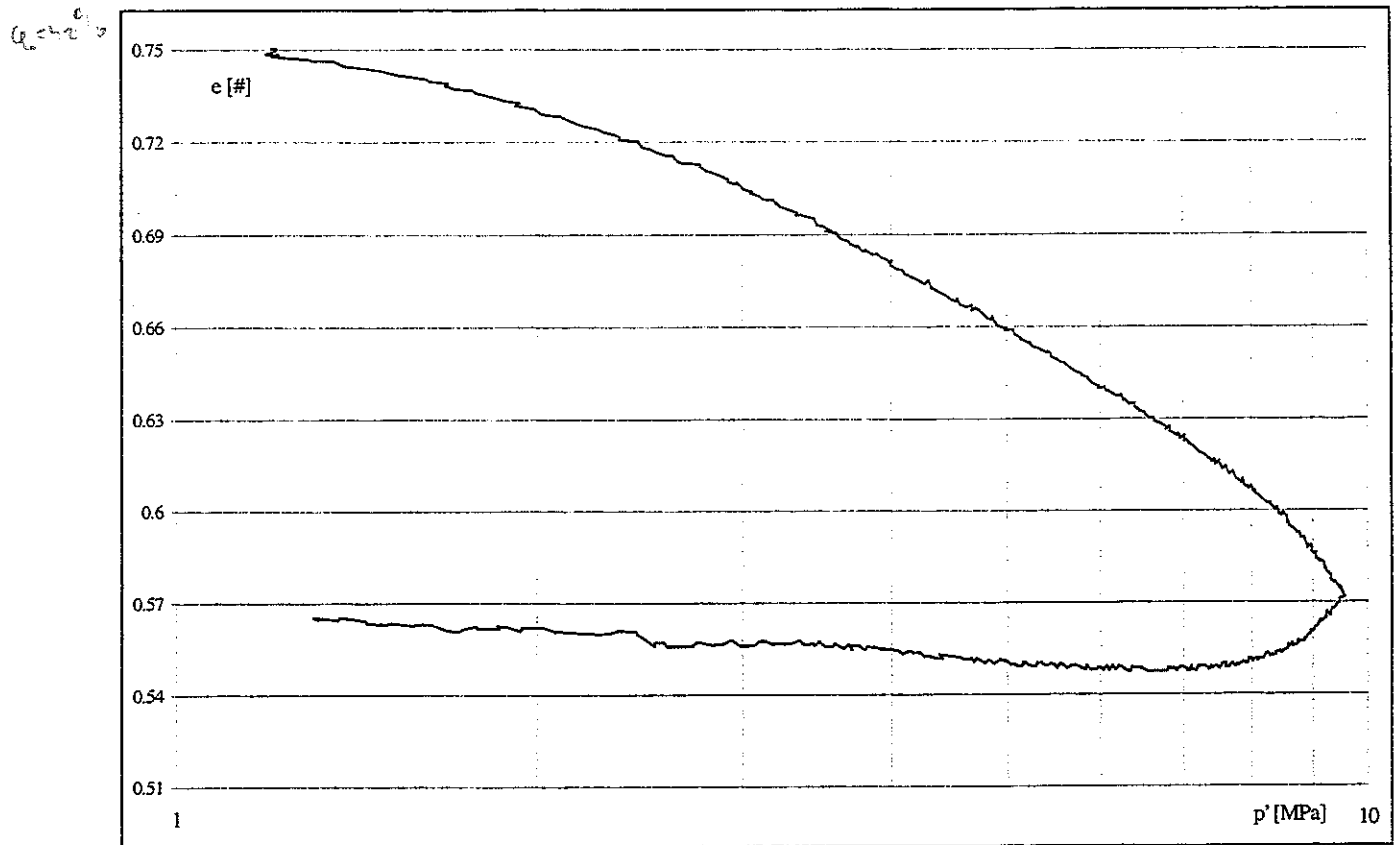


Fig 22 : Void ratio versus the effective stress - Zoersel (B) 120 m

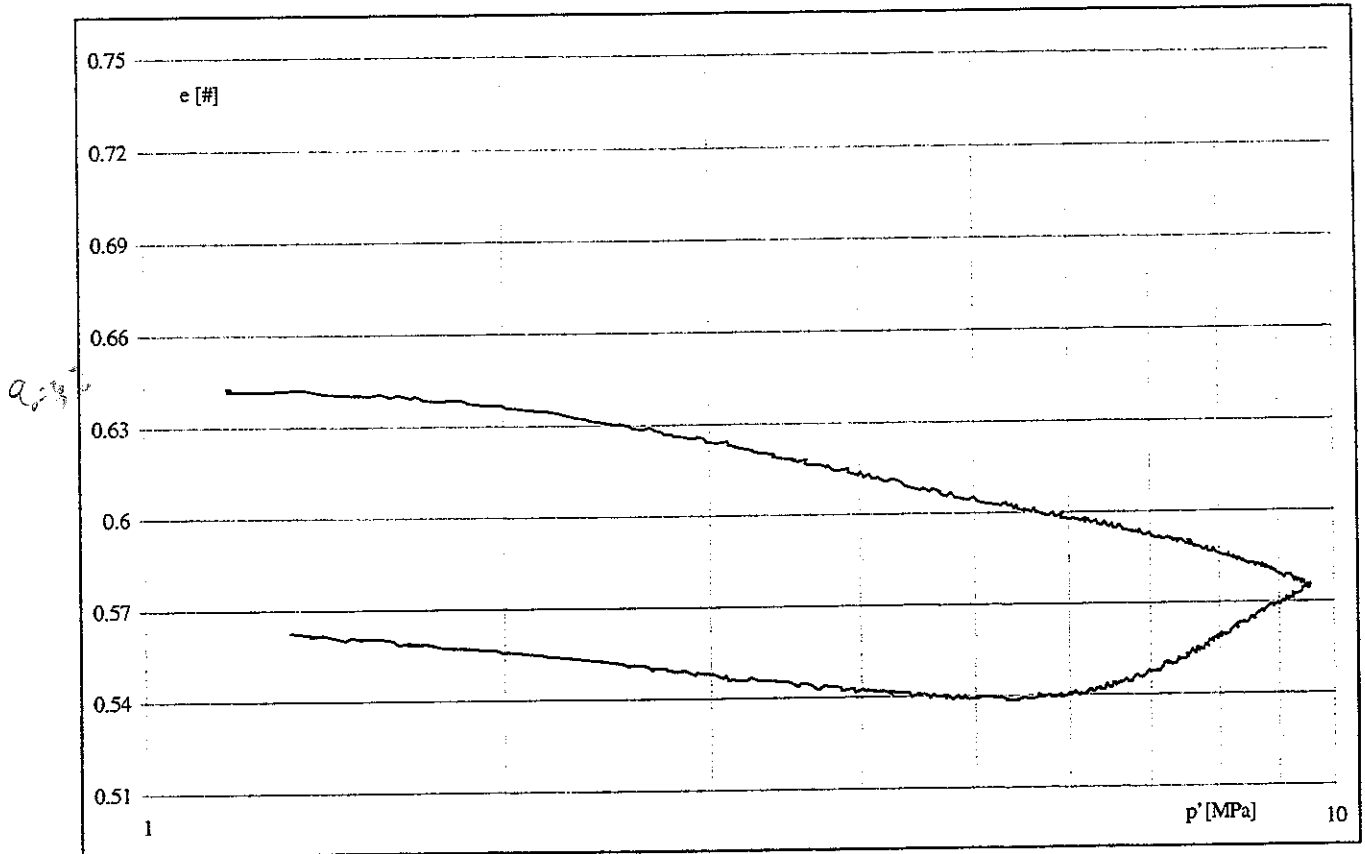


Fig 23 : Void ratio versus the effective stress - Mol (B) 229 m

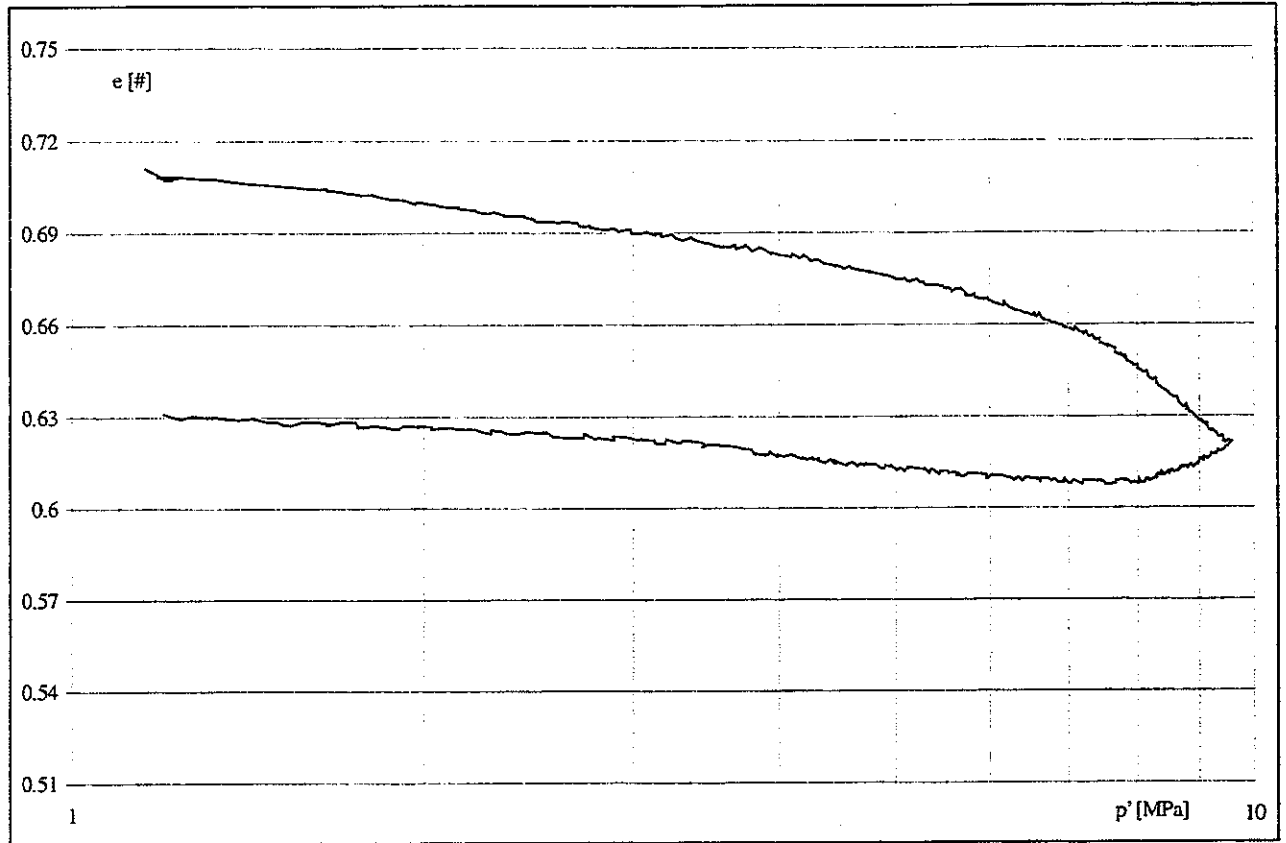


Fig 24 : Void ratio versus the effective stress - Weelde (B) 313 m

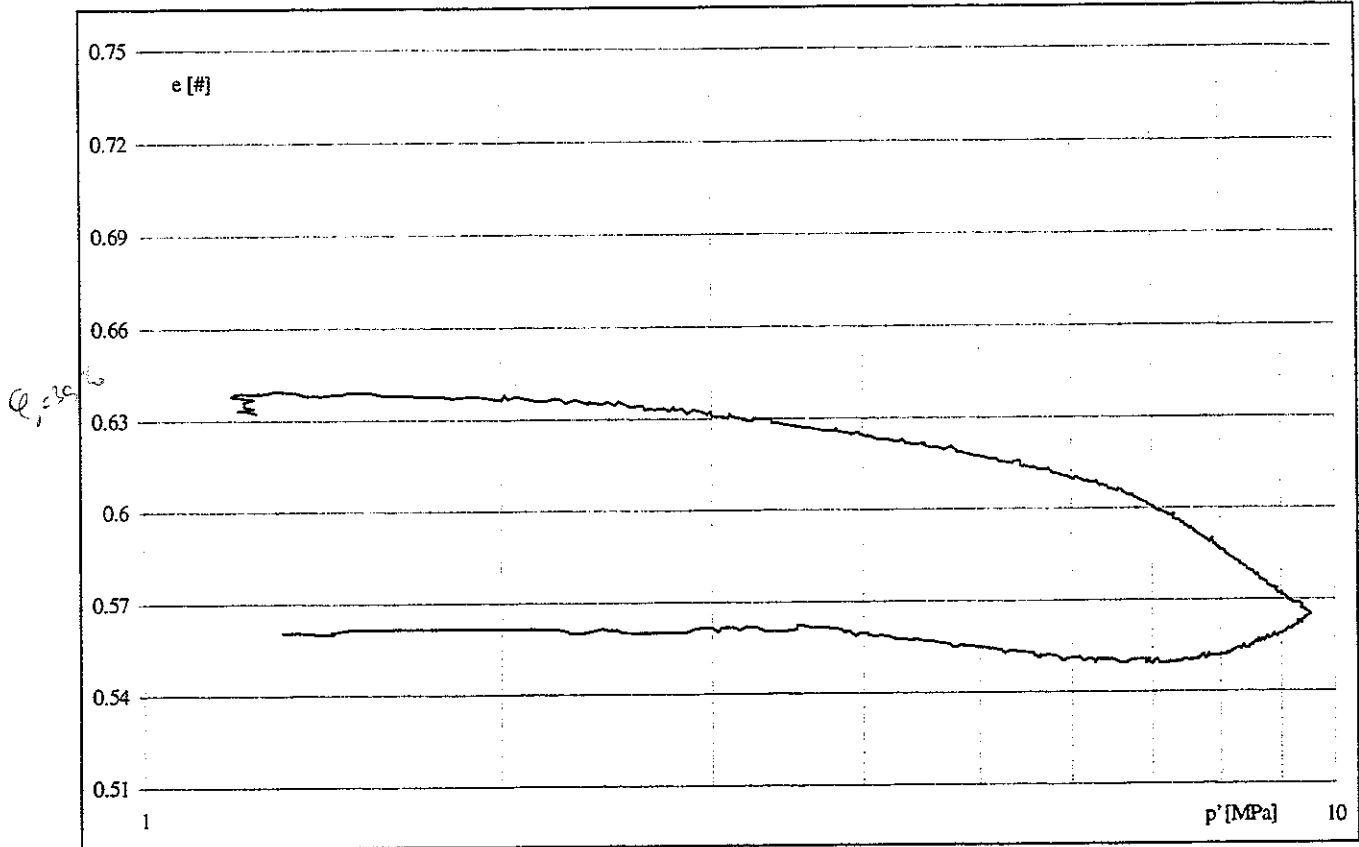


Fig 25 : Void ratio versus the effective stress - Blija (NL) 478 m

5.3.2 Parameters of the Cam-Clay model

These curves allow to calculate the parameters of the Cam-Clay model : p_c , λ and κ (table 5). The parameter M is the slope of the critical state line plotted on a p' - q diagram (Fig. 4 to 8).

Table 5 : Parameters of the Cam-Clay model

Depth [m]	λ [-]	κ [-]	p_c [MPa]	M [-]
69	0.1577	0.02377	2.317 - 8.6560	0.6865
120	0.2195	0.01326	2.492 - 6.4990	0.3421
229	0.0685	0.02048	2.366 - 7.9039	0.3541
313	0.1433	0.01639	- 7.5538	0.4081 ⁽¹⁾ → 0.322 ⁽²⁾
478	0.1196	0.02152	- 6.9307	0.3236

The determination of the Cam-Clay parameters (λ , κ and p_c) was critical. The curves do not allow an easy evaluation of these parameters. The shape of the curves may be influenced by the stress rate that does not allow to guarantee the dissipation of the water pressure in the sample. The



determination of the value of p_c is not easy either. For Doel (69 m), Zoersel (120 m) and Mol (229 m), 2 discontinuities in the loading curve can be taken into account but neither Weelde (313 m) nor Blija (478 m) presents this characteristic.

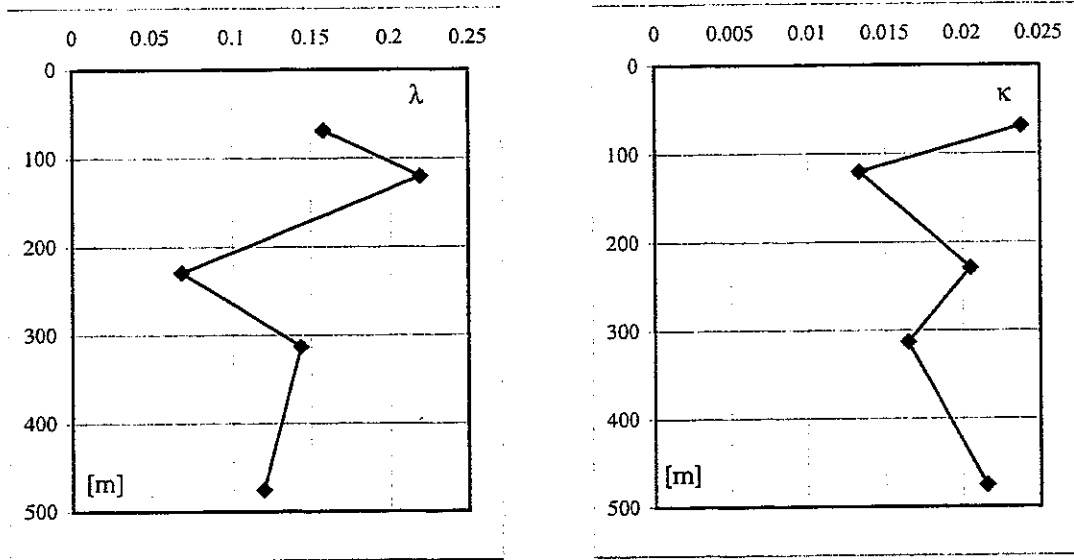


Fig. 26 : Parameters λ and κ of the Cam-Clay model versus the depth

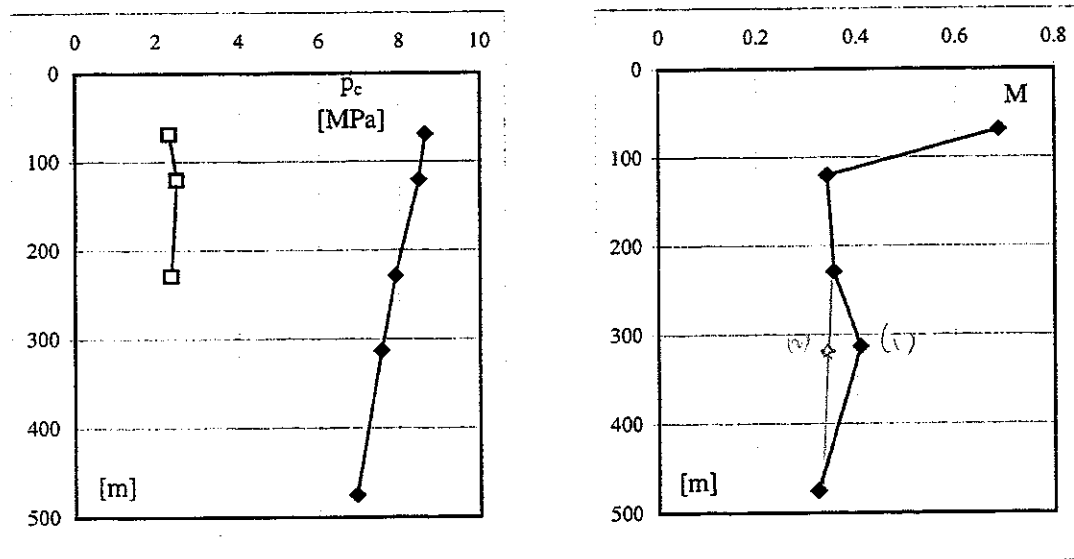


Fig. 27 : Parameters p_c and M of the Cam-Clay model versus the depth



6. Conclusions

6.1 Characteristics of the samples

The dry, saturated and specific weights increase linearly with the depth while the initial and saturated water contents decrease with the depth, except for Doel (B) where the values of the saturated water content is lower :

γ_d	from 15.11 to 16.34 kN/m ³
γ_{sat}	from 19.19 to 20.15 kN/m ³
γ_s	from 26.07 to 26.89 kN/m ³

About the sedimentation analysis, a first group (Doel 69 m, Zoersel 120 m and Mol 224 m) have less fines than a second one (Mol 229 m, Weelde 313 m and Blija 455 m) and the depth is a important parameter for Mol.

The mineralogical analysis shows that there is no significant difference between all the samples. The clay ($d \leq 2 \mu\text{m}$) is constituted for third to half of smectite. With regard to the initial sample, there is approximately between 20 and 30 % of smectite (swelling clay).

6.2 CTU tests

The critical state lines plotted on the $p'-q$ and $p-q$ diagrams allow to calculate the shear strength parameters.

The cohesions increase considerably with the depth, but the values of Weelde (confirmed by a second serie of tests) are almost two times lower than expected. About the friction angles, the effective one seems to increase while the total one decreases with the depth.

ϕ'	from 17.94 to 8.83°	c'	from 0.133 to 0.715 MPa
ϕ_{cu}	from 15.21 to 5.67°	c_{cu}	from 0.125 to 1.010 MPa

The shear modulus G , estimated owing to a loading-unloading cycle, increases with the depth and the correlation is fine ($R^2 = 0.94$).

6.3 HCD tests

The parameters of the Cam-Clay model are estimated from a diagram plotting the void ratio versus the effective stress. The determination of the 4 parameters of the the Cam-Clay model (λ , κ , M and p'_c) has raised problems :

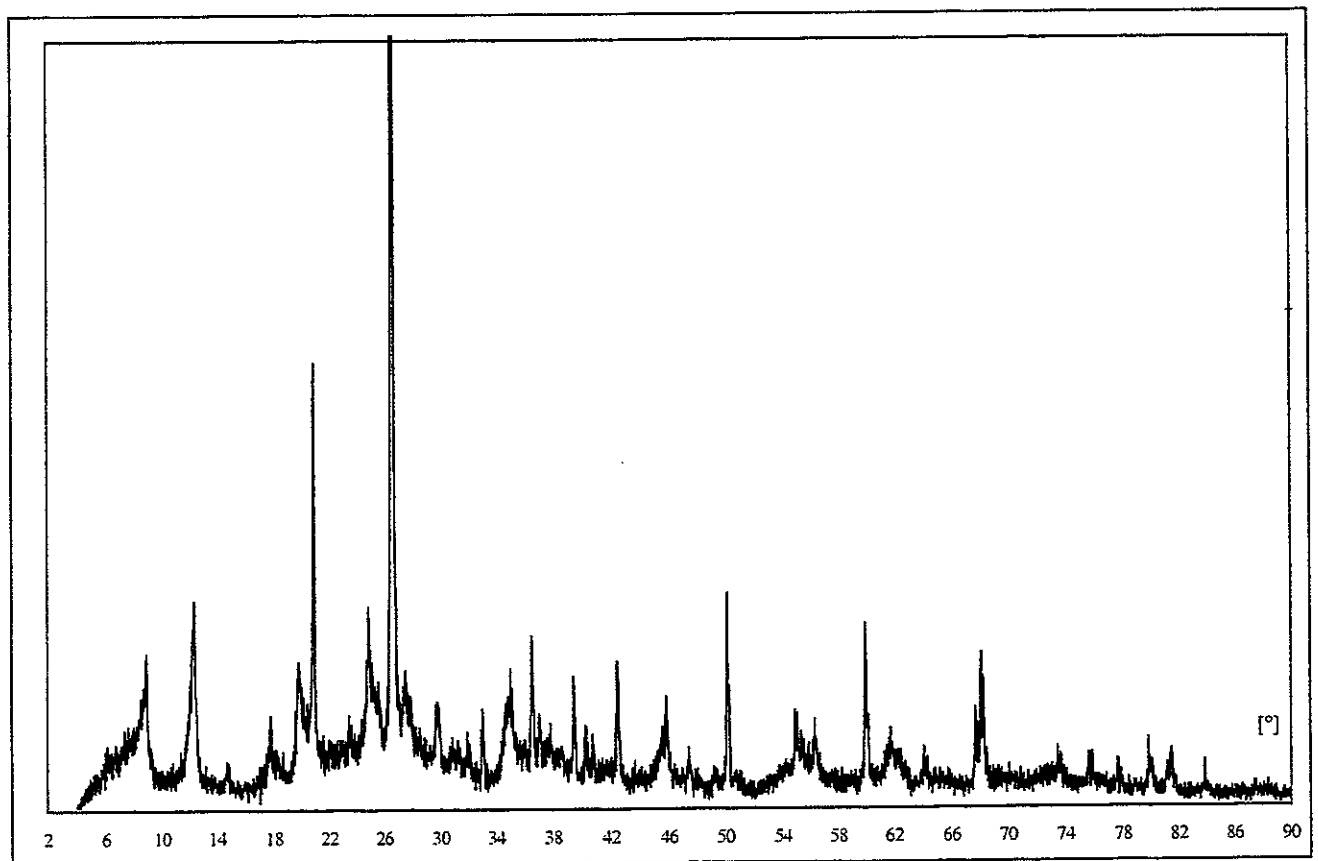
- λ The values of Zoersel (120 m) and Mol (229 m) seem to be respectively to great and to low with regard to the evolution for the other samples. One can retain that λ seems to decrease from 0.17 to 0.12 with depth.
- κ Except the value of Doel, one can conclude that κ seems to increase from 0.015 to 0.020 with depth.



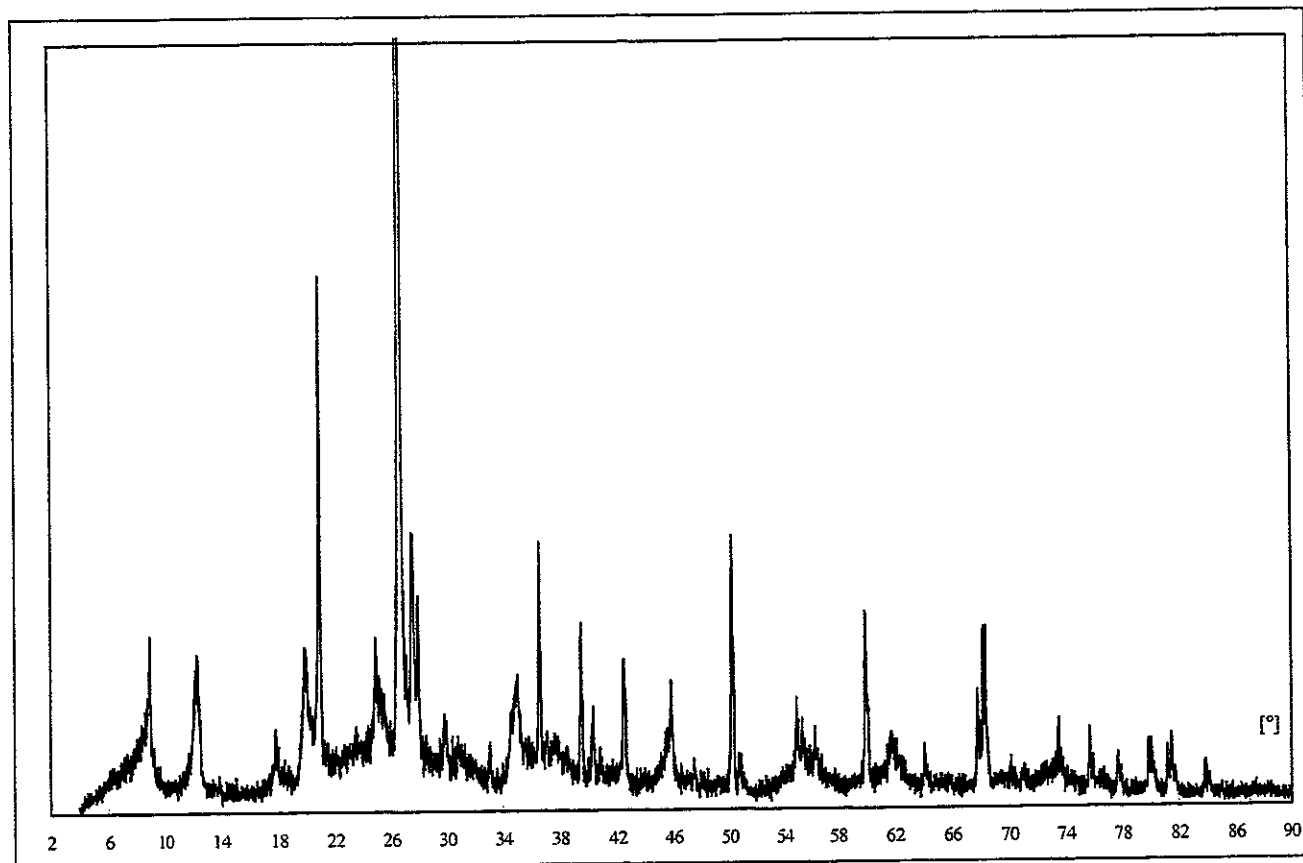
- M The value from Doel is very different from the others ; one can conclude that M seems to vary between 0.3 and 0.4.
- p_c If for each sample, we keep the greatest values, p_c decreases with the depth from 8.66 to 6.93, but with the lowest values, the mean is about 2.4 MPa for Doel (69 m), Zoersel (120 m) and Mol (229 m).

Important remark : these results have been obtained from only one test per depth and should be, thus, confirmed by other tests.

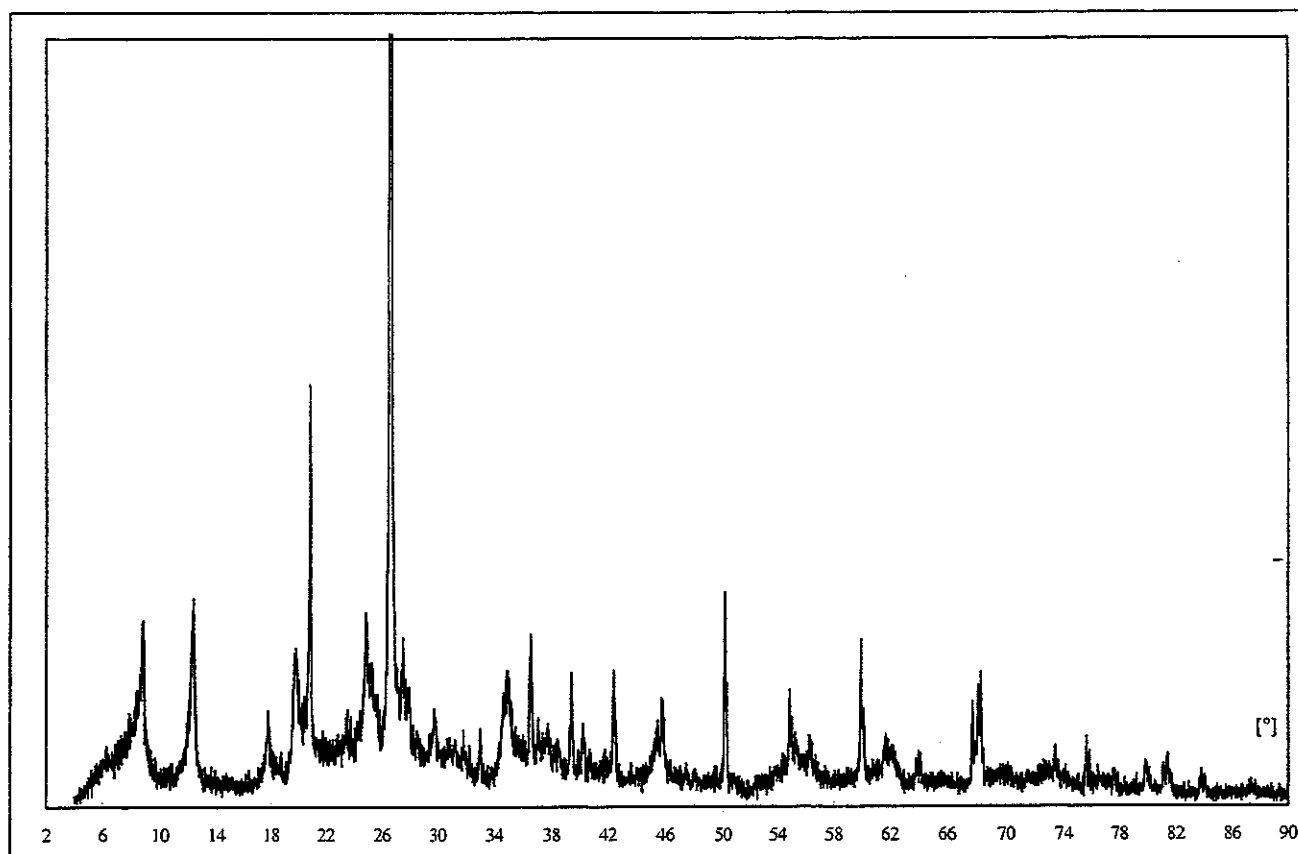
7. Appendix



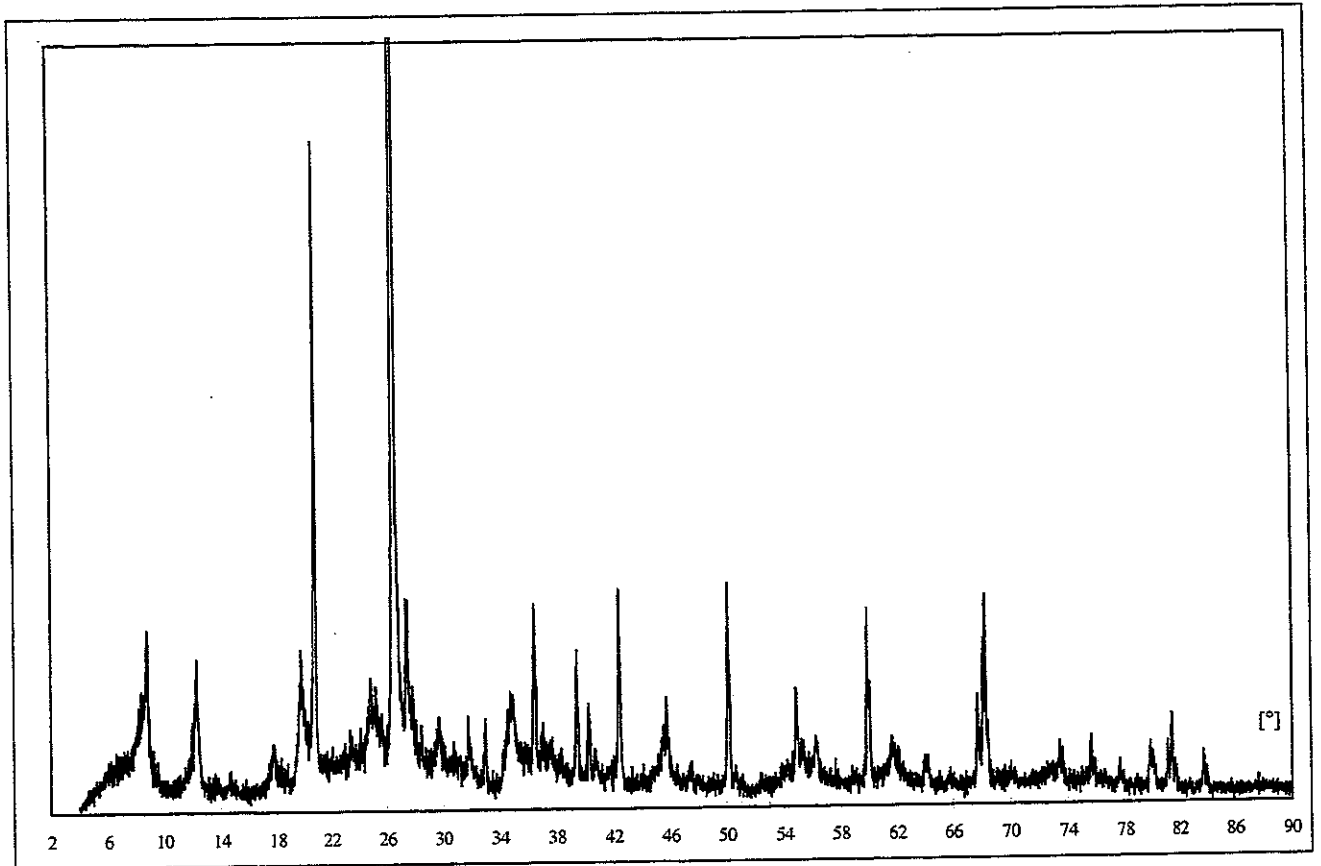
Appendix 1 : Mineralogical analysis : Total spectra for Doel (B) - 69 m



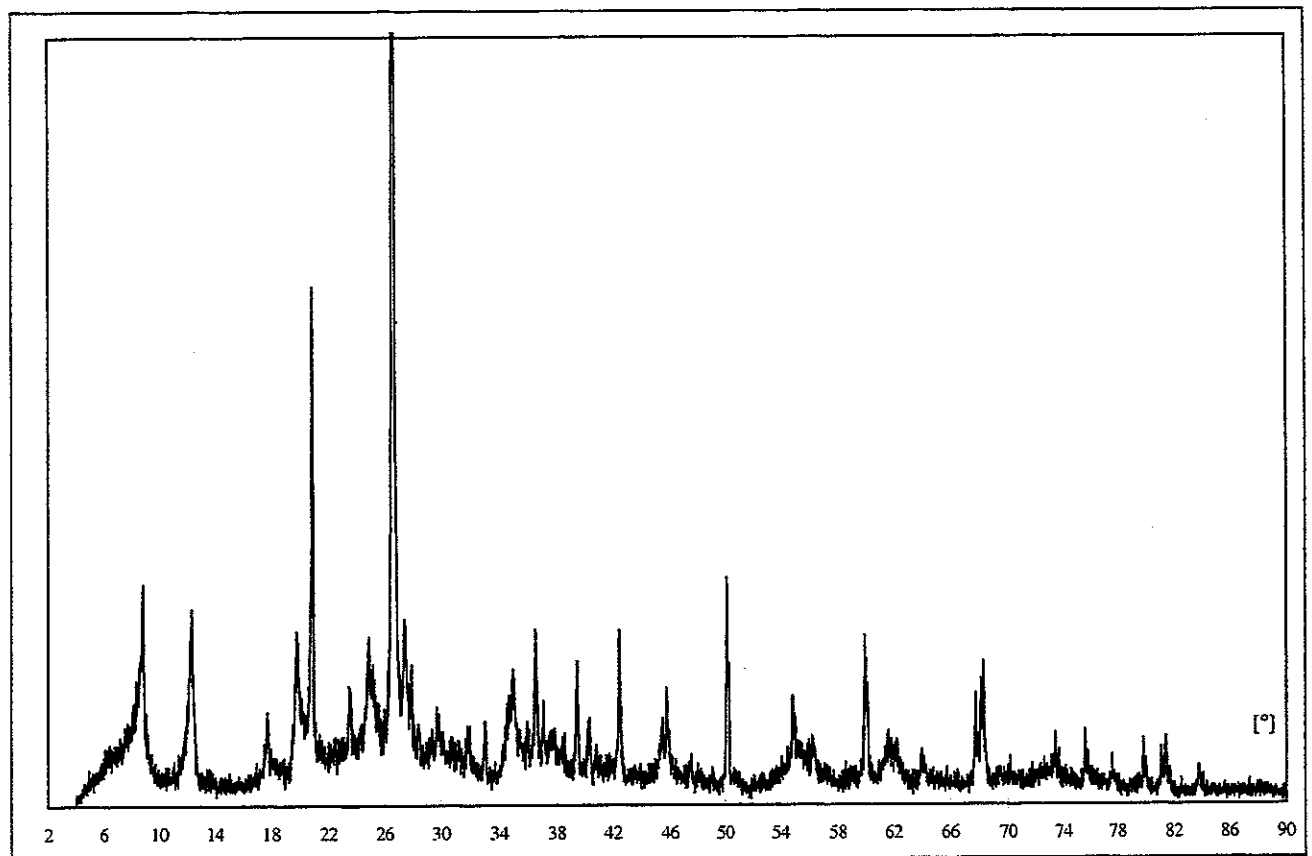
Appendix 2 : Mineralogical analysis : Total spectra for Zoersel (B) - 120 m



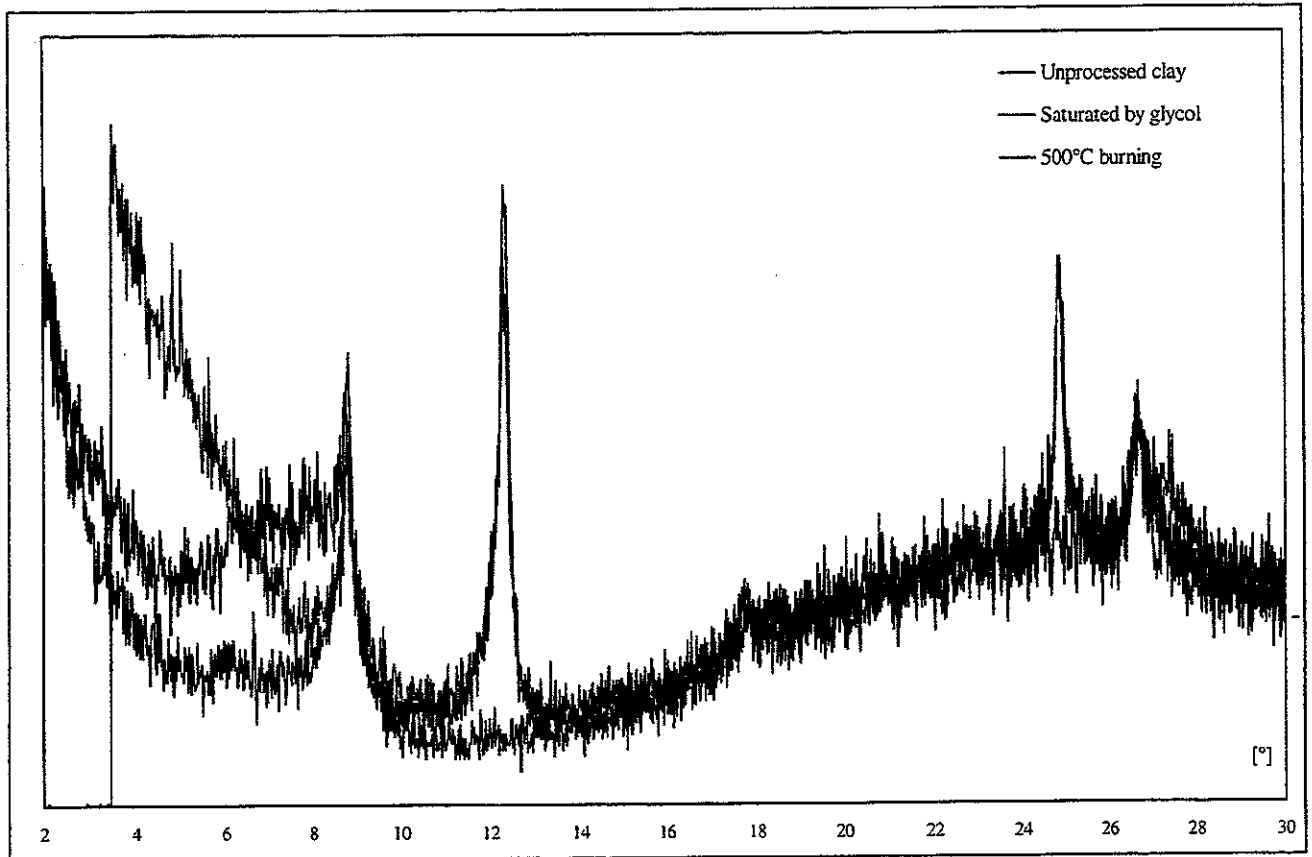
Appendix 3 : Mineralogical analysis : Total spectra for Mol (B) - 224 m



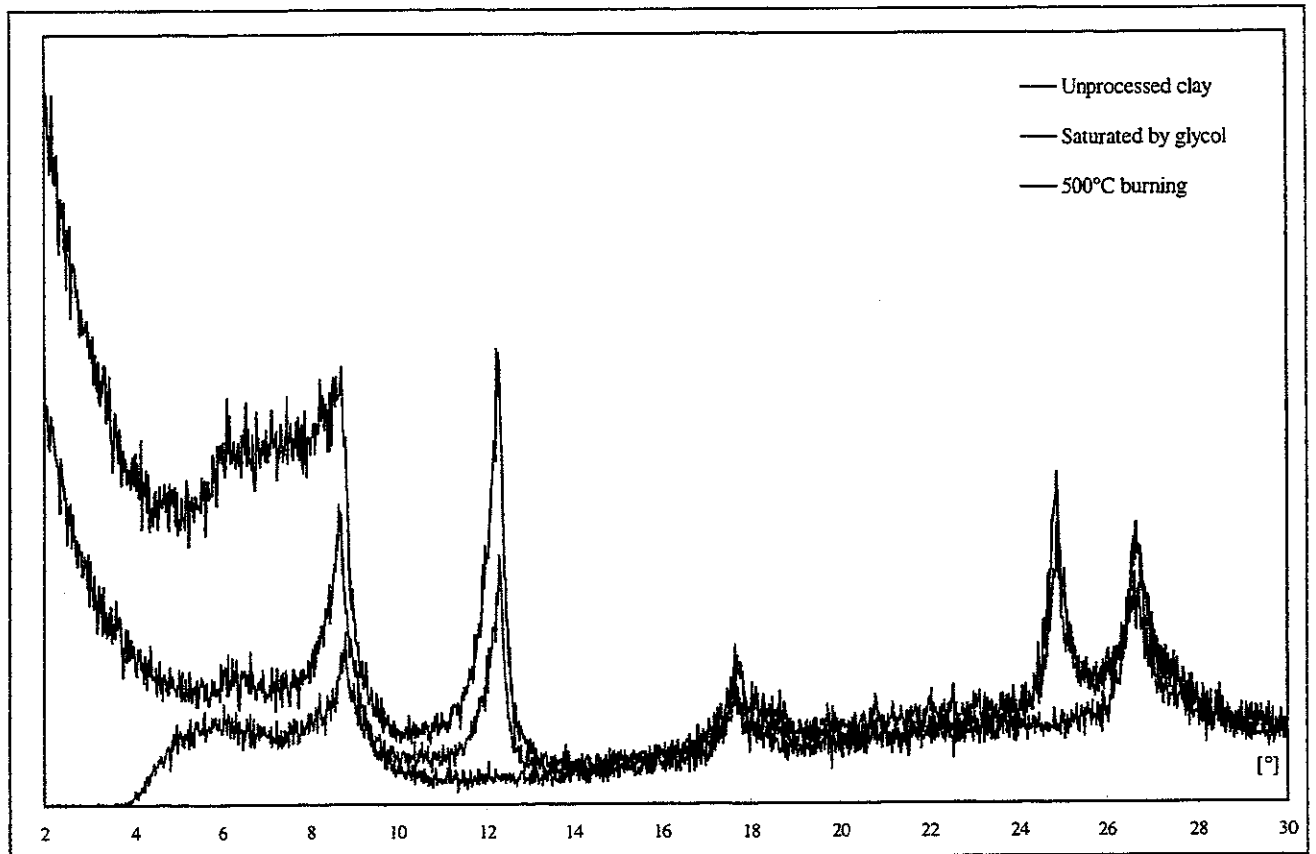
Appendix 4 : Mineralogical analysis : Total spectra for Mol (B) - 229 m



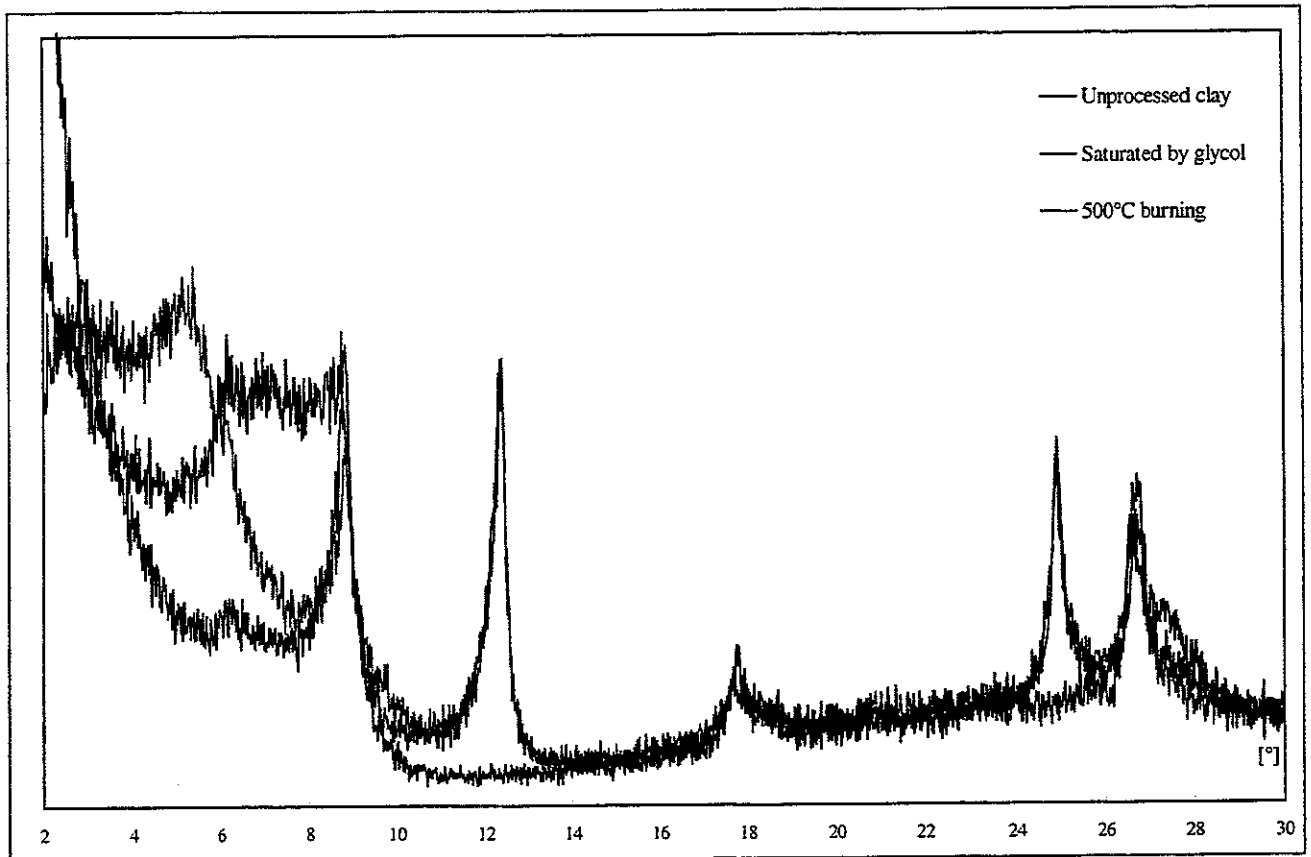
Appendix 5 : Mineralogical analysis : Total spectra for Weelde (B) - 313 m



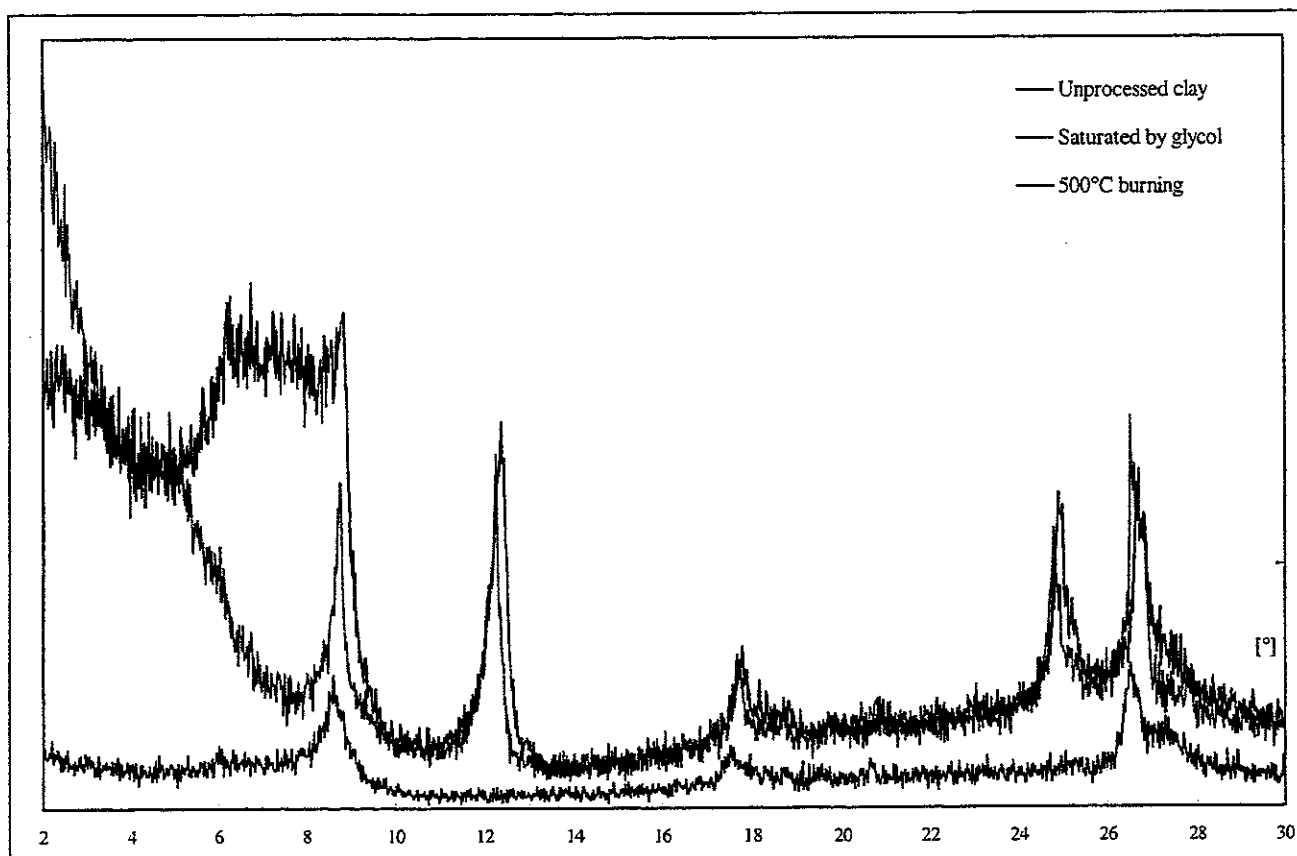
Appendix 6 : Mineralogical analysis : Spectra on the clay for Doel (B) - 69 m



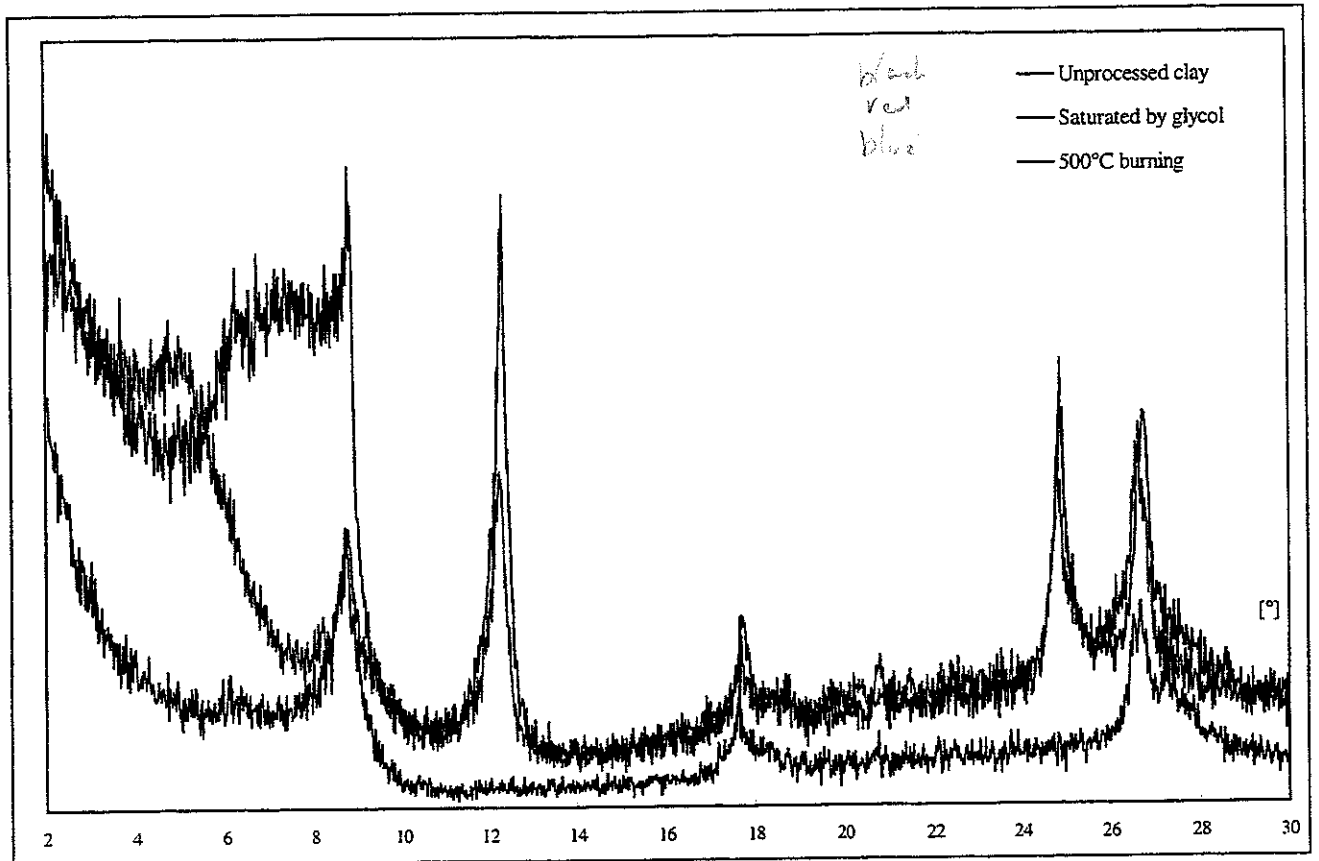
Appendix 7 : Mineralogical analysis : Spectra on the clay for Zoersel (B) - 120 m



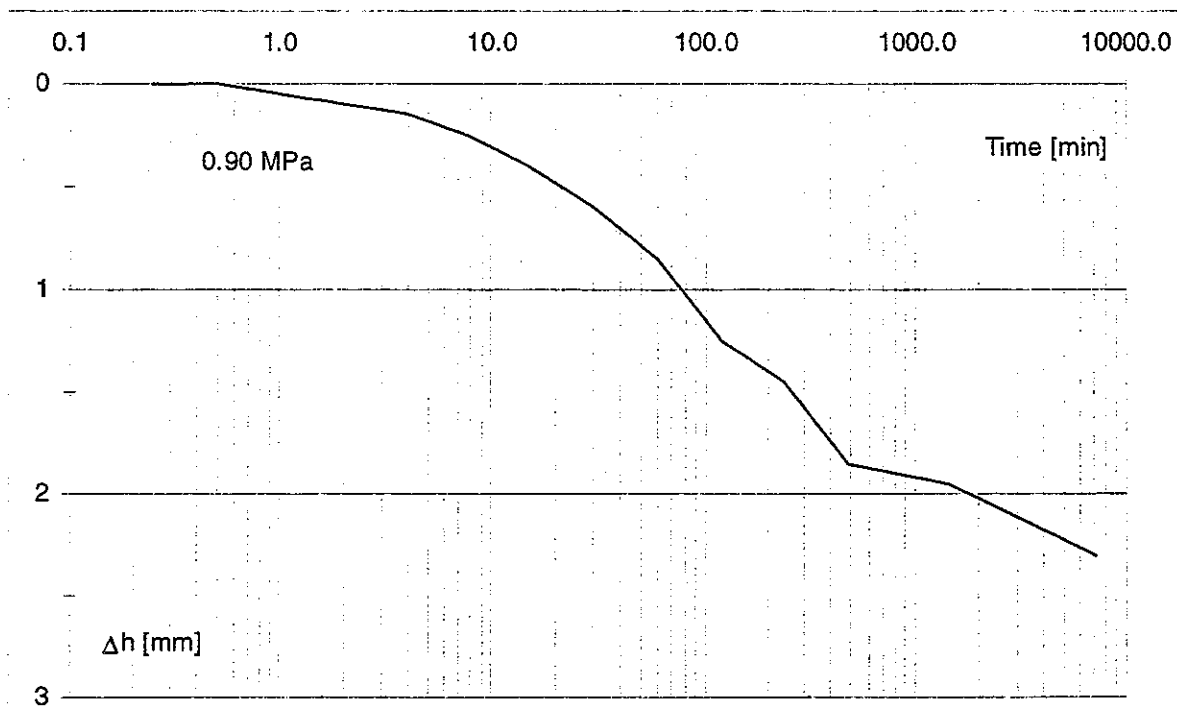
Appendix 8 : Mineralogical analysis : Spectra on the clay for Mol (B) - 224 m



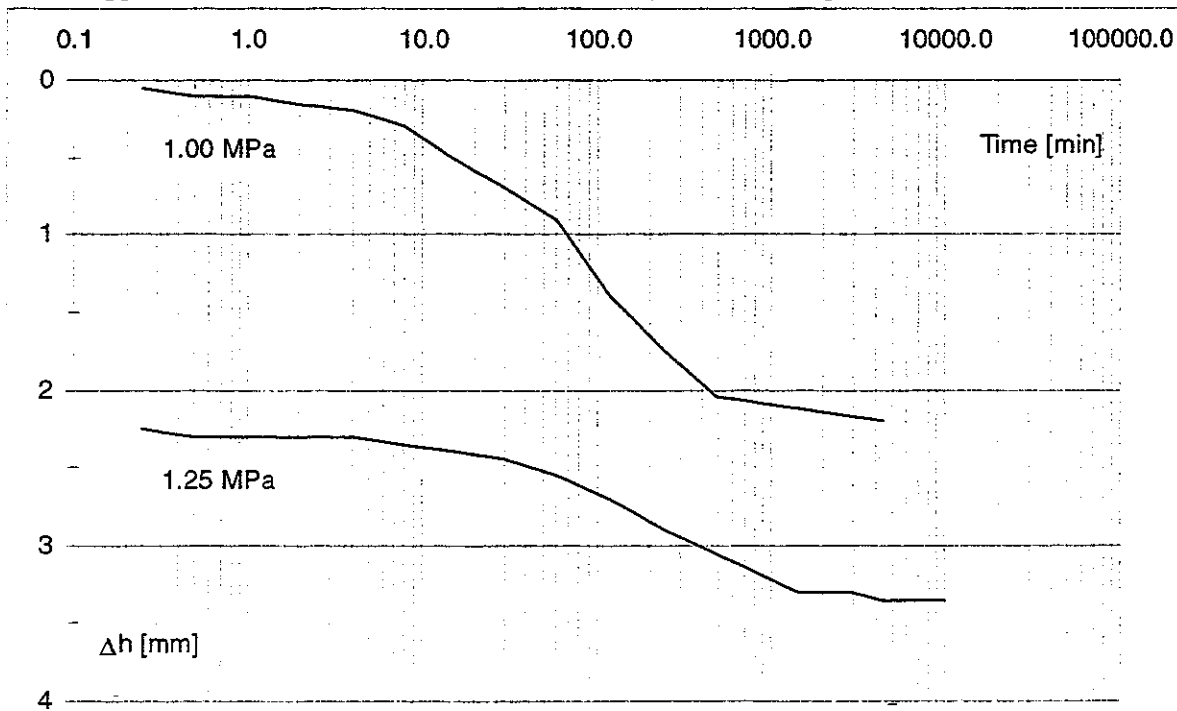
Appendix 9 : Mineralogical analysis : Spectra on the clay for Mol (B) - 229 m



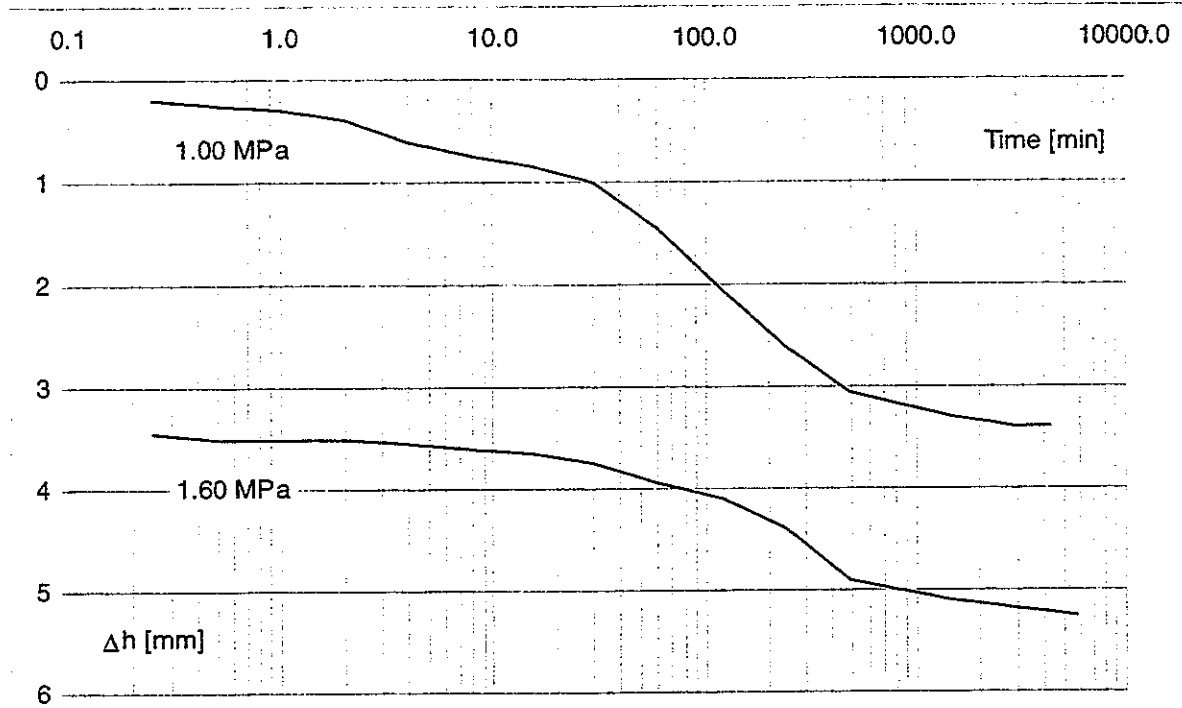
Appendix 10 : Mineralogical analysis : Spectra on the clay for Weelde (B) - 313 m



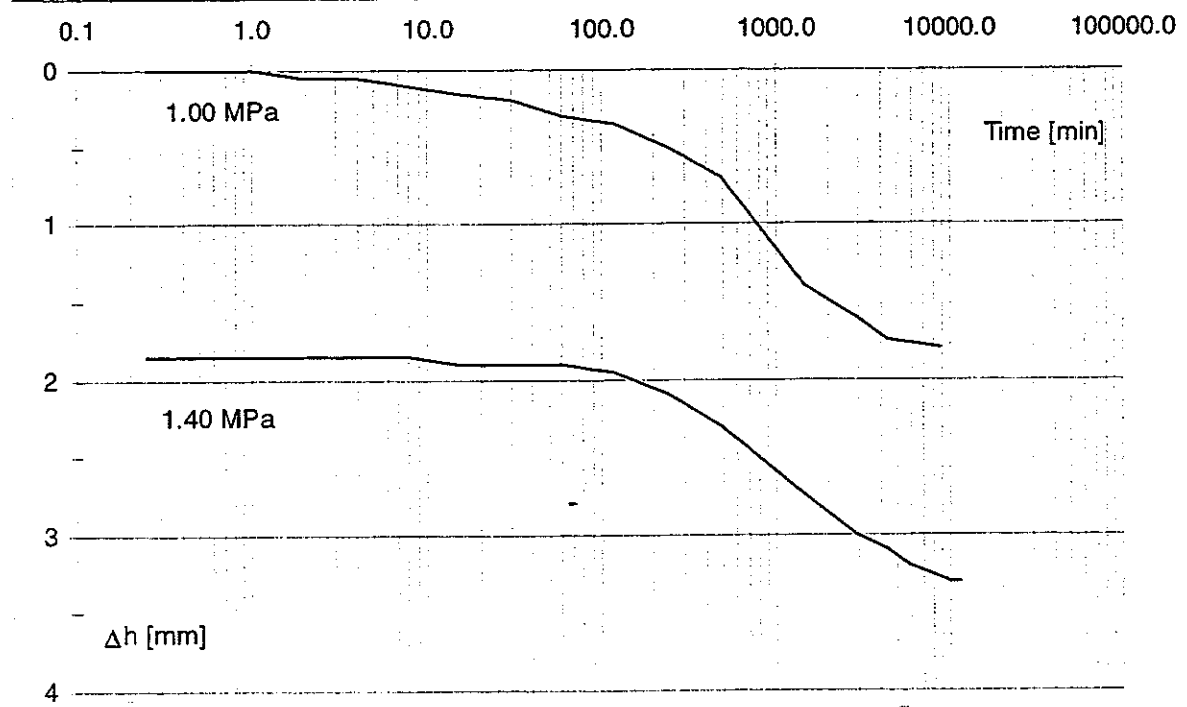
Appendix 11 : Consolidation curve - Doel (B) 69 m - Sample a : $\sigma_c = 0.70$ MPa



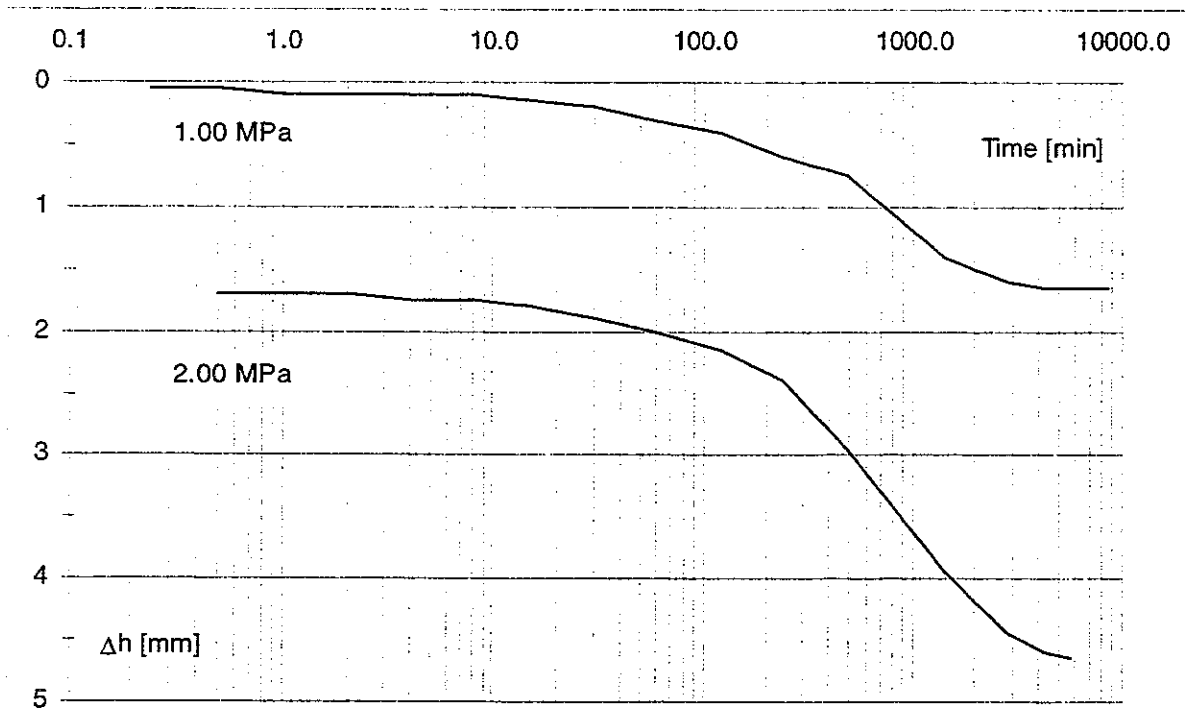
Appendix 12 : Consolidation curve - Doel (B) 69 m - Sample b : $\sigma_c = 1.05$ MPa



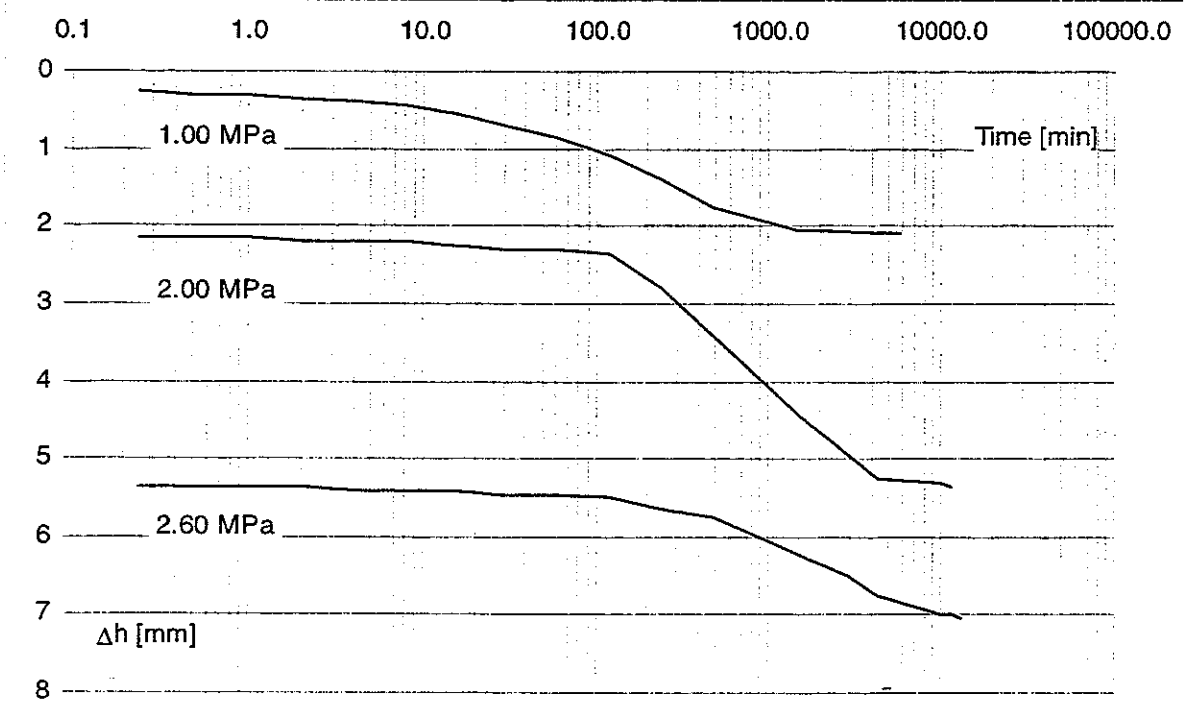
Appendix 13 : Consolidation curve - Doel (B) 69 m - Sample c : $\sigma_c = 1.40$ MPa



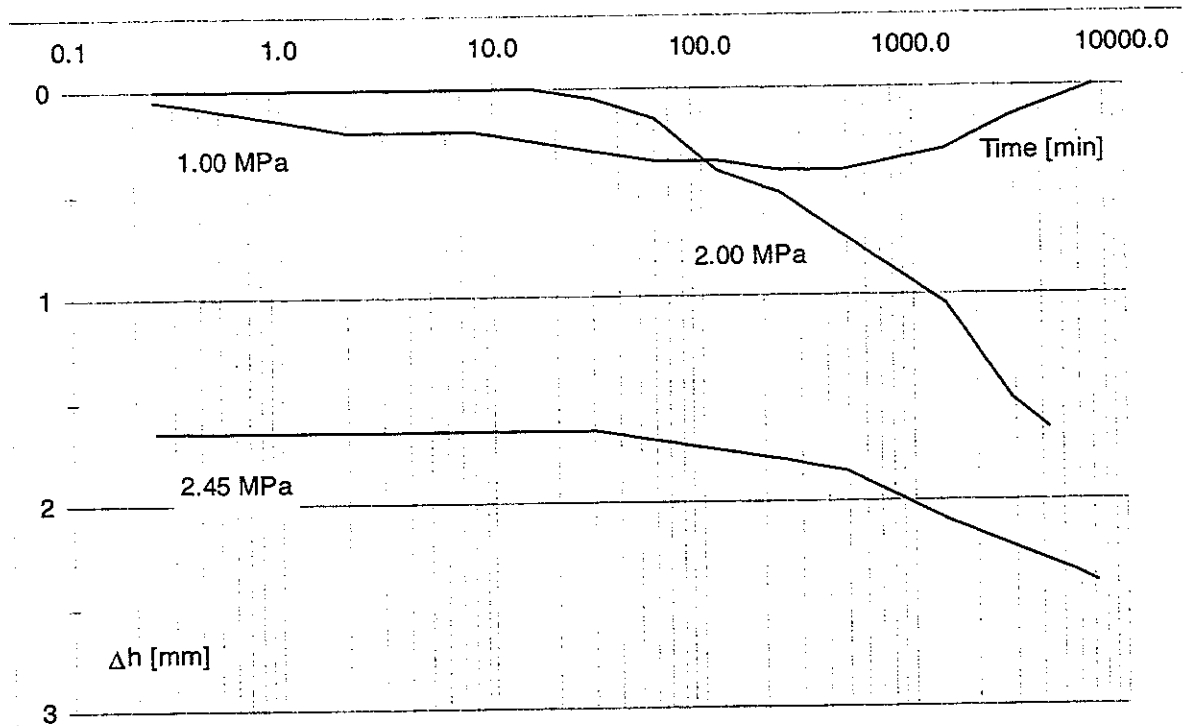
Appendix 14 : Consolidation curve - Zoersel (B) 120 m - Sample a : $\sigma_c = 1.20$ MPa



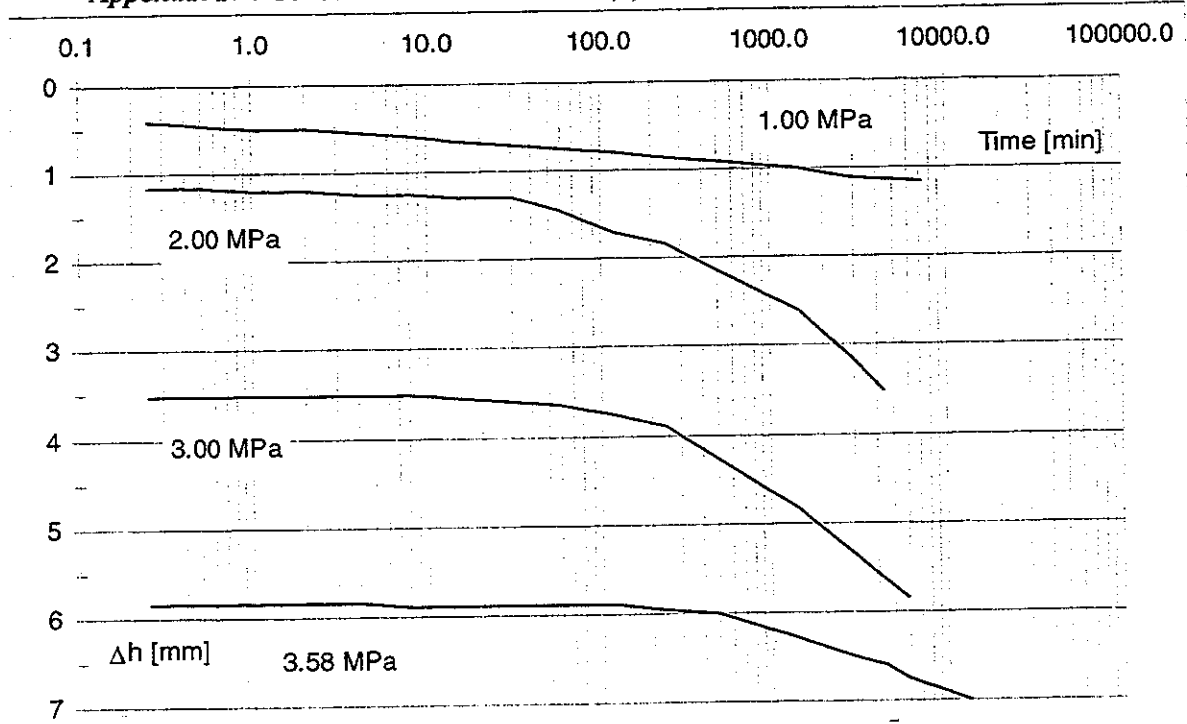
Appendix 15 : Consolidation curve - Zoersel (B) 120 m - Sample b : $\sigma_c = 1.80$ MPa



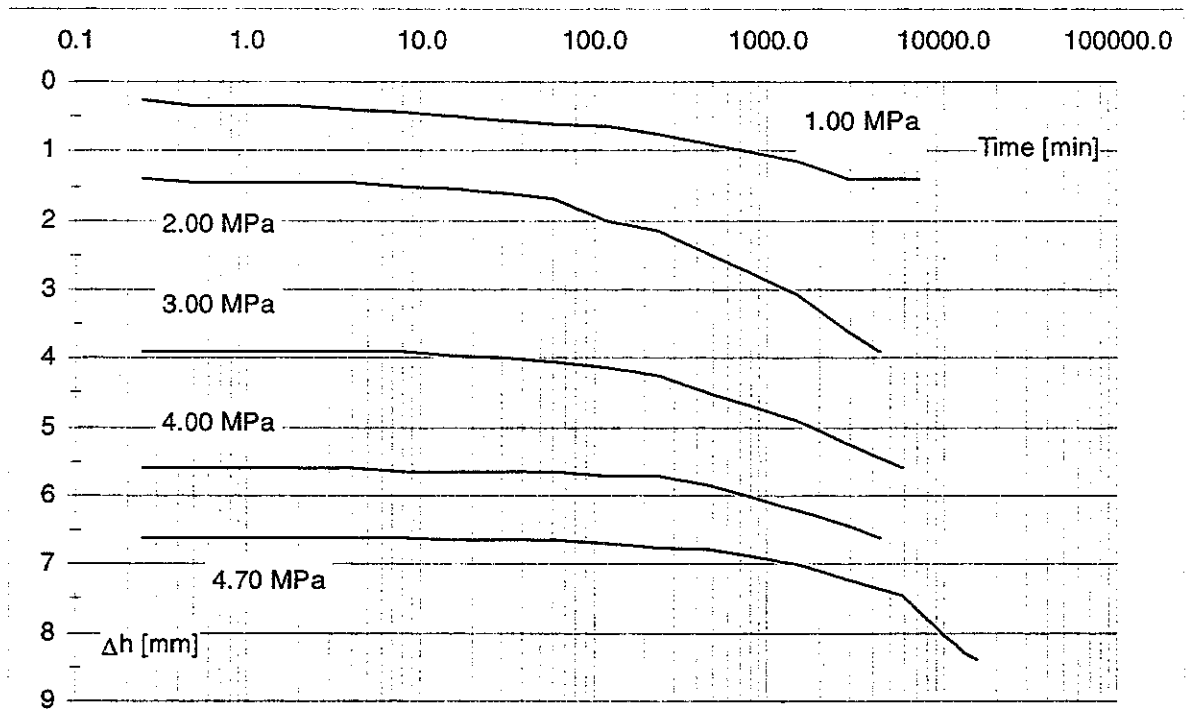
Appendix 16 : Consolidation curve - Zoersel (B) 120 m - Sample c : $\sigma_c = 2.40$ MPa



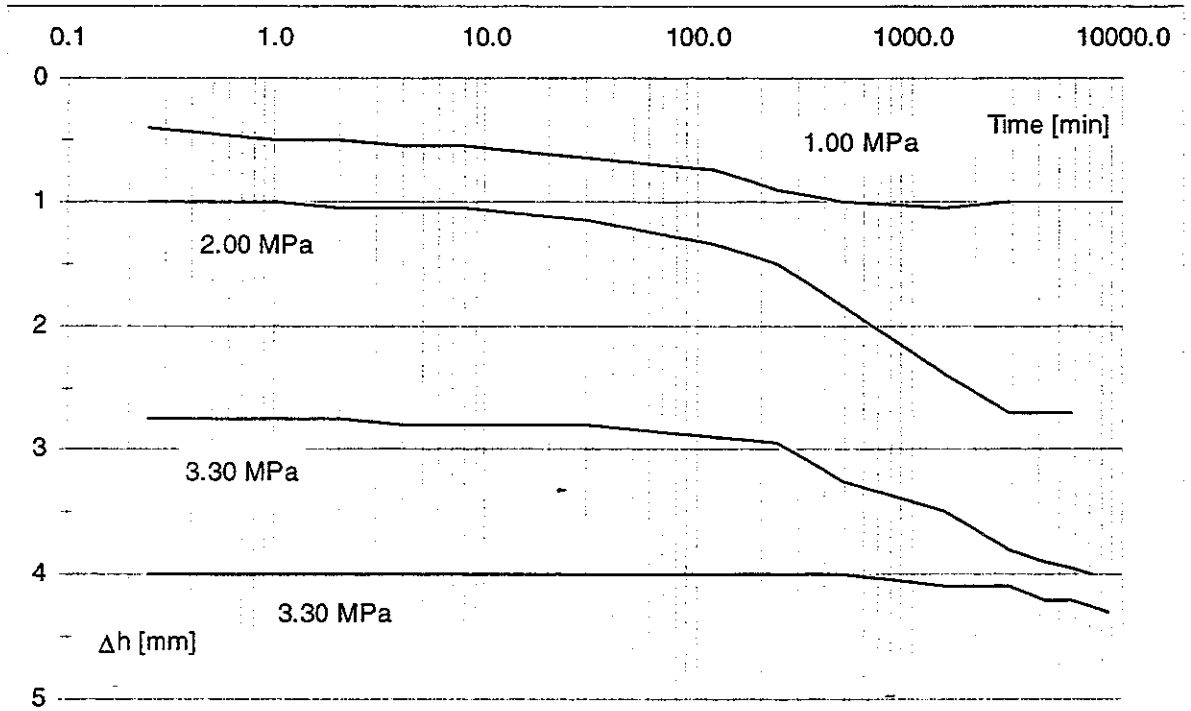
Appendix 17 : Consolidation curve - Mol (B) 229 m - Sample a : $\sigma_c = 2.25 \text{ MPa}$



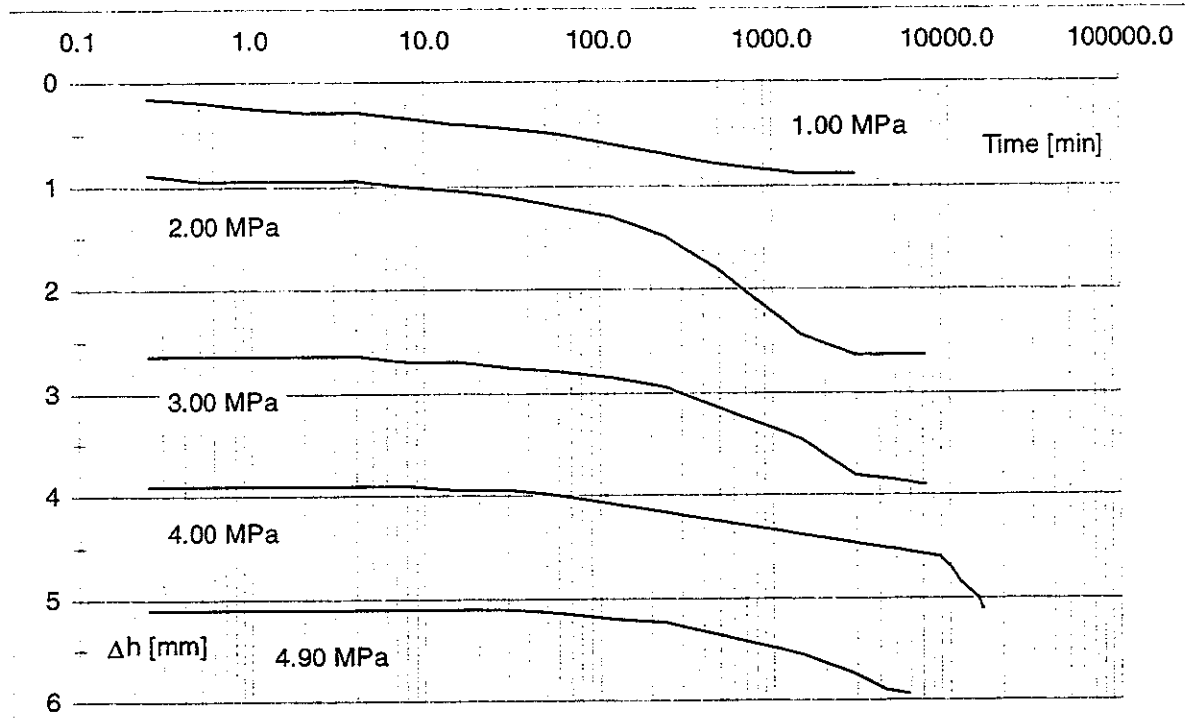
Appendix 18 : Consolidation curve - Mol (B) 229 m - Sample b : $\sigma_c = 3.38 \text{ MPa}$



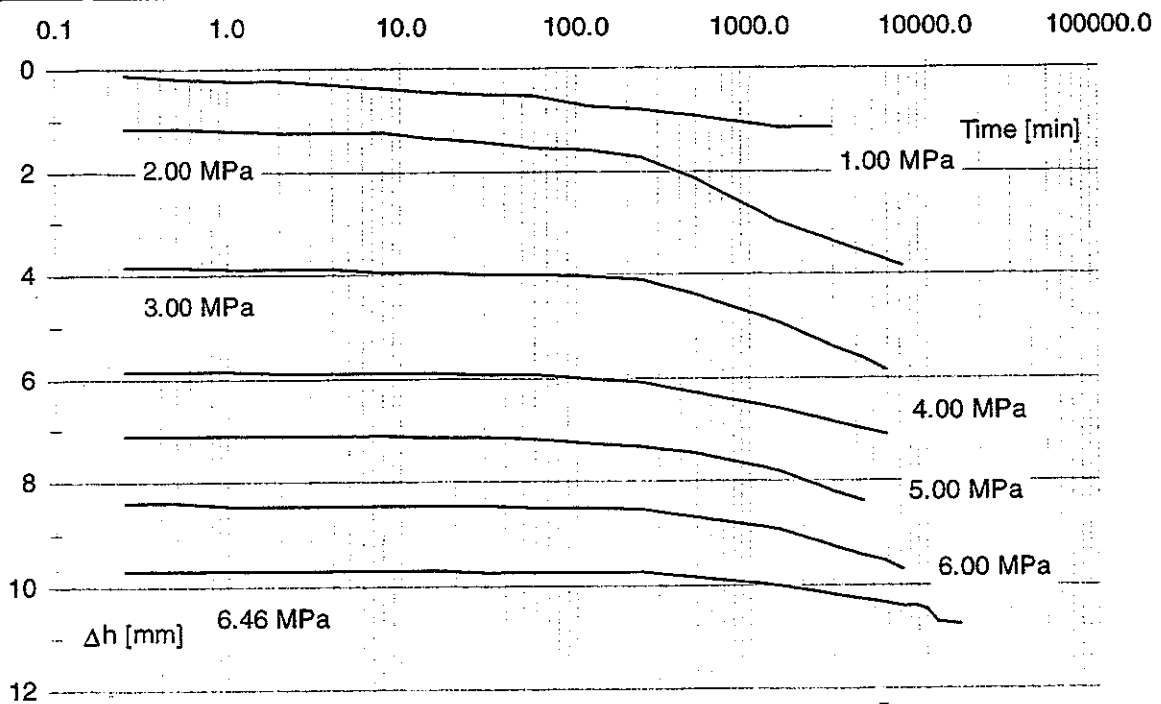
Appendix 19 : Consolidation curve - Mol (B) 229 m - Sample c : $\sigma_c = 4.50$ MPa



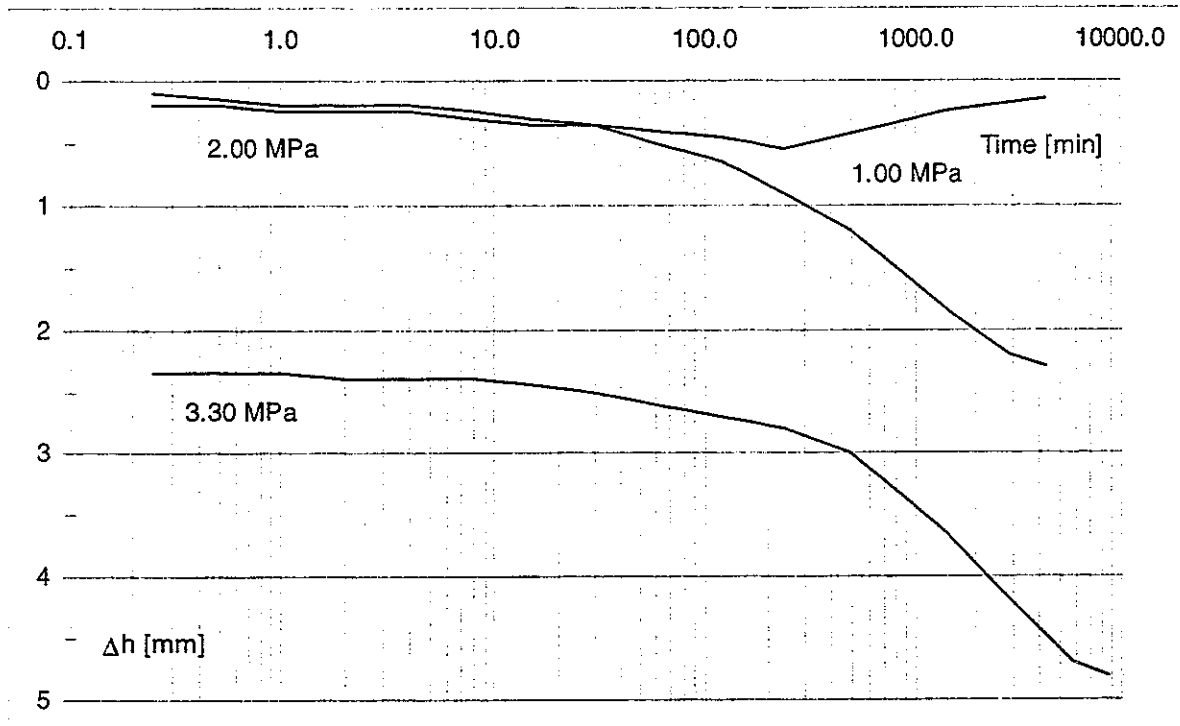
Appendix 20 : Consolidation curve - Weelde (B) 313 m - First serie - Sample a : $\sigma_c = 3.10$ MPa



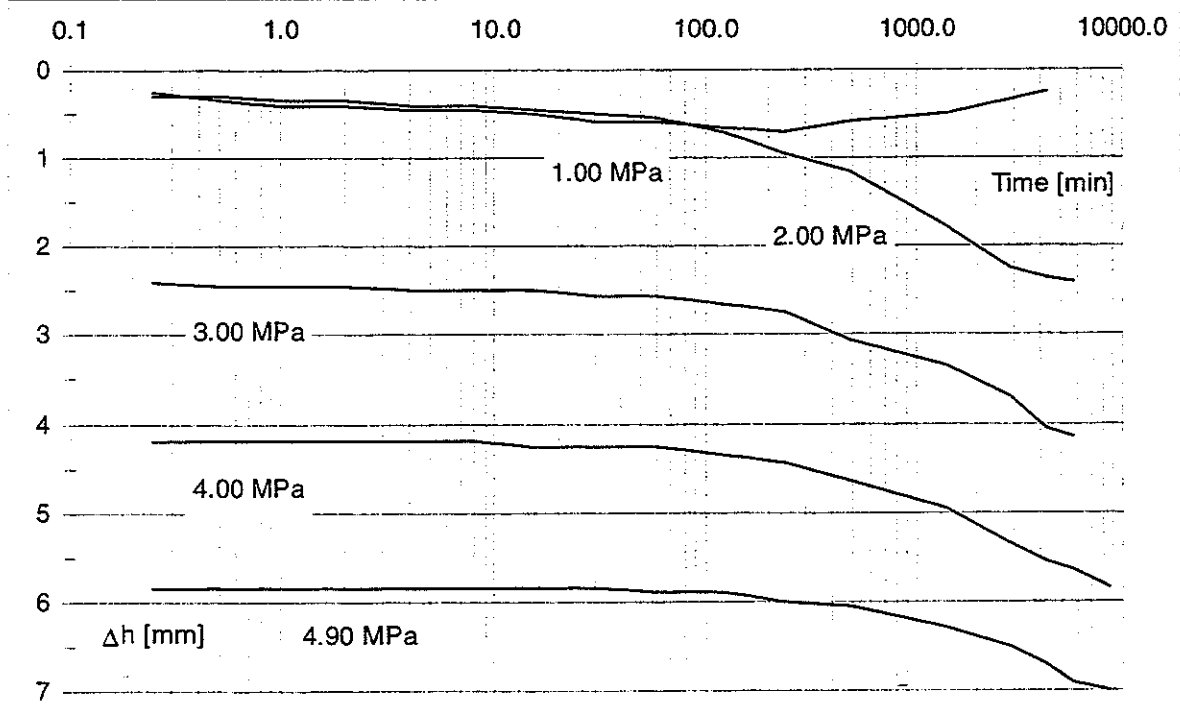
Appendix 21 : Consolidation curve - Weelde (B) 313 m - First serie - Sample b : $\sigma_c = 4.70$ MPa



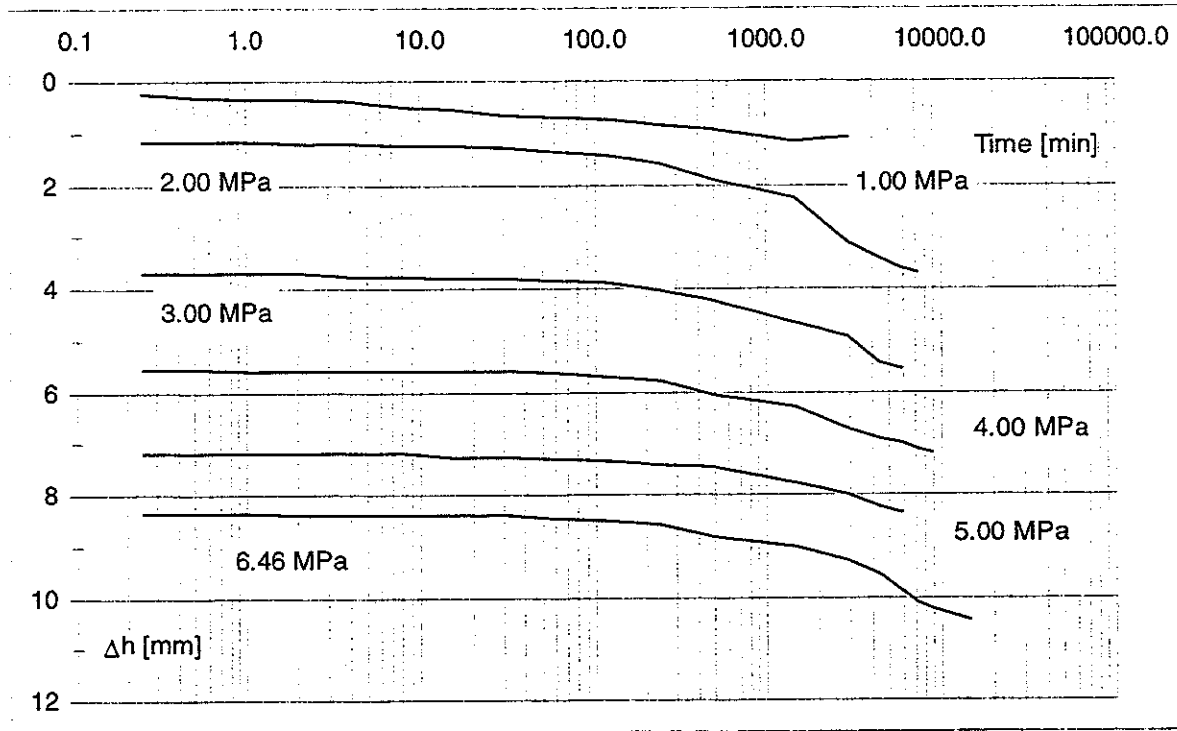
Appendix 22 : Consolidation curve - Weelde (B) 313 m - First serie - Sample c : $\sigma_c = 6.26$ MPa



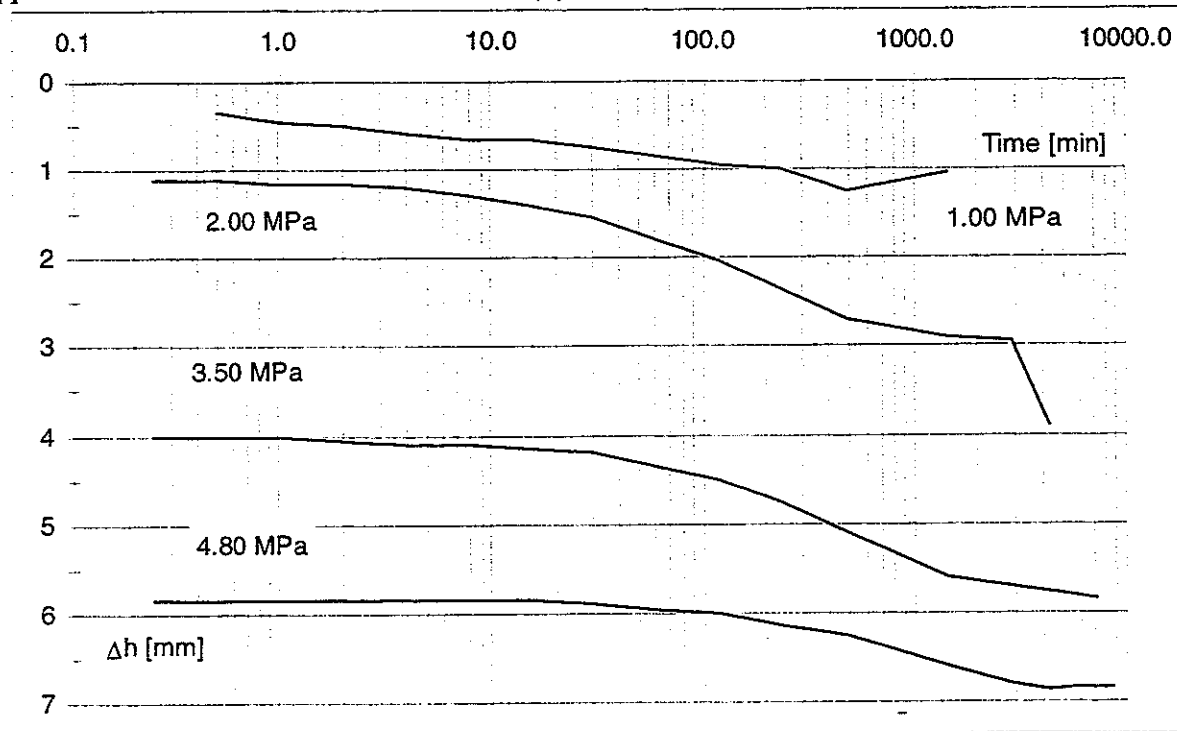
Appendix 23 : Consolidation curve - Weelde (B) 313 m - Second serie - Sample a : $\sigma_c = 3.10$ MPa



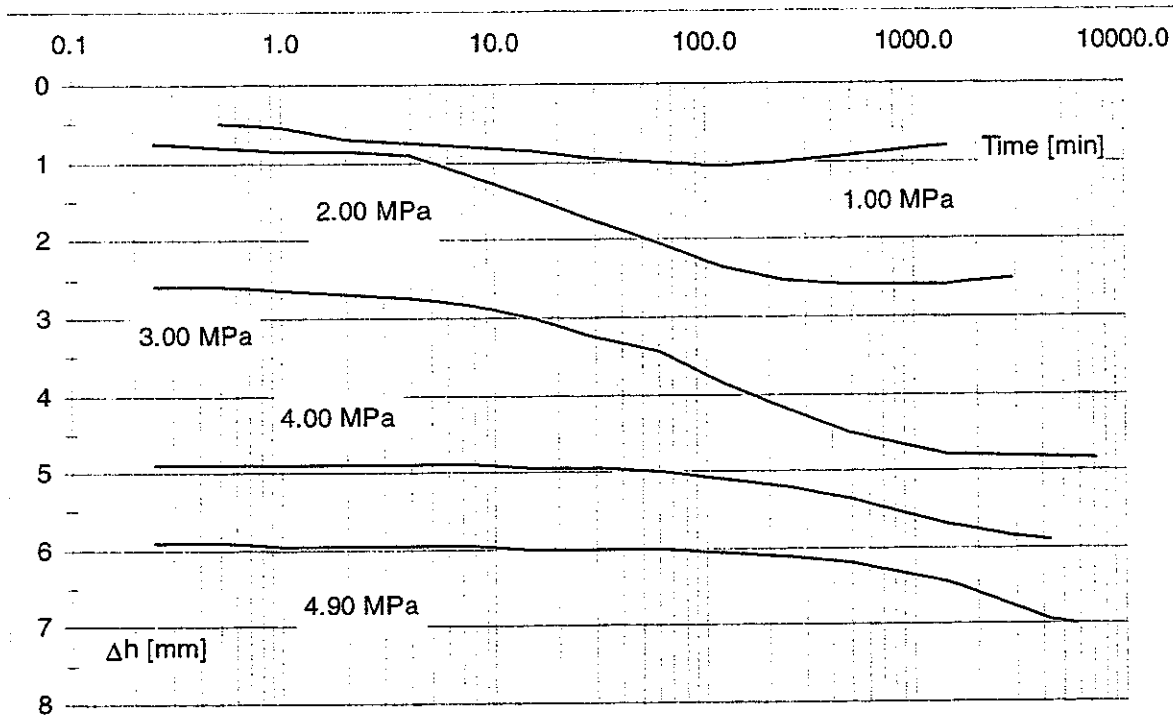
Appendix 24 : Consolidation curve - Weelde (B) 313 m - Second serie - Sample b : $\sigma_c = 4.70$ MPa



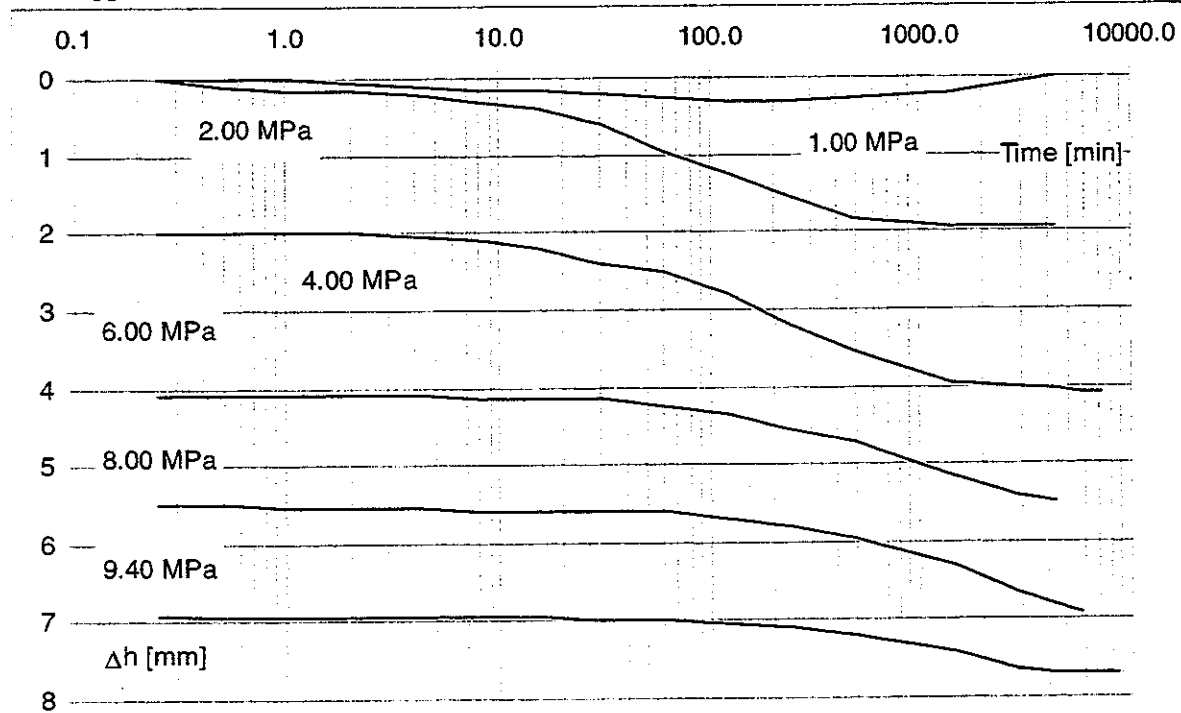
Appendix 25 : Consolidation curve - Weelde (B) 313 m - Second serie - Sample c : $\sigma_c = 6.26$ MPa



Appendix 26 : Consolidation curve - Blija (NL) 455 m - Sample a : $\sigma_c = 4.60$ MPa



Appendix 27 : Consolidation curve - Blija (NL) 455 m - Sample b : $\sigma_c = 6.90$ MPa

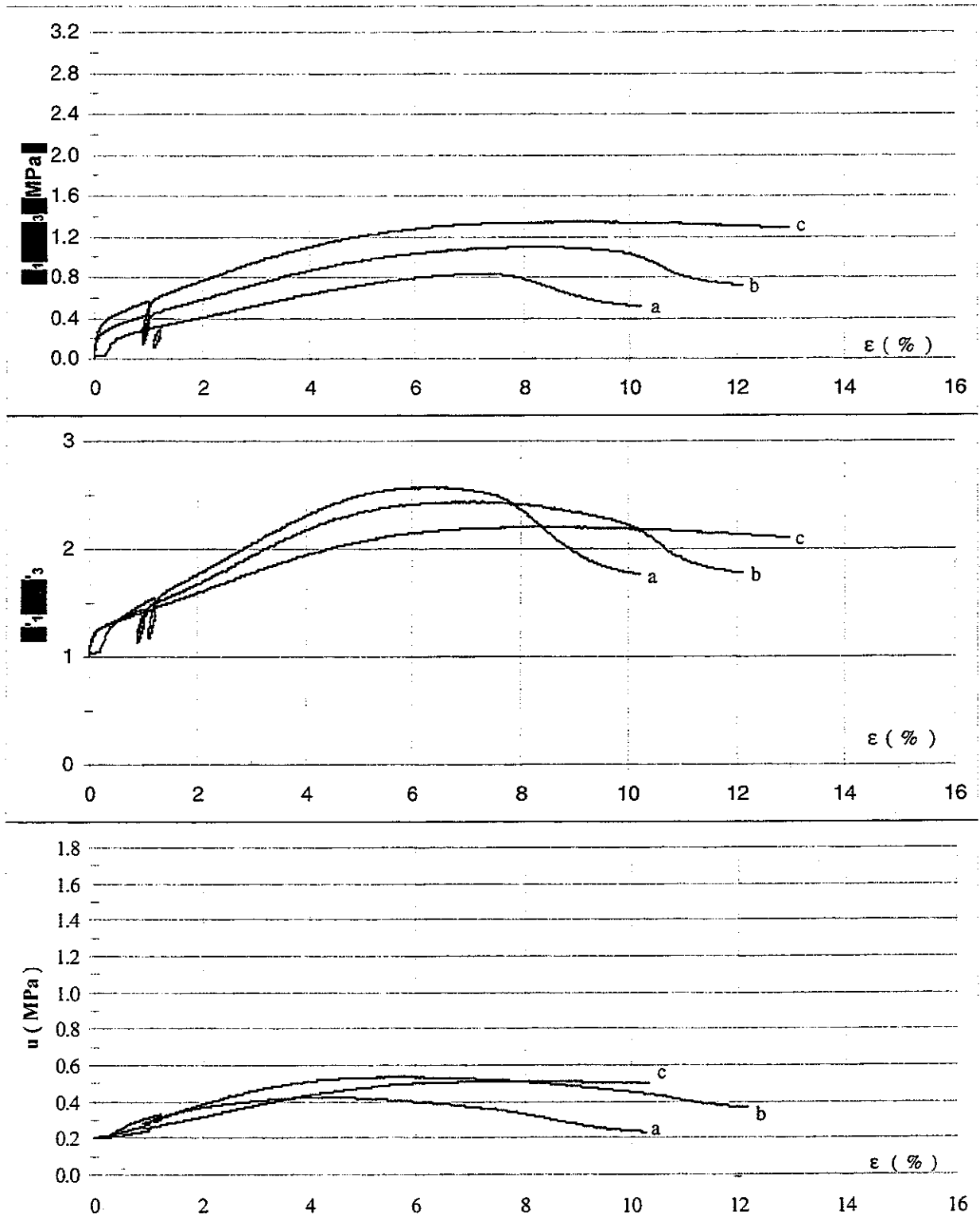


Appendix 28 : Consolidation curve - Blija (NL) 455 m - Sample c : $\sigma_c = 9.20$ MPa



<u>Sample a</u>		
σ_c	MPa	0.90
$(\sigma_1 - \sigma_3)_{\max}$	MPa	0.831
ε	%	7.422
$\sigma_{\text{tot},1}$	MPa	1.537
$\sigma_{\text{tot},3}$	MPa	0.706
u	MPa	0.359
$\sigma_{\text{eff},1}$	MPa	1.380
$\sigma_{\text{eff},3}$	MPa	0.549
u_0	MPa	0.202
<u>Sample b</u>		
σ_c	MPa	1.25
$(\sigma_1 - \sigma_3)_{\max}$	MPa	1.098
ε	%	8.159
$\sigma_{\text{tot},1}$	MPa	2.184
$\sigma_{\text{tot},3}$	MPa	1.086
u	MPa	0.506
$\sigma_{\text{eff},1}$	MPa	1.877
$\sigma_{\text{eff},3}$	MPa	0.779
u_0	MPa	0.199
<u>Sample c</u>		
σ_c	MPa	1.60
$(\sigma_1 - \sigma_3)_{\max}$	MPa	1.345
ε	%	9.027
$\sigma_{\text{tot},1}$	MPa	2.773
$\sigma_{\text{tot},3}$	MPa	1.428
u	MPa	0.508
$\sigma_{\text{eff},1}$	MPa	2.465
$\sigma_{\text{eff},3}$	MPa	1.120
u_0	MPa	0.200
<u>Friction angles and cohesions</u>		
c_{cu}	MPa	0.125
φ_{cu}	°	15.21
c'	MPa	0.133
φ'	°	17.94

Appendix 29 : Numerical values for Doel (B) - 69 m

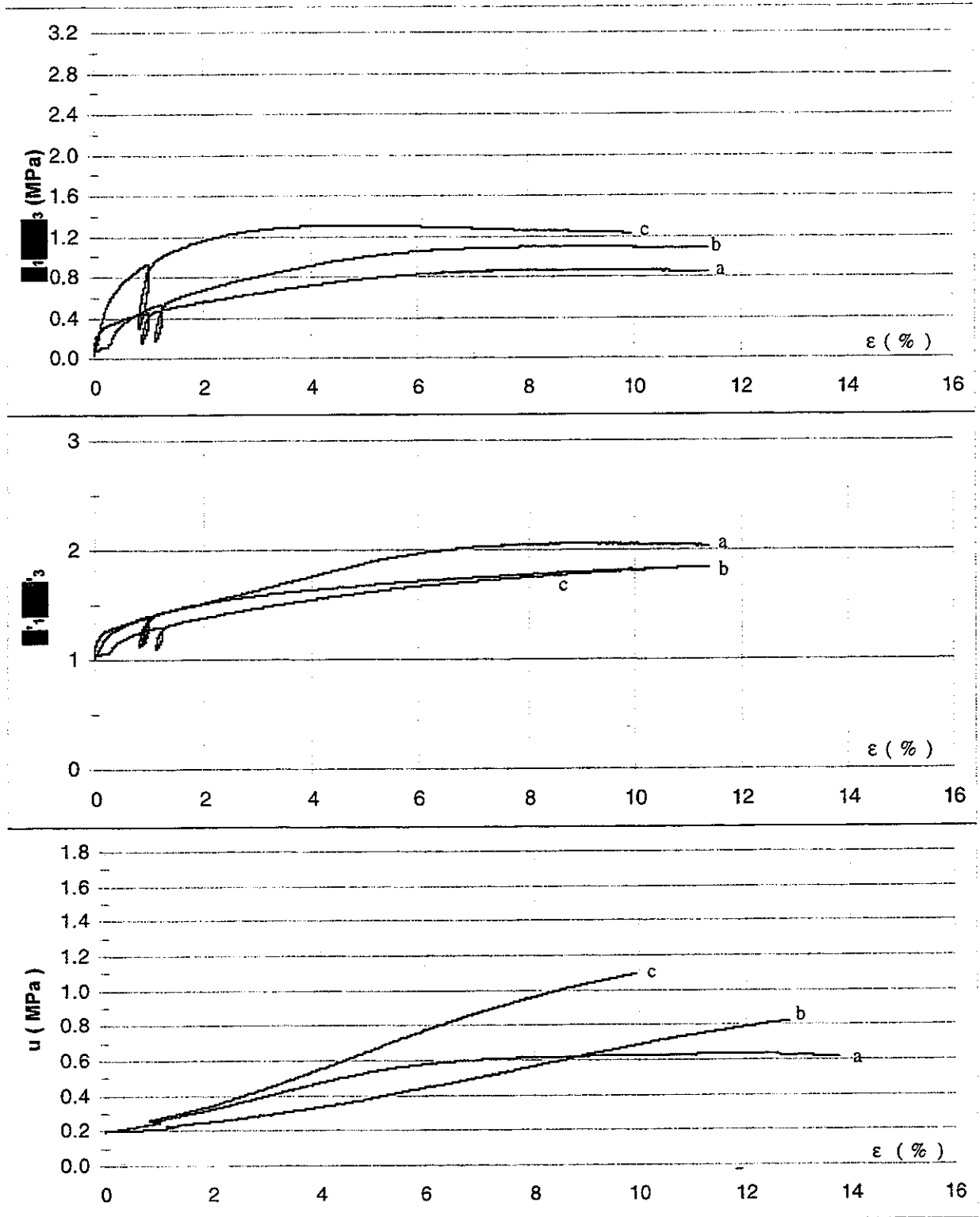


*Appendix 30 : Deviator stress, principal stress ratio and pore pressure versus deformation
Doel (B) - 69 m*



<u>Sample a</u>		
σ_c	MPa	1.40
$(\sigma_1 - \sigma_3)_{max}$	MPa	0.866
ϵ	%	8.950
$\sigma_{tot,1}$	MPa	2.111
$\sigma_{tot,3}$	MPa	1.245
u	MPa	0.622
$\sigma_{eff,1}$	MPa	1.688
$\sigma_{eff,3}$	MPa	0.822
u_0	MPa	0.199
<u>Sample b</u>		
σ_c	MPa	2.00
$(\sigma_1 - \sigma_3)_{max}$	MPa	1.096
ϵ	%	8.570
$\sigma_{tot,1}$	MPa	2.924
$\sigma_{tot,3}$	MPa	1.828
u	MPa	0.603
$\sigma_{eff,1}$	MPa	2.521
$\sigma_{eff,3}$	MPa	1.425
u_0	MPa	0.200
<u>Sample c</u>		
σ_c	MPa	2.60
$(\sigma_1 - \sigma_3)_{max}$	MPa	1.305
ϵ	%	4.770
$\sigma_{tot,1}$	MPa	3.697
$\sigma_{tot,3}$	MPa	2.392
u	MPa	0.634
$\sigma_{eff,1}$	MPa	3.263
$\sigma_{eff,3}$	MPa	1.958
u_0	MPa	0.200
<u>Friction angles and cohesions</u>		
c_{cu}	MPa	0.168
φ_{cu}	°	9.20
c'	MPa	0.233
φ'	°	9.31

Appendix 31 : Numerical values for Zoersel (B) - 120 m

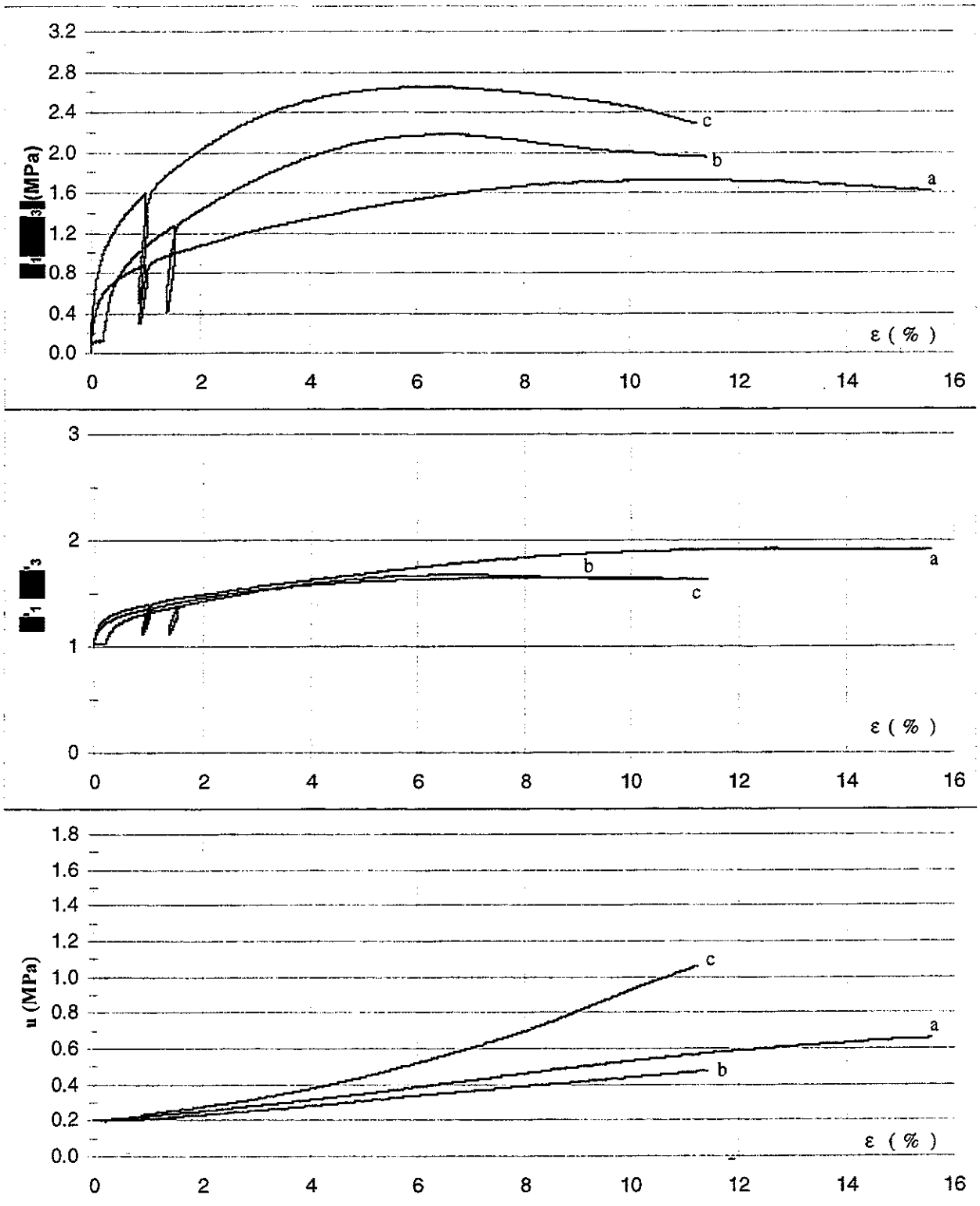


*Appendix 32 : Deviator stress, principal stress ratio and pore pressure versus deformation
Zoersel (B) - 120 m*



<u>Sample a</u>		
σ_c	MPa	2.45
$(\sigma_1 - \sigma_3)_{max}$	MPa	1.723
ϵ	%	10.997
$\sigma_{tot,1}$	MPa	3.980
$\sigma_{tot,3}$	MPa	2.257
u	MPa	0.562
$\sigma_{eff,1}$	MPa	3.619
$\sigma_{eff,3}$	MPa	1.896
u_0	MPa	0.201
<u>Sample b</u>		
σ_c	MPa	3.58
$(\sigma_1 - \sigma_3)_{max}$	MPa	2.179
ϵ	%	6.568
$\sigma_{tot,1}$	MPa	5.571
$\sigma_{tot,3}$	MPa	3.392
u	MPa	0.353
$\sigma_{eff,1}$	MPa	5.418
$\sigma_{eff,3}$	MPa	3.239
u_0	MPa	0.200
<u>Sample c</u>		
σ_c	MPa	4.70
$(\sigma_1 - \sigma_3)_{max}$	MPa	2.650
ϵ	%	6.145
$\sigma_{tot,1}$	MPa	7.161
$\sigma_{tot,3}$	MPa	4.511
u	MPa	0.531
$\sigma_{eff,1}$	MPa	6.831
$\sigma_{eff,3}$	MPa	4.181
u_0	MPa	0.201
<u>Friction angles and cohesions</u>		
c_{cu}	MPa	0.333
ϕ_{cu}	°	9.82
c'	MPa	0.396
ϕ'	°	9.62

Appendix 33 : Numerical values for Mol (B) - 224 m

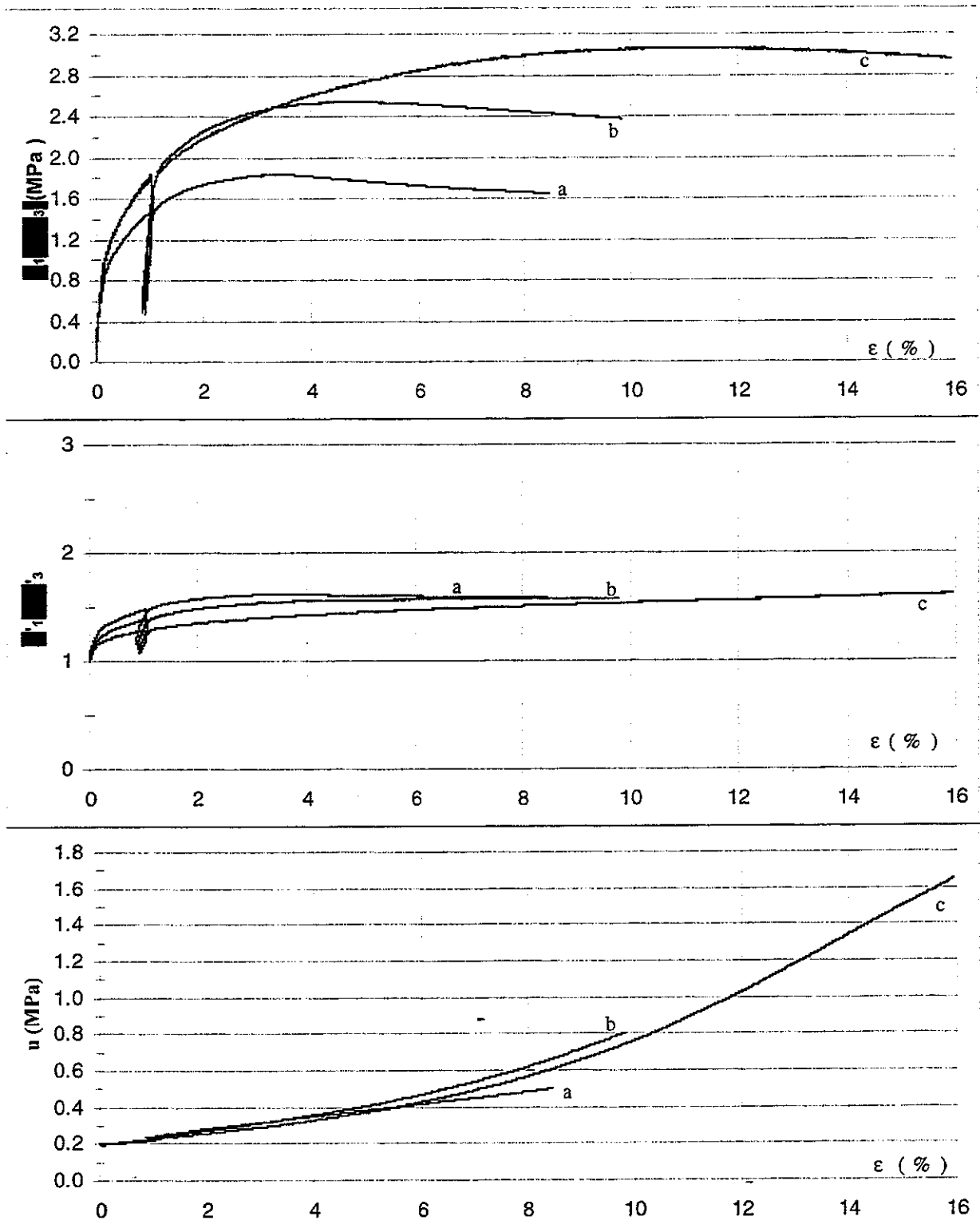


*Appendix 34 : Deviator stress, principal stress ratio and pore pressure versus deformation
Mol (B) - 224 m*



Sample a		
σ_c	MPa	3.30
$(\sigma_1 - \sigma_3)_{\max}$	MPa	1.840
ε	%	3.495
$\sigma_{\text{tot},1}$	MPa	4.943
$\sigma_{\text{tot},3}$	MPa	3.103
u	MPa	0.334
$\sigma_{\text{eff},1}$	MPa	4.808
$\sigma_{\text{eff},3}$	MPa	2.968
u_0	MPa	0.199
Sample b		
σ_c	MPa	4.90
$(\sigma_1 - \sigma_3)_{\max}$	MPa	2.541
ε	%	4.784
$\sigma_{\text{tot},1}$	MPa	7.250
$\sigma_{\text{tot},3}$	MPa	4.709
u	MPa	0.397
$\sigma_{\text{eff},1}$	MPa	7.053
$\sigma_{\text{eff},3}$	MPa	4.512
u_0	MPa	0.200
Sample c		
σ_c	MPa	6.46
$(\sigma_1 - \sigma_3)_{\max}$	MPa	3.064
ε	%	11.220
$\sigma_{\text{tot},1}$	MPa	9.328
$\sigma_{\text{tot},3}$	MPa	6.264
u	MPa	0.917
$\sigma_{\text{eff},1}$	MPa	8.616
$\sigma_{\text{eff},3}$	MPa	5.552
u_0	MPa	0.205
Friction angles and cohesions		
c_{cu}	MPa	0.281
φ_{cu}	°	9.35
c'	MPa	0.177
φ'	°	11.01

Appendix 35 : Numerical values for Weelde (B) First serie - 313 m

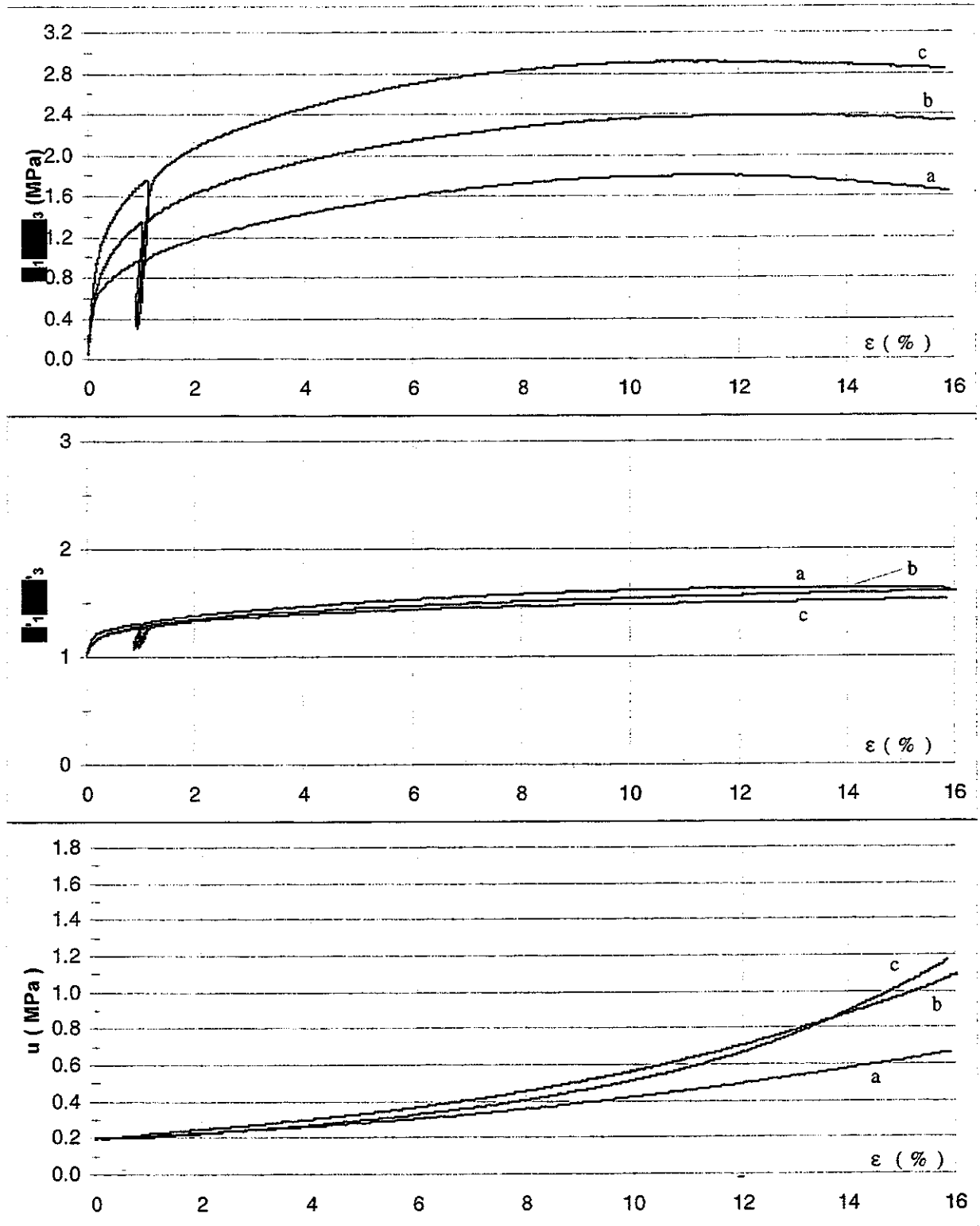


Appendix 36 : Deviator stress, principal stress ratio and pore pressure versus deformation
Weelde (B) First serie - 313 m



	<u>Sample a</u>	
σ_c	MPa	3.13
$(\sigma_1 - \sigma_3)_{\max}$	MPa	1.800
ε	%	11.521
$\sigma_{\text{tot},1}$	MPa	4.941
$\sigma_{\text{tot},3}$	MPa	3.141
u	MPa	0.476
$\sigma_{\text{eff},1}$	MPa	4.663
$\sigma_{\text{eff},3}$	MPa	2.863
u_0	MPa	0.198
	<u>Sample b</u>	
σ_c	MPa	4.90
$(\sigma_1 - \sigma_3)_{\max}$	MPa	2.387
ε	%	12.528
$\sigma_{\text{tot},1}$	MPa	7.105
$\sigma_{\text{tot},3}$	MPa	4.718
u	MPa	0.748
$\sigma_{\text{eff},1}$	MPa	6.560
$\sigma_{\text{eff},3}$	MPa	4.173
u_0	MPa	0.203
	<u>Sample c</u>	
σ_c	MPa	6.46
$(\sigma_1 - \sigma_3)_{\max}$	MPa	2.912
ε	%	10.768
$\sigma_{\text{tot},1}$	MPa	9.188
$\sigma_{\text{tot},3}$	MPa	6.276
u	MPa	0.564
$\sigma_{\text{eff},1}$	MPa	8.826
$\sigma_{\text{eff},3}$	MPa	5.914
u_0	MPa	0.202
	<u>Friction angles and cohesions</u>	
c_{cu}	MPa	0.298
φ_{cu}	°	8.67
c'	MPa	0.345
φ'	°	8.81

Appendix 37 : Numerical values for Weelde (B) Second serie - 313 m

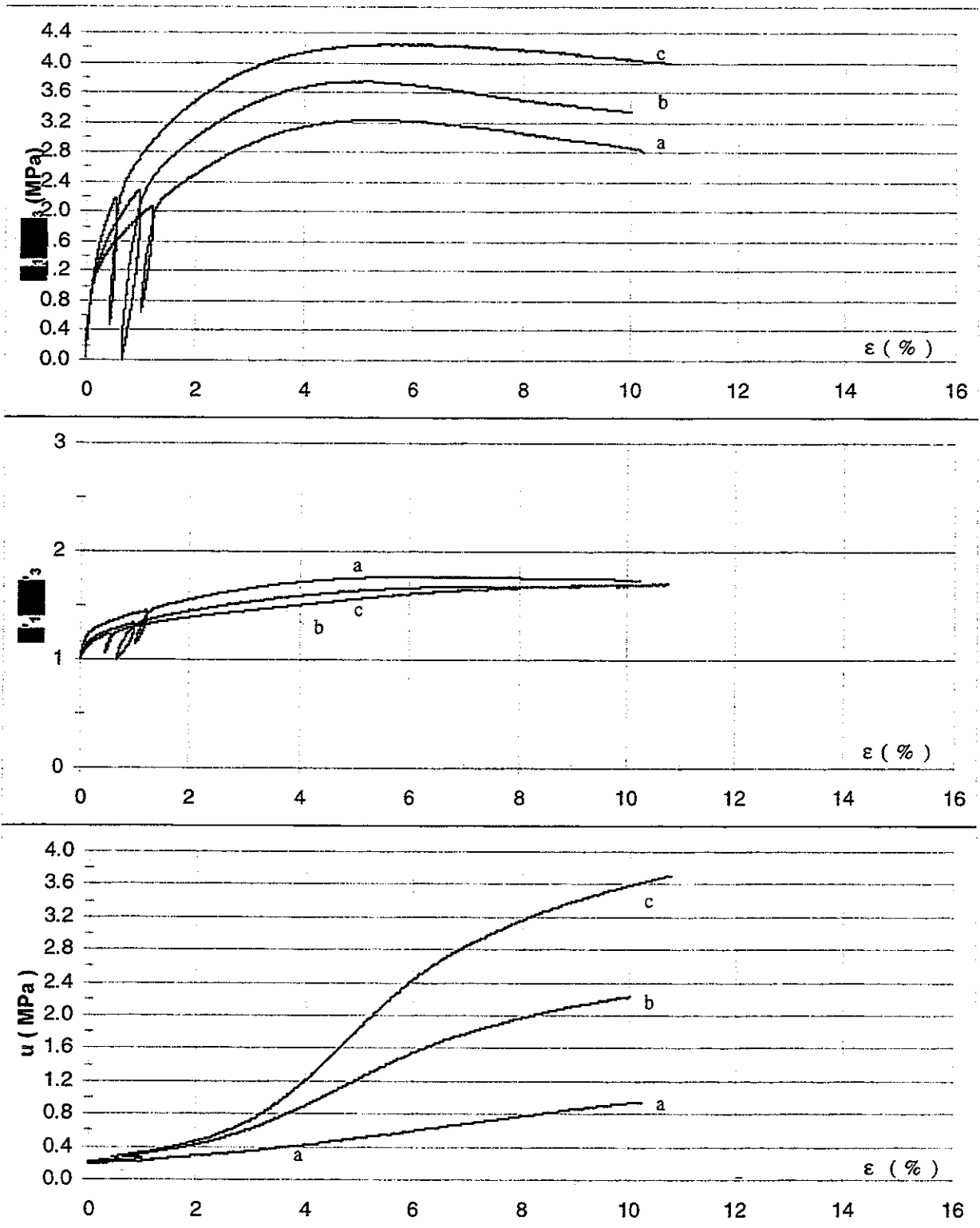


Appendix 38 : Deviator stress, principal stress ratio and pore pressure versus deformation
Weelde (B) Second serie - 313 m

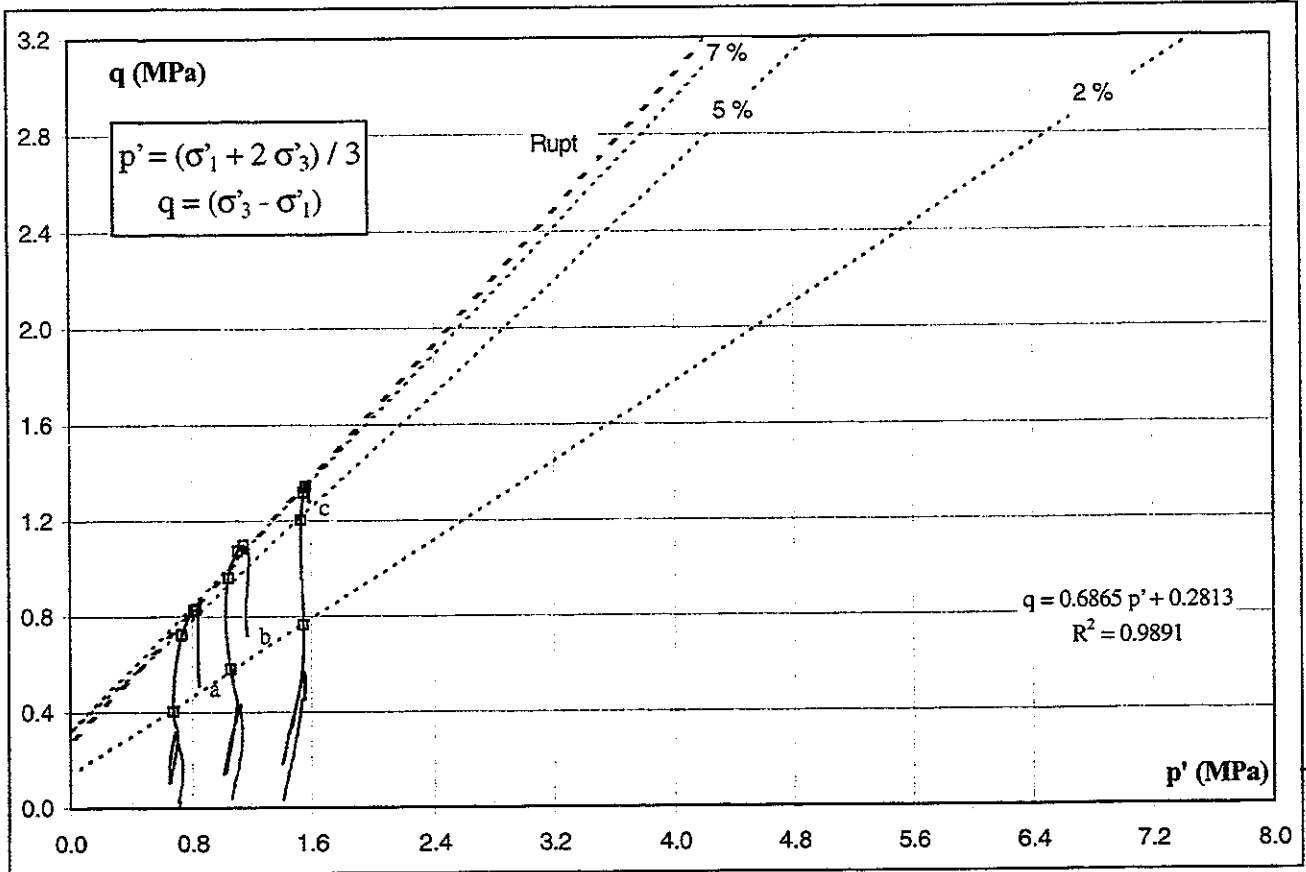


<u>Sample a</u>		
σ_c	MPa	3.13
$(\sigma_1 - \sigma_3)_{max}$	MPa	3.236
ϵ	%	5.323
$\sigma_{tot,1}$	MPa	7.831
$\sigma_{tot,3}$	MPa	4.595
u	MPa	0.535
$\sigma_{eff,1}$	MPa	7.497
$\sigma_{eff,3}$	MPa	4.267
u_0	MPa	0.201
<u>Sample b</u>		
σ_c	MPa	4.90
$(\sigma_1 - \sigma_3)_{max}$	MPa	3.745
ϵ	%	5.057
$\sigma_{tot,1}$	MPa	10.650
$\sigma_{tot,3}$	MPa	6.905
u	MPa	1.249
$\sigma_{eff,1}$	MPa	9.601
$\sigma_{eff,3}$	MPa	5.856
u_0	MPa	0.200
<u>Sample c</u>		
σ_c	MPa	6.46
$(\sigma_1 - \sigma_3)_{max}$	MPa	4.247
ϵ	%	5.900
$\sigma_{tot,1}$	MPa	13.457
$\sigma_{tot,3}$	MPa	9.210
u	MPa	2.380
$\sigma_{eff,1}$	MPa	11.277
$\sigma_{eff,3}$	MPa	7.030
u_0	MPa	0.200
<u>Friction angles and cohesions</u>		
c_{cu}	MPa	1.01
ϕ_{cu}	°	5.67
c'	MPa	0.715
ϕ'	°	8.83

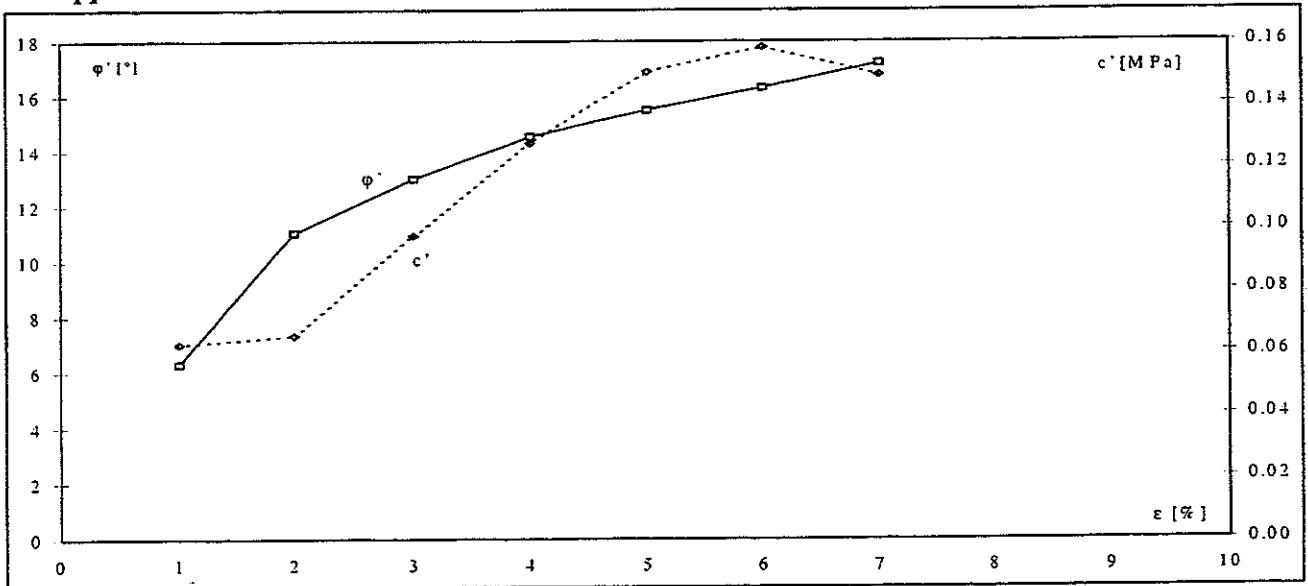
Appendix 39 : Numerical values for Bljia (NL) - 455 m



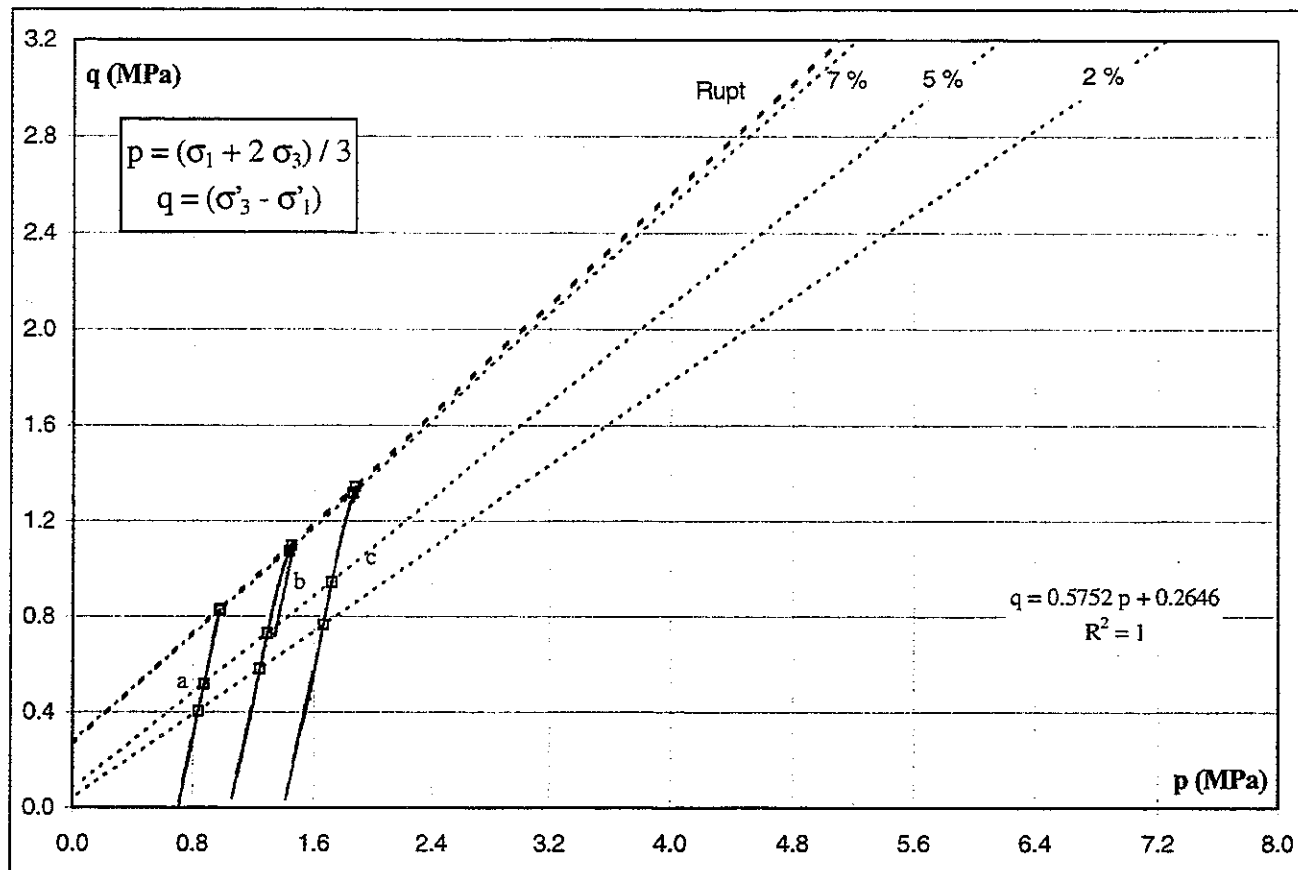
Appendix 40 : Deviator stress, principal stress ratio and pore pressure versus deformation
Bljka (NL) - 455 m



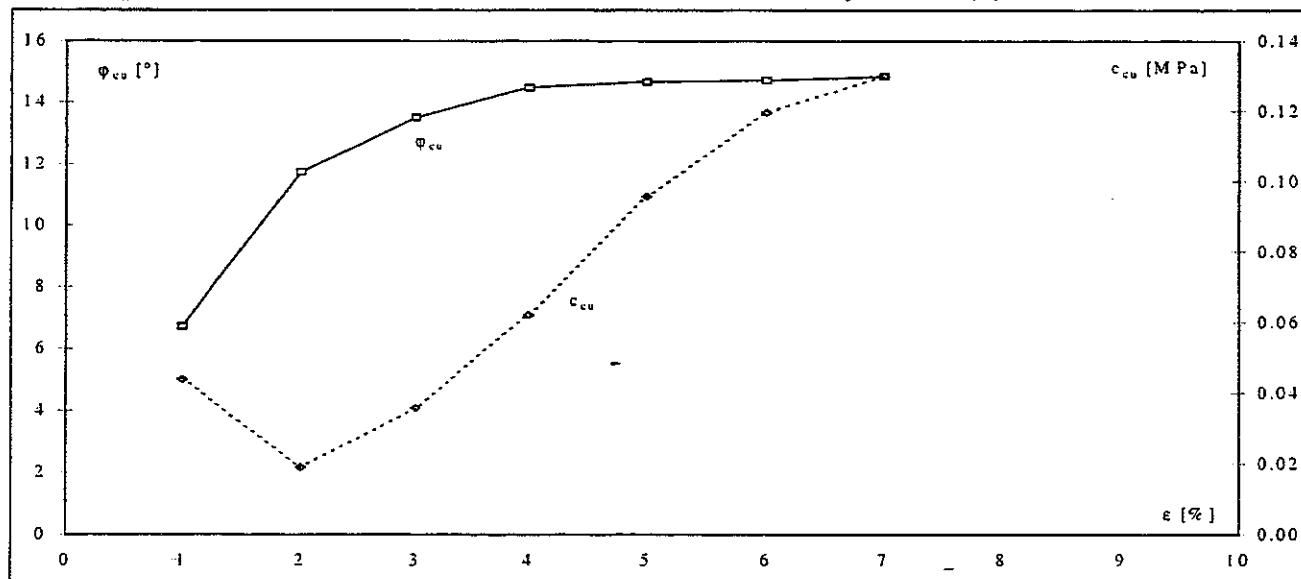
Appendix 41 : Deviator stress versus the mean effective stress for Doel (B) 69.23 - 69.68 m



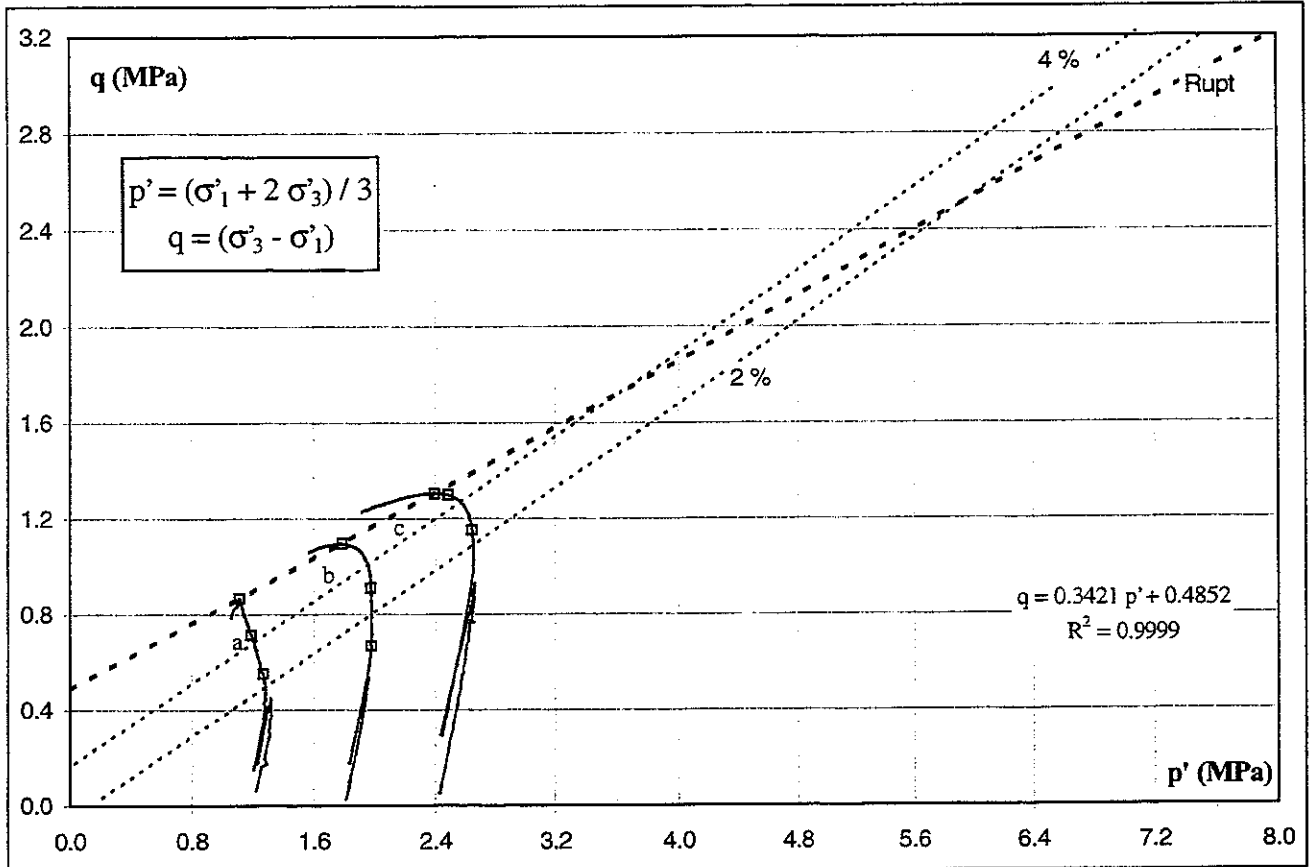
Appendix 42 : Effective 'shear strength parameters' versus deformation for Doel (B) 69.23 - 69.68 m



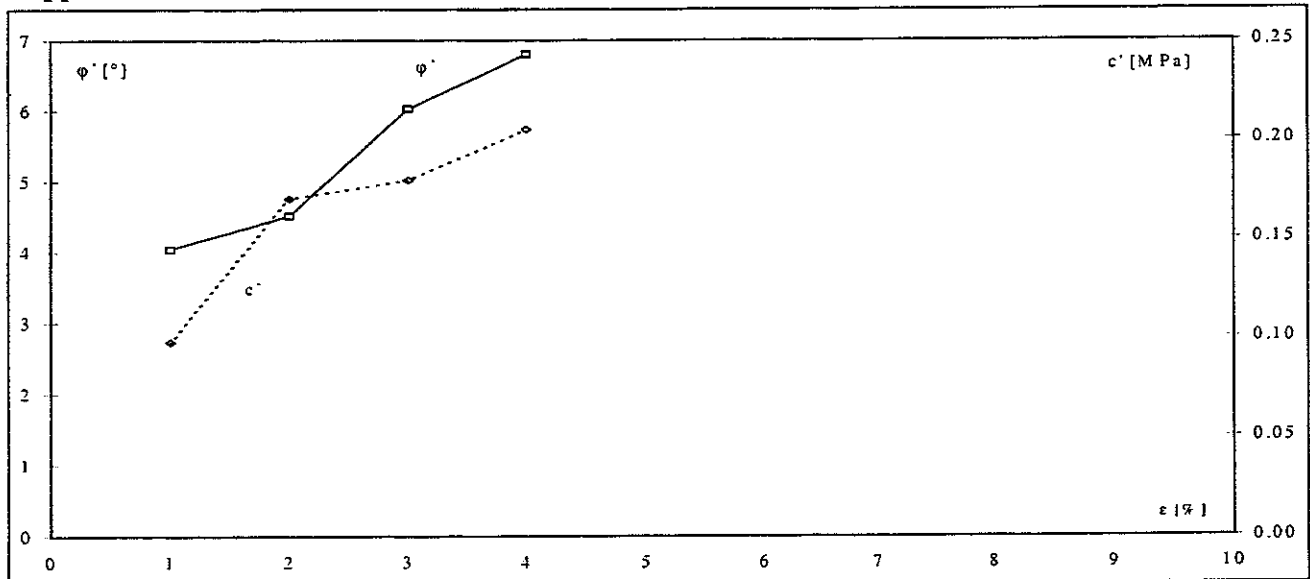
Appendix 43 : Deviator stress versus the mean total stress for Doel (B) 69.23 - 69.68 m



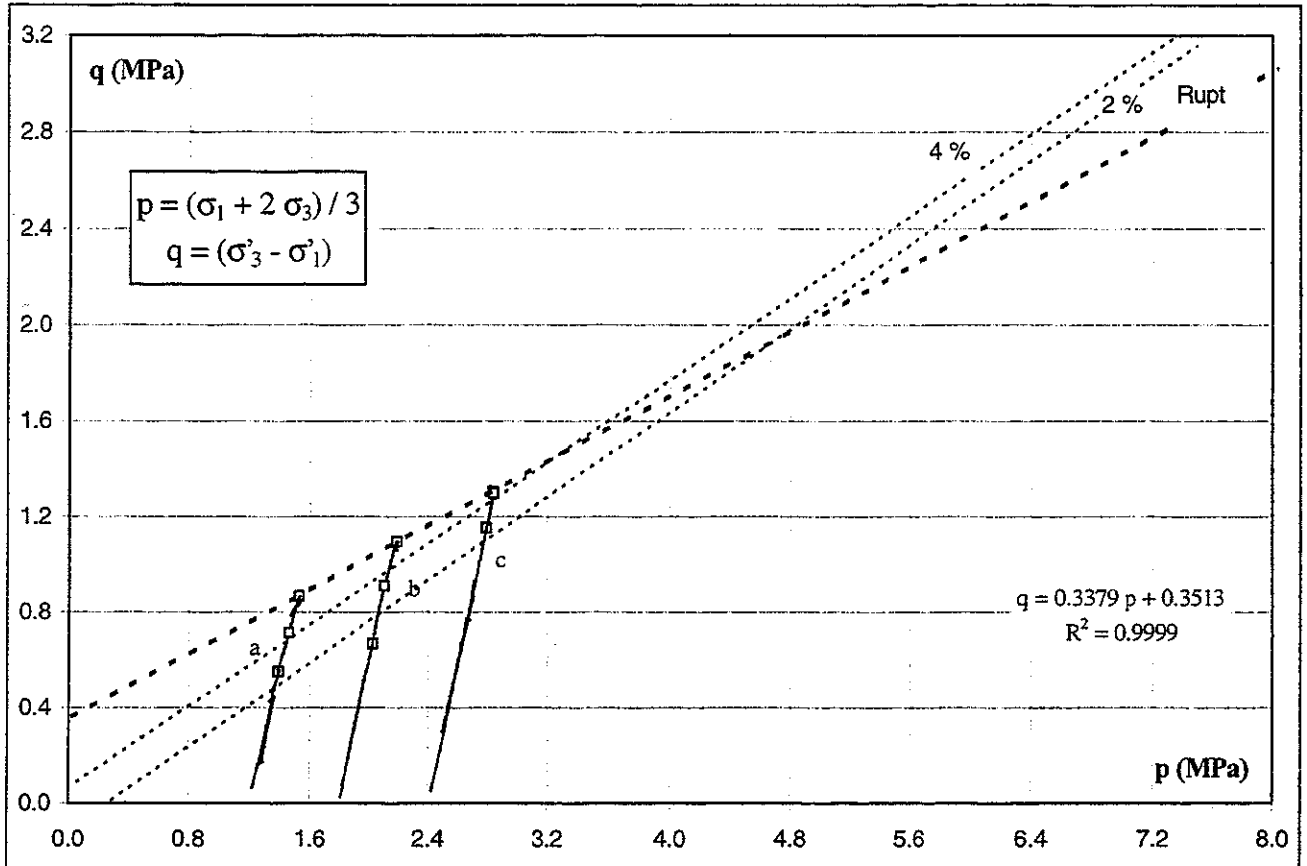
Appendix 44 : Total 'shear strength parameters' versus deformation for Doel (B) 69.23 - 69.68 m



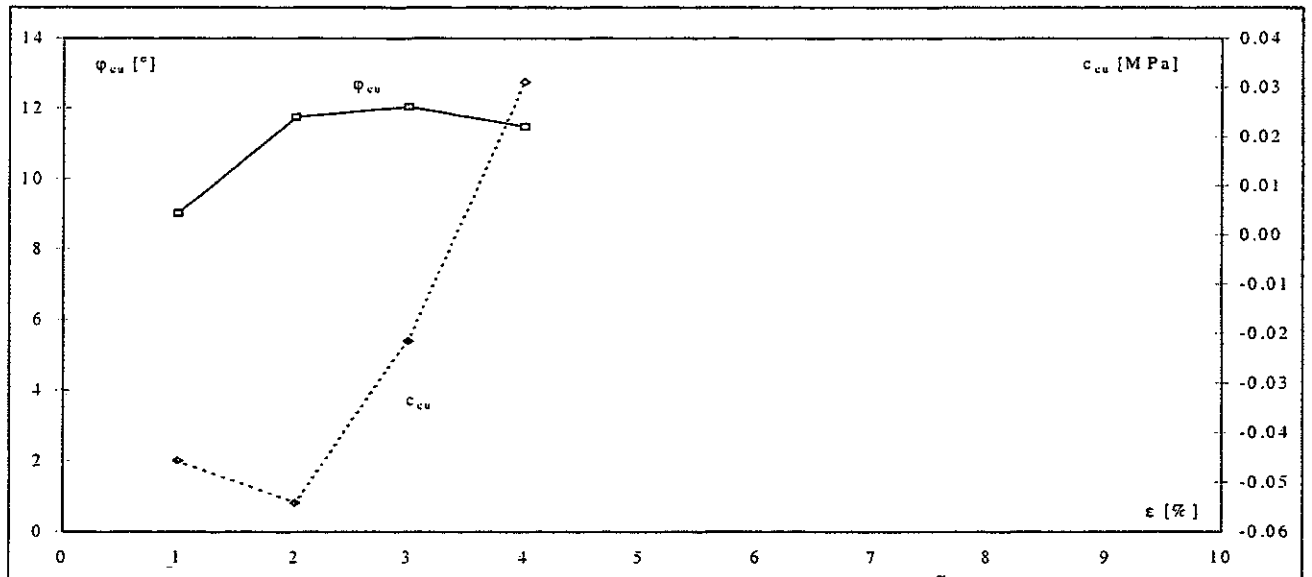
Appendix 45 : Deviator stress versus the mean effective stress for Zoersel (B) 120.47 - 121.22 m



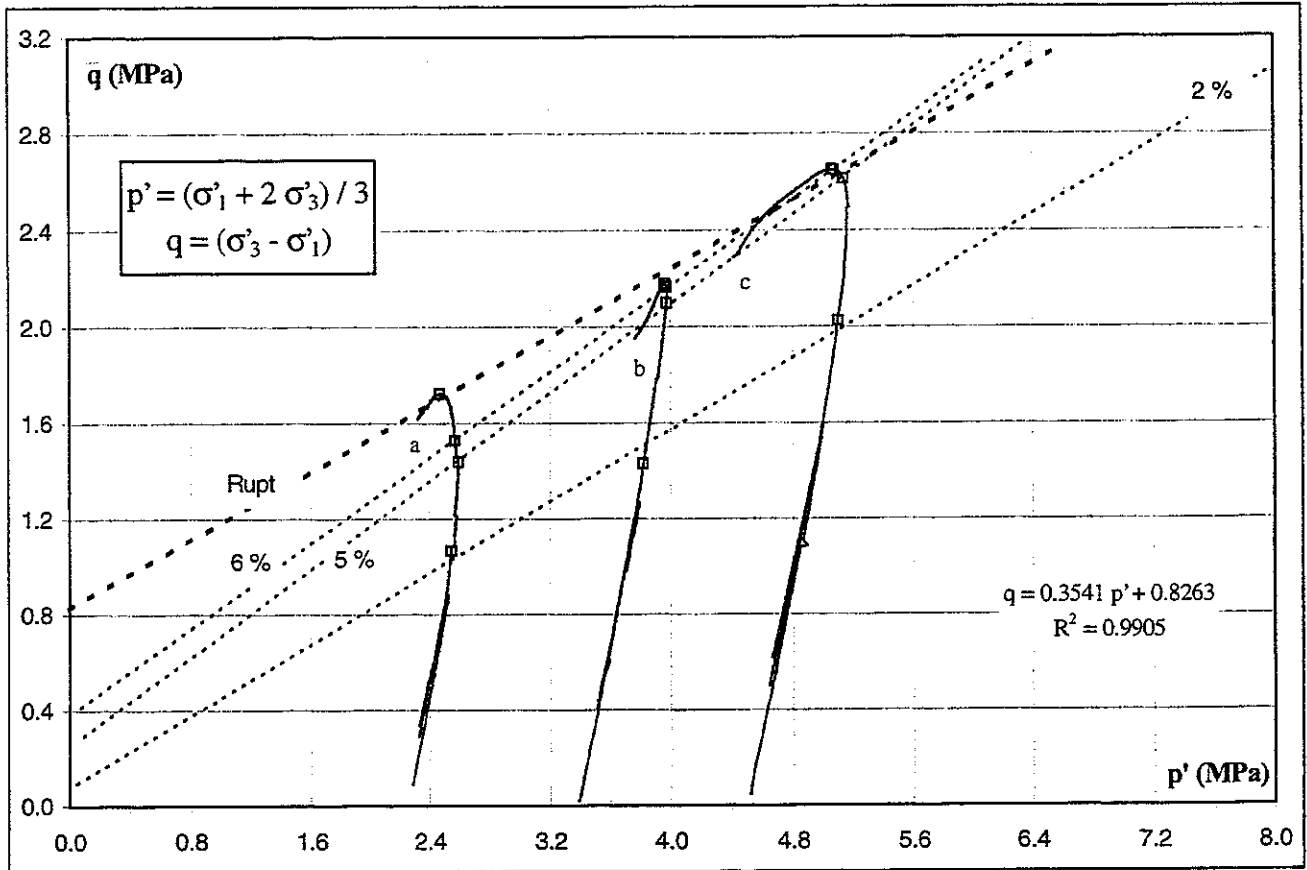
Appendix 46 : Effective 'shear strength parameters' versus deformation for Zoersel (B) 120.47 - 121.22 m



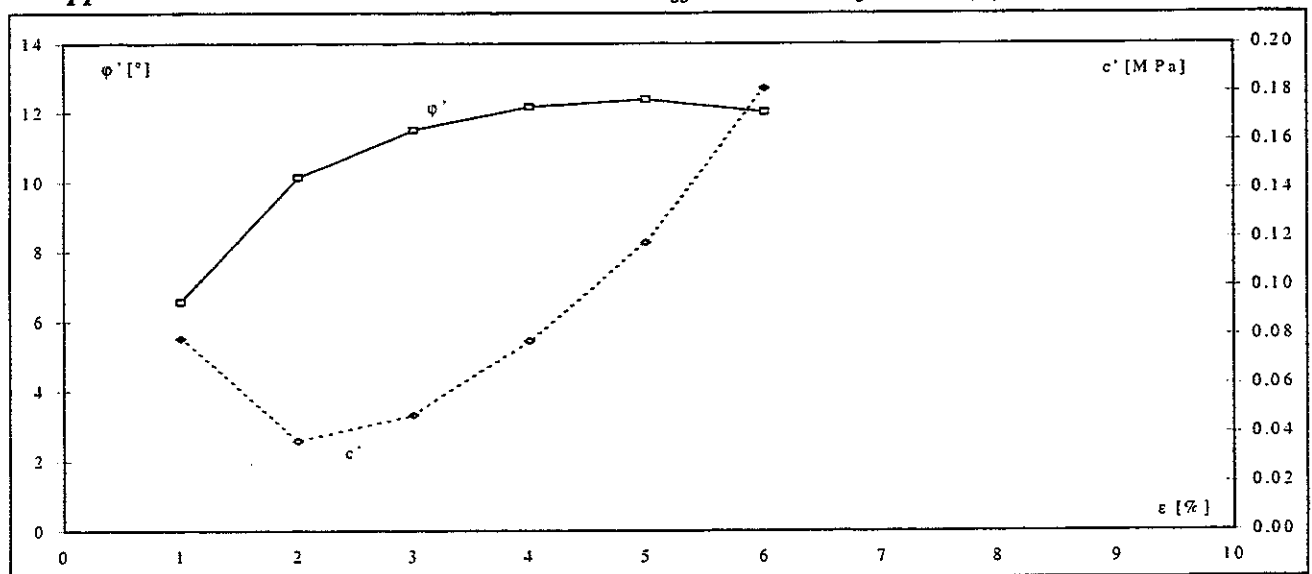
Appendix 47 : Deviator stress versus the mean total stress for Zoersel (B) 120.47 - 121.22 m



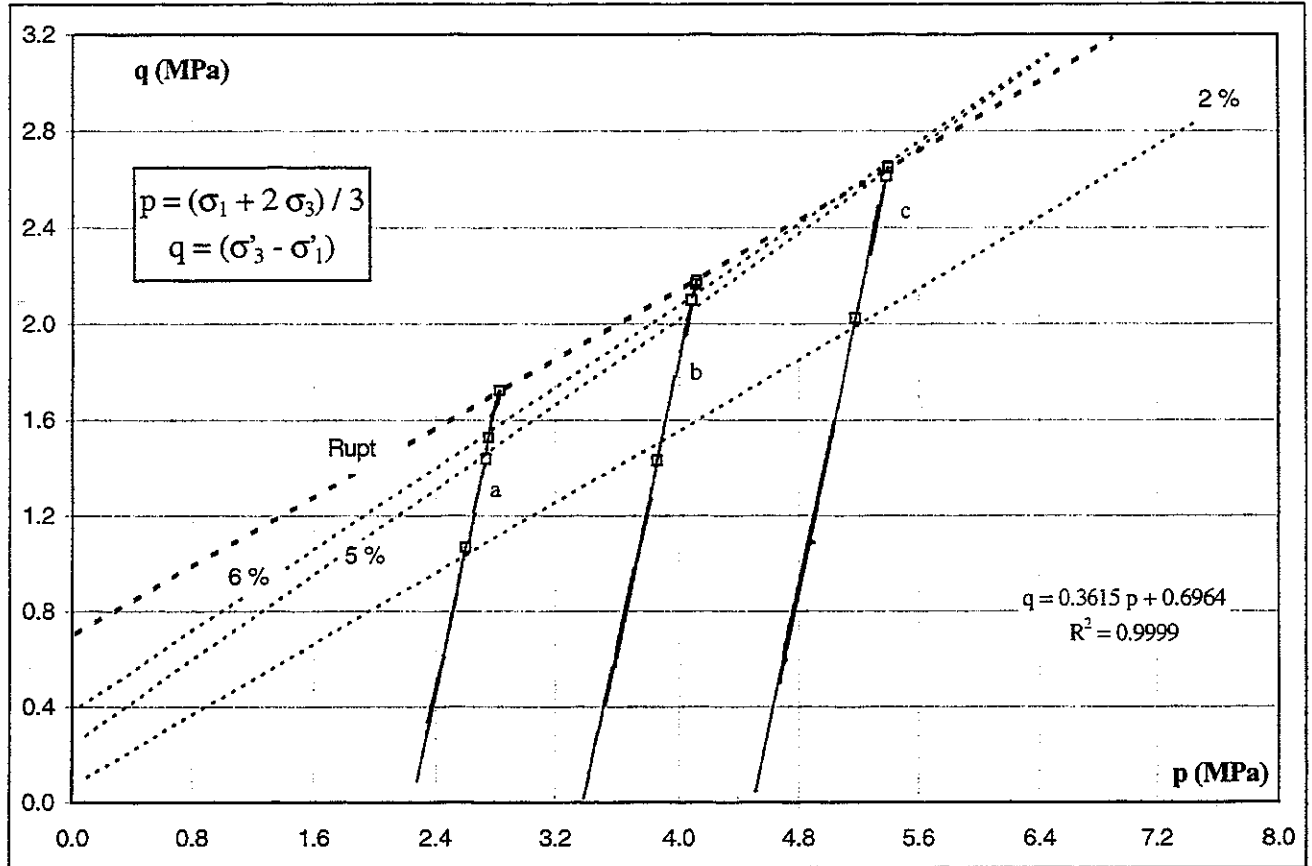
Appendix 48 : Total 'shear strength parameters' versus deformation for Zoersel (B) 120.47 - 121.22 m



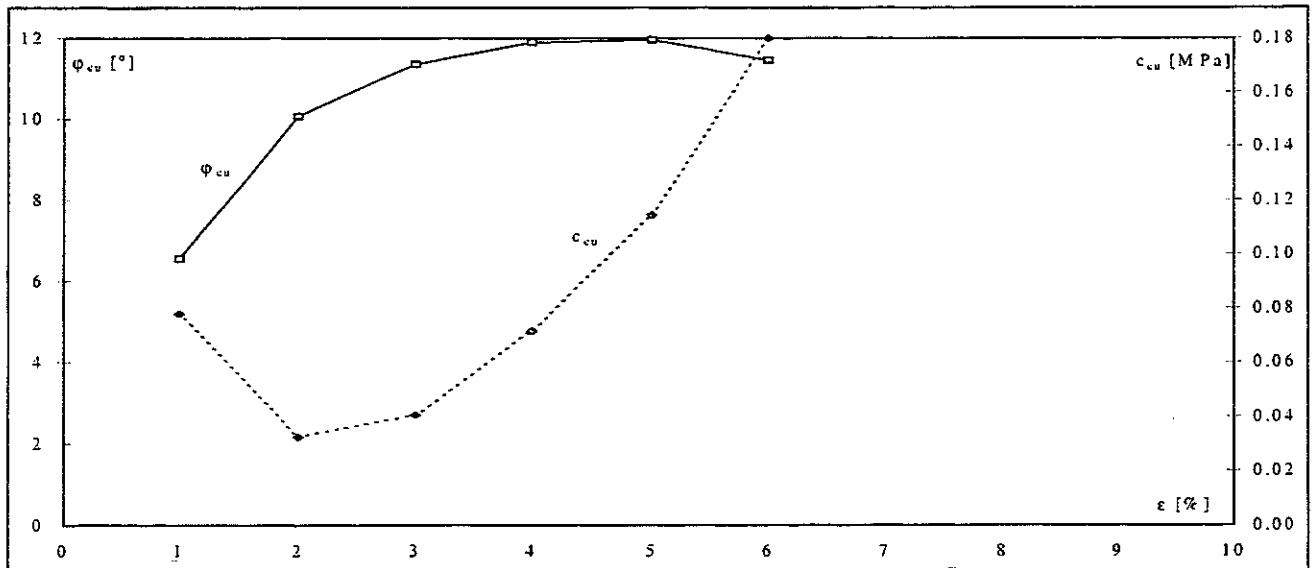
Appendix 49 : Deviator stress versus the mean effective stress for Mol (B) 229.18 - 229.28 m



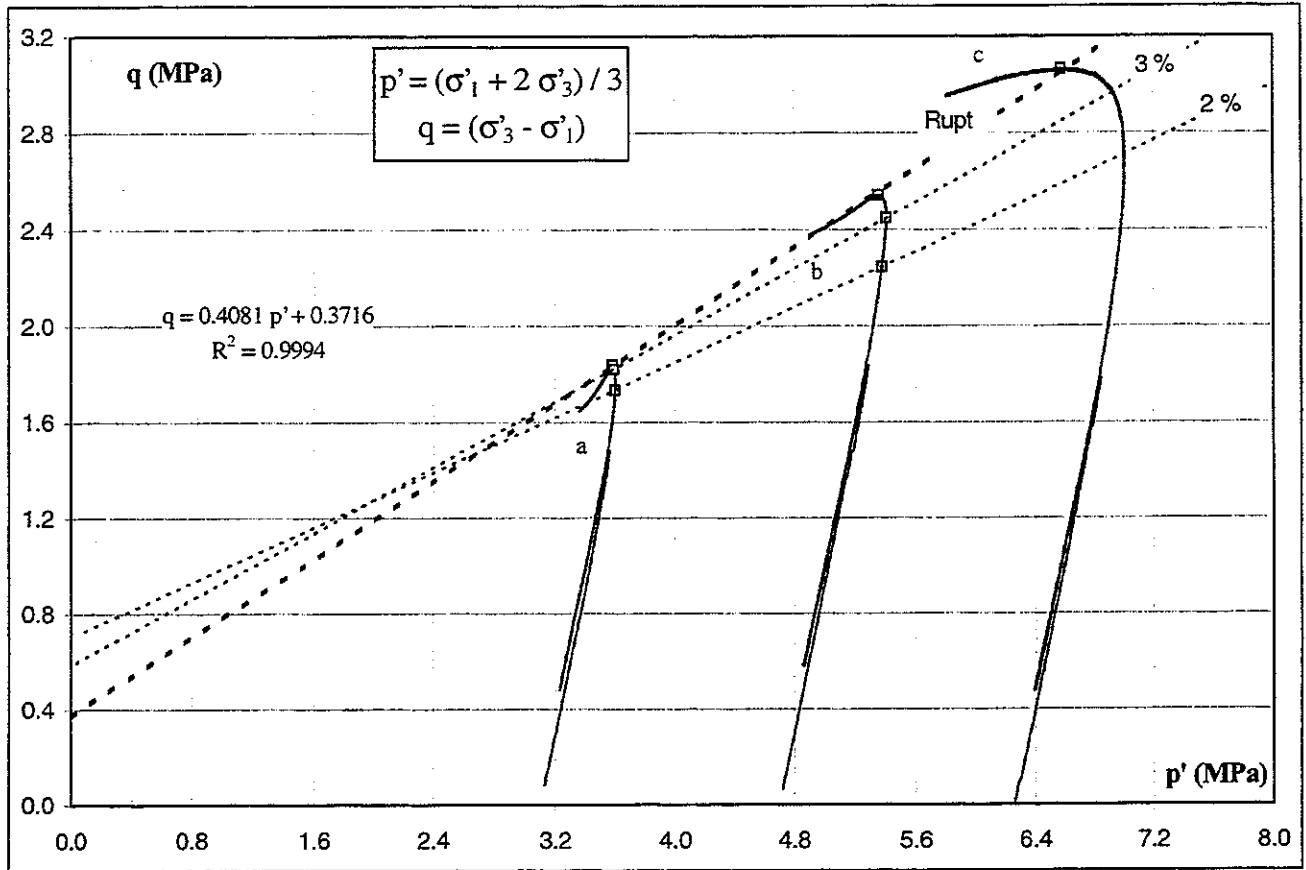
Appendix 50 : Effective 'shear strength parameters' versus deformation for Mol (B) 229.18 - 229.28 m



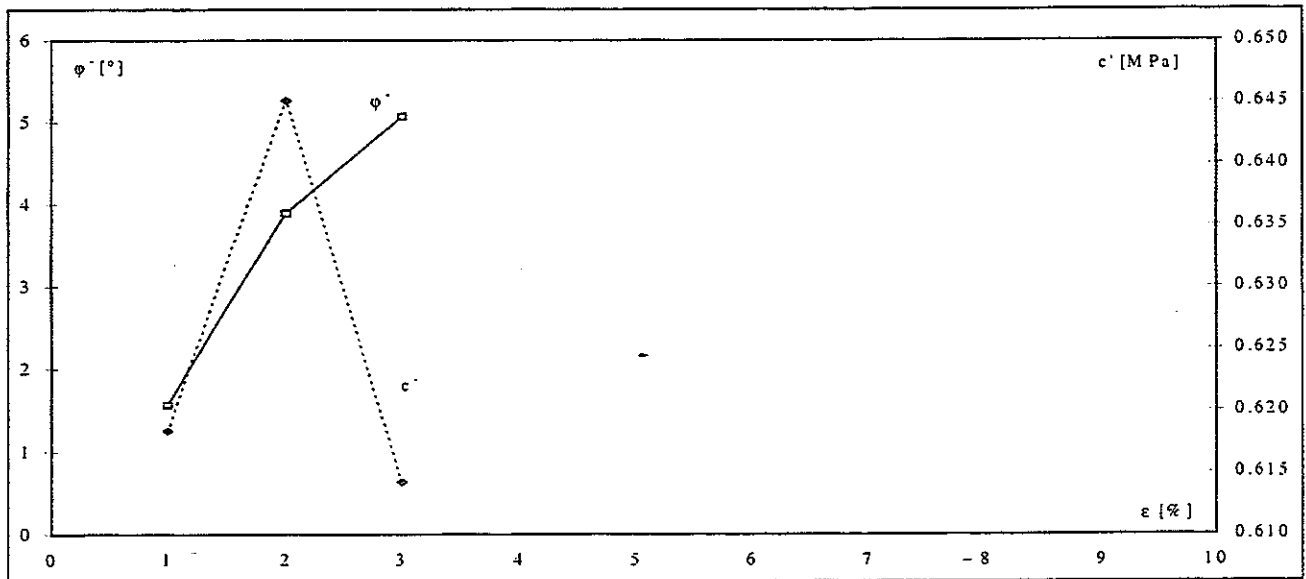
Appendix 51 : Deviator stress versus the mean total stress for Mol (B) 229.18 - 229.28 m



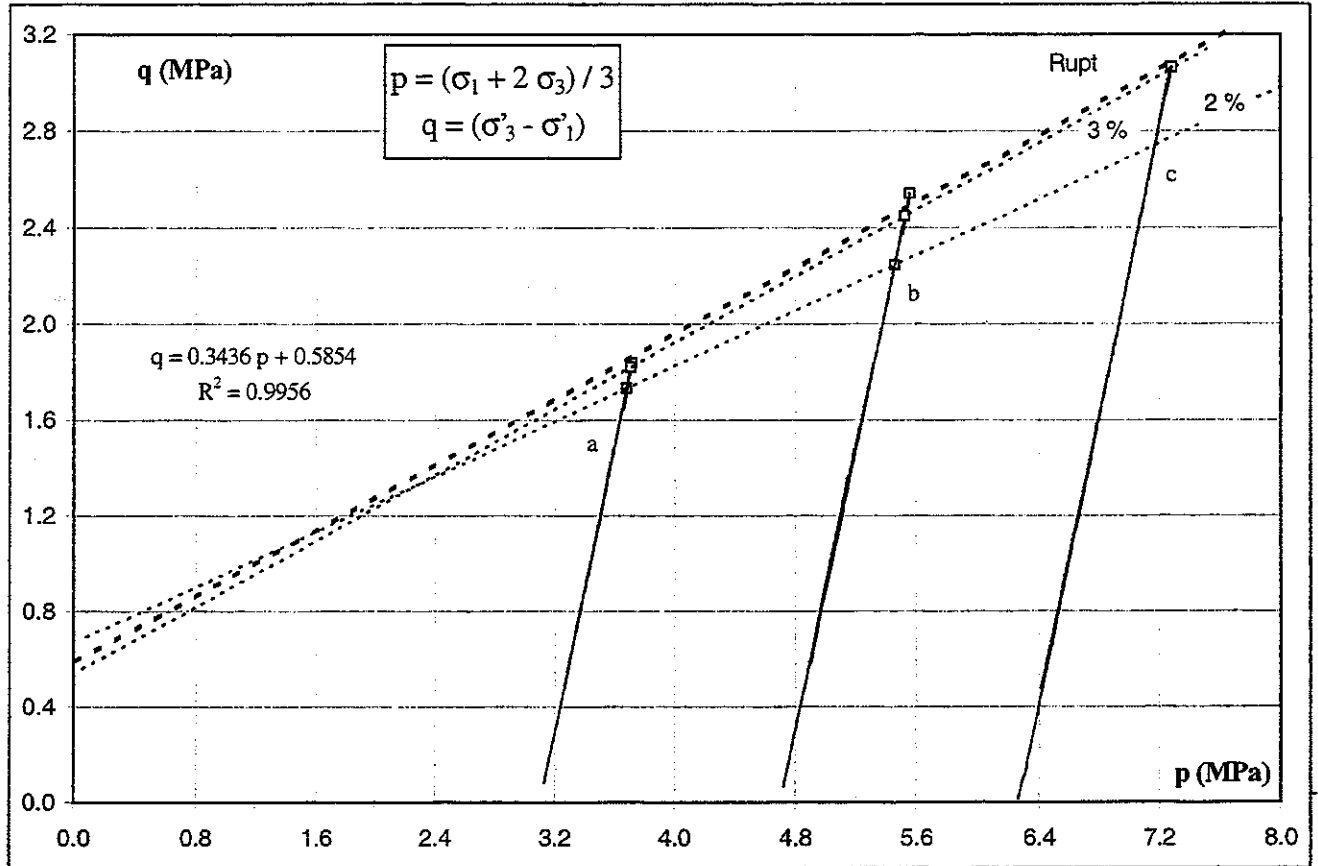
Appendix 52 : Total 'shear strength parameters' versus deformation for Mol (B) 229.18 - 229.28 m



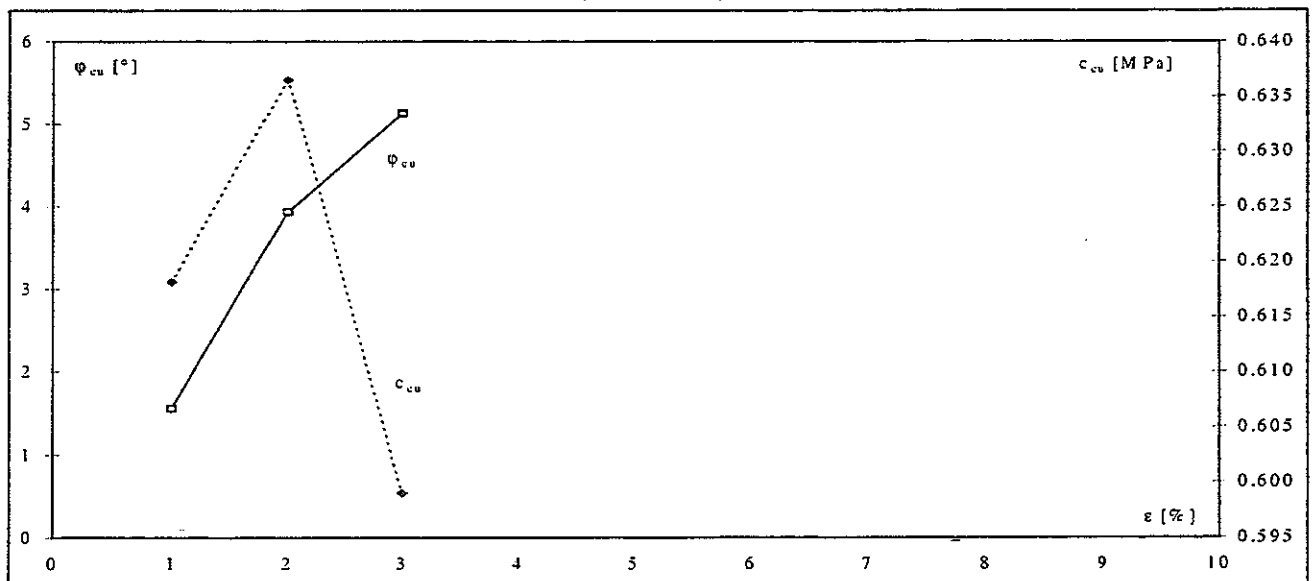
Appendix 53 : Deviator stress versus the mean effective stress for Weelde (B) 313.22 - 313.55 m (First serie)



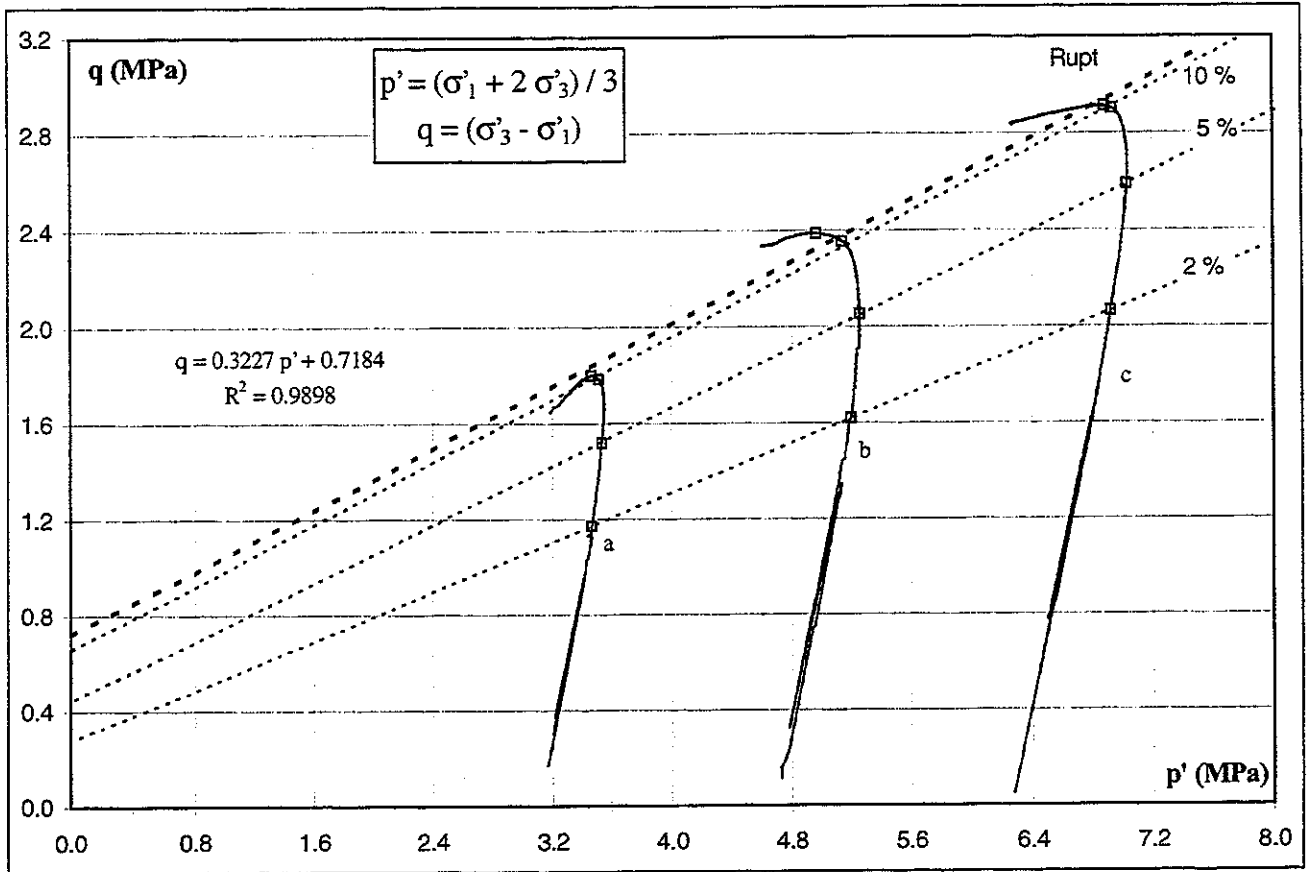
Appendix 54 : Effective 'shear strength parameters' versus deformation for Weelde (B) 229.18 - 313.55 m (First serie)



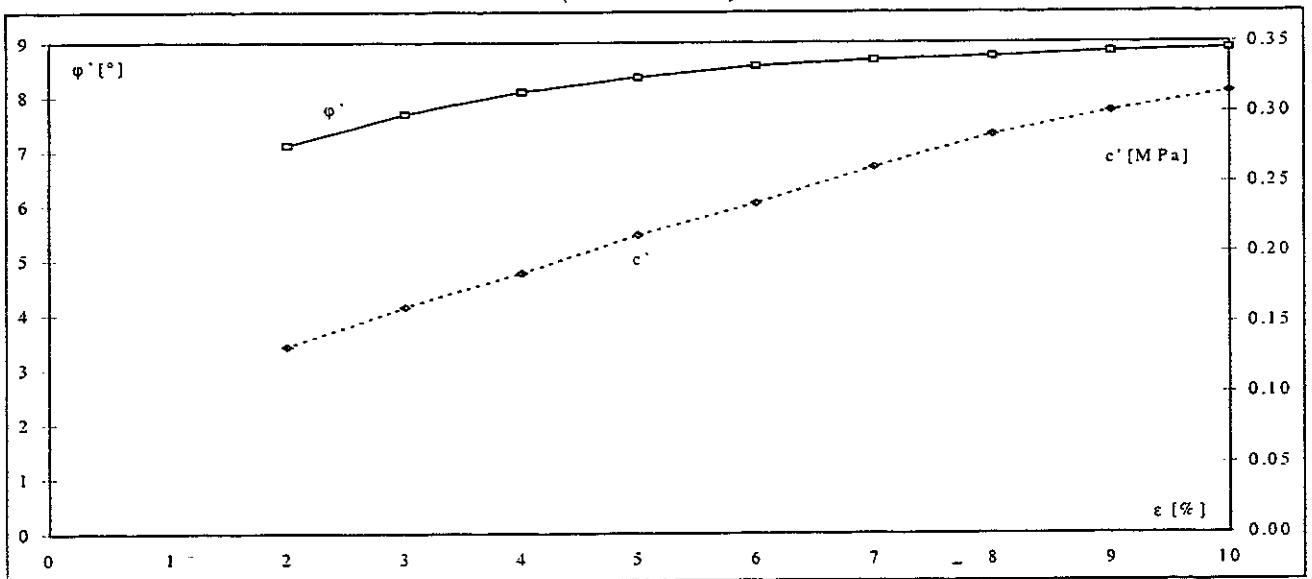
Appendix 55 : Deviator stress versus the mean total stress for Weelde (B) 313.22 - 313.55 m (First serie)



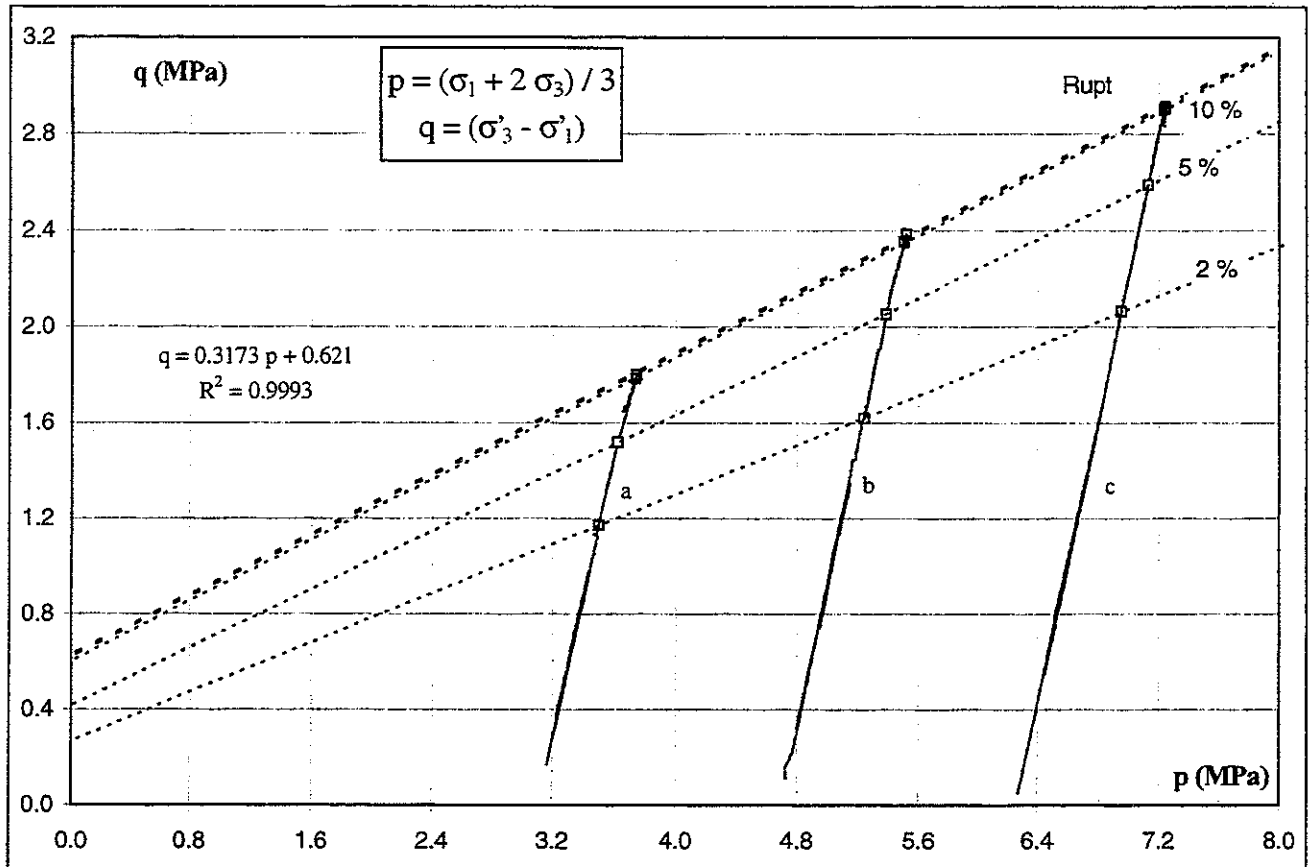
Appendix 56 : Total 'shear strength parameters' versus deformation for Weelde (B) 313.22 - 313.55 m (First serie)



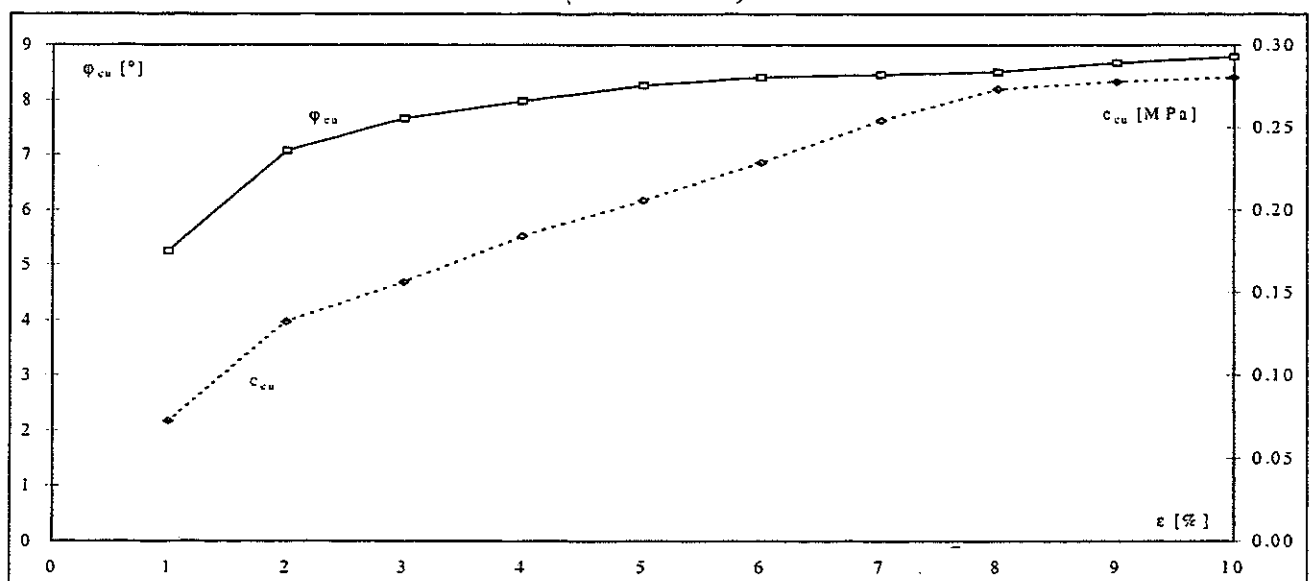
Appendix 57 : Deviator stress versus the mean effective stress for Weelde (B) 313.22 - 313.55 m (Second serie)



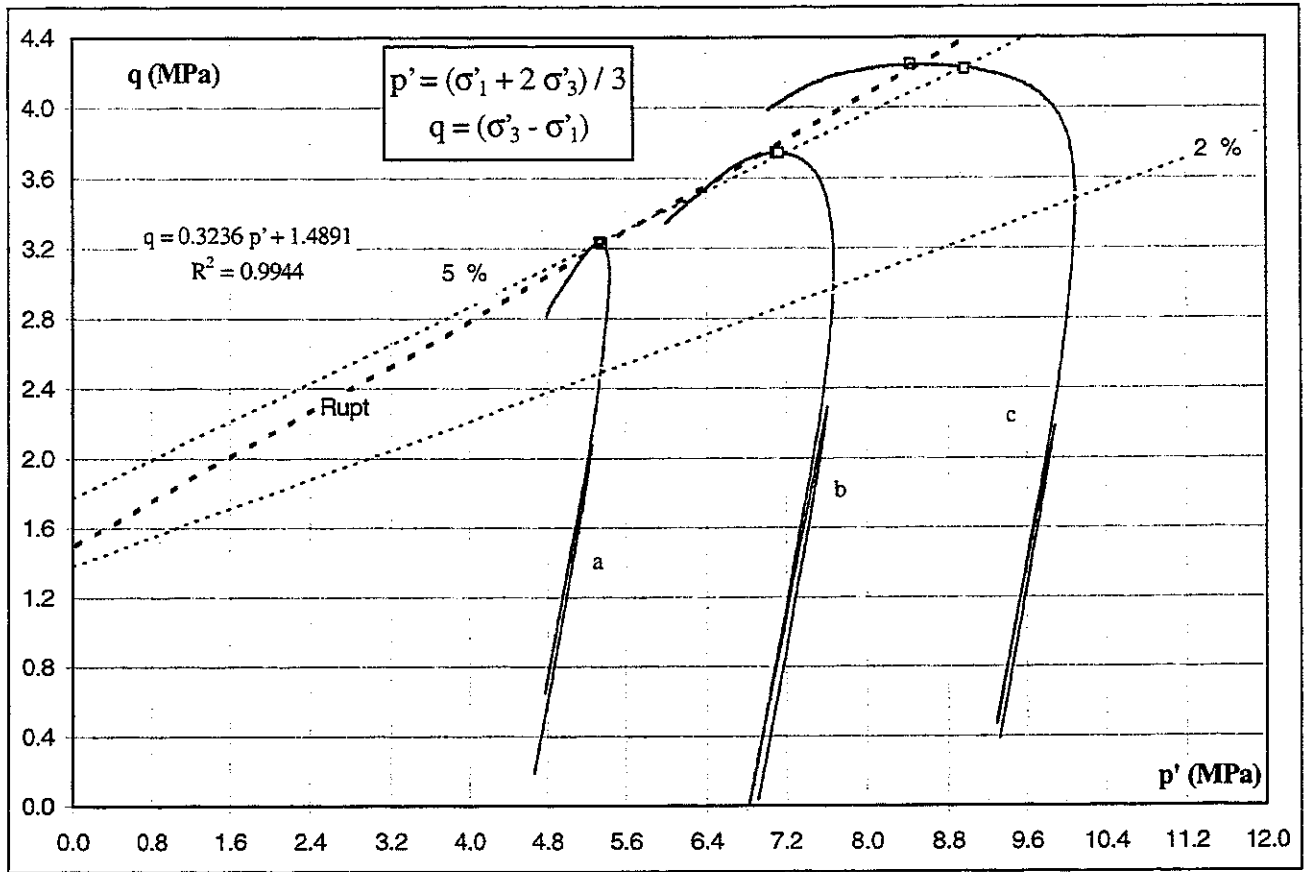
Appendix 58 : Effective 'shear strength parameters' versus deformation for Weelde (B) 313.22 - 313.55 m (Second serie)



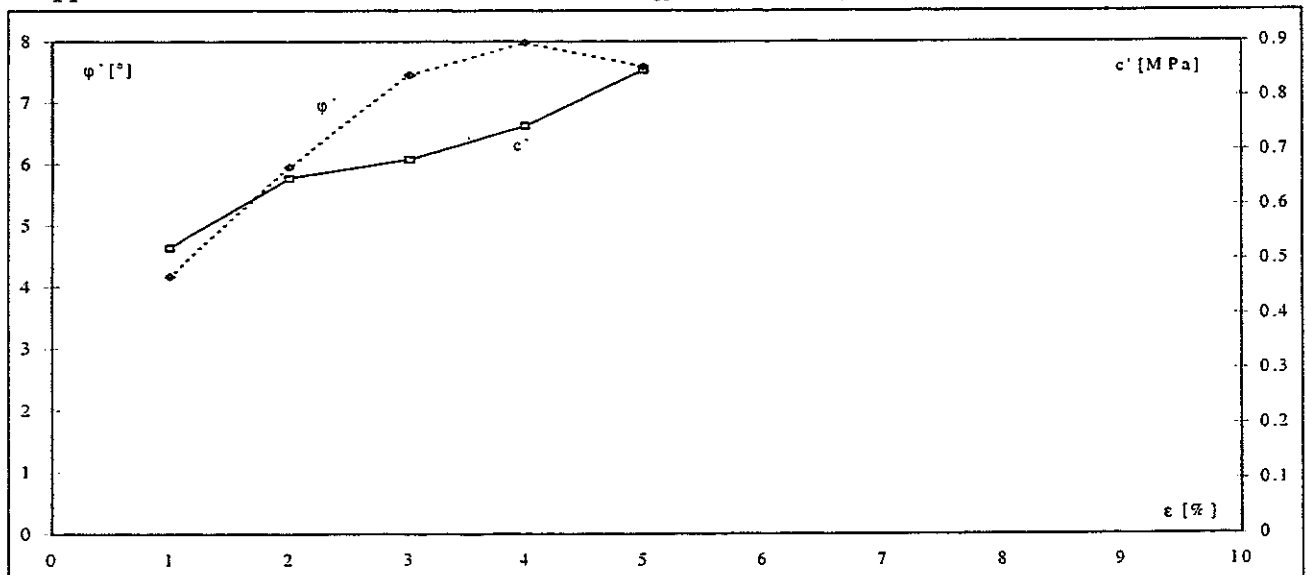
Appendix 59 : Deviator stress versus the mean total stress for Weelde (B) 313.22 - 313.55 m (Second serie)



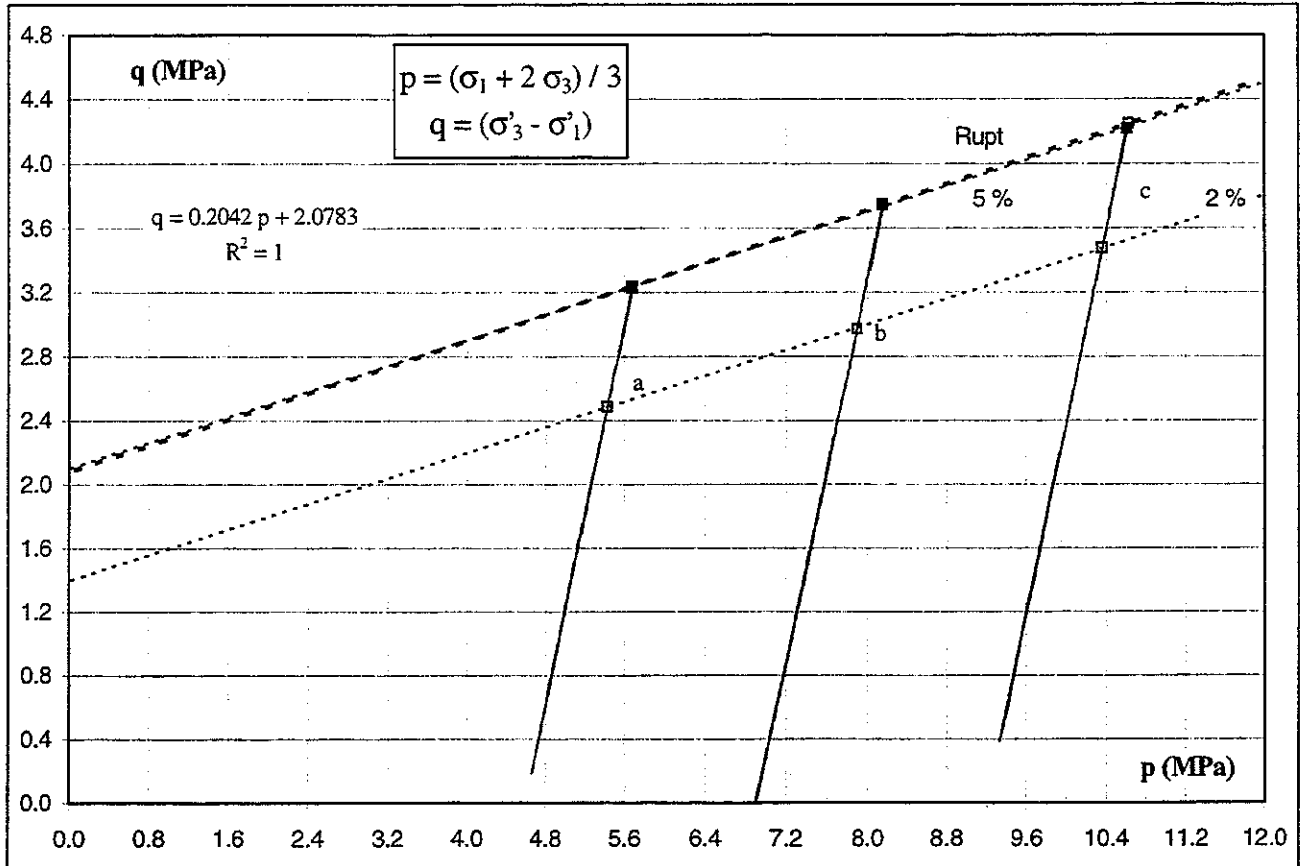
Appendix 60 : Total 'shear strength parameters' versus deformation for Weelde (B) 313.22 - 313.55 m (Second serie)



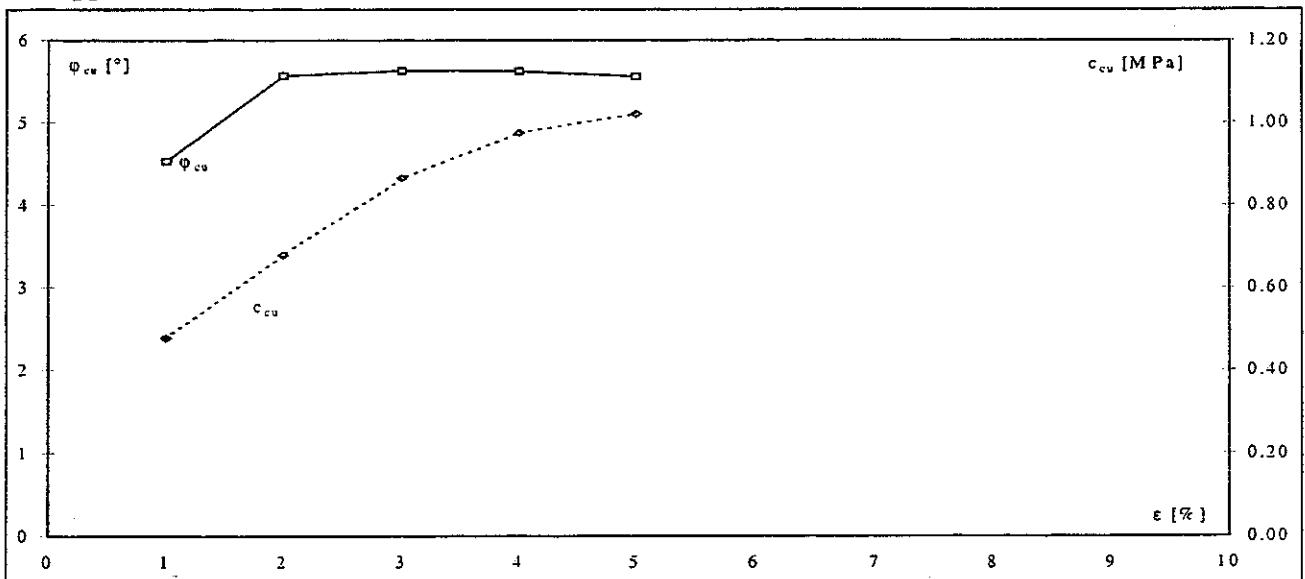
Appendix 61 : Deviator stress versus the mean effective stress for Blija (NL) 454.50 - 455.00 m



Appendix 62 : Effective 'shear strength parameters' versus deformation for Blija (NL) 454.50 - 455.00 m



Appendix 63 : Deviator stress versus the mean total stress for Blija (NL) 454.50 - 455.00 m



Appendix 64 : Total 'shear strength parameters' versus deformation for Blija (NL) 454.50 - 455.00 m